UNIVERSITY OF SOUTHAMPTON

Faculty of Medicine

Bone and Joint Research Group

THE USE OF TRANSLATIONAL MODELS TO ASSESS POTENTIAL NOVEL STRATEGIES IN BONE TISSUE ENGINEERING

by

Cameron RM Black

Thesis for degree Doctor of Philosophy

May 2017

UNIVERSITY OF SOUTHAMPTON

ABSTRACT

FACULTY OF MEDICINE

Bone Tissue Engineering

Thesis for degree Doctor of Philosophy

THE USE OF TRANSLATIONAL MODELS TO ASSESS POTENTIAL NOVEL STRATEGIES IN BONE TISSUE ENGINEERING

Cameron Russell MacGregor Black

The success of novel developments in the disciplines of stem biology and tissue engineering can be measured by the real-world impact each strategy achieves, this impact hinges on the transformation of core science into clinical application. In the field of Bone Tissue Engineering, progression from *in vitro* and small animal *in vivo* research towards a clinical application is constrained by a common translational barrier; designing and implementing a suitable pre-clinical experimental model in which to demonstrate any relevant clinical efficacy. In this thesis, a translational pathway is set out, mapping the progression from early *in vitro* development through successive upscaling into a true translational large animal segmental defect model, potentially bridging the gap from benchtop to bedside.

Multi-modal novel therapeutics in bone tissue engineering are formed of basic units. The cellular building block, scaffold material which acts as a vector for cell delivery whilst providing a framework to deliver and facilitate the growth of cells and host tissue and, biologically active stimulating factors which regulate the differentiation of both host and delivered cell components. The intelligent development of relevant large animal translational models needs to be able to address each of these core elements of a bone tissue engineering strategy, and prior to any large animal experimentation it was first necessary to characterise the host stem cell population so that accurate comparisons could be made from any data generated.

Chapter III characterises the ovine skeletal stem cell population selected for by Stro-4 antibody, its growth, capacity for self-renewal and differentiation both *in vitro* and through a functional assay *in vivo*.

Simultaneously we examined the potential of a novel extracellular matrix hydrogel to enhance bone formation in the absence and presence of a skeletal stem cell precursor. These promising results using basic *in vivo* models identified a candidate therapy for translational investigation.

As part of the developmental pathway towards establishing a large animal model, it was necessary to work first with a more conservative orthopaedic model, and the ovine condyle drill defect model was chosen accordingly. Chapter IV documents the condyle model development over successive experimental procedures, a standard surgical protocol was established and the model validated with positive and negative controls, resulting in a characterised model in which to assess novel tissue engineering strategies.

A nanosilicate hydrogel, which had been developed by the Bone and Joint Research Group and had demonstrated clinical promise in small animal work, was then examined in the newly developed ovine condyle model. Chapter V documents the application of the ovine condyle model investigating the ability of nanosilicates to control the delivery of a biologically active peptide, Bone Morphogenic Protein-2 in low doses within a large bone defect.

In Chapter VI, building on the experience developed through the ovine condyle model and, in collaboration with Queensland University of Technology, we utilised the Stro-4 and ECM hydrogel constructs characterised in Chapter III in an ovine tibial critical sized defect model. This model, considered as a true clinically-relevant model demonstrated the importance of large animal experimentation in translational medicine as results generated *in vitro* and using small animal models *in vivo* were not emulated in the large animal model.

A Pathway from early basic science through subsequent *in vivo* models into a clinically relevant translational model was established. An enriched stem population was characterised and the potential of the stem cell population in engineering new bone growth evaluated in combination with a novel ECM hydrogel. Concurrently, a proprietary nanosilicate hydrogel was successfully progressed though the translational pathway revealing exciting directions for future work.

Table of contents

List of tables

List of figures

DECLARATION OF AUTHORSHIP

I, Cameron Russell MacGregor Black .....

declare that this thesis and the work presented in it are my own and has been generated by me as the result of my own original research.

THE USE OF TRANSLATIONAL MODELS TO ASSESS POTENTIAL NOVEL STRATEGIES IN BONE TISSUE.

.....

I confirm that:

1. This work was done wholly or mainly while in candidature for a research degree at this University;
2. Where any part of this thesis has previously been submitted for a degree or any other qualification at this University or any other institution, this has been clearly stated;
3. Where I have consulted the published work of others, this is always clearly attributed;
4. Where I have quoted from the work of others, the source is always given. With the exception of such quotations, this thesis is entirely my own work;
5. I have acknowledged all main sources of help;
6. Where the thesis is based on work done by myself jointly with others, I have made clear exactly what was done by others and what I have contributed myself;
7. Parts of this work have been published as:

   Black CRM, Goriainov V, Gibbs D, Kanczler J, Tare RS, Oreffo ROC. 2015. Bone Tissue Engineering. Current Molecular Biology Reports 1:132-140

Signed: .....

Date: .....

Acknowledgements

The Lord my God, You have sustained me with wisdom and peace; the stronghold of my life.

Nearest and dearest

My dear family and loved ones, I have received more support and understanding whilst writing my PhD than I could have ever asked for, Hazel and Ian Black, this was my Black Sable project, and you were right there with me. To my sisters, thank you for being an ever-present help and sounding board, we got there in the end.

Joanna, you have walked with me through the hardest part and got me through the other side, this will always be ours. You have picked me up and kept me going and never once faltered, thank you.

Patrick, David, Edo and Tsiloon, you bore the brunt of my less favourable side and you were constant, I am truly thankful to have had you to rely on.

Bone and Joint Research Group

Group leader Professor Richard Oreffo; the door was always open, I am grateful for his council and sincere understanding in all circumstances. Working for the Bone and Joint Research Group has been a fulfilling experience, thank you.

Janos Kanczler; the man who makes it all happen, I am sincerely thankful to Janos for all his support and advice, there were more than a few times when I was ready to leave but your support kept me there!

The group has always worked well together and my thanks goes to many, but I must single out some superstars; Julia Wells, I don't want to think what my PhD would have been like without her professional and personal support, thank you. Kate White, Stef Inglis and Katrina Jones for holding the BJRG ship together. Jon "Laponite or Bust" Dawson, as a colleague and friend, our coffee talks helped many an ill. May De Andres Gonzalez…….. terrific!

Jon's Magimix Nespresso coffee maker

Everyone who has ever brought-in cake

Thank you to everyone for your companionship, support and understanding, we all get there in the end.

List of abbreviations

α-MEM Alpha Minimum Enrichment Media

µA Micro Amperes

µCT Micro-Computed Tomography

A/S Alcian Blue Sirius Red

AFM Atomic Force Microscopy

AM Additive Manufacturing

ANOVA Analysis of Variance

ASTM American Society for Testing and Materials

BMC Bone Mineral Content

BMD Bone Mineral Density

BMP Bone Morphogenic Protein

BTE Bone Tissue Engineering

BRF Biomedical Research Facility

BV Bone Volume

CAD Computer aided design

C-AM Computer-aided manufacturing

CAM Chorioallantoic Membrane

CE European Conformity

CD4 Helper T-cell

CD8 Cytotoxic T-cells

CVC Central Venous Catheter

DBB Deproteinised Bovine Bone

DBM Demineralised Bone Matrix

DXA Dual X-Ray Densitometry

E.T Tube Endotracheal tube

ECG Electrocardiogram

ECM Extracellular Matrix

EU European Union

FDM Fused Deposition Modelling

GDF Growth Differentiation Factor

HO Home Office

HR-QCT High Resolution Quantitative Computed Tomography

i.m. Intramuscular

ISO Isos, International Organisation of Standardisation

i.v. Intravenous

IGF Insulin-like Growth Factor

IHC Immunohistochemistry

IVFT Intravenous Fluid Therapy

kV Kilo Volts

Mcg/KG/hr Micrograms per kilogram per hour

MMPs Matrix Metalloproteinases

MERF Medical Engineering Research Facility

Mg/kg Milligrams per kilogram

MI Micro-Indentation

MIS Mullerian Inhibiting Substance

MMA Methyl Methacrylate Monomer

NHS National Health Service

NJR National Joint Registry

NK Natural Killer Cells

NVS Named Veterinary Surgeon

OBMMNCs Ovine Bone Marrow Mononuclear Cells

ONS Office of National Statistics

PBS Phosphate Buffered Saline

PCL Polycaprolactone

PDGF Platelet Derived Growth Factors

PEG Polyethylene glycol

PET Polyethylene terephthalate

PGA Polyglycolide

PIL Personal License

PLA/PLGA Poly(L-Lactide/poly(glycolide)

PLDLLA Poly(Lactide-co-D, L Lactide)

PLGA Poly(L-Lactide-co-glycolide)

PLGA/PEG Poly(lactide-co-glycolide)/poly(ethyleneglycol)

PLGA/PVA Poly(lactide-co-glycolide)/polyvinyl alcohol

PLL Poly(L-Lactide)

PLLDL Poly(L-Lactide-co-D, L-lactide)

PPF Poly(propylene-glycol-co-fumarate)

PPL Project License

QUT Queensland University of Technology

RPI Reference Point Indentation

ROI Region of Interest

RPM Revolutions per minute

s.c. Sub-cutaneous

SIBLINGs Small Integrin Binding n-Linked Glycoproteins

SLRPs Small Leucine Rich Proteoglycans

SSCs Skeletal Stem Cells

TC Tissue Culture

TGf-β Transforming Growth factor beta

TV Tissue Volume

VEGF Vascular Endothelial Growth Factor

VOI Volume of Interest

"… there was a sound like a rattling of bones, and the bones came together, bone to bone, and I looked, and tendons appeared on them, then muscle and then skin covered them." Ezekiel 37:8

Chapter I

1 Introduction

1.1 Pathway to modern bone tissue engineering

"The only rational means of treatment are those based on the natural recuperative power of the body" John Hunter. John Hunter, an inspired surgical pioneer of the 1700s recognised that the key to optimal healing lay within the body and that our function as physicians was to nurture and not supplant the bodies' capacity for self-healing.

1.2 Clinical context for novel therapies in Bone Tissue Engineering

In the United Kingdom the estimated life-time adjusted risk for hip and knee arthroplasty in men and woman is 7% and 11% (Culliford et al., 2012). The annual incidence of fractures in both sexes is estimated at 11 fractures per 1000 adults each year. Men and woman over 50 years of age face a lifetime risk from all fractures of approximately 20% and 53% respectively (van Staa et al., 2001; Court-Brown and Caesar, 2006). Further, according to the World Health Organisation 2012 Technical report (WHO, 2012), 1 in 5 men and 1 in 3 women diagnosed with osteoporosis will experience a disease related fracture, WHO (Johnell et al., 2005) and findings by Melton (Melton et al., 1998).

Fractures are debilitating; affected individuals experience severe physical pain and potential loss of function to the affected anatomy. These factors contribute to a reduction in overall quality of life which negatively impact on a patients' psychological well-being (Lubeck, 2003).

Due to complications of healing and concurrent damage to associated tissues, many of those affected by musculoskeletal disease will continue to experience related morbidity well after the initial onset of trauma or disease (Schnell et al., 2010) (Braithwaite et al., 2003; Colón-Emeric and Saag, 2006).

Under optimal conditions, a fractured or damaged bone will heal without the need for intervention. Bone repair is a well-balanced and coordinated biological process that recapitulates embryological skeletogenesis, leading to a return of physiological and mechanical function in the repaired organ (Gerstenfeld et al., 2003).

The implementation of modern surgical techniques, advanced implants and improved peri-operative management have improved clinical outcomes in fractures and bone loss related to high energy trauma, neoplasia and disease (Paley and Maar, 2000; Quarto et al., 2001; Marcacci et al., 2007). Complications, including interruptions to blood supply, wound contamination, poor mechanical stability and other deleterious factors can create large areas of bone tissue with an inherently compromised potential for repair (Mirhadi et al., 2013).

The treatment of large volume bone defects caused by complex trauma and bone disease is beset by complications of delayed and non-union; salvage procedures resulting in limb reduction and removal are sometimes a surgeon's only choice. These options-of-last resort place an irrevocable lifetime burden a patient but are unavoidable in the absence of effective alternative treatment (Ghert et al., 2005; Phieffer and Goulet, 2006; Papakostidis et al., 2011).

Patients experience prolonged physical and psychological difficulty and are subjected to extended periods of hospitalisation, and may require multiple surgical interventions. Such bone tissue healing insufficiencies pose a significant socio-economic and medical challenge which can greatly undermine the health and well-being of all affected (Perry, 1999).

The current best clinical practice employs the use of bone graft and bone graft alternatives to replace lost bone material and supplement bone regeneration (Lane et al., 1999). Autologous bone is an ideal like for like graft material and is the standard to which all material should be compared (Sen and Miclau, 2007; Misch, 2010). Although not as efficacious, allograft is widely used and accounts for higher use by volume than autograft due relative ease of harvest preparation and storage (Zimmermann and Moghaddam, 2011).

Despite the clinical benefits of bone graft, major inadequacies remain, complications such as fracture non-union, failed engraftment and delayed graft fracture remain commonplace, particularly in large defect reconstruction (Muramatsu et al., 2003; Cancedda et al., 2007; Delloye et al., 2007).

Auto and allogenic bone graft are limited in availability, harvest may cause significant donor site morbidity, carry an infection risk and are not clinically reliable (Giannoudis et al., 2005; Laurencin et al., 2006). Therefore, a conspicuous clinical need exists for a readily available, effective and low-cost alternative to bone graft material.

Between 2003 and 2014 the National Joint Register recorded over 700,000 primary hip replacements in the UK, with numbers rising year on year from 14,424 in 2003 to over 83,000 in 2014. A corresponding increase in hip revisions from 1,423 in 2003 to over 8,000 in 2004 were also registered, National Joint Registry 2016 (Registry, 2016).

Over 600,000 primary knee replacements were recorded over the same period. Primary hip and knee replacement statistics in the USA closely match those of the UK (Organisation for Economic and Co-operation and Development).

Most patients undergoing joint arthroplasties are over the age of 50 and, in the UK, the number of people aged 65 and over is projected to increase by 32.7% between 2014 and mid-2039, with the number 75 years and older predicted to rise by 89.9%, Office of National Statistics (Schnell et al., 2010), see Figure 1-1.

1.2.1 Office of National Statistics population projection

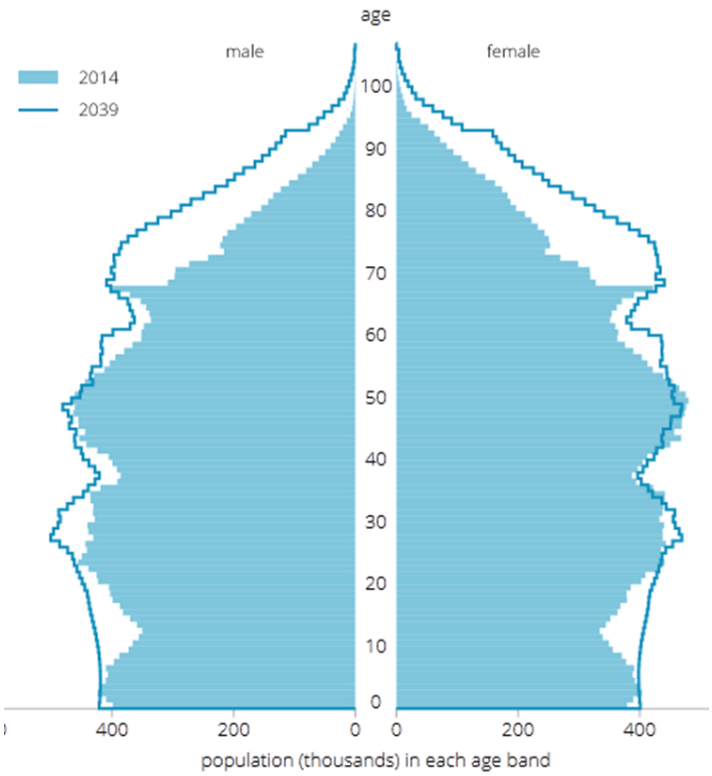

Figure 1-1 Population age change 2014-2039. Office of National Statistics projections for net population change, by number age and sex (ONS, 2015)**..**

This flattening of the population age pyramid is expected to correlate with an increase in primary and secondary joint arthroplasties in concert with an increase in the number of older-age associated musculoskeletal conditions. The current and potential burden to national health care systems is clear and carries with it a significant financial cost. Financial costs are not only limited to direct spending on the treatment of musculoskeletal conditions, the indirect economic impact to a labour force is often underplayed. In 2011, NHS England total spend on musculoskeletal disease exceeded £5 billion for surgical and physiotherapy care and over £1 billion on chronic pain management (NHS Programme Budgeting Data 2013/2014) (NHS, 2013).

The broader economic implications relating to work disability and impact to the labour force are more difficult to quantify. In the USA the estimated monetary impact of associated costs in musculoskeletal disease is 1% of GDP (Yelin, 2003). The overall clinical, social and financial impact of musculoskeletal disease is of importance globally, its significance providing the impetus behind next generation therapies.

1.3 Bone

1.3.1 Function

Bone is a ubiquitous calcified tissue in all vertebrate classes and is the most abundant of all connective tissues within the skeleton.

Bone is a metabolically active organ with functions including:

i) Structural support, providing the rigid framework forming the shape of the body, and locomotion, providing muscle attachments, a centre of moments and moment arm for axial skeletal movement and joints, allowing directional change of forces during fine motor control and ambulation.

ii) Mineral regulation; bone is a reservoir for inorganic ions and the osteocyte is a prolific producer of FGF-23, MEPE, PHEX and DMP-1 serving in a coordinated manner locally and in circulation to regulate bone mineral composition and systemic mineral homeostasis (Bonewald, 2011).

iii) Macro and microenvironment for haematopoiesis, marrow cavities and finer trabecular structures provide a haematopoietic niche for myeloid and lymphoid progenitor cells (Morrison and Scadden, 2014).

iv) Protection of internal organs; the spine, skull, rib cage and pelvis shelter delicate internal organs from external trauma.

v) Reservoir for haematopoietic and mesenchymal stem-cells, and a bone microenvironment shown to harbour a population of multipotent progenitors required for musculoskeletal maintenance and repair.

vi) Endocrine regulation; independent to bone's capacity for mineral homeostasis, osteocytes secrete osteocalcin contributing to glucose metabolism, adipocyte regulation and testosterone production (Guntur and Rosen, 2012).

1.3.2 Structure

Bone is a composite material with mineral elements conferring strength and stiffness (Martínez-Reina et al., 2010) with the organic component providing strength (Zioupos, 2001). Bone structure is hierarchical and varies according to bone type, species, sex, age, activity and health status (Rho et al., 1998).

Macroscopically bones are described as long, flat, sesamoid or irregular, with the sub-structure of each bone type varying according to its function *in vivo*. Bone is broadly formed of two types of osseous tissue; dense, highly mineralised cortical bone and open-structured less-dense cancellous or trabecular bone, the proportions of each varying between bone types.

Cortical bone forms the majority of the skeleton by mass and is denser, stronger and stiffer than cancellous bone. Cortical bone is surrounded externally by a tough fibrous vascularised membrane called the periosteum which is matched on the internal bone surface by a thin cellular membrane known as the endosteum.

Cancellous bone by comparison is finer, less dense and open in structure forming delicate trabeculae branching from a cortical origin, its primary function is to provide the structural domain hosting the haematopoietic activities of long bones, sternum and ilium. Trabeculae orientate along the line of force distribution and offer a secondary, elastic load sharing capacity, augmenting the primary function of cortical bone (Weiner and Traub, 1992; Rho et al., 1998; Story et al., 1998). The typical structure of a long bone is shown in Figure 1-2.

Structure of long bone

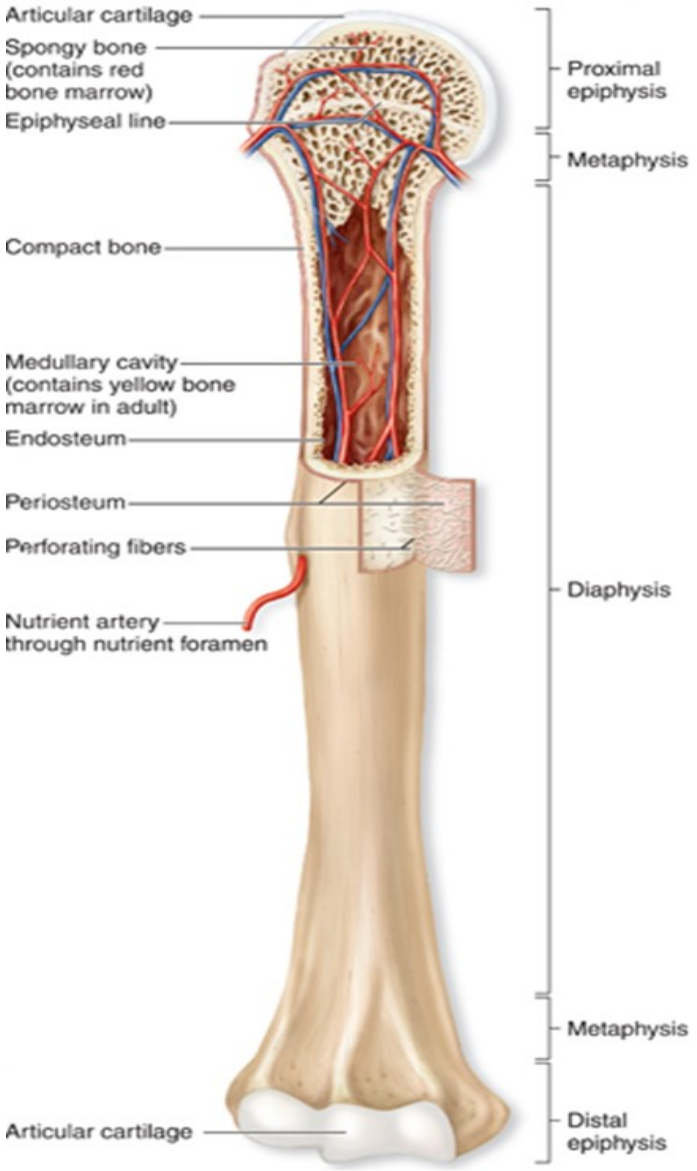

Figure 1-2 Hierarchical structure of a long bone. Source: Hexanatomy.weebly.com, November 2016

The osteon forms a central repeating unit of cortical bone, it consists of a blood vessel and nerve innervation located in a central canal, which is encased by concentric lamella of osteocytes and calcified extracellular matrix (ECM). As each osteoblast matures, its polygonal morphology alters to form spindle-like projections that lay down ECM. As matrix is produced and calcifies, it surrounds and encases proximate osteoblasts in osteoid material, this in turn directing osteocyte differentiation. In this way, concentric layers of calcified material consisting of mature osteocytes and surrounding matrix are formed.

The macroscopic and higher order structure of bone may vary considerably but the building block of all bone is the mineralised collagen fibril (Reznikov et al., 2014). Type I collagen is the most abundant protein type in bone and is found in the ECM as a triple helical structure which are coalesced into fibrils which themselves organise into bundles.

In the human, bundles are found in three common structural orientations: i) aligned parallel along the long axis, as is found in Sharpey's fibres and alveolar bone (Aaron, 2012) ii) Random orientation of fibres with loose structural organisation known as woven bone, as is found in neonatal bone and unresolved fracture callous prior to remodelling. iii) Organised structure resembling plywood as found in lamellar bone, wherein the fibres of each layer are offset by varying degrees relative to the layer immediately adjacent (Reznikov et al., 2014) (Weiner and Traub, 1992).

The second core element of the mineralised collagen fibre is water. Water is pervasive through the fibre, fibril and bundle structure and forms an important mechanical component with noticeable differences in mechanical properties of wet and dry bone (Nyman et al., 2006).

The essential mineral element of bone is hydroxyapatite, $Ca_5(PO_4)_3(OH)$, which is present as plates of nano-crystals aligned around collagen fibrils. Compositions of these three elements vary between bone types, in general the collagen volume remains consistent and any changes in mineral content occurring at the expense of water (Nyman et al., 2006; Martínez-Reina et al., 2010).

1.3.3 Bone development and growth

Bone formation occurs by two pathways: Endochondral and intramembranous ossification (Kronenberg, 2003). Endochondral, translating as "from cartilage" forms the majority of bones within the adult skeleton when formed in utero. The process is initiated when chondrocyte progenitors form a cartilaginous template into which osteogenic cell populations infiltrate, differentiate and produce mature bone. The cartilage template is infiltrated, first centrally and then peripherally to form primary and secondary centres of ossification (growth plate). Template forming chondrocytes participate in well-ordered growth phases, forming zones of i) rest ii) proliferation iii) hypertrophy, and iv) apoptosis. Longitudinal bone lengthening occurs as proliferative chondrocytes continually create new template material for osteogenesis, increasing the distance between growth plates in the process.

Pre-hypertrophic chondrocytes differentiate and become post-mitotic hypertrophic chondrocytes that secrete extracellular matrix which subsequently starts to mineralise, chondrocytes then become apoptotic and degrade.

As chondrocytes die and degrade, so to do the transverse septa of matrix between cells, whilst vertical septa are largely intact (Mackie et al., 2008). During maturation of the hypertrophic zone, blood vessels infiltrate along septal lines, bringing with them osteogenic precursors, osteoclasts and early bone marrow. Osteoclasts aid in the removal of the cartilage matrix, with the remaining material used as a scaffold for new matrix deposition by maturing osteoblasts. This matrix is then mineralised and new calcified tissue is formed, extending the new bone.

Intramembranous ossification is the formative mechanism for the bones of the skull and pelvis and ribcage, it is also a vital component of bone repair in the adult. The process initiates as mesenchymal progenitors condense and differentiate directly into early osteoblasts. Osteoblasts lay down organic matrix which mineralises forming calcified tissue. A key difference to endochondral ossification is the lack of a cartilaginous template, when cartilage and osteogenic progenitors differentiate to osteoblasts in response to growth cues.

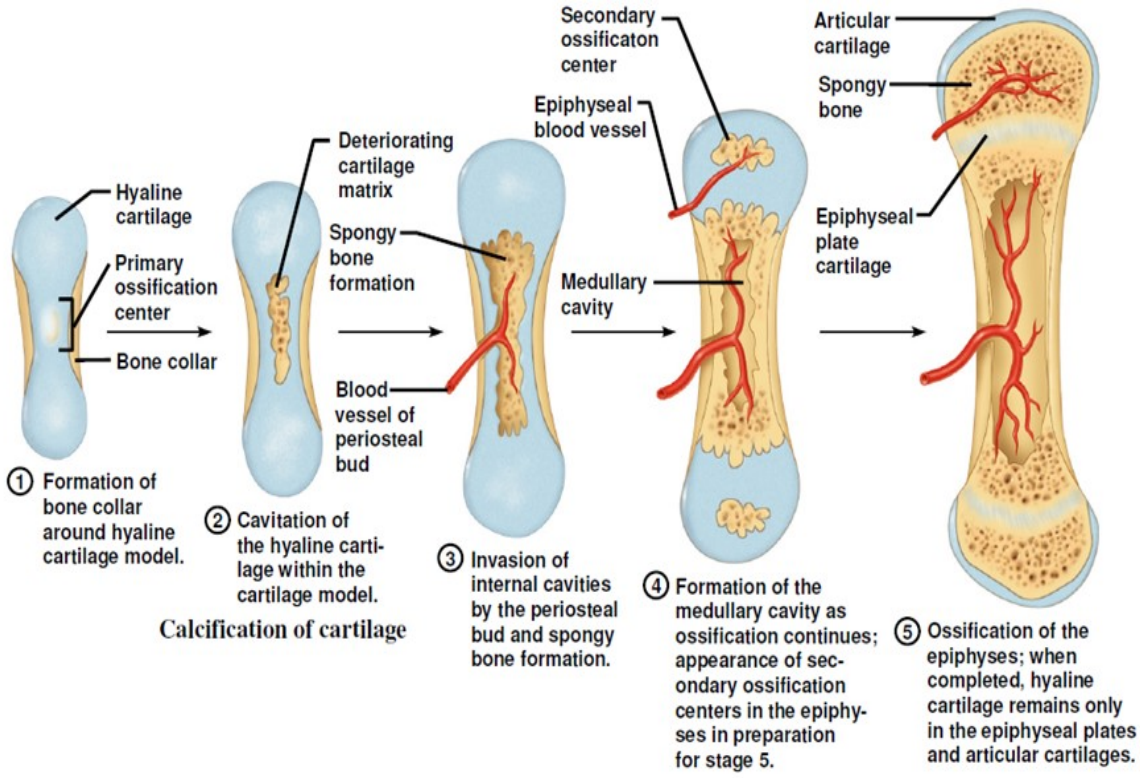

Figure 1-3 Schematic of endochondral ossification. Source: http://www.apsubiology.org/anatomy, November 2016

1.3.4 Fracture repair

Uncomplicated fracture healing is a coordinated interplay between cellular, signalling and Extracellular Matrix (ECM) elements. Fracture repair occurs by primary or secondary healing. Primary or direct repair is unusual as it requires absolute fracture apposition and minimal movement and strain between fragments (Marsell and Einhorn, 2011), this is commonly achieved in simple long bone fractures with complete anatomical reduction and surgical internal fixation. Bone union occurs without callous and is achieved as cutting cones cross the fracture line creating longitudinal cavities which are filled by osteoblasts with new bone, the new bony bridge is remodelled and a new Haversian system is created spanning the fracture boundary (Greenbaum and Kanat, 1993).

Secondary or indirect fracture healing is by the most common form of bone repair and occurs through both endochondral and intramembranous ossification (Einhorn, 1998). Indirect healing does not require strict fracture alignment and fixation, contrarily, a small degree of interfragmentary movement or relative stability enhances callous formation and promotes indirect healing (Tsiridis et al., 2007).
Bone is near unique among biological tissue as its process of repair is a replication of the biological processes occurring during foetal development. The systems of neonatal endochondral and intramembranous ossification are mirrored throughout fracture repair, where many genes expressed in early bone development are induced during fracture healing making it a truly regenerative process (Einhorn and Gerstenfeld, 2015).

Fracture repair is initiated by the ***inflammatory phase*** which is characterised by an inflammatory response following bone trauma and fracture, the healing response is initiated by platelet degranulation and inflammatory cell activation in an acute localised inflammatory reaction. Initial tissue disruption, haemorrhage and inflammation lead to a haematoma formation at the site of fracture. Activated cells release coagulation factors and pro-inflammatory cytokines such as Tissue Necrosis Factor-α (TNF-α) and interleukins -1, -6, -11 and -18 (Rundle et al., 2006) which serve in modifying the initial haematoma into a fibrous pre-callous. The immune response during the early inflammatory phase is upregulated with infiltrative phagocytic cells removing necrotic debris and facilitating formation of granulation tissue.

In addition to Tumour Necrosis Factor (TNF-α) and Interleukins -1, -6, -11 and -18, the coordination of fracture repair is orchestrated by cytokines and growth factors including members of the Transforming Growth Factor (TGF) Superfamily; TGF-β2 and -β3, the Bone Morphogenic Proteins (BMPs), Vascular Endothelial Growth Factor (VEGF), Basic Fibroblast Growth Factor (FGF-2), Macrophage Colony-Stimulating Factor (M-CSF) and Platelet Derived Growth Factor (PDGF) produced by infiltrating immune, vascular and progenitor cell types. These factors stimulate the periosteum, bone marrow and surrounding soft tissue encouraging bone precursor recruitment, vascular bed development and activation of osteogenic precursors.

At the cessation of the inflammatory phase, the second phase of ***endochondral ossification*** commences with infiltration and differentiation of MSCs into chondroblasts and chondrocytes. As these cells proliferate and mature they lay down cartilage specific matrix proteins rich in type II collagen forming a fibro-cartilaginous soft-callous which aids in stabilising the fracture. Stimulation of mature chondrocytes and pre-osteoblast by VEGF, BMPs, FGF and TGF-β leads to callous mineralisation and osteoblastic infiltration. Hypertrophic chondrocytes undergo apoptosis and the cartilaginous matrix is degraded by chondroclasts and osteoclasts, creating channels for new blood vessel ingress. Populations of MSCs with specific skeletogenic capacity, Skeletal Stem Cells (SSCs), are then recruited from surrounding tissue including periosteum, bone marrow sinusoids and blood vessels which infiltrate the maturing callous (Crisan et al., 2008). SSCs undergo osteoblastic differentiation and maturation, replacing cartilaginous ECM with mineralised type I collagen rich osteoblastic ECM, thus the soft callous transitions into a harder woven bone with random fibre orientation.

Intramembranous ossification occurs concurrently to soft callous formation at the fracture-callous interface. Vascular components and SSCs present in the periosteum activate in response to VEGF, TNF-α, IL-1, IL-6 and BMP-2 release from surrounding tissue. Activated SSCs proliferate and advance over the fracture defect, SSCs then differentiate into matrix producing osteoblasts, secreting ECM which is then mineralised and in turn remodelled forming new bone. In contrast to bone repair by endochondral ossification, osteoblast infiltration, proliferation and maturation occurs without the formation of cartilaginous callous precursor. In comparison to long-bone repair, flat-bones of the skull, pelvis sternum and ribs heal almost exclusively by intramembranous ossification.

The final stage of fracture repair is ***bone remodelling.*** As the hard callous continues to mineralise, the balance between anabolic bone formation and catabolic bone remodelling is controlled in a cyclical process by the expression of osteoprotegrin, RANK-Ligand and M-CSF (Simonet et al., 1997). The initial woven bone is remodelled into the original lamellar structure and the hypertrophic callous gradually reduces in volume. A new Haversian system is formed and the vascular network, increased during injury and repair, reforms to its pre-injury state (Melnyk et al., 2007). Thus, damaged bone regenerates remodelled mature bone which is structurally sound and physiologically functional. In the context of bone tissue engineering it is important to highlight that successful fracture repair is dependent on fracture stability, alignment, patent vascular supply, a reserve of pro-osteogenic cells and coordination by cytokine and growth factors (Tsiridis et al., 2007). Failure of any of the components will result in delayed or failure repair, conversely manipulation of any and all of these elements may prove effectual targets for tissue regeneration.

1.3.5 Vascular Supply

Establishment of a blood vessel network by vasculogenesis, the process of vascular tree formation from mesoderm derivatives, and angiogenesis, the maturation of this primitive vascular tree by the sprouting of smaller capillary networks from established vascular components, is essential for cellular gaseous exchange, nutrient supply and waste product removal during new tissue formation (Patan, 2004). There is evidence that blood vessels act as a reservoir for an undifferentiated skeletal progenitor that translocates with new vessel in-growth to areas of tissue damage and repair (Crisan et al., 2008; Murray et al., 2014). Furthermore, the interaction between inflammatory cues, cellular components and vascular elements is a highly intricate, spacio-temporal event essential in bone tissue repair. It is therefore not surprising that the complex biochemical and physical associations between skeletal cells and neighbouring blood vessels have been identified as an essential requisite for dynamic bone development and repair. An inadequate or malformed vasculature will significantly inhibit bone repair contributing to the failure or delayed union of bone fractures (Mamalis and Cochran, 2011; Stegen et al., 2015). Generation and support of an abundant, patent and pervasive vasculature is crucial in the long-term success of bone graft and tissue engineered solutions for fracture repair.

The cellular and molecular events of fracture healing are summarised Figure 1-4.

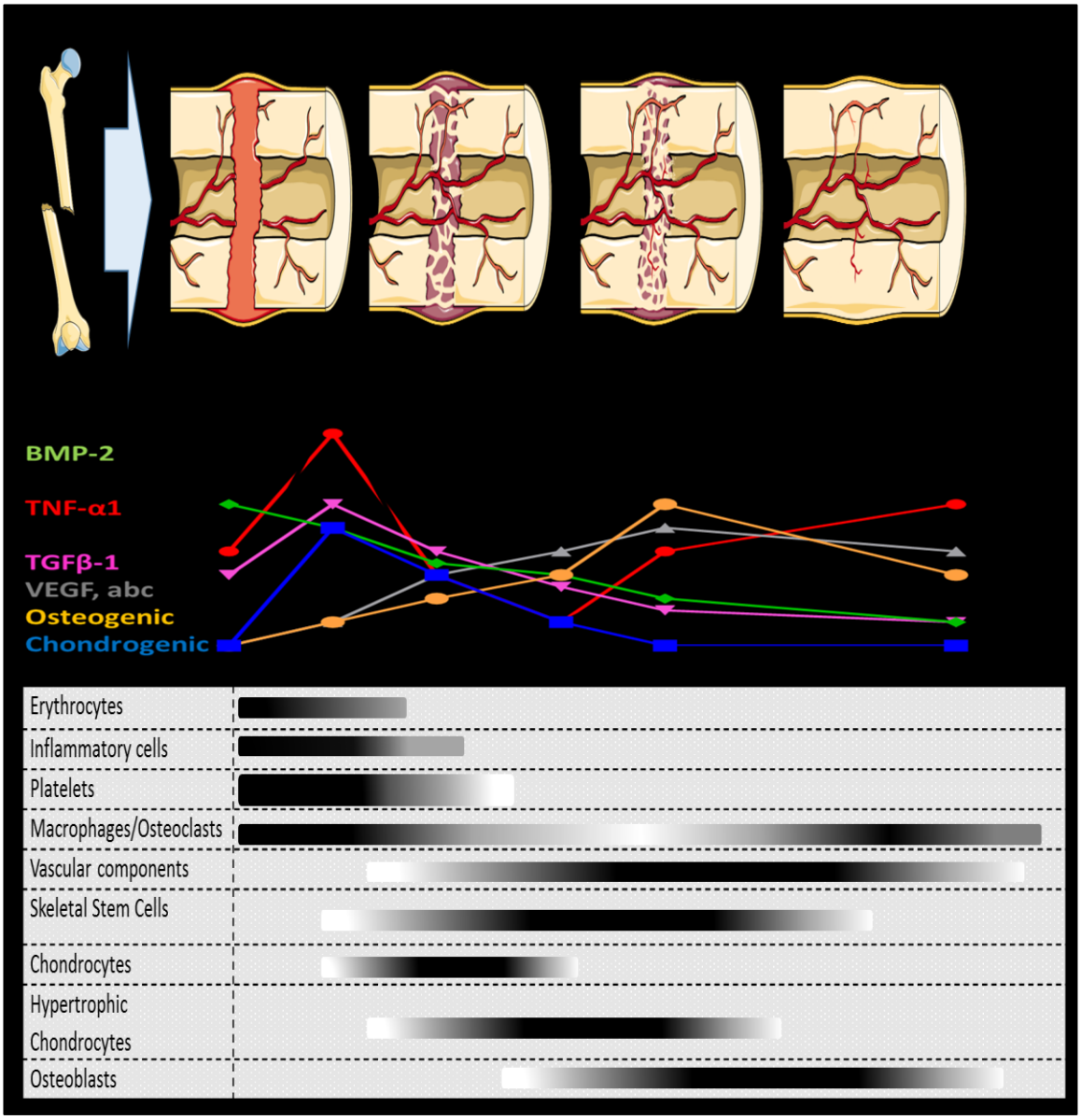

Figure 1-4 Temporal expression of cellular and molecular activity following fracture. Cell activation and infiltration within the fracture environment is coordinated by growth factor and cytokine release. Both cellular and molecular events overlap and sustain through positive and negative feedback systems. Selected growth factors include BMP-2, osteogenic factors (BMP-3a, 4,7,8), chondrogenic (TGβ-2+3, GDF-5) and VEGF isoforms-(a,b+c). Inflammatory markers limited to TNFα-1 and Il-1. Cell activity graded from baseline in (white) to peak concentration (Black). Figure adapted from Kon et al, Einhorn and Gerstenfeld 2015, and Cho et al 2002. Acknowledgement: Servier medical

1.4 Growth factors in fracture healing

1.4.1 Transforming Growth Factor β Superfamily

The TGF-β superfamily represent a group of structurally related morphogenic polypeptides which include; isoforms of TGF-β, Bone Morphogenic Proteins, Growth and Differentiation Factors (GDFs), activins, inhibins and Mullerian Inhibiting Substance (MIS) (Tardif et al., 2004). Members of the TGF-β superfamily are amongst the most intensively documented group of factors in skeletal repair (Rosier et al., 1998) and have been shown to promote SSC differentiation into osteogenic and chondrogenic lineages. Many factors in this group appear to overlap functionally and the interplay between select members of TGFβs, GDFs and BMPs have been shown to orchestrate endochondral and intramembranous ossification (Cho et al., 2002).

Bone Morphogenetic Proteins (BMPs)

Members of the large BMP family are divided into groups according to protein sequence similarities, with only BMP-1 not considered structurally part of the TGF-β superfamily. BMPs are morphogens critical in the activation, recruitment and differentiation of SSCs and play a key role in bone development and repair with BMP-2, -6 and 9 the most potently osteo-promotive, only BMP-3 and 12 failing to induce alkaline phosphatase *in vitro* (Cheng et al., 2003). BMPs have been administered clinically, preparations using doses at supra-physiological levels as such these therapies have become prohibitively expensive to manufacture, and may carry risks associated with ectopic calcification *in vivo* (Starman et al., 2012; James et al., 2016) .The main reservoir of BMPs come from ECM produced by osteoprogenitors, SSC, osteoblasts and chondrocytes. As a result, careful processing of bone and ECM in the production of ECM biomaterials is essential in ensuring bioactivity on application.

Growth Differentiation Factors (GDFs)

GDFs form a sub-group of the BMP family with many members sharing common symbol identifiers for example GDF-5, -6 and -7 with BMP-14, -13 and -12. Improved understanding in the function of individual BMP family members has led to a change in naming convention, with the BMP and GDF functional interrelation highlighted by their shared terminology, with both BMPs and GDFs contributing a regulatory role in skeletogenesis, endochondral and intramembranous ossification. It has been shown that BMP heterodimers such as BMP-2/-7 and BMP-4/-7 produce enhanced osteoinductive activity in SSCs (Zhang et al., 2015) and that BMPs function in tandem with GDFs in regulation of skeletal development and repair (Cho et al., 2002).

GDF application in musculoskeletal injuries shows promising results in tendon and ligament repair *in vivo* (Bolt et al., 2007; Jiang et al., 2016) and may prove effective in combination with BMPs for the treatment of avulsion injuries, damage of the bone-tendon interface and regenerative methods of joint arthroplasty.

Transforming Growth Factor beta (TGF-β)

Five isoforms of this multifunctional polypeptide are described in mammalian tissue (Kingsley 1994), with exclusion of functional homologues leaving three recognised conventional isoforms TGFβ-1,-2 and-3, all of which functioning through shared receptor pathways (Cheifetz et al., 1987). TGF-β subfamily is released by activated platelets during the inflammatory phase, it is also produced by osteoblasts and chondrocytes with bone ECM serving as a storage reservoir. They are potently chemotactic directing cell migration and activation in early callous formation, post inflammatory phase functions include activation and differentiation of SSCs, pre-osteoblasts, osteoblasts and chondrocytes. TGF-β also induces the production of cartilaginous and osteoid matrix proteins performing an essential role in cartilage formation and bone repair (Salgado et al., 2004). The success of TGF-β *in vivo* has been mixed but recent combinations of hybrid scaffold have shown promise in osteochondral and sub-chondral bone healing (Shimomura et al., 2014).

Fibroblast Growth Factors (FGFs)

FGFs are a family of polypeptides expressed in early fracture healing which are produced by SSCs, chondrocytes, osteoblasts and monocytes. Functionally FGFs promote angiogenesis, encourage proliferation and differentiation in a variety of cells including myocytes, fibroblasts, SSCs, osteoblasts and chondrocytes. Activation of SSCs and osteoblast differentiation by FGFs varies as a function of time after injury and is related to of cell maturation. These variations, in addition to the complex interplay between FGFs, BMPs and other cytokines may account for the unreliable response of FGFs when used singly in fracture healing. (Garrigue-Antar et al., 1995; Zellin and Linde, 2000). FGF1 and 2 promote callous formation and accelerate fracture healing and have shown enhanced mineralisation and ectopic bone formation *in vivo* when used in combination with BMP-2 (Fakhry et al.; Nakamura et al., 2005). Future applications of FGFs in bone tissue engineering should therefore focus on the combination of FGFs with members of the BMP family in a dose and time-controlled manner.

1.4.2 Insulin-Like Growth Factors (IGFs)

IGFs exist biologically as one of two isomers IGF-1 (somatomedin) and IGF-2 (skeletal growth factor) and are produced by endothelial cells, osteoblasts and chondrocytes and, much like other growth factors in skeletal repair, are stored in bone ECM. IL-1 and 2 act independently to stimulate osteo- and chondrogenesis and are closely regulated by growth hormone and modulated by IGF receptors and binding proteins (Guntur and Rosen, 2012). IGF-1 supports canonical Wnt signalling, enhancing osteoblast proliferation, and stimulates osteoblast function promoting collagen type I synthesis and ECM production, (Canalis; Giustina et al., 2008), IGF-2 is a less potent promotor of ECM production and is also able to induce SSC osteoblastic differentiation, a function not shared by IGF-1. Controlled IGF-1 release in an ovine bone defect model enhanced new bone formation but was associated to dose release kinetics in a poorly defined relationship (Luginbuehl et al., 2013). IGF-1 and TGF-β administered by collagen sponge was used successfully to treat tibial and maxillofacial defects in rat models (Srouji et al.; Srouji et al., 2005).

1.4.3 Platelet Derived Growth Factor (PDGF)

PDGF exists in three forms combining A and B chains; AA BB and AB. It is an extracellular factor produced by endothelial cells, monocytes, macrophages and osteoblasts in response to bone injury. It exerts a potent chemotactic and osteoblastic effect on SSCs, enhancing proliferation and ECM production in during callous formation (Lieberman et al., 2002). The response to PDGF delivery *in vivo* has been mixed with several studies showing a failure of PDGF to enhance new bone formation (Kaipel et al., 2012; Gothard, 2014). There has been some promise using PGDF-BB in the treatment of osteoporosis in humans with more work required to understand the spacio-temporal interplay between PDGF and other factors during fracture healing (Graham et al., 2009).

1.4.4 Angiogenic Factors

Development of the vascular bed is essential in fracture repair. Neovascularisation provides a route of removal for necrotic debris, provides oxygen and nutrient supply to regenerating tissues and contains a source of SSCs crucial for new tissue formation.
Two separate pathways regulating angiogenesis are acknowledged, Vascular Endothelial Growth Factor dependant pathway and the Angiopoietin pathway. VEGF comprises a family of 5 homologous glycoproteins, VEGF-A, B, C, D and placental growth factor, with VEGF-A the best elucidated. VEGFs are essential initiators and mediators of new blood vessel formation through (but not limited to) endothelial mitogenesis (Ferrara et al., 2003) to also exert chemotactic and stimulatory effects on adult bone marrow derived cells (Hattori et al., 2001) .

VEGF has been delivered *in vivo* as a sole growth factor and in combination with other mitogens in animal models of bone repair. There is clear evidence of upregulation in blood vessel formation but its influence on new bone formation is unclear (Li et al., 2009). Angiopoietin 1 and 2 regulate the vascular structure, stimulating and controlling vessel dimension and collateral formation. In contrast to VEGF, the role of angiopoietin 1 and 2 in bone repair is poorly understood although its complementary action with VEGF in early blood vessel formation is established (Visconti et al., 2002). It may therefore prove sensible to investigate the importance of VEGF/Angiopoietin co-administration in the formation of new patent structured vessels *in vivo*. Studies linking the pro-angiogenic function of VEGF with the stabilising effects of PDGF and angiopoietin 1 should be considered when designing large scale tissue engineering solutions (Rouwkema et al., 2008).

1.4.5 Wnt signalling molecules

Wnts are a group of functionally diverse glycoproteins essential in embryonic development and are essential for normal skeletogenesis with alterations to Wnt pathway components causing numerous disease phenotypes in murine models including; failed mineralisation, limb shortening, osteopenia, osteopetrosis amongst others (Monroe et al., 2012). Two main arms to the Wnt signalling pathway are described based on Wnts ability to activate β-catenin, "Canonical" and "Non-Canonical" Pathways, however the function of Wnt signalling pathways is explored the distinction becomes less binary. Within the context of bone, Wnts, Lrp5 and β-catenin are pivotal to SSC fate determination with β-catenin and Wnts contribute to osteoblast survival. β-catenin promotes osteoblast function and moderates osteoprotegrin expression and is therefore an important contributor to bone turnover and structure throughout adult life (Glass Ii et al., 2005).

Clinical application and delivery of Wnts is made difficult by the unstable and lipophilic nature of Wnt proteins, attempts at therapeutic delivery have been made using cell transfection and liposome carriers. Novel drug transport vehicles could aid in the targeted delivery of Wnts intracellularly opening the possibility of use in fracture therapy in the future.

Table 1-1 Lists the source and biological effect of signalling molecules in fracture repair.

Signalling Molecule	Source	Biological effect
Cytokines; IL-1, IL-6, TNFα	Macrophage, monocytes, SSCs	Pro-inflammatory, Angiogenesis, ECM synthesis and bone resorption
TGF-β	Degranulating platelets, SSCs, Monocytes, ECM, Chondro- and Osteocytes	Pre-osteoblast mitogenic effect, Angiogenic, Chemotactic for bone forming cells, inhibits terminal chondrocyte differentiation
PDGF	Degranulating platelets, osteoblasts, endothelial cells and monocytes	Pro-osteoblastic effect on SSCs, and potent SSC chemotactic effect
BMPs	Osteoprogenitors, SSCs, ECM, osteoblasts and chondrocytes	Differentiation of skeletal precursors into chondrocytes and osteoblasts
FGFs	Bone ECM, SSCs, Osteoblasts, chondrocytes, endothelial cells	Chondrocyte maturation (FGF-1) Osteoblast proliferation. Bone resorption (FGF-2)
IGFs	Bone ECM, osteoblasts, chondrocyte, hepatocyte, endothelial cells	IGF-1 SSC recruitment and proliferation IGF-2 Proliferation and matrix synthesis
VEGFs Angiopoietin 1 and 2	Osteoblasts, myocytes, platelets Larger Vessels	Potent angiogenic factor, endothelial proliferation, blood vessel formation Osteoblast proliferation Promote vessel integrity
Metalloproteinases	Musculoskeletal ECM	Cartilage and bone degradation allowing blood vessel invasion during fracture repair

Table 1-1 Signalling Molecules associated with fracture repair. TGF-β Transforming Growth Factor beta, PDGF Platelet Derived Growth Factor, BMP Bone Morphogenic Protein, FGF Fibroblast Growth Factor, IGF Insulin-like Growth Factor, VEGF Vascular Endothelial Growth Factor. Adapted from Dimitriou et al 2005 and Devescovi et al 2008

1.5 Skeletal Stem Cells

The biological ability of bone to repair itself without scar-tissue formation through a recapitulation of embryonic skeletogenesis makes bone healing a true regenerative process. This unusual capacity for regenerative repair logically requires the presence of bone forming cellular elements either within bone marrow or within the supportive structures of mature bone. Cells with renewal and healing capacity are considered an essential element in tissue engineering strategies (Langer and Vacanti, 1993), crucial in successful tissue repair. A standout reason that the oft stated "gold standard" in graft and graft substitutes, cancellous autograft, is considered so effective *in vivo* in part relates to large numbers of pro-osteogenic cells, cellular signalling activity, inherent matured bone structure serving as an osteoinductive and conductive network (Delloye et al., 2007) (Pneumaticos, Triantafyllopoulos, Basdra, & Papavassiliou, 2010). Autograft's status as the "gold-standard" is no longer as clear as has been in the past decade and the emergence of graft substitutes and novel surgical techniques present viable alternatives to in some clinical scenarios. These points are discussed in section 1.8.1.

Whether the cellular component of tissue regeneration is present innately in the wound site (low-grade damage to healthy tissue), is resident in transplanted tissue (bone and tissue autograft) or is applied exogenously to a scaffold or wound, one aspect of tissue repair remains constant; the presence of a regenerative cell source.

The most fundamental principle of a stem cell is governed by two properties, its ability to **self-renew** and the concept of **potency.**

Self-Renewal: Refers to the ability of cell to undergo repeated cycle cycles without altering its state of maturation. Stem cell must both replace themselves and give rise to cells that differentiate, stem cell numbers in the body are not constant and fluctuate with life stage and response to injury (Kimble and White, 1981; Wright et al., 2001). This implies a mechanism allowing stem cells to increase in number whilst also contributing differentiated cells to participate in growth and repair. The need for stem cells to replicate in an adaptive manor has produced two theories of growth: Asymmetric and Symmetric reproduction.

In *asymmetric* replication*,* a stem cell undergoes cell division and produces an undifferentiated copy of itself alongside a differentiated daughter cell. *Symmetric* replication whereby a stem cell produces two undifferentiated daughters, which may be balanced by the production of two differentiated cells in parallel divisions. These two process are thought to work in concert maintaining a balance of undifferentiated and differentiated cells according to the systemic need. The process of self-renewal is outlined in Figure 1-5.

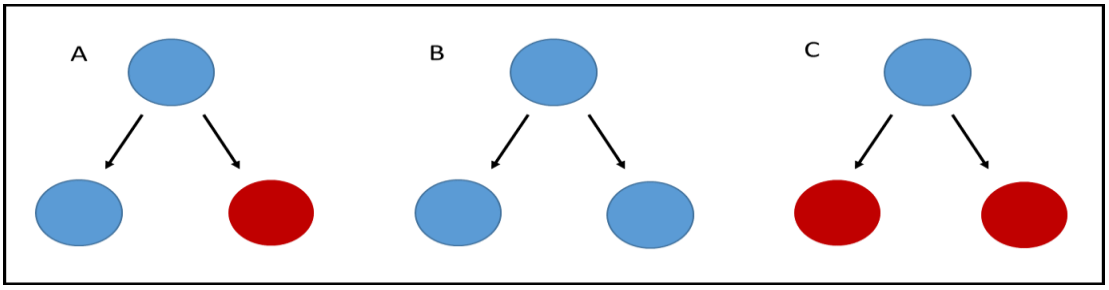

Figure 1-5 Schematic of symmetric and symmetric cell division. A) Asymmetric replication; A single undifferentiated stem cell gives rise to one undifferentiated and one differentiated daughter cell. B) Symmetric replication maintaining undifferentiated status of daughter cells. C) Symmetric replication producing two differentiated daughter cells.

Potency: Refers to the capacity or potential of a stem cell to differentiate into functionally mature cell types. Differing degrees of potency are recognised: *Totipotent* cells can differentiate into all cell types of the mammalian adult, reproducing cells of the three embryonic germ layers, totipotent cells can generate an entire organism. Totipotency is restricted to cells within the first 2 cell divisions of embryogenesis. As embryogenesis continues, forming the early foetus and extra-embryonic layers, *Pluripotent* cells may be isolated, possessing the potential to form all adult tissue types but not in themselves able to generate a whole organism (Shamblott et al., 1999) . Cells which are restricted to a particular lineage are referred to as *Multipotent*, these possess potential for producing differentiated offspring related to the tissue in which they reside, and multipotent cells are the adult organism's reservoir for repair and replacement.

1.5.1 Skeletal Stem Cells or MSCs?

Bone marrow derived stromal cells, described by Pittinger (Pittenger et al., 1999) and Caplan (Haynesworth et al., 1992b) as Mesenchymal Stem Cells which are products of their environment, capable of occupying one of two phenotypes: The *constitutive phenotype* expressing multipotency *in vivo* and *ex vivo*, proving a functional capacity *in vivo*, and the *regulatory phenotype* which responds to tissue damage and fulfils an active role as a multipotential cell source, capable of tissue regeneration and providing a chemotactic or immune-modulatory role in wound repair (Haynesworth et al., 1992b) (Caplan and Correa, 2011; Pittenger, 2013).

Alternatively, as a stem cell population with specific capacity for growth and repair of tissues of the musculoskeletal system, defined as a known physical and conceptual entity by Bianco and co-workers as Skeletal Stem Cells (SSCs) (Paolo Bianco, 2013), SSCs are described as multi-potent cells with the capacity for self-renewal and ability to generate a complete bone marrow organ, capable of supporting haematopoiesis and producing cell types of the embryonic mesoderm lineage including bone, cartilage, fat, muscle and connective tissue (Pittenger, 2013) .
For consistency, the term SSC will be used and refers to the cellular elements within Bone Marrow Mononuclear Cells (BMMNCs) demonstrating enhanced skeletogenic capacity and are identified prospectively by a known phenotype. The term MSC is used when referring broadly bone marrow stromal elements which adhere to tissue culture plastic and has the capacity to form distinct self-renewing colonies (CFU-F) *in vitro,* SSCs by comparison being a defined cell population within the stromal environment.

Early experiments to isolate and test the phenotypic potential of bone marrow derived non-haematopoietic cells took the broad approach of using the unrefined bulk BMMNC fraction, containing all the cells types with bone marrow, inoculated *in vivo*, and assessed for differentiation (Tavassoli and Crosby, 1968). Analysis of implanted cells showed the formation of a discrete heterotopic bone organ containing cortical bone, trabeculae and interstitial stromal components including adventitial cells, pericytes and adipose tissue (Strobel et al., 1986). Subsequent work to characterise the immunophenotype of the heterogeneous population has unveiled a raft of consistently expressed markers including CD29, CD44, CD73, CD90 CD105, CD106, CD146, CD166, CD271 and Stro-1.

It was described that the non-haematopoietic component of the implanted BMMNC fraction engrafted and contained elements capable of reconstituting a bone organ but due to the heterogenous nature would be considered MSCs. MSCs are also identifiable within the bone marrow mononuclear population by a reliable absence of haematopoietic cell markers; CD11b CD14, CD19, CD34, CD45 and HLA-DR (Dominici et al., 2006b; Dawson et al., 2014). Both sets of markers can be used to either positively or negatively enrich for pro-skeletogenic sub-populations within BMMNCs.

MSCs have now been isolated and characterised in a large number of species, both laboratory and domesticated, including mouse (Soleimani and Nadri, 2009), rat (Bai et al., 2009) , rabbit (Tan *et al* 2013), cat (Munoz *et al* 2012), dog (de Bakker et al., 2013), goat (Zhang et al., 2012), sheep (McCarty et al., 2009; Berner et al., 2013b), horse (Schnabel et al., 2013), cow (Bosnakovski et al., 2006) and non-human primates (Izadpanah et al., 2005).

1.6 Stem cells in tissue engineering

SSCs are an attractive target in tissue engineering: They can be used as an autologous cell source, harvested from multiple tissue types including bone marrow and adipose tissue, expanded to clinically relevant numbers and differentiated *in vitro* prior to therapeutic use.

To refine the use of cells in bone regenerative strategies various BMMNC sub-populations have been targeted utilising prospective SSC immuno-selection for single or multiple cell surface markers, using cells from a variety of tissue sources. Cell population enrichment by immuno-selection aims to filter out non-tissue-regenerative cells from the MSC milieu and improve on stem cell yields obtained from traditional basic tissue culture plastic adherence as a means of MSC selection. Further selection aims include enriching for cell types with a predilection for tissue defined repair, specifically skeletal tissue. The development of a single monoclonal antibody enriching for a BMMNC population with superior tissue specific regenerative capacity has been the focussed goal for tissue engineers for over a decade, with the emergence of a small number of candidates, although highly sought "pan-osteogenic marker-1" remains elusive. The use of prospective candidate selection based on proven *in vivo* cell functionality could become standard best practice within tissue engineering and can enrich bone marrow derived mononuclear populations to select for cells with specific skeletal capacity; Skeletal Stem Cells or SSCs.

1.6.1 Enriched cell populations in BTE

The discovery and characterisation of adult, bone marrow derived non-haematopoietic progenitors over the past 30 years has driven the popularity of BMMNCs in a regenerative context. Populations of bone marrow and adipose derived MSC cells have been detailed *in vitro*, with cell growth profile, cell surface marker expression and capacity for multi-lineage differentiation documented (Crisan et al., 2008; Paolo Bianco, 2013; Murray et al., 2014). Isolation of the non-haematopoietic stromal cell elements occurs predominantly by means of bulk cell isolation, examples include; cell culture plastic adherence and density gradient centrifugation with novel techniques under development such as flow-cell isolation acoustic trapping utilising the physical properties of cells to discern between populations (Tatarova et al., 2016; Xavier et al., 2016).

The characterisation of certain designated populations has identified enriched BMMNC sub-populations which are more specifically suited for use in bone tissue engineering (Jarocha et al., 2008), and in tissue engineering as a whole. The use of immune-labelling based techniques such as Magnetic Activated Cell Sorting (MACS) and Fluorescence Activated Cell Sorting (FACS) to isolate bone marrow stromal subsets prospectively has been shown to enrich for CFU-F and capacity for lineage specific differentiation. Although MSCs have demonstrated multi-potency *in vitro* and *in vivo*, providing a consistent phenotype of homogenous pro-osteogenic cells within the heterogeneous MSC component has not been fully realised, although consensus in the field has produced potential candidates (Noth et al., 2002; Boxall and Jones, 2012). The heterogeneity of cell populations selected by antibody labelling does cloud thinking regarding prospective cell isolation but work by Wagner implies that gene expression of SSC sub-population is consistent *in vivo* even when surface markers are not and that gene expression and can be used in quality control when trialling novel markers (Wagner et al., 2005).

Characteristics of an optimal cell source for bone tissue engineering would include i) Selection for a homogenous population with ii) potent endochondral capacity, iii) clinical accessibility, isolated with minimal patient trauma and iv) be suitable for rapid intra-operative re-implantation or v) culture prolifically *in vitro*. Points iv and v may be influenced by the possibility of high stem-cell yield numbers, exceptional proliferation potential, or a potent secretome or paracrine effect independent of cell survival *in vivo* (von Bahr et al., 2012), all of which would minimise the negative effects of extensive *in vitro* cultural expansion.
The use of phenotypic cell enrichment in bone repair has only recently started to gain popularity. The inertia may be related to a lack of consensus on marker choice, mixed results *in vivo* and the added effort required in more complex isolation protocols.

Ideally, targets for cellular enrichment would i) allow easy cell selection based on a conspicuous cell characteristic which is, ii) persistently and vigorously expressed *in vivo* with, iii) antigen expression and cell potency maintained *in vitro*. The use of enriched populations is increasing, be it by antigen identification or other means (Xavier et al., 2016), although this remains a relatively new frontier in cell based therapies for regenerative medicine. Enriched populations have been trialled in osteochondral and maxillofacial regeneration utilising CD146+, CD90+ and CD271+ sub-populations to promising effect (Mifune et al., 2013; Kaigler et al., 2015).

1.6.2 Stro-1: Heat Shock Protein Cognate 70

Developed by Simmons and Torok-Storb (Simmons and Torok-Storb, 1991) initially to deplete human bone marrow isolates of their non-haematopoietic elements, Stro-1 was shown to select for the CFU-F and osteogenic element within the bone marrow stromal fraction (Gronthos et al., 1994a; Gronthos et al., 1994b). Stro-1 antibody is produced by a hybrid cell-line created by the fusion of lymphocytes obtained from BALB/c mice inoculated with CD34 positive human BMMNCs and murine NS1-Ag4-1 myeloma. The antigen identity of human Stro-1 was only recently confirmed as selecting for extra-cellular Heat Shock Protein cognate 70 (Hsc70), reliably expressed in early passage cells with expression declining with subsequent passage (Fitter et al., 2017).

The positive selection of Stro-1 expressing SSCs from purified primary tissue, including human bone marrow, delivers a clear CFU-F and osteogenic capacity enrichment over unselected cells both *in vitro* and *in vivo* and has shown promise as a cell target in orthopaedic regenerative medicine (Williams et al., 2013). Cells selected by Stro-1 monoclonal IgM antibody are multi-potent and possess a superior response to mitogenic cues *in vitro* and *in vivo* when compared to the unselected or Stro-1 negative fraction. Stro-1 expression within the BMMNC fraction is patient variable between 1-10%, typically between 2-5%, 95% of which are nucleated erythroid bursts with all CFU-F activity present in the Stro-1 fraction.
As an enriched SSC population, Stro-1 positive cells culture freely, will grow in standard culture media and lend themselves to larger scale *in vitro* expansion and differentiation. As a stromal fraction component, Stro-1 also express an array of stem-cell marker related adhesion molecules, VCAM, MCAM and HCAM which aid in scaffold adhesion and pre-seeding techniques often utilised in *in vitro* prior to *in vivo* use.

Hsc70 is an attractive alternative antigen target for stem cell enrichment as it is well characterised, would only require one label for selection and can be purified from cell suspensions of potentially multiple tissue types.
Single antibody selection can be harnessed as part of an in-line system of intra-operative cell selection and re-implantation, avoiding multiple procedures and the delay that can occur between tissue harvest, cell isolation, culture and eventual therapeutic use, as was successfully demonstrated by Ridgway (Ridgway et al., 2010) and reviewed by Dawson (Dawson et al., 2014).

1.6.3 Application of SSCs by delayed injection

The efficacy of current cell delivery approaches has failed to achieve consensus regarding the most effective cell origin type, density, cell combination and method of cell delivery. In many current experimental models the introduction of a cell progenitor source, either by itself or in concert with biomaterials, has occurred at the time of trauma, with cells implanted directly *in vivo* into an acute inflammatory environment. During the inflammatory phase, damaged tissue is awash with pro-inflammatory molecules including TNF-α, IL-1 and IL-6 in addition to raised serum acute phase protein concentrations. Current thinking within tissue engineering postulates that the direct cellular and paracrine effect of cell progenitors introduced into this inflammatory milieu is diminished by the predominate pro-inflammatory environment.

A recent approach to cell delivery in BTE attempts to avoid the stem-cell inhibiting acute inflammatory response by delaying the introduction of stem cells into the bone defect until after the inflammatory phase has subsided. Both SSCs and mandibular osteoblasts exert a more potent osteogenic effect *in vivo* when implantation of cells is delayed (Berner et al., 2013a). The delayed injection of MSCs have shown distinct improvements in the repair of damaged tissue compared to "time-of-trauma" applications. Tissue culture plastic adherent MSCs have been successfully expanded *in vitro* and applied in cardiac repair (Amado et al., 2005) and neuronal regeneration (Parr et al., 2007) once the acute inflammatory window has passed.

It is evident that the means and timing of cell delivery can influence the efficacy of cell based repair strategies, however positive results are seen when cells are introduced subcutaneously, intravenously as well as directly to the wound site (Dreger et al., 2014). No clinical reports of intentionally applying SSCs in a delayed manor were found on literature search but the use of autologous bone graft and SSC therapies in delayed union and degenerative bone disease is documented (Pountos et al., 2010). The application of SSCs through bone graft in chronic orthopaedic conditions corroborates the hypothesis that withholding cell delivery until after the inflammatory phase may prove efficacious in bone repair.

1.6.4 Immunomodulatory effects of MSCs

The paracrine effect of MSCs is growing as an area of research in stem cell therapeutics. Down-regulation of the immune response was of particular interest in transplant medicine wherein MSC were shown to inhibit the immune reaction between donor and recipient tissue (Barker and Wagner, 2003; Amorin et al., 2014).

This potent immunomodulatory effect has been utilised in the treatment of lethal graft vs host disease, type I diabetes and immune mediated arthritis (Le Blanc et al., 2004; Jo et al., 2014). During the inflammatory phase of fracture repair, activation of tissue and vessel resident MSCs modulate production of TNF-α and IFN-through paracrine and direct inhibition. MSCs downregulate CD8 and encourage CD4 T-cell populations whilst modulating the action of NK cells during acute inflammation (Chen et al., 2011).

These effects indicate a significant role of MSCs in limiting immune response during the chondrogenic and osteogenic phases of bone repair and offer a protective role in bone repair. The immunomodulatory effects of MSCs would further help prevent adverse inflammatory reactions against implanted scaffolds and materials and should be considered when interpreting stem-cell influenced outcomes *in vivo*.

1.7 Bone Tissue Engineering

1.7.1 What's in a bone?

The manufacture of functional new bone requires essential elements. The engineer requires cells (osteogenic and stromal), extracellular matrix, growth factors supplied via a patent vasculature, and a 3-Dimensional (3-D) framework providing the physical template which defines the organ form; it is this last element, a 3D scaffold which is perhaps the most important in BTE. Cell culture is dominated by 2-dimensional techniques, simply having the right mix of cells and growth cues will not produce a 3-D bone organ. All elements of a new tissue need to be combined within an appropriate 3-D framework in a carefully controlled manner accounting for the temporal and spacial interactions between cells, their matrix and signalling molecules. The choice of scaffold material is complex and consideration must be given to interactions between the material and biological elements.

In vivo it is the role of extracellular matrix to provide the 3-D scaffold requirement of developing and mature bone tissue, the mechanical properties are dependent on tissue type and location and can be altered in a bone environment by collagen, water and mineral content (Story et al., 1998). ECM also serves as a reservoir for nutrients, water and signalling molecules. Further, the composition and physical properties of ECM is tissue specific, directing cell phenotype and maintaining tissue function (Engler et al., 2006; Even-Ram et al., 2006). A surrogate matrix framework is required that will act as a temporary scaffold persisting in-situ, providing a frame work for cell adhesion, tissue invasion and new bone formation until the host tissue becomes capable of producing its own supportive matrix, mechanically competent and with a functional vascular supply (Hutmacher, 2000; Carulli et al., 2013).

Ideally the rate of new tissue growth would be matched by the rate of scaffold subsidence within the defect environment, newly formed tissue would no longer contain any element of the original implant and upon remodelling would be considered a new regenerated organ, indistinguishable from pre-existing host tissue.

The generation and maintenance of larger volumes of new bone material is dependent on the formation of a new vascular network, which invades and permeates all areas of the scaffold/new tissue with patent functionally mature vasculature. It follows that a scaffold structure should be compatible with vessel ingress and may promote vasculogenesis (Hutmacher, 2000; Khademhosseini and Langer, 2016)

The scaffold quickly takes centre stage in bone tissue engineering with importance placed not just on the type of material, but scaffold macro and micro architecture as well. A schematic of the Bone Tissue Engineering Paradigm is shown in Figure 1-6

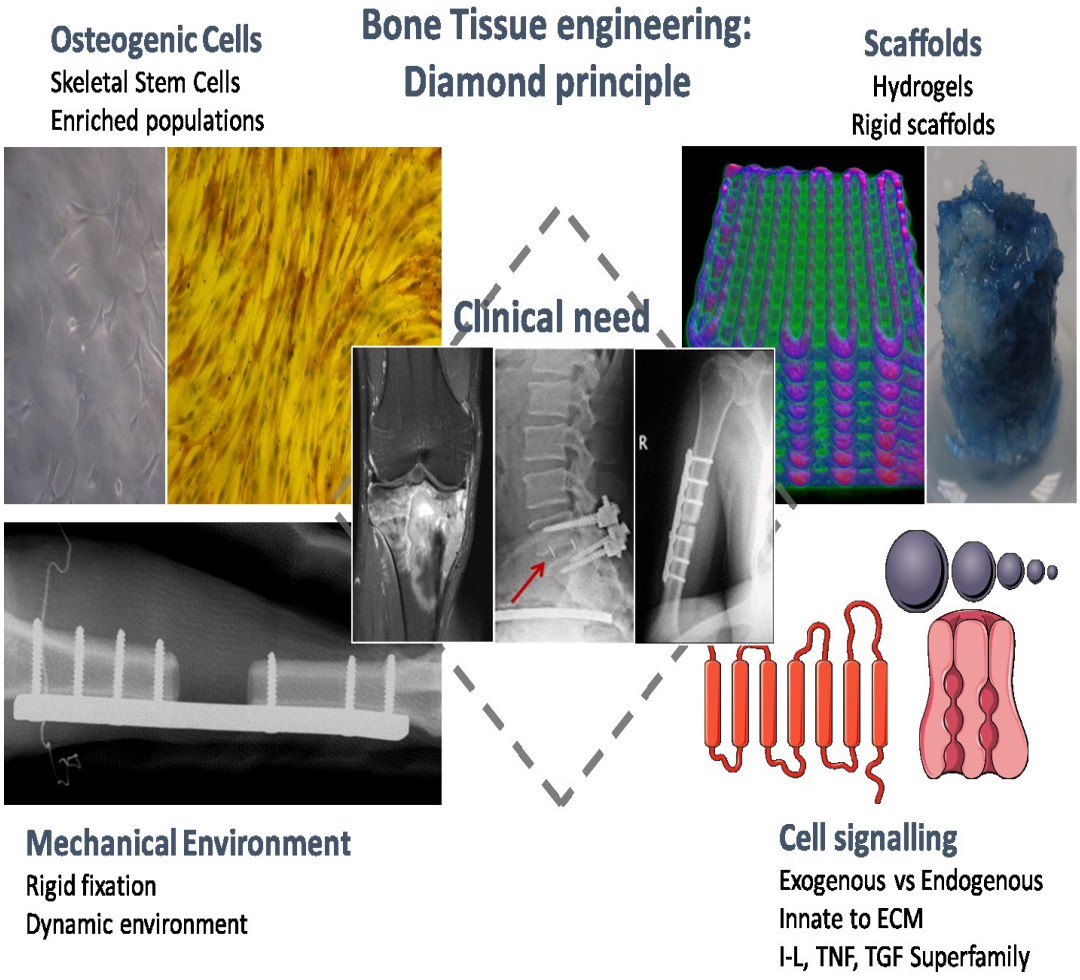

Figure 1-6 Bone Tissue Engineering paradigm, the diamond principle. Tissue engineering is a combination of scaffold materials delivering bioactive agents and cells to meet the clinical need. Images are the author's with cell signalling drawings sourced through Servier medical

1.7.2 Scaffold physical and functional properties, a balancing act

Several properties are integral to successful bone tissue engineering. Optimising a scaffold's biocompatibility often compromises the scaffold's material and mechanical properties, conversely, manufacturing a mechanically robust structure tends to hinder cellular and physiological integration. In understanding the interaction between biological and synthetic elements it is useful to set out clear definitions of core principles used in bioengineering.

Biocompatibility – A minimum requirement for a biomaterial scaffold. The term reflects on the neutral or assimilative interaction between scaffold and the recipient organism. The implant should not elicit a humoral or innate immune response relating to its physical and material properties, nor should its components, bulk or degraded, activate an inflammatory response within the host tissue (Langer and Vacanti, 1993; Yang et al., 2001).

Cytocompatibility - A contributing factor to biocompatibility with particular emphasis on the scaffold's *in vitro* capacity to accommodate cell adherence, long term cell survival, proliferation and differentiation.

The role of a scaffold can be described relating to its cellular and tissue function, these functions are summarised from Albrektsson (Albrektsson and Johansson, 2001), given in Table 1-2 below.

Table 1-2 Definitions of scaffold biological properties

Osteoinductive Stimulating the differentiation of skeletal elements within the graft and surrounding tissue, these may include SSCs, chondrocytes and osteoblasts.
Osteoconductive - Refers to promoting the growth and proliferation of bone forming cellular elements along the scaffold and matrix components, leading to the formation of new bone along scaffold axis. Osteoconduction must occur in 3-D resulting in complete propagation along all the scaffold axis, in many ways osteoconduction can only occur if pro-osteogenic cells have been successfully activated through osteoinduction.
Osteointegration – Used to define the end-point of scaffold and host tissue assimilation, whereby innate tissue is considered contiguous with regenerated tissue and scaffold material. Osteointegration infers an element of tissue remodelling whereby the mechanical and histological features of host and new bone are regarded as part of the same whole.
Osteogenesis – The formation of new bone from cellular, matrix, scaffold and molecular elements. Osteogenesis occurs as an extension of successful *Osteoinduction*, *Osteoconduction* and *Osteointegration.*

1.7.2.1 Scaffold degradation,

The strength, stiffness and durability of a scaffold are influenced by the behaviour of a material within the body, scaffold biocompatibility and integration are influenced by how a material responds to a physiological environment. For clarity, brief definitions as outlined by Vert (Vert et al., 1992) are used when describing scaffold degradation *in vivo*. Definitions regarding biomaterial degradation are given in Table 1-3 with schematic examples of the modes of polymer degradation given in Figure 1-7.

Table 1-3 Definitions; modes of polymer degradation

Biodegradable – Bulk degradation of solid polymeric scaffolds. Biodegradable polymers break down through macromolecular degradation and can be the result of biological elements. Break down by-products maybe dispersed throughout the organism but there is no detectable elimination form the body.
Bioresorbable – Solid polymeric scaffolds which undergo bulk degradation with subsequent elimination of degradation by-products. Elimination can occur as a result of filtration and excretion or metabolism of by-products by the body's enzymatic pathways. Conclusive proof of elimination must be shown.
Bioerodable – Refers specifically to degradation occurring at the surface of solid polymers. Eroded by-products must themselves be eliminated as in bioresorption.
Bioabsorbable - Solid polymer materials which dissolve in body fluids without polymer chain cleavage or loss of molecular mass. Bioabsorbable materials can be bioresorbable if conclusive proof of elimination exists.

Examples of three common modes of polymer degradation

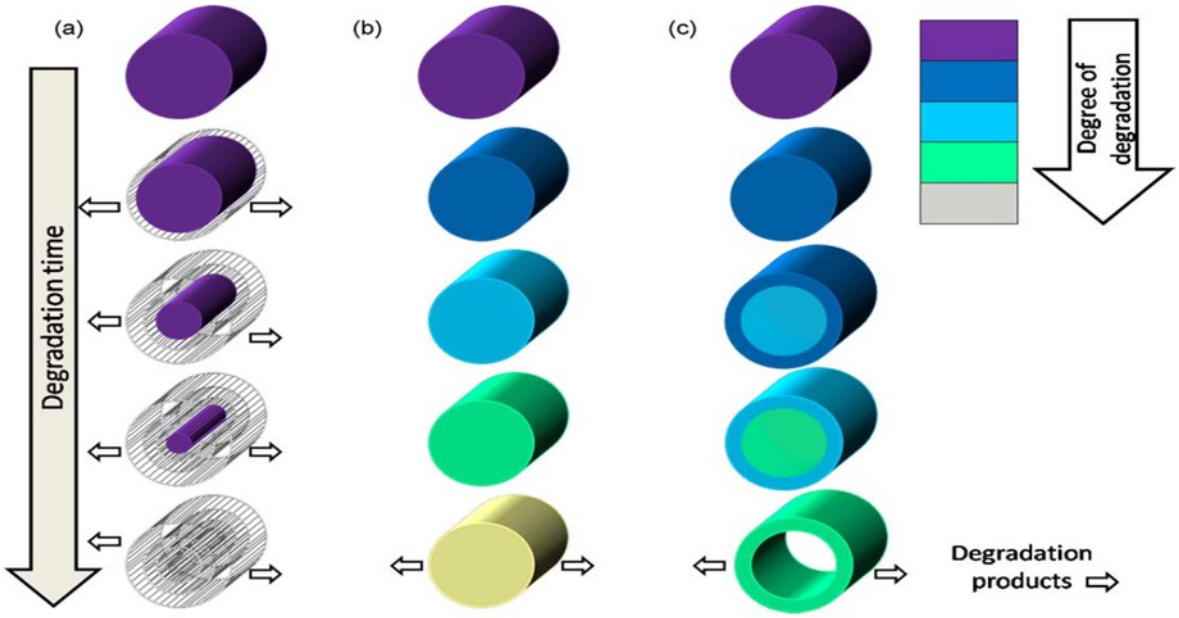

Figure 1-7 Schematic of polymer degradation. A) Surface erosion, only surface material undergoes polymer hydrolysis and polymer break down. B) Bulk erosion is the most common mode of polymer degradation and occurs throughout the polymer mass uniformly. C) Bulk degradation with autocatalysis; a central area of hydrolytic polymer alters the pH microenvironment of a polymer and accelerates further hydrolysis. Reproduced with permission, Professor Mia Woodruff, Queensland University of Technology

1.7.2.2 Porosity

A scaffold acts as a framework for cell adhesion, proliferation and differentiation, continuing as a template for new tissue formation, vessel invasion and tissue remodelling, culminating in the generation of adult, mature vascularised tissue.

Pores are essential to providing a macro environment for tissue ingrowth and integration, a microenvironment for cell adhesion and differentiation, and an architectural framework for blood vessel formation. A highly porous structure with interconnected pores and large surface to volume ratio will encourage new blood vessel formation and promote tissue growth, also strengthening the tissue-implant interface (Story et al., 1998). Crucially, it has been established that pores are essential for new bone growth and porosity is a critical structural element in bioengineering scaffold design (Kuboki et al., 1998).

Pore structure, size and degree of interconnectivity influence bone formation and blood vessel growth (Hulbert et al., 1970; Feng et al., 2011). The Haversian system present in adult human bone consists of a central channel no smaller the 100µm, a biological requirement linked to the diffusion limit of oxygen of 100-200µm.

Consistent with this *in vivo* structure, it has been shown that pore sizes smaller than 100µm restrict blood vessel growth into the scaffold, further, a macroscopic pore and improved pore interconnection improve tissue growth and blood vessel ingress (Henkel et al., 2013).

Larger pore sizes enhance the rate of neovascularisation and promote osteogenesis (Tsuruga et al., 1997), conversely, smaller pores have been shown to reduce oxygen tension and promote osteochondral formation (Oh et al., 2007). The importance of pore structure and the variable distribution of pore geometries throughout bone tissue *in vivo* has led researchers to develop biomimetic scaffolds with controlled pore hierarchy (Sobral et al., 2011).

An improved understanding of pore structure under 10µm highlights the importance of micro-porosity in scaffold design, by increasing surface area, promoting ion-exchange and delivery of osteogenic signalling molecules (Yuan et al., 1999). Furthermore, scaffold features in the sub-micron range contribute to cell adhesion and growth.

Cell differentiation can be controlled topographically which contributes to the overall osteogenic function of the scaffold without the use of exogenous molecular growth cues (Dalby et al., 2014). Although macro porosity and pore interconnection are essential elements in scaffold design, increases in overall porosity compromises structural integrity (Lin et al., 2003).

Biodegradation, absorption and erosion are influenced by the surface area to volume ratio of a scaffold, which in turn is affected by total scaffold porosity.

Although pore sizes in the millimetre range have been reported to promote osteointegration, the benefits of enlarging pore diameter diminish over 600-700µm. Work by Yang and Yuan and others suggests an optimum range for pore diameter of 300-500µm (Yang et al., 2004; Zong et al., 2010). As with material selection and composition, porosity is another part to the balancing act that is bioscaffold design.

1.8 Materials in Tissue Engineering

Commonly used materials in bone tissue engineering can be allocated into 4 broad categories, with a fifth category used to describe bone derived materials. i) Synthetic organic polymers; aliphatic polyesters and poly-ethylene glycol, ii) organic polymers of natural origin; collagen, fibrin, hyaluronic acid and alginate iii) inorganic material of natural origin; coralline hydroxyapatite, deer antler, mother of pearl and iv) synthetic inorganic materials; hydroxyapatite, tricalcium phosphate, ceramics and bio-silicates. Bone is a biological composite organ formed of inorganic and organic elements. Bone graft products; autograft, allograft and demineralised bone matrix are considered as a fifth category unique from other materials.

1.8.1 Bone graft and bone graft derivatives

1.8.1.1 Autologous bone graft

In clinical practice the traditional opinion holds that the most suitable and effective material for replacing bone, is bone. Coined “the gold standard”, autologous bone grafts, wherein a patient is both the donor and recipient of bone material, have yet to be matched in efficacy by synthetic alternatives although increasing evidence suggests that allograft preparations, synthetic material used alone or in combination with osteoinductive molecules and osteogenic cells may now offer subtle alternative to autograft in selected cases (Blokhuis, Calori, & Schmidmaier, 2013). Bone is not just a material but a compound and alternatives to autograft need to reconstitute bone’s complex structural and biological functions. Cancellous autologous bone provides an optimal osteoconductive, osteoinductive and osteogenic environment ideal for clinical use (Delloye et al., 2007)(Griffin et al., 2015) . Cancellous bone is highly cellularised containing pro-osteogenic SSCs, resident osteoblasts and chondrocytes with an intact ECM network (Cypher and Grossman, 1996). The cellular osteogenic cellular component plays important role in the ability of autograft to produce bony union and stimulate new bone formation, this concept is supported by the success of cellularised allograft in tarsal arthrodesis and lumbar fusion comparative to autograft and superior to allograft alone (Adams, White, Gross, & Parekh, 2016) (Rush et al., 2009).

Due to its open trabecular structure, cancellous graft readily promotes blood vessel invasion and tissue integration but is at a disadvantage mechanically when compared to cortical graft. Cancellous autograft can be harvested from several sites, most commonly the Iliac crest, and can be implanted during the same procedure without an immunological response.

Evidence suggests that non-osteoblastic cells survive for up to a day after transplant but that osteoblasts themselves have a poor survival rate following explant (Bae and Waters, 2006) (Rogers and Greene, 2012). Questionable cell survival and a short half-life of signalling molecules dictate that any graft material needs to be used immediately to be considered osteogenic (Delloye et al., 2007; Rogers and Greene, 2012).

Although autologous graft possesses many desirably properties as a graft material, it also has its very real limitations. The donor site can experience many detrimental effects including; pain, haemorrhage, infection, nerve damage and cosmetic deficits (Arrington et al., 1996; Giannoudis et al., 2005).

In a comparison of autograft versus allograft applied within an intervertebral cage device in 40 patients, autograft demonstrated more rapid fusion at 3 and 6 months although no differences were noted at 12 month follow, importantly 5 out of 20 patients receiving autograft experienced persistent pain associated with donor site (Putzier et al., 2009).

Work by Buser et al. compared 27 studies investigating the use of autograft, allograft and synthetic alternatives including HA, β-tricalcium phosphate and polymethylmethacrylate (PMMA) (Buser et al., 2016) in lumbar and cervical spinal fusion. No significant differences were found between groups regarding fusion rates and functional outcomes are supportive of the motion that autologous graft may not the only effective option available to surgeons. The authors acknowledge that differences in study design, data collection and analysis complicate any direct comparison of outcomes.

Autograft has been used successfully in many applications including tarsal arthrodesis (Herscovici & Scaduto, 2012), repair of tibial plateau fractures (Dorr, Ranawat, Sculco, McKaskill, & Orisek, 2006) , intervertebral body fusion (Bishop, Moore, & Hadley, 1996) and cranioplasty (Aydin, Kucukyuruk, Abuzayed, Aydin, & Sanus, 2011) and continues to represent a highly reliable and effective material for orthopaedic surgery. The deleterious effects of its harvest, particularly in larger volumes, and the emergence of materials with the potential for enhanced efficacy necessitates continued investigation into viable graft alternatives.

1.8.1.2 Cortical Autologous bone graft

Cortical bone is a highly organised and mineralised material, mechanically strong and resilient. In contrast, cancellous bone is highly cellular and vascularised but offers poorer mechanical stability. Low cellularity combined with evidence for osteoblast death during grafting reduce cortical graft's osteogenic potency (Khan et al., 2005; Roberts and Rosenbaum, 2012). Cortical bone's most

appealing quality, its structural stability, is also its limitation; dense cortical bone graft is slow to vascularise owing to poor vessel penetration and the larger volumes of calcified material needing enzymatic degradation to allow for vascular ingress. Graft integration is limited by the rate at which osteoclasts can degrade and remodel the graft material to make way for new tissue growth and blood vessel formation, a process known as creeping substitution (Khan et al., 2005). Harvest of cortical autograft is limited to sites such as the fibula, scapula, iliac crest and rib. These sites tend to act as support structure and site of muscle attachment thus grafting, although painful, is tolerated with minimal loss of function.

Cortical grafts can be transplanted with vasculature intact, providing a readymade, pre-vascularised graft material which is non-immunogenic. This strategy has been employed positively to treat skeletal defects relating to trauma, tumour excision and osteomyelitis (Sun *et al* 2010, Tu *et al* 2001). Vascularised fibular grafts are used to treat defects with large bone loss in tibial fractures, resulting from neoplasia, infection, delayed and non-unions (Kim et al., 2015). Bone grafting in tibial fractures is another direct comparison to the segmental tibial defect model used in orthopaedic research and helps validate the real-world application of the tibial defect model.

1.8.1.3 Allogenic bone graft

Allogenic bone graft refers to bone which not of recipient origin, and is primarily sourced from cadaveric donation. Commonly, the femoral head of patients undergoing hip arthroplasty is kept, sterilised and processed for graft use, the harvest of cadaveric bone by comparison is not site restricted.

Processing of allograft often removes osteoblasts and SSC population thus diminishing the osteogenic potential of the graft. Although limited in osteogenic potential, allograft is highly collagenous, contains intact ECM, ECM associated proteins and provides a biologically structured framework for cell invasion and proliferation. As the ECM is resorbed and degraded, matrix associated growth factors are liberated improving the graft's osteoconductive and osteoinductive potential. Proactive management of allograft reserves and widespread introduction of bone banks has increased the availability of allograft, this has led to the production of bone graft products in various forms.

The use of allogenic material carries an inherent risk of disease transmission, most seriously from Hepatitis C and HIV, concern of infection within musculoskeletal tissue is the main cause of allograft tissue recall in the USA (Mroz et al., 2008). Improved processing and screening for infectious agent within tissue banks has vastly improved biosecurity but an infection risk remains. The control of disease transmission a clinical imperative but the comprehensive processing techniques employed to achieve this goal dramatically reduce the biological activity and clinically efficacy of allograft (Keating and McQueen, 2001). Allograft is considered non-allergenic as its cellular elements have been stripped, unfortunately cell loss removes the osteogenic component of any graft material. Most allograft is prepared using two methods, freeze drying and demineralising, removing cellular components, exposing growth factors through removal of mineral content and reducing infection risk.

1.8.1.4 Demineralised bone matrix

Demineralised Bone Matrix (DBM) refers to a material consisting of the entire non-mineralised portion of bone. It is produced by various means of demineralisation, leaving a trabecular collagen network, intact ECM and associated proteins. The osteoinductive effects of the BMP family were discovered after noting ectopic bone formation on DBM *in vivo* (Urist, 1965). The processes of demineralisation do not completely inactivate nor remove all growth factors and DBM is more osteoinductive than allograft due to removal of the mineral phase, improving growth factor bioavailability (Sandhu et al., 1999). Processing steps as published by Dinopolous and Gianoudis in 2005 include: Low-dose gamma irradiation, high pressure wash in antimicrobial solution, mechanical dissection, morselisation, alcohol decontamination, acidic demineralisation followed by washing and storage (Giannoudis et al., 2005). DBM is available in several preparations; as a gel, malleable putty and flexible strips. Despite the osteoinductive potential for DBM, results have been inconsistent clinically. It is suggested that the variability in bone source and variations in processing are to blame.

An in depth study examining the growth factor activity in various commercial DBM products showed variation in growth factor and protein yield, both between batches and between products (Wildemann et al., 2007). DBM has been used in combination with autograft and with bone marrow aspirate as a bone graft extender, stimulating new bone formation. Although the information regarding the efficacy of DBM across its range of applications is inconsistent and scarce, DBM is clinically useful and has a valuable potential.

1.8.1.5 Inorganic materials of synthetic and natural origin

Bioceramics

Ceramics are formed by heat firing or high sintering temperature of mineral salts. The formed synthetic is highly crystalline, hard, heat resistance and brittle. The primary material used in bioceramics is calcium phosphate and its derivatives; tri-calcium phosphate (TCP) and hydroxyapatite (HA). HA and TCP are not themselves osteoinductive nor osteogenic but are exceptionally well tolerated biologically. This biocompatibility is linked to the Ca_3PO_4 stoichiometry between HA, TCP and mineralised tissue *in vivo*, predominantly with dahllite in bone (Vallet-Regí and Ruiz-Hernández, 2011).

Neither TCP or HA are osteoinductive and rather serve as condensation foci for osteoid deposition and aggregation for regenerative osteoblasts. As the new osteoid mineralises and subsequently remodels, the ceramic scaffold material is resorbed and replaced with new bone. TCP crystalline structure is more similar to adult bone than is HA as its surface properties encourage osteoclastic degradation and resorption, its open formation also encourages blood vessel growth (Eggli et al., 1988). TCP has a low porosity, approximately 30-40%, with poor interconnectivity and is often sold as granules to overcome this shortcoming, unfortunately at the cost of mechanical strength. HA ceramics are highly crystalline and dissimilar structurally to calcium phosphate in bone, as a result resorption is slow and HA scaffolds persist *in vivo*. The *In vivo* persistence of HA ceramic implants can result in implant failure through fatigue and inhibit bone-implant integration and the tissue-HA interface.

The introduction of nanomaterial manufacturing techniques has led to HA scaffolds with enhanced yield strength, reduced stiffness whilst also improving cell invasion and scaffold integration (Gao et al., 2014). The crystalline structure of HA and TCP ceramics, and their lower overall porosity limit implant integration. A move to small particle size granular preparations has improved graft response with an optimal particle size ranging between 100 and 500um optimal (Prieto et al., 2015). Biocompatibility of HA has allowed its use in many SSC based therapies success clinically as a treatment for segmental bone loss (Marcacci et al., 2007) and as a scaffold based drug delivery platform in hip arthrodesis (Choe et al., 2015).

Coralline Hydroxyapatite

Certain marine coral species produce a natural porous calcium carbonate structure. These structures have large pores of reliable size and reproducibility but a variable pore interconnectivity. Calcium carbonate structures are brittle, rapidly dissolve *in vivo* and their low compressive strength makes them unsuitable as bone graft substitutes clinically (Jones et al., 2007). Coralline calcium carbonate can be converted to coralline hydroxyapatite through the application of high heat manufacturing to yield a porous, high strength scaffold with a macrostructure well suited to tissue and blood vessel invasion. Improvement sin mechanical properties cannot alter the brittle nature of these materials, and complete tissue integration is hampered by incomplete pore interconnection. Despite clear drawbacks as a material, coralline HA products have been used successfully in management of radial and tibial fractures and in some cases may be seen as a viable alternative to autologous bone graft (Wolfe et al., 1999).

Bioactive glasses

Bioactive glasses are hard, amorphous solids manufactured from minerals including calcium, silicon, sodium and phosphorous oxides. Dental and orthopaedic engineers have favoured bioglassses owing to their osteointegrative and osteoconductive properties. Bioglassess are cytocompatible and have been show to direct differentiate immature SSCs into osteoblastic phenotype (Hench, 1998).The characteristic property of bioglass is its efficient and rapid bonding at the implant-bone interface. Solution leaching of sodium into body fluids leads to subsequent release of calcium and phosphate from the glass substance into the peri-implant space. A silica rich gel is formed between glass products and physiological fluids, calcium and phosphorous then crystallise onto the gel forming hydroxyapatite. As this interface layer is assimilated and remodelled the process of leaching and HA formation advances and the bioglass implant is absorbed contingent with new bone formation (Cao and Hench, 1996). The ability of bioglass to modulate its implant environment imparts an antimicrobial effect and bioglassses have been used effectively to treat fixation related osteolytic lesions (van Gestel et al., 2015). Composite material solutions seek to take advantages of the bio-integrative and antibacterial properties of bioglassses, improving implant-bone interface strength and cell adhesion performance of next generation biomaterials. Promising outcomes include the use of bioglass coated metal implants, glass-ceramic hybrids and TCP-bioglass composites (Kokubo and Yamaguchi, 2016; Lopes et al., 2016).

1.8.2 Polymers

Polymers are considered as either biological in origin; which include collagen, fibrin and hyaluronic acid or, synthetic; including aliphatic polyesters and polyethylene glycol. Scaffold design is dictated by its intended clinical and anatomic location, parameters such as strength, porosity and required degradation rate all bear influence on the choice of material used.

Polymers may need to be physically strong and resilient to cyclic loading or may perform a void filling non-supportive role negating the need for high compressive and tensile strength. Polymer materials must be biocompatible and biodegradable, and neither the material nor its degradation products should illicit an immune response *in vivo*. The breakdown of a polymer can be tailored and altered such that it degrades as new tissue invades and is remodelled.

1.8.2.1 Naturally derived polymers

Natural polymers such as collagen offer distinct advantages over synthetics due to their biological nature. Cells recognise, bind and proliferate more readily on polymer surfaces these materials show advantageous integration *in vivo*.

Organic polymers undergo enzymatic cleavage and are further metabolised and in many instances excreted. The use of organic polymers can trigger and immune response and immune rejection. Literature is ambiguous regarding the macrophage and T-cell response to collagen and fibrin specifically. A study comparing two commercially available xenogenic ECM products showed a variable mononuclear response with demonstration of both M1 and M2 macrophage activation in both the processed ECM and positive xenograft muscle control (Badylak et al., 2008).

Natural polymers are hampered by inter-batch variations and their availability being dependant on the availability of donor xenogenic material. The degradation of natural polymers is harder to customise as biological cleavage sites are inherently present, although this feature can be advantageous in natural-synthetic blends. A major disadvantage comes due to their inherent mechanical properties. The natural origin or these peptides makes them susceptible to denaturation at elevated temperatures and vulnerable to many of the solvents commonly used in scaffold manufacturing.

As a result the use of biological polymers is seen predominantly in hydrogels, although synthetic-biological polymer blends and 3-dimensional printing of organic polymers are documented (Inzana et al., 2014).

1.8.2.2 Synthetic polymers

Synthetic polymers account for a vast group of materials with applications in tissue engineering, with aliphatic polyesters and ethylene glycol the most commonly used polymers are the (Jones et al., 2007). Synthetic polymers are produced with high uniformity and purity yielding both structurally and molecularly consistent scaffolds in a controlled manor. Many synthetic polymers have FDA approval in craniofacial and orthopaedic applications reducing the regulatory hurdles in translation from research to clinical environments.

The ester bonds in aliphatic polyester are hydrolytically labile and undergo hydrolytic (non-enzymatic) bulk degradation, the degradation products are acid and will alter both osmolality and pH of surrounding tissues. Scaffold degradation rates can be controlled by altering polymer blends, changing polymer molecular weights and polymer chain entanglement.

The toxic effect of low pH and metabolite accumulation can be mitigated by minimising total material volumes within a scaffold and enhancing local blood vessel growth and tissue perfusion. The time taken for bulk mass loss in a variety of polymers is known, this information can be used to pre-soak or leach a scaffold in a physiological fluid prior to use *in vivo*. With continual solution changes and adequate buffering, the pre-soaking or leaching process can coincide with cell culture *in vitro*, creating an established tissue construct ready for implantation (Hutmacher, 2000; Woodruff et al., 2012).

Manufacturing techniques, degradation times and applications of common synthetic polymers used in tissue engineering are listed in Table 1-4

Polymer	Processing method	Use	Degradation time (months)	Example (Publication/product)
Poly(L-lactide)	Extrusion, Inj. Moulding, Solvent casting	Ortho. surgery, Maxillofacial surgery, Oral	6 to 12	Bergsma et al 1995 Shikinami et al 1998 NeoFix® Fixsorb®
Poly (lactide-co-D, L-lactide) Blends 98/2, 50/50, 70/30	Extrusion, Inj. moulding, Compression moulding, Solvent casting	Spinal surgery, Orthopaedic surgery	16-12-8	Todd et al 2002 Reise et al 2012 Smidmaier et al 2005
Poly(L-lactide-co-glycolide) Blends 10/90, 85/15, 50/50 etc.	Extrusion, Inj. Moulding, Compression moulding, Solvent casting	Suture, General surgery, Orthopaedic, drug delivery	5-6	Fu et al 2008 PolySorb® Vicryl®
Polyglycolide	Extrusion, Inj. Moulding, compression moulding, Solvent casting	Orthopaedic surgery, Dental Surgery, Suture	≥24	Middleton 2000 Pillia 2008 Serino 2007 Dexon® Biofix®
Poly(lactide-co-glycolide)/poly(ethyleneglycol)	Porogen dissolving	Orthopaedic Spinal Surgery, Drug delivery	6-12	Lin 2010
Poly(lactide-co-glycolide)/polyvinyl alcohol				Nuttelman Meneghello 2009
Polyethylene terephthalate	Melt-blowing	Vascular repair	2-6	Ma 2005
Poly(propylene-glycol-co-fumarate)	Gas foaming	Maxillofacial		Lui 2015
Polyethylene glycol		Small molecule delivery	6-12	Fu 2012 Cui 2010
Polycaprolactone	Extrusion, Inj. Moulding, Compression moulding, Solvent casting, electrospinning	Drug delivery, Suture, Cranial surgery	≥24	Reichart *et al 2010* Berne *et al* 2012 Capronor® Ethicon®

Table 1-4 Synthetic polymers in tissue engineering. Adapted from Woodruff et al 2012 (Woodruff et al., 2012).

Hydrogels

Hydrogels are materials defined by a highly-hydrated networks of cross-linked polymer chains. Hydrogels can be natural in origin; collagen, fibrin, alginate and hyaluronic acid or, synthetic; polyethylene glycol polymers, and recently semi-synthetic polymer blends such as PEG/Collagen and PEG/polysaccharides have been described (Drury and Mooney, 2003; Gibbs et al., 2016a).

Natural polymers are inherently biocompatible, both cells and signalling molecules persist in a hydrogel environment and natural polymers are often easily cleaved and metabolised *in vivo*. Natural polymers although enticing, are not without disadvantages, including inconsistent hydration and variable elastic properties. Gels derived from synthetic polymers are by contrast, highly consistent and are more easily adapted to modify degradation profiles and influence cell binding by the addition of RGD sites (Guan et al., 2017). Hydrogels have been adopted in a number of areas of clinical practice, such as spinal surgery (Kim and Wright, 2011) and wound dressings (e.g. Anaspet™); although their promise has yet to be matched by any pervasive uptake into clinics.

There is a broad body of evidence demonstrating the ability of natural and synthetic hydrogels to enhance the delivery of growth factors for bone regeneration. While this effect was noted even in cases in which a growth factor was subject to a rapid release, further adapting its release through hydrogel use may enhance the growth factor response. Effective delivery of Bone Morphogenic Protein family members using hydrogels has proven to enhance new bone formation *in vivo* (Gibbs et al., 2016b). Enhancement of osteogenesis was also noted through controlled delivery of minerals in the absence of growth factors. Limitations of hydrogels in clinical applications are still experienced relating to hydrogel migration and off target delivery.

Promising steps have been made to overcome the inherent low compressive strength of hydrogels and some materials approaching the mechanical strength of bone have been produced but these materials failed to demonstrate the ability to withstand mechanical loading in a segmental defect model. A promising clinical application using PEG hydrogel loaded graft material was described by Hoffman (Hoffman et al., 2014). MSCs were effectively localised within an engineered periosteum TE construct using a photo polymerised hydrogel/allograft composite. Cells and construct were successfully introduced in a mouse femur defect model showing sufficient strength and resilience to resist motion, remain localised and to promote cell proliferation and differentiation.

The study by Hoffman is an example of the hybrid application potential of hydrogels in concert with other material forms. It also demonstrates the use of hydrogels as a cell delivery and localisation modality. Cell localisation on reinforced hydrogels co-administered with bioactive molecules appears to offer the most viable clinical application of hydrogels in tissue engineering (Guan et al., 2017).

The potential applications of hydrogels in orthopaedic tissue engineering are reviewed by the author and colleagues, (Gibbs et al., 2016a).

Two areas of application were apparent:

i) A hydrogel-mediated injectable growth factor delivery vehicle to enhance fracture healing; in this regard, hyaluronic acid has shown promise. Assessment of such hydrogels would benefit from *in vivo* models more closely aligned to fracture repair.

ii) Development hydrogel growth factor and cell delivery system to be used in concert with engineered rigid scaffolds. The hydrogel delivery and scaffold should be designed to work synergistically with a gel-scaffold interface built into the design; such as a “Luer-lock” syringe port. Pore hierarchy of the scaffold should be optimised to permit hydrogel infiltration and subsequent cell adhesion and proliferation.

Application of the scaffold/hydrogel delivery system should be amenable to intraoperative use, providing mechanical stability whilst delivery cells and bioactive molecules in one application. A complete assessment of biocompatibility, including cell viability, resistance to mechanical forces and degradation characteristics would need to be carried out prior to further development.

1.9 Scaffold manufacturing

1.9.1 Traditional techniques

The design parameters of a scaffold are critical to its function *in vivo*. Macroscopically a scaffold must be able conform to suit the defect site and contain design elements conferring resistance to tension and compression where appropriate. Optimal pore geometry, size and interconnection is important in allowing tissue and blood vessel in growth and scaffold-bone integration. Further, a scaffold should contain within its design a suitable zone allowing integration with a fixation system to prevent graft/scaffold migration. Microscopically the design and structure of a scaffolds surface can positively influence angiogenesis, osteoconduction, osteoinduction and osteogenesis, finer details on a nano-scale can influence cell adhesion and differentiation. The ability to accurate and reliably control all these elements during scaffold design and manufacture is important in producing effective bioengineering solutions.

Traditional manufacturing techniques in tissue engineering are expertly reviewed by (Salgado et al., 2004; Jones et al., 2007; Henkel et al., 2013). A brief overview is given herein with references given for technology application within 5 years if appropriate and available.

Solvent casting/particulate leaching or "porogen foaming", a pore forming salt or particle is dispersed and dissolved into a polymer mix. The porogen is then selectively dissolved or leached from the solid polymer leaving a porous scaffold (Lee and Sah, 2016). The pore size and pore interconnections can be manipulated although accurate control of either parameter is technically challenging. Effervescent salts can be incorporated in a foam freeze-drying approach whereby the polymer solution is subjected to low temperatures creating a solid phase scaffold with pores created by evaporating the gas phase. A freeze-drying approach can be used to take advantage of thermally induced phase separation between two materials, the remaining non-solid phase is extracted or dissolved to leave a porous solid.

Super critical CO_2 processing exposes polymers to carbon dioxide at temperatures and pressures approaching the critical point for CO_2. As environmental conditions are returned to standard temperature and pressure, absorbed CO_2 expands and creates pores within the polymer (Davies et al., 2008). This technique is an adaptation of a process long used in the pharmaceutical industry and it allows the creation of a porous scaffold under mild environmental conditions, which could be used to incorporate bioactive molecules into the scaffold blend.

Melt technologies such as melt moulding and microcellular injection moulding see the heating of a polymer/porogen mix above the glass point temperature, at which point the porogen is dissolved and the remaining material cooled. This process can be adapted to alter pore size and geometry (Mi et al., 2013).

Other melt technologies include *melt extrusion;* a polymer or polymer blend is heated, changing its viscoelasticity and then extruded through a fine nozzle. Two or more polymers can be extruded and combined to create a composite scaffold, subsequent selective dissolution creates a porous scaffold (Gomes et al., 2001). This approach can be adapted as extrusion free form technologies advance to make use of multiple extrusion heads and materials in combination.

Fibre bonding creates woven mesh structures from a variety of polymers by first interweaving the fibres as desired and sintering fibres at contact points. This process uses substantial amounts of solvent and has poor reproducibility, fibre bonding has in large been superseded by micro and nano-fibre methodologies in additive manufacturing.

1.9.2 Additive manufacturing

Traditional manufacturing techniques are subtractive in nature, portions of the scaffold are removed until the intended design remains. As such they are beset by limitations, which include the precise control over structural parameters such as pore geometry and pore interconnectivity. Similarly, it is beyond the scope of many of these techniques to control the micro and nano scale topographies which are so important in cellular and tissue integration. Furthermore, many of these techniques utilise organic solvents which reduce the scaffold's cyto- and biocompatibility and may prove teratogenic in long term implants (Sachlos and Czernuszka, 2003).

Additive manufacturing (AM) offers distinct advantages over traditional subtractive manufacturing techniques. In AM, a 3-D construct is formed in a computer controlled layer-by-layer manufacturing process. It also permits precise positioning of biological components such as signalling molecules and cells such that the biological and structural elements are constructed simultaneously with exquisite spatial control. A digital template is created either by computer aided design (CAD) or from medical imaging modalities such as SPECT, CT or MRI. The image file is then manipulated and converted into an international standard .STL (derived from STereoLithography) file format. .STL files convert data from a 3-D object scan into a series of horizontal, 2-D slices with x- and y- axis coordinates. The computer-aided manufacturing (C-AM) process, then recapitulates the horizontal slices in a characteristic layer-by-layer approach, resulting in a 3-D construct.

Historically these techniques have been referred to as Rapid Prototyping (RP); turning a CAD concept in 3-D reality with minimal cost and quick turnaround, and Fused Deposition Modelling (FDM); related to the layered manufacturing process of first generation techniques. For consistency both these terms now fall under the Additive Manufacturing umbrella (ISO/ASTM terminology). Additive manufacturing can be categorised, according to its approach methodology as; Biomemetic, autonomous self-assembling and, mini-tissue building blocks (Murphy and Atala, 2014).

Biomimicry derives its inspiration from structures and designs seen in nature and seeks to replicate them artificially. This approach is the most common in tissue engineering with researchers attempting to replicate biology in a like-for-like manner. Attempts to reconstruct the vascular tree, produce ECM-like tissue and printing of artificial trabecular bone are all examples of a biomimicry approach.

Autonomous self-assembly is a cell driven tissue engineering approach whereby the tissue structure and function are provided by developing tissue precursors (Marga et al., 2007).

This technique could be seen as the pinnacle of advances in embryological and stem-cell disciplines, as intimate knowledge of cell signalling and developmental pathways is required and manipulated to direct tissue self-formation. Whole or partial organ synthesis could be achieved using a self-assembly approach in an advanced bioreactor set-up, ready for *in vivo* implantation.

Mini-tissue building blocks are described as the functional or repeating elements of much larger tissues. Examples include the renal nephron, portal triad in the liver and an osteon in adult long bones. These building blocks are either assembled using a biological inspired design, as in biomimicry, or produced by self-assembly. This modular approach has been successful in producing elements of a branched vascular network (Alajati et al., 2008). Creating a complete functional organ element can be used in an organ-on-a-chip approach for disease screening and therapeutic testing.

The precise control and detailed designs afforded by AM techniques have transformed the scope of biomedical engineering and a number of techniques have been described. Manufacturing techniques fall in to three broad categories: i) Laser based, which include stereolithography and selective laser sintering, ii) Printing solutions such as 3-D printing and wax modelling, iii) Nozzle based technologies including extrusion free forming and electrospinning (Henkel et al., 2013).

Figure 1-8 Examples the structure and material types produced by common additive manufacturing techniques used in tissue engineering.

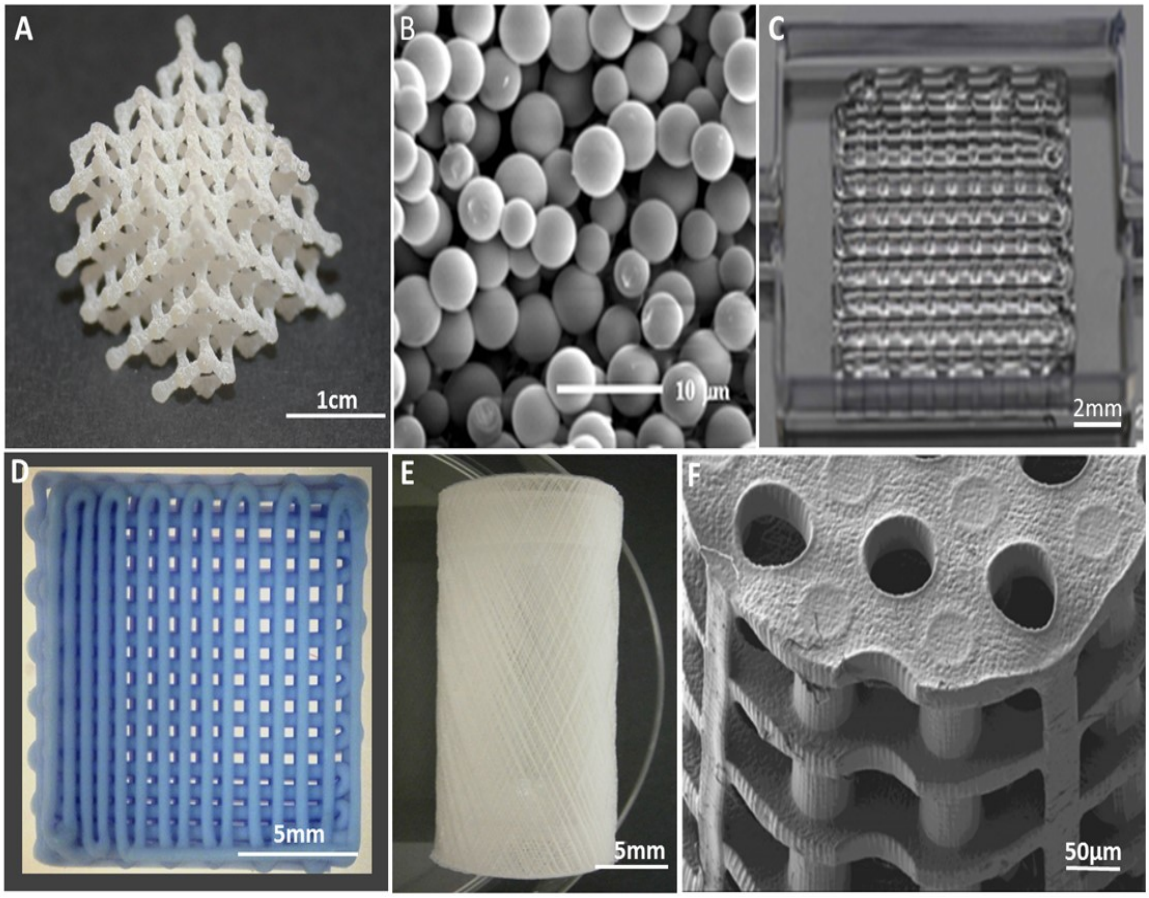

Figure 1-8 Scaffolds produced by common additive manufacturing techniques in tissue engineering.A) Porous architecture produced by Selective Laser Sintering (Kinstlinger et al., 2016) B) Nano-spheres manufactured using supercritical CO2 solvent, applications in drug and growth factors delivery (Woods et al., 2004). C) 3-D Bioprinting of vascularised hydrogels, (Kolesky 2014) D) Extrusion Free Forming of HA scaffold, demonstrating pore size variation, C.Black E) Melt Electrospun porous PCL tubular mesh, (Brown et al., 2012). F) Stereolithographic PCL porous column, (Kim et al., 2010).

1.9.2.1 Laser based techniques:

Laser based techniques utilise the energy derived from a highly-focussed laser source to alter the physical properties of one or more substrates. Selective Laser Sintering (SLS) sinters a polymer, ceramic, glass and metal causing particles to fuse, coalesce and solidify. In a typical SLS system a sample stage operates in the z-axis whilst the laser sinters substrate powder in desired pattern, as subsequent slices are formed the stage moves down and further powder is added on top. A process of sintering, stage movement and addition of fresh powder substrate continues until a 3-D form is made. Scaffold design parameters are controlled by manipulating laser movement and focal plane. The recent advances in Liquid Chrystal Displays and Digital Mirror Devices have improved print resolution and speed in both SLS and Stereolithographic solutions. Commercial materials available for SLS are not compatible *in vivo*, and bespoke solutions are required, subsequently polymer based biocompatible bone tissue scaffolds have been produced by SLS and successfully tested in large animal models, reviewed by Shirazi (Seyed Farid Seyed et al., 2015).

Stereolithography was created by Chuck Hull in 1986 and was a pioneering technology in additive manufacturing. In contrast to SLS, the photon source in stereolithography is used to polymerise a suitable photosensitive solution and not to sinter solid powders. A UV light source is focussed on a photopolymer causing it to polymerise in a very specific location. This solid polymer slice is collected on a base plate with z-axis control. As layers are polymerised they fuse and start to form a 3-D shape, the collection arm lowers, exposing the laser to new liquid polymer and the process continues. Biocompatible scaffolds have been created with high reproducibility, detailed architecture with highly interconnected pore geometry (Gauvin et al., 2012)

Laser Induced Forward Transfer (LIFT) has been applied to tissue engineering, in LIFT, the laser is used to blister or bubble a substrate, causing the bubble to interact with a collecting surface. Biological elements are contained within a liquid which sits on a metal layer (Delaporte and Alloncle, 2016). Laser heating causes the carrier fluid to vaporise and form a high-pressure bubble. This bubble projects cells and other material forward onto a suitable collecting substrate. LIFT or LAB (Laser Assisted Blotting) can be used to coat surfaces with cells at high density. Its nozzle free set-up will not clog and can be used on highly viscous material. Coating of complex topographies is challenging and the scale of structures produced by LIFT is hindered by the size and projection of formed microbubbles. In work by Ovsianikov (Ovsianikov et al., 2010), a biocompatible highly porous structure was created using two photon polymerisation (2PP) and subsequently seeded by LIFT to produce an elegant, cell-seeded bioactive construct.

1.9.2.2 Printing based additive manufacturing

Inkjet printers were among the first techniques adapted for bioengineering. A print head capable of delivering a “bio-ink” deposits scaffold and biological elements in a 2-D plane. Adjustments to the head or print stage allows movement in the x-, y- and z-axis, droplets are deposited on each other forming a 3-D stack. 3-D printing can use heat or acoustics to disperse bio-ink droplets from the printer head onto a collector surface, with both techniques preserving the activity of bioactive molecules and cells (Cui et al., 2012; Piard et al., 2015). It is possible to combine multiple printing heads and utilise an array of polymer and polymer-cell combinations. Bio-ink printing is restricted by the lack of cell compatible inks available and by the poor control of spatial resolution in reported set-ups.

3-D printing also relies of the use of liquid bio-ink derived from synthetic or natural sources, these materials are then deposited to simulate ECM or other tissue geometries in a 3-D design. Forming stable structures from liquid bio-inks often requires a cross-link or polymerisation step to increase material stiffness which can reduce printing speed and inhibit biocompatibility. In one recent approach a gelatin hydrogel was mixed with PEG cross-linker and allowed to gel in the bio-ink reservoir with viable cells, the bio-ink was printed using a custom printer with fine fibre resolution of 200µm, the same technique was applied to fibrin and collagen gels to similar effect (Rutz et al., 2015) .This approach is an excellent example of a biocompatible polymeric material containing biological elements, being manufactured in 3-Dimensions utilising a single headed printer.

1.9.2.3 Nozzle based approaches

Any system in which a material is expressed through a nozzle, uses the nozzle to control material properties and aid in material deposition is included in this varied group which includes methods of extrusion such as melt injection extrusion, Extrusion Free Forming (EFF) and Precision Extrusion Deposition (PED). The force for extrusion is provided by a range of methods including piston, screw, spring and pneumatic arrangements. Fine nozzle control is provided by piezoelectric, solenoid and pneumatic wave valves amongst other techniques (Khalil et al., 2005). A variety of materials including polymers, calcium phosphates and hydrogels are forced at variable pressure and temperature through the extrusion nozzle onto a collecting plate with x-, y- and z-axis movement capability.

Extruded materials harden either by cooling, removal of solvent or by cross-linking. It is possible to combine multiple extrusion heads to produce scaffolds from composite materials in combination with biological elements (Chia and Wu, 2015). As with all nozzle systems, the chance of blockage in the nozzle and damage to cells from shear stresses has yet to be resolved.

Alternative nozzle technologies include solution or melt electrospinning and electro-spraying. In these technologies the driving force for polymer deposition is provided by an electrical potential difference across the polymer and collection plate (Lukáš et al., 2009). The charged material is drawn out of the nozzle stretching polymers into fine fibres which can then be layered into intricate patterns. Melt electrospinning utilises polymers with low glass transition and appropriate melt viscosities which may be combined with growth factors and cells (Brown et al., 2012). An excellent review of nozzle and other AM approaches in tissue engineering was published by Veazi (Vaezi et al., 2013).

1.10 Melt-Electrospun Poly Caprolactone (PCL) Microfiber Mesh Scaffolds

In chapters III and VI, a PCL mesh construct supplied by Professor Dietmar Hutmacher's group at QUT, Australia was used to localise a thermosetting bovine ECM hydrogel. Background to the melt-electrospinning technique is provided below for reference in subsequent chapters.

For more than a decade there has been a resolute effort to produce biologically compatible, functionally relevant scaffold materials with well-defined and precise intra-structure architecture. Design parameters influencing cyto- and bio-compatibility include the choice of material and material blends used, scaffold macro-structure, filament diameter, pore size, pore orientation (Karageorgiou and Kaplan, 2005) and post production functionalisations (Liang et al., 2007).

Electrospinning is a versatile polymer based manufacturing technique which can be used to create fibres from micro to nano scale. Scaffolds can be produced from simple or blended polymers, at uniform or variable fibre diameters (biphasic production) and combined with other AM scaffolds (multimodal) to produce intricate structures in tissue engineering.

The principal of electrospinning centres on the "drawing" of fine fibres between the spinneret (material reservoir) and a collection plate. Two broad categories of electrospinning have been used in tissue engineering, solution and melt. Both methods rely on an applied electric charge to the polymer and the creation of a potential difference between the polymer and collecting plate, pulling the molten or dissolved liquid polymer towards the collector. In solution electrospinning polymer solidification occurs by solvent extraction in comparison with the controlled cooling which occurs during melt electrospinning. The use of solvent in the production of bio-materials requires adequate ventilation and fume extraction making production under sterile biologically compatible conditions impractical and expensive, added risks are associated with the incomplete removal of cytotoxic solvents (Baker et al., 2005) which may leach with use *in vivo*. Melt-electrospinning circumvents the need for solvents and by extension solvent related hazards and has also been shown to manufacture 3-D structures with larger pore sizes and more reproducible structure than are achievable with solvent based techniques. Unlike true AM techniques, the precise control and design of scaffolds produced by electrospinning has proven problematic as the charge forces causing the droplet to leave the spinneret increase as the polymer approaches the collection plate.

These forces create bending instabilities in the polymer jet (Reneker et al., 2000) causing the fibre to “whip” or spiral, accelerate laterally and stretch. Polymers used in melt-electrospinning by nature are higher purity and viscosity (owing to absence of solvent in solution), have a higher viscosity and lower conductivity, as a result the jet produced is less susceptible to bending in the electric field, can be drawn over a longer distance and deposited with more accuracy than jets in solution electrospinning (Zhou et al., 2006).

Melt-electrospinning has been developed to manufacture 3-D scaffolds with fibre diameters in orders of magnitude smaller than established additive manufacturing (AM) techniques such as Fused Deposition Modelling (FDM), Selective Laser Sintering (SLS) and Extrusion Free-forming, with melt-electrospinning also producing pore sizes large enough to allow cellular infiltration and tissue invasion using biocompatible materials without the need for harmful solvents.

Poly-Caprolactone (PCL) is a biocompatible polymer first synthesised by the Carothers group in 1930 which published the technique 1934 (Natta et al., 1934) which has been the subject of investigation for drug delivery and potential tissue engineering applications from the 1970s through to the present day. PCL is currently used in drug delivery (Capronor®) and as surgical suture material (Ethicon®, Monocryl®) and PC is increasingly seen as an attractive material in the field of tissue engineering. PCL is easily synthesised and can be produced at high molecular weight which is readily blended with thorough molecular entanglement between copolymers. The advantageous rheological and visco-elastic properties exhibited by the aliphatic polymers lend themselves to use in melt extrusion and electrospinning manufacturing techniques (Brown et al., 2012). In context of melt-electrospinning for tissue engineering, PCL has a low melt temperature, is biocompatible and has seen application in bone (Ren et al., 2014) and cartilage regeneration (Santos et al., 2013).

Based at Queensland University of Technology, Professor Dietmar Hutmacher’s group has pioneered the design and manufacture of computer aided melt-electrospun nanofiber scaffolds using PCL polymers and blends. The Hutmacher group has successfully produced biocompatible PCL mesh scaffolds and tested both *in vitro* and *in vivo* (Brown et al., 2012; Ren et al., 2014) demonstrating ectopic bone formation on spun fibres within the porous mesh substance. PCL microfiber mesh provides a membrane network similar to that found in may connective tissues and ECM (Shin et al., 2004) promoting cellular adhesion and proliferation. When combined with bimodal techniques a PCL mesh frame work could be used to target exogenous cell delivery and to localise other delivery material such as injectable hydrogels. It was envisaged that a narrow diameter PCL mesh cylinder would be suitable in both these functions to deliver an ECM hydrogel therapy into a chick femur defect using the *ex vivo* CAM model.

1.11 Animal models in bone tissue engineering

Animal models are the cornerstone of translational research, they are used in a variety of ways to prove safety, efficacy and suitability for clinical use. The *in vivo* model stage is a crucial make or break for many novel therapies (Hollister and Murphy, 2011); success is a fast track to clinical trials, whereas a negative outcome condemns a treatment hopeful as an "also-ran". The use of appropriate animal models is stipulated by guidelines issued from a range of voluntary and governmental regulatory bodies including ASTM International, FDA, EU (CE) and ISO (ISO 10993) all governing and advising on best practice in the development and certification of medical devices and biomaterials. All approved FDA and ISO certified implants and devices have at some point in their development been trialled in an animal model and proven safe for use in humans. Does successful testing at the preclinical level justify and support the continued use of animal models in tissue engineering? Can we therefore assume that animal models are an accurate predictor for efficacy in human clinical use?

After all, a human is not a 60kg mouse.

Standard Operating Procedures for *in vivo* experimental design are not outlined in EU/ISO nor FDA/ISO guiding literature, although corroborative evidence of safety and efficacy in appropriate models is required . There are an extraordinary number of variables for a researcher to consider when designing an *in vivo* experiment, and the lack of standardisation complicates the decision-making process. The confusion is related in part to the lack of reliable data correlating an animal model to known consistent outcomes in the human. Animal models are deemed essential in research translation, researchers and policy makers agree, as is evidenced by their pre-requisite at regulatory level. The following section details the various *in vivo* approaches in tissue regeneration research.

1.11.1 Development of *in vivo* models

Basic *in vitro* science has shaped our fundamental understanding of the cellular components of bone generation and repair and their responses to key regulatory molecules and growth factors (Erlebacher et al., 1995). *In vitro* assays have become progressively intricate, with modern bioreactors it is possible to co-culture multiple cell types in 3-Dimensions, offering new insights into bone formation and repair (Martin et al., 2004; Zhao and Ma, 2005) . New developments into how we mimic biology in the lab have been mirrored by expert computer modelling solutions *in silico* (Reifenrath et al., 2014).

Despite these advances there simply no comprehensive alternative to the living organism. *In vitro* techniques are unable to simulate the cellular, molecular, physiological and biomechanical intricacies present at the whole organism level. Biological elements critical to bone repair, such as a patent vascular network and biomechanical stimulation have proven difficult to reproduce outside of the living organism. When it comes to understanding how a construct will interact within a living organism, no suitable alternative to well-designed *in vivo* experimentation presents itself, *in vivo* models remain essential to therapy development. The many considerations facing a researcher in developing the appropriate *in vivo* model is presented in Table 1-5.

***In vivo* species and breed selection criteria**	**Considerations for *in vivo* model design**
• Size and anatomical characteristics • Biomechanical characteristics • Physiological similarity to humans • Gene sequence and protein homology to humans • Genetic variability between cohorts • Availability • Husbandry and handling, risk to staff • Housing requirements • Resistance to disease and environmental stress • Lifespan and life-stage progression throughout study duration • Existence of anaesthetic, surgical and post-operative protocols • Robust nature, tolerant of experimental model • Surgical survivability • Ethical and societal implications	• Model design addresses the research question • Develop model to improve data relevance • Modification to eliminate procedural short-comings of previous techniques to address short comings • Should only take place after thorough *in vitro* toxicity, cytocompatibility and efficacy assays • *In vitro* feasibility must justify use of animal model • Study group design, including appropriate controls • Adequate group numbers, avoiding excessive animal use • Avoid wasteful experimental duplication. Study design should include accurate power calculations, 3R considerations and longitudinal study methodology. • Impact of model on animal behaviour • Model design closely simulates possible clinical usage • Consider methods of post-experimental analysis

Table 1-5 Factors in small animal *in vivo* design. From (Black et al., 2015)

1.11.2 Small animal models

Pre-clinical models in bone repair act as bioreactors assessing biomaterial and cellular performance at a whole-organism level. These precursory models provide information on a range of factors including; toxicity, tumour formation, biological compatibility, vascular integration and any potentially deleterious off-target effects. Commonly used small animal models are split between those providing an in-bone environment (orthotopic) and those out with the bone environment (ectopic).

Orthotopic simulations include complete and partial osteotomy or drill defect creation long bones (Hollinger and Kleinschmidt, 1990), calvaria (Sawyer et al., 2009), sternum, pelvis and mandible (van Leeuwen et al., 2012).

Ectopic models offer two benefits, firstly they can rapidly assess biocompatibility in an easy to approach model and, secondly, assess bone forming capacity in an environment devoid of innate osteogenic potential, including bone related cytokines and osteogenic cell precursors (Scott et al., 2012). The premise in ectopic models is that any new bone formation recorded is directly caused by the treatment under examination as there are not any of the bone forming elements found within host bone. By extension, the expectation is that the bone forming capacity of the treatment will be enhanced when tested orthotopically, i.e. when a system, cells and/or materials, generates functional bone in the absence of osteogenic elements such as cells and signalling molecules (ectopically), the same system will then be enhanced when used in the presence of host bone forming elements (orthotopically).

These assumptions do not always hold true in osteogenic systems which are working at the upper dose response limit, further stimulation may trigger a paradoxical bone resorption (Pobloth et al., 2015). Further undesired effects are possible in excessive upregulation with the production of poor quality bone, bone cysts and damaging unregulated hypertrophic bone (Zara *et al* 2011).

The degree of new bone formation seen in small animal models will vary depending on the model used and the material in question, these variations should be kept in mind when planning a translational set-up (Lissenberg-Thunnissen et al., 2011). Ectopic models are almost exclusively sub-cutaneous or intra-muscular although several variations of organ sub-capsular implants in the kidney, testes and liver are also documented (Scott et al., 2012). These models are performed predominately in the mouse, rat and rabbit, and can produce high experimental numbers in a short experimental timeframe.

The sub-cutaneous model involves a simple full thickness skin incision under aseptic conditions with the followed by implantation between dermal and hypodermal connective tissue layers. Many implants can be accommodated in a single animal, with control and test groups performed in parallel, providing data over a range of time varying from days to months. The sub-cut model is a first step on the *in vivo* pipeline, providing base information on overall biocompatibility, material integration, degradation and metabolism. As a secondary attribute, sub-cut modelling offers preliminary information on vascular compatibility and bone regeneration simultaneously with the use of contrast enhanced micro-computed tomography (μ-CT), and supplemented by traditional histological techniques. An adaptation of the sub-cut model is the intra-muscular implantation or muscle pouch model. Commonly deployed in the biceps-femoris, triceps and dorsal spine muscles in mice and rats, this model addresses the need for experimentation in a musculoskeletal microenvironment and may offer improvements in vascular supply and exposure to non-bone SSC elements.

Ectopic models provide general information on biocompatibility, the need to better understand how scaffolds behave in a bone environment led to the development of models using the flat bones (calvarial) and long bones (femoral), in critical- and non-critical sized defect models. Segmental bone defects in the mouse, rat and rabbit have been described in bones of the axial skeleton. The relative reduction in body mass and structural bone differences permit the creation of self-stabilising defects alongside those requiring surgical fixation. Mouse and rat long bone defects can be created with relative ease with relative stability commonly provided by modified internal nailing/pinning.

The larger femoral dimensions in rabbit breeds (particular the large New Zealand White) allow the use of modified plate and external fixator systems which are analogous to a clinical scenario. Modified systems have been described in smaller species but in the opinion of the author, unnecessarily complicate the surgical protocol, increasing the risk of haemorrhage and anaesthetic related depression and may further introduce post-surgical risk factors regarding implant failure and infection.

Small animal models are comparatively cheap, accessible and offer useful information on biological performance but are restricted by their small scale and lack of clinical relevance. Although the value of any correlation between small animal models and clinical translation is restricted, a great deal of fundamental data has been generated using these models as part of a high throughput, rapid turn-around feasibility experimental design.

The subject of small animal models in musculoskeletal research is broad and falls out with the focus of translational models in bone tissue engineering. A comprehensive review is given by Gothard (Gothard, 2014). Examples of common small animal models are given in Figure 1-9.

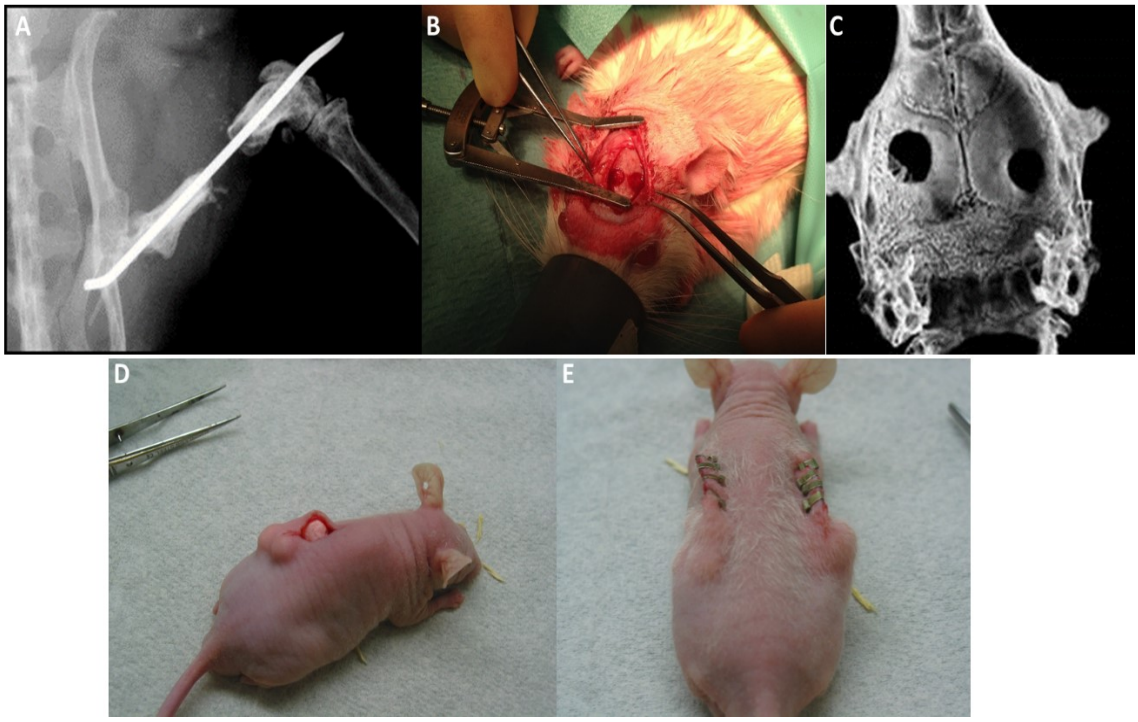

Figure 1-9 Examples of small and *in vivo* models. A) Mouse, femoral segmental defect with i.m. pin, radiograph. B) Rat, cranial defect, *in vivo* C) Mouse, cranial defect, post-harvest, µCT. D and E) Mouse, sub-cutaneous implant, implant inserted D and after wound closure E. Images provided by Dr Janos Kanczler, Bone and Joint Research Group

1.11.3 The need for large animal models in bone tissue engineering

Historically, rodent and rabbit animal models have not reliably predicted bone formation in experimental models using larger species nor within the human clinical setting. Bone formed in both sub-cutaneous and bone defect studies using dogs, sheep and pigs is inconsistent with small models, as either bone fails to form in the rat, mouse and rabbit models or the type and volume of bone recorded does not correlate between large and small species (Kan and Kessler, 2011; Wang et al., 2014), with a failed correlation between orthotopic rodent models and human clinical trials also recorded (Meijer et al., 2008). The causes of this effect are poorly understood; bone biology and morphology, cell characterisation, growth factor activity and availability, enzyme presence and activity, biomechanics, physiology, metabolism and overall size and morphology are all potential contributors. Huipen, Yuan and colleagues demonstrated a distinct separation between larger species (such as cows, pigs, dogs and non-human primates) and smaller model species (such as lagomorphs and rodents) in the performance of therapies forming new bone (Zong et al., 2010).

Although this observation is important in interpreting data derived from small animal models it does not imply that we cannot correlate between rodent and large animal models of new bone formation. Work by Yamada and colleagues demonstrated new bone formation in a rat ectopic subcutaneous model and a subsequent canine orthotopic mandibular segmental defect model (Yamada et al., 2004).

Extensive work on the therapeutic bone forming potential of Nell-1 protein has demonstrated significant new bone formation in the rat calvarial and spinal fusion models, this work was successfully scaled into an ovine model of spinal fusion with 100% fusion achieved across test groups ((Lu et al., 2007). The rodent long bone orthotopic model was used to assess bone forming capacity of an AM PCL scaffold loaded with recombinant BMP-2 by Sawyer (Sawyer et al., 2009) , this informative work was effectively repeated in the ovine tibial segmental defect model demonstrating enhanced new bone formation over autologous “gold standard” bone graft (Berner et al., 2013a).
These are three examples of common large animal models; mandibular defect, spinal fusion and long bone critical defect and support that significant orthotopic new bone in a rodent model can be correlated to similar outcomes in large animal models.

Following on, the absence of bone formation in ectopic and orthotopic rodent models does not predict negative outcomes in larger translational models, whilst the presence of new bone orthotopically (in rats) correlates to outcomes seen in translational models.

The prevalence of studies linking successful experimental outcomes in large animals such as the pig, sheep and dog, and positive clinical outcomes in humans continues to increase (Warnke et al., 2006) reviewed by (Dawson et al., 2014) and (Cancedda et al., 2007).
There is confusion on which models we should be using and how we should correlate data between small and large animal studies and a clinical impact, this complicates *in vivo* experimental design. Based on the data available, the only reliable method of assessing clinically relevant new bone formation *in vivo* is using a well-designed appropriate large animal model with due consideration given to inherent properties of species and intended clinical use.

Large animal models in bone repair research are documented in various guises, intended to mimic normal fracture repair, delayed union, large volume bone loss, fracture non-union, spinal fusion and joint arthroplasty. Models which replicate segmental bone loss and fracture mal-union tend to do so by an intentional compromise of the wound healing environment, either by tissue trauma or inadequate fracture stability. A separate group of models uses a critical sized bone defect in the presence of a biologically competent wound environment to assess large scale bone regeneration in a healthy animal. Inhibition of natural healing is caused simply by the large volume of bone tissue removed which exceeds the physiological limit for repair and is unrelated to impedance of the fracture microenvironment. Segmental defect models can be modified to include further biological compromise of the fracture environment, which may be achieved by damaging or removing the periosteum or less commonly, through thermal injury to bone and soft tissue structures involved in the defect.

It is important that the design and implementation of translational animal models addresses both the physiological and pathophysiological elements relevant to the research question. It should also address more common research questions such as tolerance of treatment, biomechanical performance, and involve well-planned characterisation of newly formed bone and vascular integration into the study design. The choice of model and species must be considered within the experience and capacity of the researcher and available facilities (Black et al., 2015). It should aim to achieve a large sample number, obtaining clinically relevant data over a short time frame (Egermann et al., 2005), with considerations regarding availability the animal species, husbandry requirements, tolerance to captivity, ethical considerations and societal acceptance.

1.11.4 Justification of the ovine as a suitable research model species

Before detailing the development of an ovine model, it was first necessary to justify the use of sheep over other documented large animal species in research.

1.11.4.1 Canine

The dog has been a popular model species in orthopaedic research from the early years of modern bone tissue engineering (Neyt et al., 1998). When compared with the cow, rabbit, pig, sheep and goat, canine bone was found to be most similar to human long bone in bone particle size, total inorganic mineral content, hydroxyproline, extractable protein and assayable IGF-1 (Aerssens et al., 1998). Macroscopic bone changes are present between dogs and humans and consistent with expected dissimilarities between a smaller digitigrade quadruped and a larger plantigrade bipedal skeleton.

In human adult long bones a secondary osteonal structure dominates, osteons are characterised by a central blood vessel carrying canal approximately 100µm in diameter, surrounded concentric lamellae with a cement line between lamellae (Reznikov et al., 2014). In dogs, the osteonal structure is present in only the central most diaphyseal regions within the middle most cortical bone but the bulk of bone mass is plexiform in structure (Wang and Agrawal, 1998). Plexiform bone is prevalent in rapidly growing skeletons in large animals and is also prominent in the skeletons of children during periods of rapid growth (Pearce et al., 2007a). The use of canine models in orthopaedic research between 1991 and 1995 was recorded at 11% (Neyt et al., 1998), and again by Martini in 2001 at 11% (Martini et al., 2001). The canine segmental bone defect model continues to be used and is readily documented from 2001 onwards.

Canine orthopaedic surgery is a developed discipline within veterinary medicine and the availability of modern customised implants used in and advanced surgical protocols is attractive when designing a model with clear human parallels. Dogs are sociable and easy to condition, with convenient husbandry contributing to their widespread use. The US National Research Council (Gov, 2009), EU directive 2010/63/EU and related UK Animals (Scientific Procedures) Act 1986 (Committee, 1986) outlines its position that all vertebrate species do sense pain and that it is the duty of researchers to ensure that appropriate attention is given to the choice of animal species and models with due consideration towards pain and pain alleviation. The development of accurate behaviour and pain monitoring scoring systems in companion animals has highlighted that dogs overtly display pain and fear responses in response to painful stimuli (Livingston, 2010).

The canine response is more marked than for species such as the cat, sheep and cow, the reasons for which are uncertain.

Two possibilities are proposed, that canines are more susceptible to pain sensation and less adapted to tolerate noxious stimuli, or that as a result of their developed social hierarchical structure, dogs have development a variety of non-verbal communicative traits which are expressed under duress, making it easier to visually assess a pain behaviour. The response to pain and an enhanced display of fear and distress should be considered when selecting the use of canine species in *in vivo* response.

Objectively, the case for the dog as an orthopaedic model is contrasting; bone mineral content and bone mineral density in humans is more analogous to the dog than other large animal species (cow, sheep, goat and pig) (Aerssens et al., 1998). Macroscopically, canine bones are smaller (in almost all breeds) and morphologically distinct from those of the human and require veterinary specific implants, many of which are only slight modifications of those used in human surgery. Canine bone remodelling and turnover is variable between body locations and comparison to humans is difficult, as a rule fracture repair time, rate of turnover and remodelling are accelerated in dogs (Pearce et al., 2007a).

Moral considerations are influenced by societal tolerances which may be attributed to the selection of a canine model as either acceptable or morally challenging and may account for the use of canines across differing geographical locations. From a veterinarian's perspective, the dog shows closer similarities in bone microstructure than other large animal species, (although not in the case of mature sheep) yet disparities in other areas such as accelerated turnover, hierarchical bone structure and reduced body mass, coupled with strong ethical concerns regarding the uses of companion animals in research indicate that other more ethically justifiable candidates exist.

1.11.4.2 Porcine

The pig has been used as an important model in tissue engineering as a discipline and orthopaedic research in particular and are as commonly used as sheep (Martini et al., 2001). The use of pigs is limited in the first instance by practical reasons related to excessive size, vocal nature and potential for aggressive behaviour.

Modified mini and nano-pig breeds have sought to overcome these limitations but the use of pigs remains specialised. The axial limb of pigs is condensed, femoral and tibial lengths are considered too short for defect surgery and implant use. The trabecular network density and cortical thickness are greater than in the human (Li et al., 2015) although similarities in femoral cross-sectional diameter have been shown (Raab et al., 1991).

Pigs are intrinsically muscular and access of the long bones and joints requires transection and distraction of significant soft tissue structures in comparison to surgery of the small ruminants. Regarding physiology, bone repair and remodelling the pig is considered homologous with humans and is therefore a good candidate species in bone tissue research (Thorwarth et al., 2005).

Similarities between pigs and humans are not significant and are not sufficient to justify the use of a pig model outright in favour of small ruminants or dogs. The level of expertise and intensive husbandry requires of the species limit their attraction as a model (Rubessa et al., 2017)

1.11.4.3 Ovine and small ruminants

The use of sheep in musculoskeletal use has risen over the last 20 years. Use between 1991 and 1995 was recorded at 9-12 % in bone lengthening and osteoarthritis, compared with 5% in the preceding decade (Pearce et al., 2007a). Increasing use of the sheep model may be in part a response to ethical concerns relating to the use of companion animals in research.

Demeanour

Sheep are for the most part docile (highly breed variable) animals which respond well to conditioning of indoor intensive housing systems. They can be habitualised in a research context making them suitable for serial assessment and ongoing monitoring post operatively. Polled sheep breeds (without horns) are commonly used in research and are readily available, sheep do not pose the same bite threat as dogs and display fear as aversion behaviour rather than aggression, these and other general physical attributes reduces the risk of accident and harm during husbandry. Sheep were first domesticated over 10,000 years ago and their husbandry requirements are well understood. Their amenability to domestication, adaption to an artificial environment, linked with their docile manner and low-risk to handlers makes sheep an ideal species for management throughout the experimental duration.

Musculoskeletal system

Macroscopically, the dimensions of ovine long bones are complimentary to humans, permitting the use of human implants in experimental models (Reichert et al., 2009). Additionally, prosthesis developed in the sheep model can be transferred into humans with minimal adaption, reducing any uncertainty associated with upscaling the implant for human use (Cancedda et al., 2007). As the importance of the sheep model has grown, understanding into ovine biomechanics has improved the value of data and its correlation to the human scenario.

Work examining the gait cycle and tibio-femoral forces during rising and ambulation indicate that forces experienced in the sheep are similar to those in the human during resting and low levels of activity (Bergmann et al., 1984; Duda et al., 2006). Peak forces such as those noted in humans through running and the use of stairs are more than twice the magnitude recorded in sheep during high activity (Duda et al., 2006). These larger differences are in part attributed to the quadruped gait and reduced range of motion in ovine skeletal systems. Forces noted in the ovine proximal femur at slow and fast walk femur are comparable to humans relative to body mass, although total measured forces in the sheep are approximately half of those in humans.

The distribution of forces in the frontal and transverse planes of sheep and humans is also comparable (Bergmann et al., 1999). It is clear the overall forces recorded in motion are significantly greater in humans, forces relative to body weight are congruent.

Similarities in force distribution indicate that sheep are an appropriate model for human orthopaedic research but care must be taken to factor in the larger forces experienced in human patients at rising running and climbing.

Dissimilarities in the microstructure of young adult sheep bone and humans are more marked than for the differences in force distribution. The long bones of young sheep, less than 7 years old, have a primary bone structure characterised by poorly organised woven bone with plexiform bone elements, in contrast to the secondary osteonal bone structure in humans (Eitel et al., 1981; Reznikov et al., 2014). Ovine breeds undergo secondary remodelling between 7 and 9 years (Newman et al., 1995) of age taking on a similar structure to human bone (Liebschner, 2004), albeit with less frequent Haversian canals in a less organised orientation. After this remodelling period, the macroscopic architecture and microscopic bone characteristic in sheep and humans are more closely aligned. Although no one animal species (other than non-human primates) approximates humans for bone physiology and anatomy, the aged ovine in a healthy state possess many suitable structural traits with the human. Analogues in macro and micro architecture, comparable body mass and suitability to housing support the justification for the use of sheep as an orthopaedic model in research.

Other ruminants?

The use of goats in orthopaedic research is documented (Anderson et al., 1999) although is far less prevalent than sheep (Martini et al., 2001), unlike sheep, the use of goats in musculoskeletal research is centred on cartilage and ligamentous repair (An and Friedman, 1999). Larger goat breeds offer similar advantages as sheep in body mass and bone size and may be suitable for large critical bone defects. Goats and sheep both show similar variations in microstructure with a non-uniform Haversian distribution, with the cranial aspect of bone demonstrating the presence of a canal system and caudal aspect of long bones comprised primarily of lamellar bone with a small number of blood vessels.

Remodelling, fracture repair and metabolism in the goat sheep and humans is comparable, lending credibility to their use in implant development.

These metabolic and remodelling similarities did not appear to be hold true in models assessing bone graft integration as vessel penetration and bone turnover was more rapid in the goat compared with humans, 3 months and 8 months respectively (Lamerigts et al., 2000).

Issues relating to husbandry may prove the deciding factor in the use of goats, they're natural inquisitive nature and higher level of activity than the sheep make them less suited to intensive indoor research set-ups. Goats are considered a more intelligent species which could lead to learnt aversion behaviour to research protocols, increasing negative behaviours with subsequent handling, inhibiting follow up treatment and serial monitoring.

The use of goats over sheep may be an issue of availability and prior operator experience rather than decision based on scientific merit.

Use of a bovine model is recorded but appears limited to spinal fusion, and documentation is scarce (Wedemeyer et al., 2007). The use of a cow model was logistically not possible and without scientific justification.

1.11.4.4 Mineral content and bone strength

When investigating the mineral and biomechanical elements of bones from different species no clear candidate species has been identified (with the exception of non-human primates). Aerssens and colleagues (Aerssens et al., 1998) reported a large variability in bone mineral density (BMD) and bone mineral content (BMC) in spinal trabecular core samples from the dog, pig, sheep, rat and cow. Based on these data the pig and dog are most similar to human regarding BMD and BMC. BMD and BMC for sheep and cows were higher than all other species. When expressed graphically, BMD, BMC and fracture stress formed distinct interspecies groups with little or no overlap. Data relating BMD and BMC to fracture stress did not show a clear correlation in non-human species. This observation is at odds with those in humans where BMD and BMC are shown to predict up to 70% of bone strength (Leichter et al., 1982), and a well-documented association between BMD and fracture risk exists (Johnell et al., 2005). This is not to say that BMD differences between species are not important as part of an overall understanding of bone quality and its correlation to *in vivo* models in bone repair, a researcher needs to be aware that a less distinct correlation in animal species may have implications when translating result to the preclinical environment.

The use of BMD as a surrogate indicator of bone quality has long been recognised for its potential inaccuracy and alternatives are described in clinical literature. In an attempt to rationalise the important components contributing to overall bone quality, work by Felsenberg and Boonen formulated a Bone Quality Framework (Felsenberg and Boonen, 2005). Using known factors affecting bone strength as guidance (Bouxsein et al., 2001), the Bone Quality Framework relates bone quality (structural and material properties) and the effects of bone turnover, to bone strength. Mechanical properties include bone geometry, macro and microstructure. Material qualities relate to organic and inorganic content, matrix composition and distribution and size of micro-damage (controlled by healthy turnover).

In a controlled study of fracture properties between humans and animal species, the canine showed the highest value of fracture toughness ahead of human, followed by baboon, rabbit and cow (Wang and Agrawal, 1998). Values for the human were statistically separate from canine and bovine bones yet similar to baboon and rabbit. Here again we see that BMD, which is highest in bovine cortical bone, does not correlate to bone quality as measured by resistance to fracture and that correlating the interspecies differences in organic and mineral phase composition with any valuable predictive clinical outcome proves unreliable.

1.11.5 Conclusion on choice of model species

It is clear that no one animal model is more suited to translation research in bone tissue engineering. The mineral content, compressive strength and mineral density in dogs is the most similar to humans out of commonly used species but an overall smaller skeletal structure, mismatched secondary structure, accelerated turn-over and strong ethical concerns limit the attractiveness of canine use.

Large ruminants such as the cow are physically intensive to work with, have dissimilar BMD and BMC values and microscopically vary considerably with humans.

Bone physiology and metabolism in the pig is comparable with humans although increased trabecular and cortical density coupled with a well-developed musculature deviate from humans. The large body mass, aggression and learnt aversion behaviours limit the use of pigs to specialist facilities.

Small ruminants such as the goat and sheep have a body mass comparable with humans, bones share macroscopic similarities and undergo bone secondary remodelling in later life to have a microscopic structure consistent with the adult human. Variations do exist between ruminants and humans in BMD, fracture strength and biomechanics, although the variations are small and data do overlap. The range of similarities coupled with their docile nature and tolerance of surgical procedures, promotes the use of sheep as a highly suitable large animal model in translational medicine (Pearce et al., 2007b; Reichert et al., 2010; Li et al., 2015).

1.12 Hypothesis

The application of early stage *in vivo* models do not predict outcomes in ovine translational models when investigating novel therapies in bone tissue engineering.

1.13 Aims

This thesis covers four results chapters; the intended purpose is take the reader from early *in vitro* and *in vivo* investigation in small animal models and progress toward the establishment of basic and more challenging translation models in sheep. The story is to follow a translational "pipe-line" through which novel material and cell therapies combinations are evaluated as potential solutions in Bone Tissue Engineering.

1.13.1 Chapter III

Chapter III seek to ascertain whether the enrichment of bone marrow mononuclear cells by Stro-4 antibody linked isolation selects for a potent cell type for application in bone tissue engineering. This question will be answered by *in vitro* analysis and *in vivo* functional assessment.

Aims:

→To document the *in vitro* growth and differentiation characteristics of a Skeletal Stem Cell population subset selected using the Stro-4 antibody. This will inform the translational merit of ovine studies using unselected bone marrow mononuclear cells and Stro-4 enriched skeletal stem cell populations.

→To assess the functional osteogenic capacity of Stro-4 cells in a tissue engineering platform consisting of an Extracellular Matrix Hydrogel and Melt-Electrospun Poly-Caprolactone mesh scaffolds cultured in the chick chorioallantoic membrane model

1.13.2 Chapter IV

Ovine bone defect models have been developed in young female and older male sheep and in mixed populations. The model is challenging to establish using aged female sheep which are representative of a clinical demographic in humans. Chapter IV investigates whether an ovine condyle model utilising exclusively aged female sheep is feasible as a reliable standardised protocol in translational medicine. This question will be addressed by documenting husbandry, surgical and analytical procedures.

Aims:

→To develop and establish surgical, infrastructural and analytical protocols necessary to implement an ovine condyle defect experimental model in an aged female sheep population.

→To validate the model by demonstrating statistical significance between negative and positive controls, provide baseline data for bone repair in the selected model population.

1.13.3 Chapter V

The clinical application of Bone Morphogenic Protein-2 has shown promise, however the prohibitive production costs of the protein and off-target deleterious effects undermine its adoption as a reliable therapeutic adjunct. Chapter V investigates whether a nano-silicate hydrogel can effectively deliver a low concentration of BMP-2 in a controlled spaciotemporal manor stimulating new bone formation in an ovine condyle model.

Aims:

→To successfully implement the validated ovine femoral condyle model to examine growth factor mediated bone formation and to continue to refine ovine condyle model protocols as required.

→To document the efficacy of Medtronic InductOS® at a reduced dose in an ovine cortical defect model.

→To deliver Medtronic BMP-2 using a 2.5% Laponite gel and compare efficacy to Medtronic InductOS® as described in (2) above.

→To assess the potential use of Laponite gel as a sole delivery agent for bio-active peptides in bone regeneration, in this scenario, BMP-2.

1.13.4 Chapter VI

Stro-4 selected bone marrow mononuclear cells are osteogenic *in vitro* and in small animal *in vivo.* Chapter VI investigates whether Stro-4 cells can cause new bone formation delivered with a novel extracellular matrix hydrogel in an ovine tibial segmental defect.

→To isolate and culture sufficient numbers of Stro-4 ovine skeletal stem for use in a tibial segmental model.

→To successfully implement a segmental defect study comparing the bone forming capacity of seeded (n=8) and unseeded (n=8) bovine ECM hydrogels localised to a defect by use of a Poly-Caprolactone microfiber mesh

→To demonstrate the use of a bovine derived ECM hydrogel as an effective therapeutic in bone tissue engineering showing comparative efficacy to the clinical gold standard, autologous bone.

→To demonstrate an enhanced bone forming effect in ECM hydrogels seeded with Stro-4 SSCs

Chapter II

2 Materials and Methods

The methods described below apply to the techniques which were applicable between results chapters. Chapters IV, V and VI each document the development and refinement of translational model protocols and all methods specific to those goals are provided in the relevant chapter.

Unless otherwise stated, all reagents were purchased from Sigma-Aldrich, USA. All cell culture occurred in a Class II Biological Safety Cabinet (Nuaire®, UK) maintaining strict aseptic technique.

2.1 Cell culture

2.1.1 Culture media

Standard cell culture media, alpha minimum essential medium without foetal calf serum: αMEM Gibco Life Technologies, UK) media supplemented with 100 U/ml of Penicillin G and 100 µg/ml of Streptomycin (Gibco Life Technologies, UK).

Complete media, alpha minimum essential medium with 10% foetal calf serum: αMEM media supplemented with 100 U/ml and 100 µg/ml of Penicillin G and Streptomycin, respectively, and 10% foetal bovine serum (FBS).

2.1.2 Culture protocol

Cells were plated at a density of approximately 1-3 $x10^4$ per cm^2 of tissue culture plastic. Typically, 1 $x10^5$ per T150 (Corning, UK Ltd). 10% α-MEM was used as standard for both human and ovine cells, media was changed every 2-3 days depending change to media colour (as an indicator of pH change) and rate of cell growth. Cells were cultured in 5% CO_2, atmospheric oxygen at 37°C.

Cells were passaged at no more than 70% confluence; culture media was aspirated off, cells were then washed three times in Phosphate Buffered Saline (PBS) (Gibco Life Technologies, UK) then incubated in 1x Trypsin for 5 minutes. Trypsinised cells were then counted and re-plated at appropriate density.

2.1.3 Multi-lineage differentiation of Ovine BMMNCs.

2.1.3.1 2-Dimensional *in vitro* culture assay

The potential and capacity of Stro-4 Ovine BMMNCs to differentiate into Osteogenic, Chondrogenic and Adipogenic lineages was assessed by tri-lineage differentiation and was carried out as previously stated for human BMSC (Tare et al., 2012) with adaptions due to the accelerated growth characteristics of ovine cells outlined briefly.

Osteo- Chondro- and Adipogenic differentiation was assessed at day 21 by both histological and molecular techniques of cells grown in monolayer culture. Each donor sample was plated in a 6 well tissue culture plastic plate (Corning, UK) at 2 x 10^4 cells per well, two wells per lineage specific condition. This set-up was repeated for both Stro-4 selected and unselected cells. Two wells per condition for both cell types were cultured in basal media as experimental controls. Cells were first cultured in basal media; 10% FCS, 1% P/S Alpha-MEM until 20-30% confluent then switched to 1.5ml per well of lineage specific media,

Osteogenic media; α-MEM with 10% FCS, 100 µM Ascorbate-2-phosphate, 10 nM Dexamethasone, 25 nM 1 α, 25-dihydroxy Vitamin D3, 25 nM inorganic phosphate.

Chondrogenic; α-MEM with 100 µM Ascorbate-2- phosphate, 10 nM Dexamethasone, 1% ITS medium supplement, and 10 ng/ml TGF- β3.

Adipogenic; α-MEM with 3 g/l D-Glucose, 10% FCS, 3µg/ml ITS, 100nM Dexamethasone, 0.5 mM IBMX, and 1µM Rosiglitazone.

Culture media was changed twice a week over 21 days. Cells were either fixed appropriately for histological staining or lysed in preparation for molecular analysis.

2.2 Isolation of mononuclear cell fraction from primary ovine bone tissue

Bone marrow was obtained from sample sheep by a unilateral iliac crest harvest immediately post-mortem. The iliac crest was exposed by gross dissection, taking care not to introduce skin surface contaminants through into the muscle and bone tissue. Iliac crest muscle attachments were resected and a window made in the bone using an osteotome. Approximately 10-20 ml of primary bone marrow was obtained and stored in 20 ml of basal media in a sterile 50ml Falcon tube.

In a biosafety cabinet, bone marrow samples were topped up with basal media and vigorously shaken for 2 minutes. The bone marrow suspension was then pipetted through a 100µm cell strainer (BD Cell sciences, UK) into a new 50ml Falcon and the suspension topped up with basal media. The suspension was then pelleted by centrifugation at 1100rpm (250*g*) for 4 minutes at room temperature. The pellet was re-suspended in basal media with wash steps repeated 2 more times, passing the suspension through a 75µm cell strainer each time, with the final re-suspension in 20ml of basal media, to produce a clean single cell suspension. Using a 3ml pastette, the cell suspension was gently layered onto 25ml of Lymphoprep (Stem Cell Technologies, UK) in a 50ml Falcon tube, taking care not to mix the cell suspension and Lymphoprep layers. The Falcon was then centrifuged at 2200rpm (800g) for 40 minutes with the brake off. The central mononuclear cell layer was carefully removed and placed into a universal tube and washed in 10ml of basal media. This process was repeated twice before a final resuspension in basal media, providing a single cell suspension of mononuclear bone marrow derived cells. Cells were either plated as unselected populations at the following densities: T25 – 2 x 10^5 cells (approx. 5ml in flask) or T150 – 3 x 10^6 cells (approx. 25ml in flask) and transferred to an incubator at 37°C, supplemented with 5% CO_2. If further enrichment was required, bone marrow mononuclear cells were processed by MACS as described below, 2.3.

2.3 Isolation of an enriched skeletal stem cell population by Stro-4 supernatant Magnetic Activated Cell Sorting

Reagents

Blocking buffer: 17mL α-MEM, 2mL human serum, 0.2g Bovine Serum Albumin (BSA), 1mL Foetal Calf Serum (FCS). Weigh the BSA into a tube, add α-MEM and FCS and mix, draw the mixture into a 20ml syringe and sterilise by passing through a 0.22µm syringe filter (Millipore, UK).

MACS buffer: 1L PBS, 5g (0.5%) Bovine Serum Albumin (BSA), 0.745g EDTA (disodium salt, 2mM). Filter sterilise before use, place the vacuum pump in the hood and use a 500ml flask top filter steriliser unit (Thermo Scientific, UK). The bottle can be de-gassed prior to use if made on the day.

Stro-4 cell isolation from whole bone marrow was based on published methods (Gronthos et al., 2009) by an adaption of standard laboratory protocol for the isolation of human Stro-1 from human femoral heads (Gronthos et al., 1994b). Approximately 5-8ml of sheep iliac crest bone marrow aspirate was obtained from animals immediately post mortem using aseptic technique. Marrow samples were stored in basal media at 4 degrees centigrade (°C) for no longer than 24 hours until processed for Stro-4 isolation. Single cell suspensions were produced as described 2.2 above, with the mononuclear fraction enriched for by density dependant centrifugation.

The enriched mononuclear fraction was prepared for antibody labelling by incubation in a protein blocking solution containing 2% human and bovine serum (Sigma-Aldrich, USA). Stro-4 hybridoma was produced in a similar method to Stro-1 (routinely used in the Bone and Joint Research Group) and a decision to maintain protocol continuity between Stro-1 and Stro-4 was agreed on. Blocked and PBS washed cells were centrifuged and re-suspended and approximately 1 x 10^8 cells were incubated in a saturated Stro-4 IgG supernatant (provided by Professor Andrew Zannettino, University of Adelaide) on ice for 30 minutes, gently shaking every 5 minutes. After washing, Stro-4 labelled ovine BMMNCs were incubated with goat anti-human IgG (Miltenyi Biotech, UK) at 20ul per 1x10^7 cells (approximately 200µl of beads) for 15 minutes on ice.

After resuspension in MACS buffer and washing, the MACS bead labelled cell suspension were passed through MACS magnets and columns (QuadroMACS and MACS columns, both Miltenyi Biotech). The positive fraction from each sample was collected, counted and seeded onto

standard tissue culture plastic cell culture flask at 1x 10^4 cells per square centimetre, and cultured in Alpha- MEM containing 10% Foetal Calf Serum (FCS), and 1% streptomycin/Penicillin at 37°C, 5% CO_2 in balanced air (Nuaire Cell Culture Incubators).

2.4 Histology

All appropriate Personal Protective Equipment was used throughout all protocols, adhering to laboratory Health and Safety guidelines and laboratory Standard Operating Procedures.

2.4.1 Haematoxylin and Eosin staining

Reagents (Sigma-Aldrich, USA unless stated)

Weigert's A: Haematoxylin (Fisher Scientific, UK) 10g in 1L of 100% ethanol, left to mature for one month in a dry dark cupboard. **Weigert's B**: 6 g Ferric Iron Chloride in 500ml distilled water and 5ml concentrated HCL. **Acid alcohol**, 1% Hydrochloric acid (HCL) and 70% ethanol mixed by mixing 10ml of HCL, 700ml 100% ethanol and 300ml distilled water. **Eosin**: 3g Eosin Y mixed in 300ml distilled water, 200µl acetic acid, filtered before use.

Protocol: Rehydrate slides through descending ethanols (100%, 100%, 90%, 50% for 2 minutes each), mix Weigert's and A and B 1:1 and allow to colour change to purple-black before use. Apply to slides in a rack and leave for 10 minutes before washing for 5 minutes in tap water. To differentiate the colour, dip in acid alcohol for approximately 30 seconds followed by a 5 minute rinse in tap water. Add Eosin with a pastette and leave for 10- 20 minutes. Wash slides again in tap water for 5 minutes before dehydrating through ascending alcohols and mount in DPX and coverslip.

2.4.2 Alcian Blue and Sirius Red

Reagents (Sigma-Aldrich, USA unless stated)

A standard solution of Alcian Blue was made by mixing 1.5g Alcian Blue 8GX (Fisher Scientific, UK) in 300ml Distilled H_2O and 3ml of acetic acid. **Sirius Red** was made by mixing 0.3g Sirius Red F3B in 200ml distilled water and 100ml Picric acid. 3 g of **Molybdophosphoric acid** was mixed with 300ml of distilled water to produce a 1% stock acid. Both Sirius Red and Alcian Blue were mixed using a magnetic stirrer and filtered before use.

Protocol: Rehydrate slide and stain with haematoxylin as described above. Dip slides in acid alcohol and rinse as above then apply Alcian Blue stain for 10 minutes and rinse in water for 1 minute. Stain in molybdophophoric acid for 10minutes, rinse in water then stain with Sirius Red for between 45 and 60 minutes, again rinse in water and dehydrate prior to mounting in DPX and apply a coverslip.

2.4.3 Goldner's Trichrome staining:

Reagents (Sigma-Aldrich, USA unless stated):

A working solution was made by combining 5 ml Ponceau-fuchsin solution, 2ml Azophloxin and a 0.2% Acetic acid solution. Light green was made by adding 1g Light Green in 500ml distilled water and 1ml Acetic Acid. Phosphomolybdic acid/orange G solution was made by dissolving 3g of Phosphomolybdic acid, 2 g Orange G in 500ml of distilled water and a crystal of thymol.

Protocol: Dewax slides in histoclear (Agar Scientific, UK) and rehydrate slides through decreasing ethanols. Rehydrated slides were stained in Weigert's A/B solution for 10 minutes then rinsed in tap water for 10 minutes, slides were then dipped three times in acid alcohol. Slides were again rinsed in water before staining in Ponceau-fuchsin-azophloxin solution for 5 minutes. Slides were dipped in 1% acetic acid for 15 seconds to enhance staining colour and then stained in phosphomolybdic acid/orange G solution for 20min and again rinsed in 1 % acetic acid for 15 seconds. Slides were counter stained in Light Green for 5 minutes, rinsed in acetic acid then water before being blotted dry. Stained slides were mounted in DPX and a coverslip.

2.5 Chorioallantoic Membrane (CAM) Assay

Fertilized, embryonic day 1 (E1) chicken eggs were incubated for 11 days at 37°C and 40% humidity in a Hatchmaster incubator (Brinsea Ltd) with auto rotation turned ON. Prior to experimental set-up (E8) all eggs were confirmed fertile and viable by the visible presence of an air cell, embryonic vasculature and central cranial shadow by egg candling (EggTech), any non-viable eggs were discarded, with only confirmed viable eggs selected for use in the assay.

Eggs were carefully moved from the Hatchmaster, again confirmed viable and placed into an active and laminar floor biosafety cabinet. Use of the candling procedure allows identification CAM and egg air pocket, eggs were always orientated such that window creation occurred over the membranes and not the comparatively poorly vascularised egg yolk.

Eggs were cleaned with bactericidal (Trigene) prior to window creation. Once identifying an area of shell overlying the air cell, a rectangular window measuring no more than 10 x 15 millimetres was cut using a sterilised saw blade taking great care not to crack the shell. The teeth of the blade were gently oscillated on the egg's surface, first penetrating the tough outer shell cuticle and cancellous layers stopping at the underlying fibrous inner shell membrane. The cut shell window was loosened from any small attachments and then completely excised. Remaining intact inner shell membrane was then incised and removed by use of a scalpel. At this stage, complete access is gained to the viable developing chick and the Chorioallantoic Membrane is visualised permitting experimental access. Once more the membrane is assessed for viability and suitability for experimental use. Experimental materials are carefully implanted onto the membrane with extreme care taken not to disrupt membrane vessels in any way. Chicken egg membrane was sealed by stretching sterile Parafilm (Bemis, USA) over the aperture then taped in place.

All appropriate labelling completed externally prior to return of the egg to the Hatchmaster, with rotation turned off, for incubation. Caution was taken not to keep eggs outside of the incubator environment for any extended duration, an experimental duration per egg of 30 minutes was adhered to. Eggs with still exposed windows/CAM were kept inside the biosafety cabinet at all times. Eggs were incubated for 7 days and culled on embryonic day 18. Structures of the early chick embryo are shown in Figure 2-1.

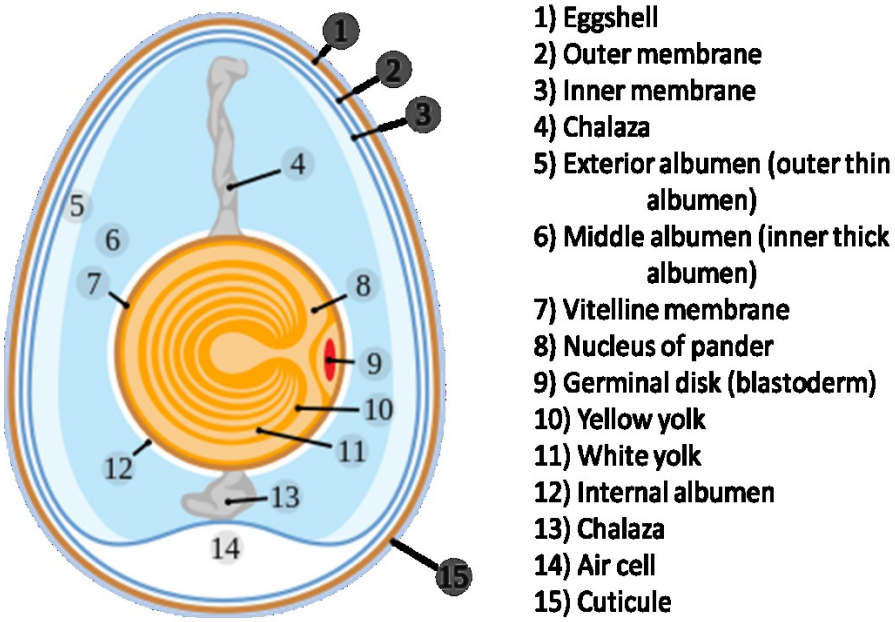

Figure 2-1 Schematic: Structures of the developing chick egg. Image release for public use, GNU Free License.

2.5.1 Harvest

Eggs were removed from incubator in batches of 6. The taped parafilm seal covering each window was carefully removed exposing the developing chick within the egg. Viability was easily confirmed by chick movement and pulsation of foetal vessels and a basic visual inspection confirms egg viability. Photographic documentation was obtained for each egg, linking survivability to assay performance for each construct. Eggs were carefully opened into a large petri dish exposing all membrane constituents and implant. Viable chicks were terminated immediately in compliance with Home Office and EU guidelines for the ethical use of animal for scientific procedures. Implants were excised with sharp surgical scissors with care taken to secure 5-10mm borders of CAM tissue on all edges, excised tissue was fixed in 4 % Paraformaldehyde (or alternative fixation as necessitated). All waste material was discarded in clearly marked biohazardous material waste bags and disposed of appropriately. Strict adherence to Home Office guidelines was maintained throughout all uses of the CAM model and no animal permitted to live beyond E18.

2.6 Bovine Extra-cellular Matrix hydrogel production

Bovine ECM was provided as a lyophilised powder by Dr Lisa White, University of Nottingham and produced by published protocols (Sawkins et al., 2013).

To produce a stock 14mg/ml ECM digest, 1.4g of bovine ECM powder was mixed with 100mg of porcine gastric pepsin (Sigma-Aldrich, Australia). Reagents were combined in a 500ml Erlenmeyer flask (Corning, USA), a metal stirrer bar was added and the solution mix at constant rate for 2-4 days at room temperature. Once the solution appeared clear of macroscopic particles (up to 5 days of stirring), solution by centrifugation at 400 x g-force for 10 minutes to remove any non-visible particulate matter. The resultant solution was then frozen at minus 20°C or used immediately.

The stock solution was neutralised and buffered with NaOH and PBS prior to *in vivo* use. To produce a 10 ml aliquot of 12mg/ml working solution, 0.95ml of 10x PBS was mixed with 0.86ml 0.1 Molar NaOH and 0.44ml 1x PBS. The PBS NaOH solution was kept on ice at all times. 8.6ml of stock solution was added to the buffer solution and mixed thoroughly with a 1ml pipette. The solution was centrifuged to remove air bubbles and the pH confirmed at 7.4. Once the working ECM was mixed, it was kept on ice until used. Using the ECM *in vivo* or *in vitro* above 30°C initiated the cross-linking reaction causing the ECM hydrogel to set.

2.7 Statistical analysis

Statics undertaken for analysis in each section are detailed in the relevant chapters

Chapter III

3 *In vitro* characterisation and *in vivo* functional assessment of a Stro-4 enriched ovine Skeletal Stem Cell populations

The application of prospectively targeted stem cell subpopulations in a clinical environment is preceded by thorough in vitro characterisation. When attempting to correlate between translational animal models and the clinical application in humans a clear comparison is needed between the skeletal stem cell populations of both the translational model, in this case the ovine, and human bone marrow derived populations. Ovine cell populations selected for by Stro-4 have been proposed as the correlate for human skeletal stem cells selected by Stro-1 antibody enrichment. In chapter III seek to ascertain whether the enrichment of bone marrow mononuclear cells by Stro-4 antibody linked isolation selects for a potent cell type for application in bone tissue engineering and whether the in vitro characterisation yields similar findings to those already documented for human Stro-1 populations.

Acknowledgements

Ovine Stro-4 isolation, cell culture and lineage differentiation was performed with assistance from Dr David Gothard and Miss Julia wells. I am grateful to Dr Lisa White, University of Nottingham for provision of bovine Extracellular Matrix Hydrogel and to Dr Onur Bas, Queensland University of Technology for manufacturing of PCL mesh constructs. Dr Janos Kanczler for his assistance with the chorioallantoic membrane model and in further assistance with compiling written work and editing.

3.1 Introduction

3.1.1 Research need: Elucidation of SSC biology sourced from *in vivo* model species

Recent advances in tissue engineering strategies *in vitro* have increased the demand for suitable *in vivo* models in the pre-clinical translation of candidate treatments. The use of large animal models in translational medicine has been established and modulated over the past 20 years with canine, caprine, porcine and ovine species all used in varying frequencies. The use of sheep in bone tissue engineering continues to gain popularity and remains a cornerstone of orthopaedic pre-clinical research due to similarities with humans in terms of i) weight, ii) joint structure, iii) physiology and, iv) bone structure. Increasing use of ovine models in research therefore increases the translational potential of the species model. In keeping with the overall thesis aims of developing multi-faceted solutions in bone tissue engineering, it was important to examine the *in vitro* and functional characteristics of the biological lead element: the ovine bone marrow derived Skeletal Stem Cell (SCC).

For an *in vitro* characterisation to be comparable to work across species and cell sub-sets within tissue engineering, a sub set series of investigations are required:

1) Marker expression at isolation, population growth rates and colony forming ability. 2) Basic growth profiles are followed up with multi-lineage differentiation protocols examined by macro phenotypic and molecular expression. Although an understanding of the *in vitro* characteristics of a cell population is of scientific interest, elucidation of population performance *in vivo* is essential. 3) With functional testing in mind the ability of enriched ovine SSC to augment the osteogenic capacity of novel regenerative therapies was assessed by combination with a promising innovative extracellular matrix hydrogel, localised with a melt-electrospun mesh in an orthotopic CAM femur experimental set-up.

3.1.2 Enriched cell populations in BTE

The discovery and characterisation of adult, bone marrow derived non-haematopoietic progenitors over the past 30 years has driven the popularity of BMMNCs in a regenerative context. Populations of bone marrow and adipose derived MSCs have been detailed extensively in the literature with cell growth profile, cell surface marker expression and capacity for multi-lineage differentiation well documented. Isolation of the non-haematopoietic stromal cell elements occurs predominantly by means of bulk cell isolation, examples include; cell culture plastic adherence and density gradient centrifugation with novel techniques under development utilising the physical properties of cells to discern between populations as employed by microfluidic and acoustofluidic separation (Xavier et al., 2016) .

Work defining the cell surface marker expression profile of MSCs has led to spin-off analysis of MSC marker specific populations such as Stro-1. The characterisation of certain marker designated populations has identified enriched MSC sub-populations which more specifically suited for use in bone tissue engineering, indeed in tissue engineering as a whole. The use of immune-labelling based techniques such as Magnetic Activated Cell Sorting (MACS) and Fluorescence Activated Cell Sorting (FACS) prospectively isolate bone marrow stromal subsets shown to enrich for CFU-F and lineage specific differentiation capacity when compared to the parent MSC population.

The clinical use of BMMNCs requires large numbers of cells functionally purposed for the intended application. Although MSCs have demonstrated multi-potency *in vitro* and *in vivo*, providing a phenotypic description of cells primed with a more functionally specific role, for example osteogenic precursors, within the heterogeneous wash has not been fully realised although exhaustive field-wide work has produced many candidates.

An optimal cell source for bone tissue engineering would be selected on its developmental bias towards osteogenesis, be accessible with minimum patient trauma and be suitable for potential intra-operative re-implantation, negating the need for *in vitro* expansion. The use of enriched populations in musculoskeletal regeneration is in its infancy but the use of CD146+, CD34+ CD105+ phenotypes has been trialled, showing the osteogenic potential of the enriched sub-population (Matsumoto *et al* 2006, James *et al* 2012 and Aslan *et al* 2006).

The inertia limiting the selection and use of enriched populations could be related in part to the uncertainty over which marker or combination of markers best select for osteogenic precursors from within the SSC population. The wide range of cell surface makers and strategies for bone marrow stem cell enrichment has been reviewed by Harichandon and Bühring (Harichandan and Bühring, 2011) and outlines how specific marker combinations can further enrich SSCs and documents potential phenotypes for cell type specific progenitors within the umbrella SSC niche. A diagram illustrating the potential SCC location within bone marrow is given in Figure 3-1**.**

The use of stem cell enrichment may become limited when the effort and complexity of isolation protocols reaches a point of diminishing returns; when increasingly elaborate methods of enrichment provide only marginal incremental improvements in cell performance. New marker discovery and functional testing of the population for which it selects is essential in advancing our understanding of the field and in providing therapeutic targets.

Ideally a target for enrichment would allow easy cell selection based on a conspicuous cell characteristic present and simple to exploit. The use of enriched populations is increasing, be it by single marker identification or other means, although this remains a relatively new frontier in cell based therapies for regenerative medicine. SSC Stro-1 enrichment exploits a single cell epitope making it cross-compatible with magnetic and fluorescence sorting and has shown promise in small animal experimentation but there remains an unmet need to further expand our understanding of how these cells perform in a larger more clinically relevant environment.

Stro-4, recognised as an ovine correlate to human Stro-1, provides an exciting target to examine therapeutics based on stem cell enrichment within a translational frame work.

Stem cell niche within the bone organ

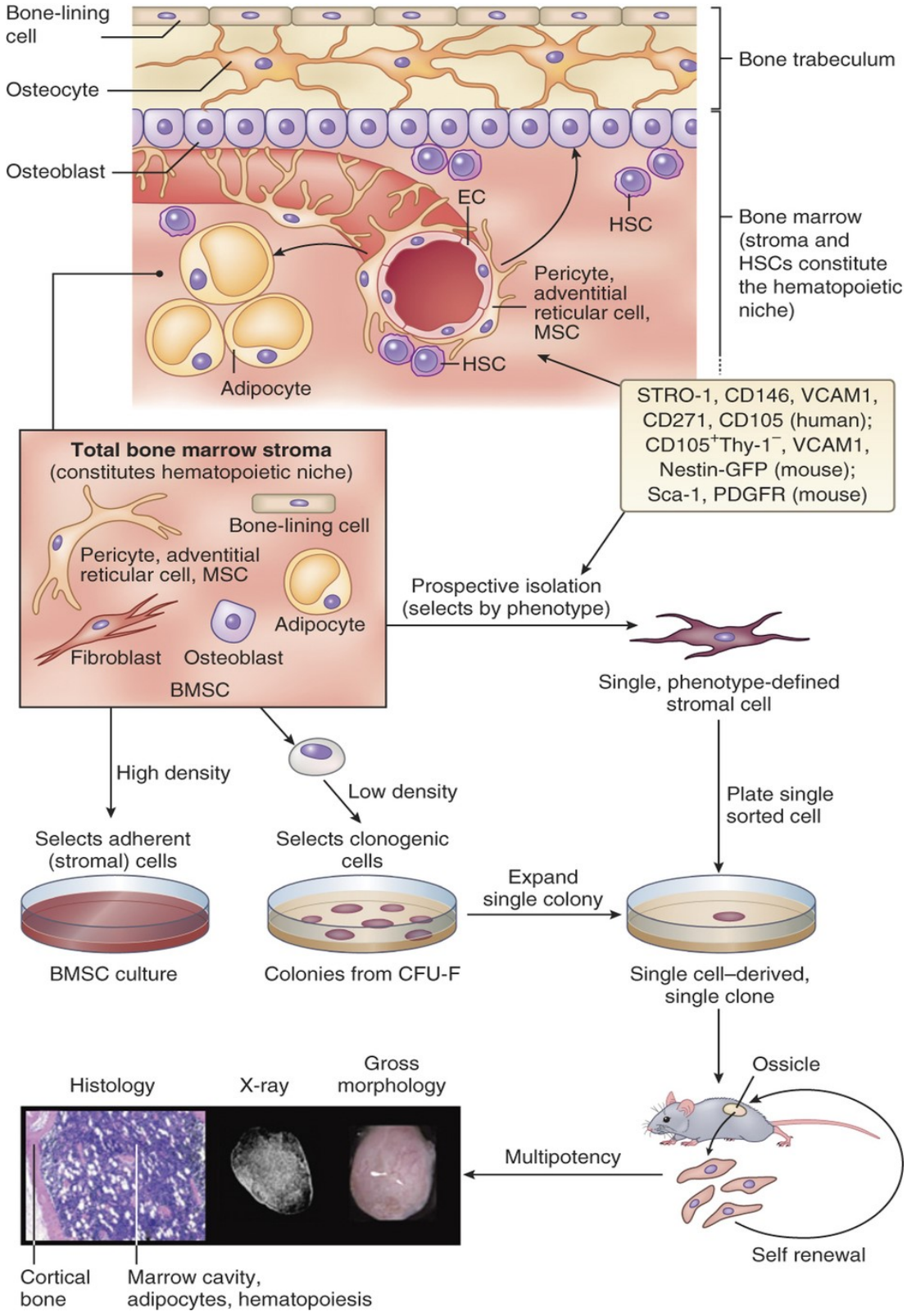

Figure 3-1 Stem cell niche within the bone organ. Image taken from Bianco et al 2015 "Stem Cells: A historical perspective" (Bianco, 2015).

3.1.3 Ovine mesenchymal stem cells and Stro-4

The need to address basic questions regarding the safety and efficacy of stem-cell therapies requires the use an *in vivo* model offering physiological and biomechanical homology to humans. This need has increasingly been met by use of ovine orthopaedic models in bone tissue engineering research.

Plastic adherent Ovine MSCs isolated from bone marrow (McCarty et al., 2009; Rentsch et al., 2010) peripheral blood (Lyahyai et al., 2012) and adipose tissue (Niemeyer et al., 2010) appear fibroblastic in culture, show similar CFU-F colony forming capacity and respond with differentiation *in vitro* and *in vivo* as the human comparator and have now been used successfully as a cell source in research utilising ovine orthopaedic models (Berner et al., 2013b).

Analysis of cell surface marker expression is hampered by the lack of species specific antibodies, this was exemplified in work by Rozemuller (Rozemuller et al., 2010) which investigated 43 human monoclonal antibodies for their cross reactivity to non-human species. Of the documented common MSC markers (CD73+, CD90+, CD105+ and CD34-, CD45-) only 22 antibodies were found to cross react and only 7 were found to be marker specific. Work to date has confirmed the expression of traditional human MSC markers on ovine MSC populations, CD29, CD44, CD146 and CD166 (Gronthos et al., 2009; Boxall and Jones, 2012).

The majority of appropriate antibodies available are not species specific and rely on species cross-reactivity for epitope identification. Therefore, confirmation of the absence or presence of antigens must be tempered by knowledge of the expected specificity of any antibodies used.

The accepted criteria for human MSC definition include the expression of CD73, CD90 and CD105 (Barry et al., 1999; Dominici et al., 2006a) as markers of cell potency. In contrast, in the sheep, confirmation of CD90, CD73, CD105 and other common human MSC marker expression has not been repeatedly demonstrated although the absence of the endothelial marker CD31 and haematopoietic marker CD45 seem shared across species. Confirming the marker phenotype as a species-specific phenotypic difference or merely an artefact of antibody specificity remains challenging.

3.1.3.1 Use of selected cell types *in vivo*

As the literature relating to the *in vitro* and *in vivo* nature of ovine MSCs accumulates, it is becoming ever clearer that ovine MSCs behave similarly, both *in vitro* and *in vivo*, to their human correlates. Ovine MSCs respond to osteogenic, chondrogenic and adipogenic differentiation cues, expressing the corresponding phenotype, assessed with both histological and molecular techniques. Ovine MSCs have been successfully isolated, culture expanded, differentiated and re-implanted as both an allogenic and autogenic cell source in various applications including cardiac, maxillo-facial and bone repair research (Sutherland et al., 2005; Reichert et al., 2009; Gallego et al., 2015).

The use of immunocompetent large animal models in translational research requires the identification and characterisation of a species specific enriched SSC population. Although candidate markers for human SSC enrichment have been detailed in the literature; CD146, CD106, CD271, MSCA-1, CD56 and Stro-1 (Gronthos et al., 2003; Aslan et al., 2006; Battula et al., 2009) therapeutic targets for use in ovine pre-clinical models remain under-developed.

Conventional anti-human Stro-1 antibody has been shown to bind to ovine BMMNCs (OBMMNCs) at low affinity, selecting for a population 1% of the total stromal fraction. This low population frequency is unattractive when choosing candidate markers for a prospective cell enrichment and to this end, Gronthos and colleagues have developed the monoclonal antibody Stro-4 as a candidate for SSC enrichment of OBMMNCs. Stro-4 designates a monoclonal antibody shown to bind specifically to human and ovine Heat Shock Protein-90, a common intra-cellular chaperone protein. Stro-4 was produced by an adaption of the Stro-1 hybridoma technique, substituting CD34 selected inoculation with a CD106 (Vascular Cell Adhesion Molecule, VCAM) BMMNC sub-population. It was later shown that Stro-4 supernatant selected for a phenotypically separate cell subset to the parent CD106 positive cells used for hybridoma inoculation.

Stro-4 monoclonal IgG antibody cross reacts with a small population of both human and ovine MSCs and cells FACS selected for Stro-4 expression enrich for CFU-F capacity 8-16 fold. Comparisons of human and ovine Stro-4 populations both demonstrated accumulations of Alizarin-Red positive mineral deposits, Alcian-Blue binding deposited matrix and intracellular oil deposits when exposed to osteo- chondro and adipogenic conditioned media *in vitro*. Further characterisation of the Stro-4 antigen by immunoprecipitation and mass spectrometry revealed Stro-4 as a 90kDa protein matching the signature of human heat shock protein 90 beta isoform (Hsp90-β).

The similarities between ovine and human MSCs have been demonstrated, furthermore Stro-4 selected ovine SSCs behave comparably *in vitro* to the human equivalent and can be regarded as a translationally relevant target for cell enrichment in ovine orthopaedic models. For full documentation of Stro-4 development see Gronthos et al., Stem Cells and Development, 2009 (Gronthos et al., 2009).

The evidence in support of the use of Stro-4 as a target of cell enrichment in ovine studies is encouraging yet further characterisation is required to understand and interpret the translational relevance of data generated from Stro-4 inclusive studies

The current study sought to isolate and enrich Stro-4 SSCs from ovine bone marrow, to document i) the cell population doubling time, ii) CFU-F formation over progressive passage, iii) multi-lineage differentiation using standard *in vitro* protocols and iv) to assess tissue specific growth characteristics using *in vivo* assays to provide a benchmark data for future translation.

3.1.4 ECM Hydrogels

Hydrogels are a class of biomaterials long recognised for as a material candidate in tissue engineering. Hydrogels are three-dimensional networks of highly hydrated macromolecular chains which have gained popularity owing to their biocompatibility, manufacturing flexibility and a wide variety of potential constituent components. Functionally hydrogels can be used for *in vivo* cell delivery and as a hydrated pliable three-dimensional matrix, providing integrity to tissue constructs. They also show exceptional promise in the delivery of morphogenic peptides and therapeutics, either as the primary material or in concert with a structural material construct, e.g. growth factor delivery onto a 3-D printed rigid scaffold. Hydrogels possess structural similarities to extracellular matrix (ECM) which can themselves be altered by material and formulation, this innate property contributes to excellent cell viability and proliferation, ideal for combining cell delivery with biocompatible scaffolds.

Extracellular matrix (ECM) is the non-cellular constitutive component of all body tissues (Frantz et al., 2010). ECM is formed by the deposition, aggregation and organisation of generic and tissue specific proteins, forming a three-dimensional network providing a biologically active frame-work, the function and structure varies between tissue types (Alford et al., 2015). As with other connective tissues, it is the acellular ECM component that forms the majority of bone tissue by dry weight, the bulk of which consists of collagen proteins, type I being the most abundant. Only 10% of bone ECM is non-collagenous with many of the more than 100 biologically important proteins forming only a very small portion of bone extracellular matrix (Chichester et al., 1993; Nanci, 1999). The ECM protein make up consists broadly of: Collagens, Glycosaminoglycans, Small Leucine-Rich Proteoglycans (SLRPs) (Bianco et al., 1990), Small Integrin Binding Ligand n-Linked Glycoprotein (SIBLINGs) (Bellahcène et al., 2008) Matrix Metalloproteinases (MMPs)and non-structural matricellular proteins (Bornstein and Sage, 2002). Osteoid and subsequent mineralisation of the tissue is a function of the osteoblast. Osteogenic cells produce an interconnected hydroxy-apatite matrix, intimately associated with bone ECM specific matrix proteins such as osteocalcin, osteopontin and bone sialoprotein (BSP-1).

ECM has been extracted from a variety of connective tissues including intestinal mucosa (Badylak et al., 1995), urinary bladder, large blood vessels (Schmidt et al 2000), heart valves and musculoskeletal tissues (Cartmell *et al* 1999, Woods *et al* 2005). Many ECM products for use in tissue engineering are commercially available, summarised by Badylak et al 2009 (Badylak et al., 2009). As has become apparent, bone ECM comprises tissue specific proteins essential in the formation and maintenance of a functional calcified matrix.

The rationale that bone ECM constituents are capable of directing cell differentiation and bone-organogenesis led collaborators at the University of Nottingham, led by Prof K Shakesheff and Dr L White, to develop and refine a process for bone ECM production.

Bone ECM hydrogels were manufactured from bovine tibiae using a protocol adapted from Pietrzak (Pietrzak et al., 2011). Bone samples underwent sequential morselisation, demineralisation to form a bovine Demineralised Bone Matrix (bDBM), chloroform/ethanol based lipid removal and a final decellularisation step producing a bovine ECM (bECM) material. bECM was then subjected to a solubilisation and pepsin digestion to prepare a functional hydrogel. The rheometric properties of bECM can be altered by varying the concentration of the bECM digest, with higher concentrations yielding more rigid gels. For further production and characterisation please see Sawkins et al 2013 (Sawkins et al., 2013).

Previous work within the Bone and Joint Research Group (BJRG) has established the use of the ex-vivo chick model and the chorioallantoic chick model as effective in early translational assessment of biomaterials in bone tissue engineering research (Kanczler et al., 2012; Smith et al., 2013). Assessment of the bone forming capacity of BMMNCs within the bECM hydrogels yielded positive results for bECM alone and bECM supplemented with exogenous growth factors. As part of a progression towards large animal translational studies it was necessary to understand and confirm the response of ovine Stro-4 within the bECM hydrogel used in a chick CAM segmental defect model.

3.1.5 *Ex vivo* femur culture in the Chorioallantoic Membrane Model

The use of a developing chick in understanding growth and development has been documented for many years, reviewed by (Wolpert, 2004). The developing embryo is an immunocompromised system which does not immune-reject xenogenic material. Use of developing chick egg as an alternative *in vivo* model capitalises on the developing structures of a chick embryo to recapitulate common *in vivo* processes whilst addressing concerns over ethical implications and intensity of resources required in large scale *in vivo* set-ups. The chick-egg model provides a significant advantage over standard and advanced *in vitro* models, providing an environment of multiple cells types with intact extracellular components developing in concert with temporo-spatial growth cues in a whole organism structure.

The long bones of a developing chick grow rapidly and are an excellent target for *ex vivo* research into musculoskeletal biology. Historically the long bones of chick embryos have been dissociated and cultured in an ex-vivo environment enabling the researcher to observe and document embryonic skeletal development including growth and resorption of cartilage and bone with subsequent tissue mineralisation. Gradually *ex vivo* models have developed by incorporated new materials and findings into their design and now allow for *ex vivo* culture up to 10 days after isolation from host tissue.

The term *ex vivo* refers to the explanted nature of tissue from an organism which is then cultured in a variety of methods. Harvested *ex vivo* tissue can be cultured organotypically or placed back into an *in vivo* model. Organotypic culture is an *in vitro* method for organ culture whereby the *in vivo* developmental environment is recapitulated outside of the living organism allowing the researcher to monitor, affect and manipulate organ development in an *in vitro* set-up (Kanczler et al., 2012).

The experimental use of *ex vivo* and organotypic culture of musculoskeletal tissue can be extended to incorporate the developing embryological membranes of the chick; the chorioallantoic membrane. In this model, scaffold constructs, cells, materials and whole organs for example chick femurs are incubated on the CAM membrane, developing alongside the underlying foetus; sharing nutrient, cellular, molecular and vascular components. Culture on the CAM membrane is not limited to the use of dissociated femurs and the CAM experimental setup is an excellent means of biomaterial and therapeutic assessment.

The CAM model is predominantly used *in-ovo*, whereby a small window is created in the developing chick egg, the material and ex-vivo organ is placed carefully onto the membrane and the egg re-sealed and permitted to grow until near-term, after which the chick is terminated and scaffolds retrieved. As a less frequently used but clever alternative, the conceptus can be cultured *ex ovo* in a modified petri dish (Samkoe and Cramb, 2003) or a novel egg surrogate (Huang et al., 2015), allowing the researcher to perform fine manipulations, such as intravascular injection and topical therapy application during the developmental process, although this culture method is less reliable.

The use of an open *ex ovo* system also lends itself to longitudinal imaging and data collection, consistent with relevant data collection and 3R principles of refinement and reduction. The CAM model is used as routine in the Bone and Joint Research Group and is a proven model for proof of concept in bone tissue engineering and was for this reason selected as the model for functional testing of Stro-4 population and ECM hydrogel constructs.

3.1.6 Aims

1 →To document the *in vitro* growth and differentiation characteristics of a skeletal Stem Cell population subset selected using the Stro-4 antibody. This will inform the translational merit of ovine studies using unselected bone marrow mononuclear cells and Stro-4 enriched skeletal stem cell populations.

2→To Assess the functional osteogenic capacity of Stro-4 cells in a tissue engineering platform consisting of an Extracellular Matrix Hydrogel and Melt-Electrospun Poly-Caprolactone mesh scaffolds cultured in the chick chorioallantoic membrane model.

3.1.7 Null Hypothesis

Selection of a sub-population of ovine bone marrow mononuclear cells by Stro-4 antibody labelled isolation techniques will not demonstrate an enhancement of skeletogenic potential.

Stro-4 selected cells will not display superiority in growth rate, colony forming capacity nor differentiation potential over the unselected population.

The novel Bovine Extracellular Matrix hydrogels will not produce an osteogenic response *in vivo* and the supplementation of ovine Stro-4 cells in Bovine ECM will not elicit an enhanced osteogenic response.

3.2 Materials and Methods

3.2.1 Multi-lineage differentiation

3.2.1.1 2-Dimensional *in vitro* Culture Assay

Differentiation of Ovine BMMNCs into Osteogenic, Chondrogenic and Adipogenic lineages were carried out as per standard differentiation protocols used for human unselected and Stro-1. Reagents are as described by Gronthos in ovine cell differentiation (Gronthos et al., 2009), methods are as described in Multi-lineage differentiation of Ovine BMMNCs. 2.1.3.

3.2.1.2 3-Dimensional *In vitro* Culture

Ovine Stro-4 selected and unselected cells were grown in micromass culture. Passage 1 Stro-4 and unselected ovine BMMNCs were trypsinised, washed in 1x PBS and centrifuged, re-suspended in basal media and counted on haemocytometer. The cell suspension was then centrifuged and re-suspended in basal media at a concentration of $1x10^4$ /µl. Micromass cultures were formed by depositing 30µl of cell suspension into a well of a 6-well plate, droplets were pipetted carefully to ensure droplet cohesion on the plate surface. 3 micromass cultures were placed per well then allowed to adhere by incubating for 2 hours at 37°C. Adherence to the plate surface and coherence between cells was confirmed under light microscope at 5 x objective. Cultures were gently covered with 1.5ml standard chondrogenic media, see Figure 3-2.

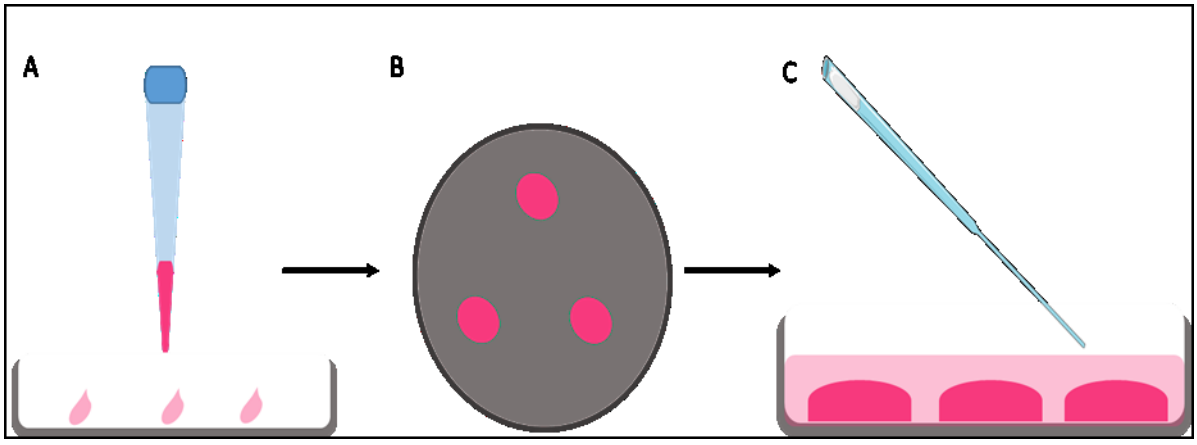

Figure 3-2 Schematic of 3-D chondrogenic micromass culture. 30µl droplets of cell suspension containing 1x104 cells/µl are carefully placed onto well surface (A). Droplets are spread across one well of a 6-well plate (B). After incubation, micromass cultures are covered with 1.5ml of conditioned culture media (C).

3.2.2 Colony Forming Unit Capacity

The Colony Forming Unit (CFU-F) capacity for ovine unselected and Stro-4 selected cells was assessed *in vitro* by modifications of standard BMMNC CFU-F assay. Preliminary work was performed on fresh cadaver samples to optimise CFU-F protocols for later work.

Optimum seeding densities for CFU-F assay of ovine cells had not yet been determined for Stro-4 cells *in vitro*, early passage (P0 and P1) cells were plated in ascending concentrations and assessed visually. Using T25 plates, which enabled good spacing and easier colony identification in the cases of high cell adherence growth occurred, passage 0 cells were plated at 1x $10^1/cm^2$, 1x$10^2/cm^2$, 5x10^2 $/cm^2$ and 1x$10^3/cm^2$, passage 1 cells were plated at 1x $10^1/cm^2$ and 1x$10^2/cm^2$. A density of 1x$10^3/cm^2$ was selected for CFU-F of passage zero cells and 1x $10^2/cm^2$ selected as an optimum seeding density for P1 and subsequent passages. Cells were cultured for 14 days in 10% FCS, α-MEM and 1% P/S, media was changed every 3 days.

3.2.3 Population Doubling Time

Population doubling time (PDT) was measured by plating 1x10^3 cells/cm^2 in a T75 flasks, growing cells in basal media until approximately 60% confluence. Cells were washed in 1x PBS, enzymatically digested (1 x Trypsin solution), washed and centrifuged before resuspension in 2ml of culture media, then counted using a haemocytometer. Total number of cells was recorded before cells were re-plated at 1x10^3 cells/cm^2. This process was repeated from passage 0 through to passage 5 from samples of five animals. Population doubling time, the time taken in hours for the total number of cultured cells to double in number, is calculated using the equation:

$$Population\ Doubling\ Time = \frac{Time\ (in\ Hours) Log\ ^2}{[Log(Final\ Cell\ Number) - Log(Seeded\ Cell\ Number)]}$$

3.2.4 Cell isolation

Cells were obtained from adult sheep immediately post mortem and processed as described in Methods, 2.22.3.

3.2.5 Melt Electrospinning of Poly(ε-Caprolactone) Tubular Scaffolds

Melt Electrospun tubular PCL fibre meshes were produced by Professor Dietmar Hutmacher and Mr Onur Bas at Queensland University of Technology, Australia as detailed in "Design and Fabrication of Tubular Scaffolds via Direct Writing in a Melt Electrospinning Mode" Brown *et al.* 2012 and summarised below.

Poly(ε-caprolactone) pellets with M_w = 50,000 (Perstop, UK) were loaded into a 3ml Luer-loc Syringe (B-Braun, Australia). The Syringe and PCL pellets were heated to controlled temperature of 78°C by recirculating water around a tank (Ratek, Australia) and through a custom-made glass syringe jacket. Material was heated for 1 hour, providing a homogenous melt. A spinneret was created by attaching a 21G Hypodermic blunt tipped "drawing" needle (Becton-Dickinson, Australia) to the Leur-Loc syringe. Polymer feed rate was kept constant to 50µl/h using a programmable syringe pump (World Precision Instruments, USA). A potential difference of 12kV was created between the spinneret and rotating collector located at a constant 40mm from the spinneret and polymer reservoir.

An electrically grounded 2mm diameter brass cylindrical rod was used as a collecting plate. The rod was connected to a stepper motor providing rotation with lateral motion supplied by a Velmex (Inc., USA) linear slide. Rotational and lateral translation was programmed by G-code, and controlled through Mach3 motion control software (Artsoft, USA). Fibres were produced at +- 60nm diameter and collected on the mandrel at constant flow rate, rotation and lateral motion. Subsequent layers of PCL fibre accumulated providing a final mesh approximately 300 fibre diameters in depth and 10cm in length. Manufacturing schematic see Figure 3-3.

PCL tubular scaffold then underwent a three stage post-production process coating each scaffold in a biomemetic calcium phosphate (CaP) layer to enhance osteo-induction. Mesh tubes were first cleaned by immersion in 70% ethanol (EtOH) solution under vacuum for 15 minutes to remove all air bubbles. The scaffold was then etched by alkaline treatment by immersion into a 2 M sodium hydroxide (NaOH) solution under vacuum for 5 minutes to activate the fibre surface for CaP coating. Scaffolds were then treated with activated Simulated Body Fluid 10x (SBF10x) under vacuum for 30 minutes, depositing CaP onto tubular surfaces. Tubes were rinsed in distilled water prior to immersion in a final NaOH solution. All samples were washed three times in phosphate buffered saline for 30 minutes and dried overnight in a desiccator and stored ready for use. Coated scaffolds were sterilised immersion in 70% EtOH for 30 minutes followed by drying in a tissue culture hood with UV exposure for 20 minutes.

3.2.5.1 Schematic of melt electrospinning process

A pure high molecular weight poly-caprolactone polymer slug is heated in a warming jacket. The molten polymer is then drawn towards a collecting plate as a result of a potential electrical difference between the polymer and collecting plate. As the rotating collecting pate rotates, layers of polymer sinter to each other creating an open structured mesh.

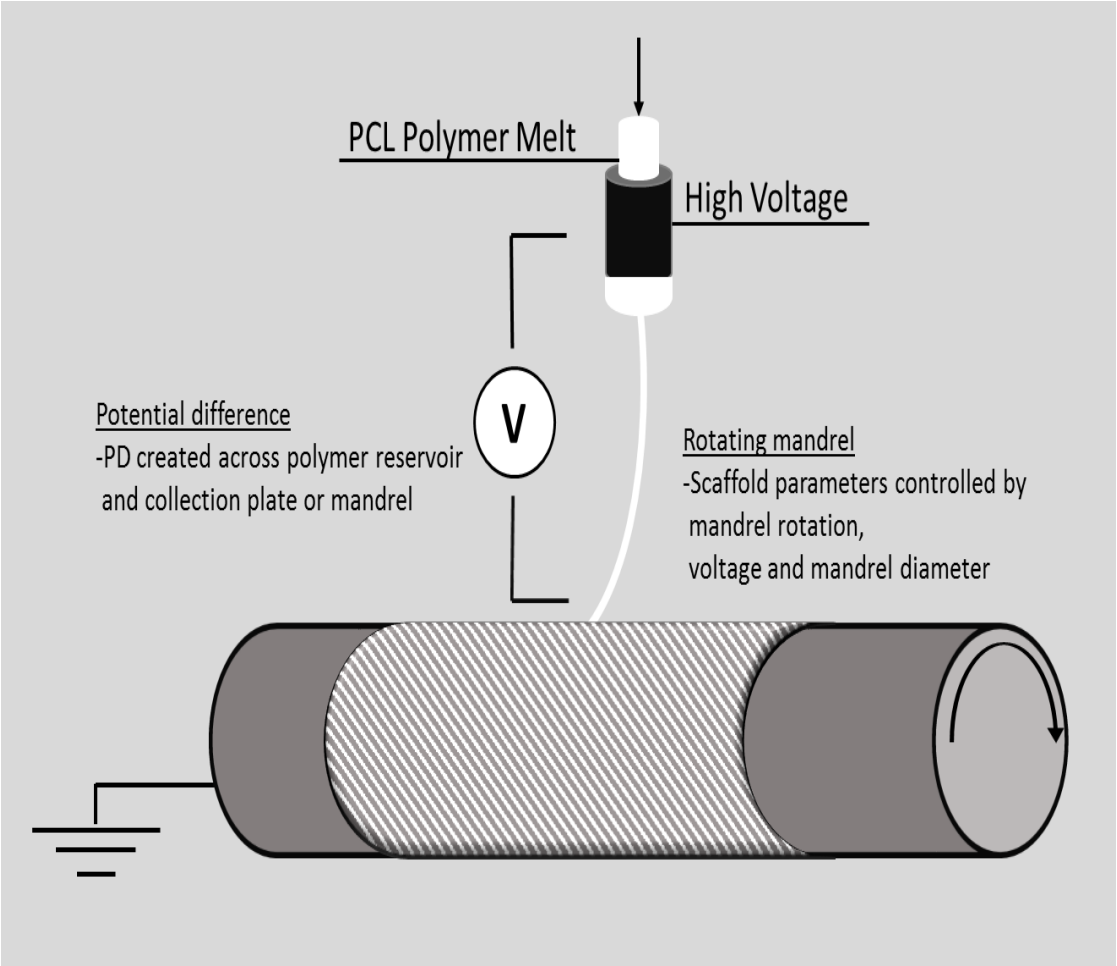

Figure 3-3 Schematic of PCL microfiber mesh production. Source: author

Histomorphometric quantification by cell profiler

Histomorphometric quantification of *in vitro* tri-lineage differentiation was performed by Cell Profiler with data analysed in GraphPad Prism. Data was obtained by measuring the colour intensity of histologically stained plates, obtained by imaging 3 regions across the culture well of each sample. Images were uploaded into Cell Prolifer® and analysed according to stain type.

Statistical analysis of comparisons in staining intensity were compared by ANOVA with multiple comparison between groups assessed by Tukey's post hoc multiple comparison test using GraphPad Prism. Graphs were generated using GraphPad Prism

3.2.6 Tri-lineage differentiation gene expression

Acknowledgement: Gene expression analysis was performed by Dr May De Andres and Miss Julia wells. All primers were designed new by Dr de Andres with guidance from published literature.

Unselected and STRO-4-enriched populations obtained from four sheep were cultured for 21 days in conditioned media for tri-lineage differentiation as per laboratory protocols, 2.1.3. Cultures were assessed for expression of adipose, osteoblastic and chondrocytic phenotype by the relative gene expression levels of differentiation markers using quantitative RT-PCR, primers given in Table 3-1.

3.2.6.1 RNA isolation and complementary DNA synthesis.

Total RNA (500 ng) was extracted from cultured samples using an Isolate II RNA Mini kit (Bioline), according to the manufacturer's instructions. RNA was immediately reverse-transcribed with TaqMan Reverse Transcription Reagents (Applied Biosystems). RNA concentration was evaluated using a NanoDrop 1000 spectrophotometer (Thermo Scientific).

3.2.6.2 Quantitative reverse transcription–polymerase chain reaction (qRT-PCR).

Relative quantification of gene expression was performed with an ABI Prism 7500 detection system (Applied Biosystems). Primer Express 3.0 software (Applied Biosystems) was used to design new primers or modify some from the literature (McCarty et al., 2009; Lyahyai et al., 2012). The 20-µl reaction mixture was prepared in triplicate, containing 1 µl of complementary DNA, 10 µl of GoTaq qPCR Master Mix (Promega), and 250 nM of each primer. Thermal cycler conditions included an initial activation step at 95°C for 10 minutes, followed by a 2-step PCR program of 95°C for 15 seconds and 60°C for 60 seconds for 40 cycles. The $2^{-\Delta\Delta Ct}$ method was used for relative quantification of gene expression, and the data were normalized to β-actin expression. β-actin was selected as a housekeeping gene as it emerged to be the most consistent from a number of other genes trialled including GAPDH, G6PD and HPRT. β-actin is also the housekeeping gene used when assessing human Stro-1 cells and was maintained for protocol consistency.

Statistical analysis of gene expression was performed by ANOVA, with LSD non-parametric post hoc testing for intergroup comparison using SPSS software, expression was normalised relative to unselected population in basal media. Graphs were generated using GraphPad Prism.

Table 3-1 Primer Sequences for qRT-PCR. Designed by Dr Rahul Tare and Dr May de Andres; Bone and Joint Research Group.

Name (length, bp)	*Function*	*Sequence (5' to 3')*
Beta-actin (336)	House Keeping	F(CCCAAGGCCAACCGTGAGAAGATGA)
		R (CGAAGTCCAGGGCCACGTAGCAGA)
COL1A1 (93)	Osteogenic	F (CCTGCGTACAGAACGGCCT)
		R (ACAGCACGTTGCCGTTGTC)
Osteocalcin (145)	Osteogenic	F (CAGCGAGGTGGTGAAGAG)
		R (CTGGAAGCCGATGTGGTC)
COL2A1 (225)	Chondrogenic	F (TGGGACTGTCCTCTGCGAC)
		R (CTGGGTCCTTGTTCACCTGC)
ACAN (108)	Chondrogenic	F (TGGGAGTGAGGACCGTCTAC)
		R (CTGGGATGTCCACAAAGTC)
Sox9 (115)	Chondrogenic	F (GCAAGCTCTGGAGGCTGCT)
		R (CTCCGCGGCTGGTACTTGT)
PPARγ (94)	Adipogenic	F (GCCCTGGCAAAGCATTTGTA)
		R (TGTCTGTCGTCTTTCCCGTC)

3.2.7 *Ex vivo* Femur cultures in CAM model

An extension of the CAM assay, the *ex vivo* femurs are cultured *in-ovo* on the CAM for 8 days. CAM set-up is as per outlined methods in Chapter II, 2.5.

Chick femurs were harvested from embryonic day 18 chicks by carefully removing the proximal and distal femoral attachments. The femur was carefully disarticulated distally from the femoro-tibial joint, and proximally at the femoro-acetabulum. Precaution was taken to ensure that neither cartilaginous epiphysis were removed from the calcified diaphysis. Once the femora were isolated, all remaining extra-osteal tissue was removed. Freshly isolated femora were placed in α-MEM kept overnight in a tissue culture incubator (37°C, 5% CO_2 balanced air).

3.2.8 Assembly of PCL Mesh, ECM hydrogel constructs and CAM implantation

On day of implant, sequentially; each femur was removed from storage media and placed into sterile filter paper to remove excess culture media, then using a scalpel, the femur was transected mid-shaft. Sections of sterile PCL Mesh were cut, approximately 5mm in length. Using fine-toothed forceps, the PCL mesh was carefully pulled over the sectioned ends of each femoral half attempting to leave a 2mm gap or defect between femoral segments.

bECM hydrogel was gently drawn into a 1ml syringe (BD Biosciences) using a 25G hypodermic needle (BD Biosciences). Each loaded syringe was kept on ice to prevent hydrogel cross linking and bECM gelation.

Once each femur was held in place by a 5mm mesh segment, the femur/mesh constructs were placed in a sterile dish and held in place by forceps. Femurs were divided according to experimental groups. In those groups containing hydrogel, the needle was inserted into the lumen of the mesh and femoral defects with great care taken not to damage any construct components nor dislodge either end of the femur. Once constructs were completed they were very gently placed through the eggshell windows and onto the CAM. Eggs were then sealed and placed into the Hatchmaster with rotation turned off. Experimental workflow is summarised in Figure 3-4**.**

3.2.8.1 Stages of CAM PCL ECM Stro-4 Experimental work flow

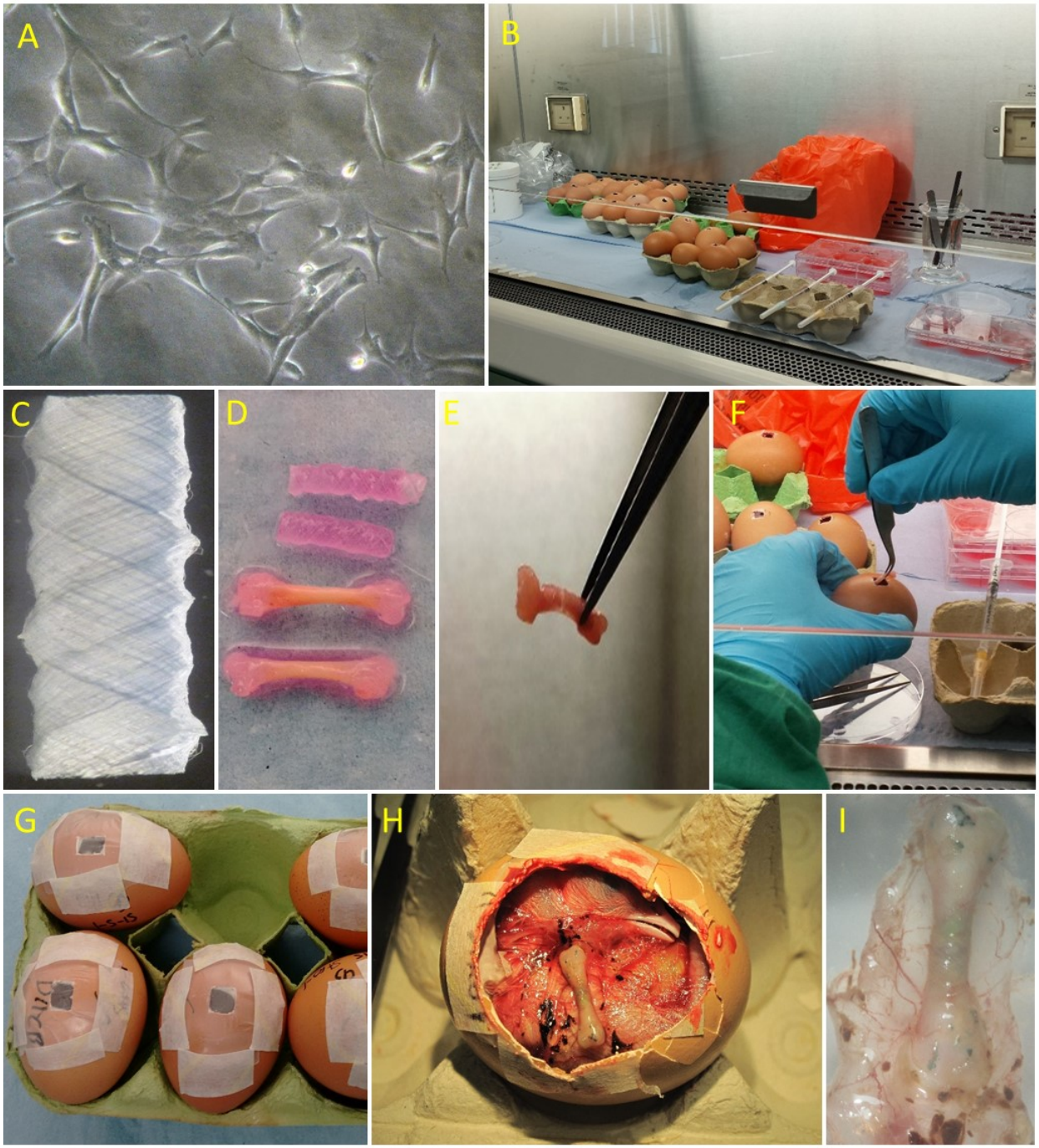

Figure 3-4 CAM experimental set-up including cell culture ECM gel and PCL mesh preparation. A) Stro-4 cells at P0 in culture B) Cell culture hood containing all elements of set-up C) 2x Magnification of Melt-electrospun mesh prior to implant D) PCL Mesh and explanted femurs prior to construct formation E) Femur mesh constructs F) Implantation onto CAM G) Sealed CAM windows H) Intact femoral constructs in situ on CAM at harvest I) explanted femur surrounding with integrated CAM at day 18.

3.3 Results

3.3.1 Stro-4 expression

Stro-4 expression of cells immediately following MACS isolation was confirmed by fluorescence microscopy on cells in suspension. Temporal expression of Stro-4 was monitored by immunofluorescence over successive passage until a signal was no longer present – this was typically by passage 3 of culture, Figure 3-5.

The presence of Stro-4 antigen expression was confirmed by fluorescent immunolabelling of freshly sorted cells, using a directly Alexa488-conjugated anti mouse-IgG to detect Stro-4 bound supernatant. The persistence of Stro-4 expression was observed through passages 1 to 3. The expression of Stro-4 declined rapidly after initial passage and was uniformly absent in passage 3 cells. The absence of Stro-4 at passage 3 subsequently determined the definition of early and late passage cells (presence and absence of Stro-4 antigen).

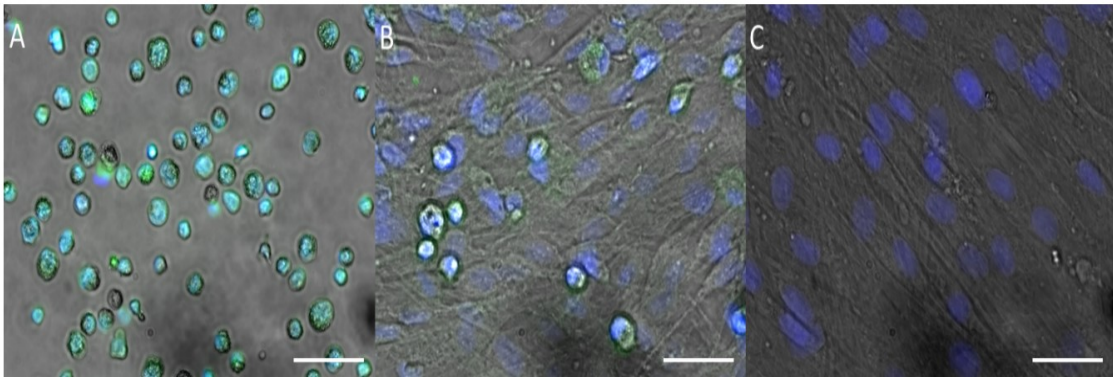

Figure 3-5 Fluorescence microscopy showing Stro-4 expression. Stro-4 in green (Alexa488), nuclear counter stained blue (DAPI). A) Cells in suspension immediately post MACS isolation of fresh ovine bone marrow mononuclear cells. B) Stro-4 expression of adherent passage 0 cells. C) Loss of Stro-4 signal by the end of passage 3. Scale bar= 50µm.

3.3.2 *In vitro* growth characteristics

3.3.2.1 Population Doubling Time (PDT)

BMMNC primary culture is characterised by and variable period of adhesion during which the cells recover from sorting protocols, expression of adhesion molecules, settling and adhering to tissue culture plastic. Both unselected and Stro-4 enriched populations followed a similar cellular proliferation profile, with no statistical difference between the PDT of selected and unselected populations at any matched time point. Population doubling time remained between 20 and 30 hours for passages 1 and 2, (SD 12 hours), **Figure 3-6**. Growth rate began to decline at passage three, PDT 24 -64 hours (SD 21). The growth profile for both selected and unselected cells over passages 4 and 5 decelerated with a PDT range between 38 and 110 hours at P5 (SD 24), **Figure 3-6.** Variation between samples across both groups increased with subsequent passage, the variation in growth profile correlated with changes in morphology and CFU-F capacity over time and passage.

3.3.2.2 Population doubling times, plotted

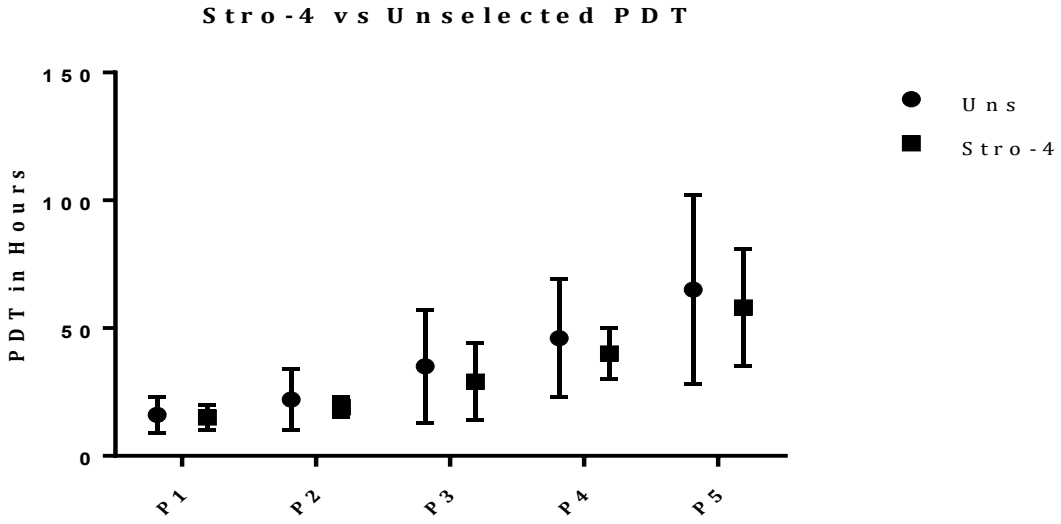

Figure 3-6 Population Doubling Time (PDT, in hours) of Ovine Skeletal Stem Cells cultured *in vitro*. Comparative growth rate of Stro-4 and Unselected Ovine-SSCs. Note: Due to large variations in adhesion and proliferation, passage zero has not been included. Variation within groups increased with passage. Error bars = standard deviation, N = 5 for all time points and both cell groups, no statistical significance found between selected and unselected populations matched for passage.

3.3.2.3 Colony Forming Unit-Fibroblast (CFU-F) Assay

Colony forming unit potential was determined by contact independent tissue culture plastic adherence and proliferation. CFU-F numbers for both selected and unselected cell populations were not significantly different when matched for passage, across all recorded passages, P0-P5. When P0 unselected vs Stro-4 were plotted individually, Stro-4 CFU-F numbers were significantly higher than unselected samples, Figure 3-8.

Passage zero CFU-F was lowest for all passages at 33-45 colonies per 10,000 cells. P0 growth was significantly lower than P1, P2 and P3 for unselected and selected populations. CFU-F numbers between passages 1, 2, 3 and 4 were similar, varying from 94-110 colonies per 10000 cells for both cells groups over all time points. Colony formation at passage 5 rapidly declined to a mean of 58 colonies per 10,000 cells in both selected and unselected populations but was not significantly lower compared with P1-P4, **Figure 3-7.**

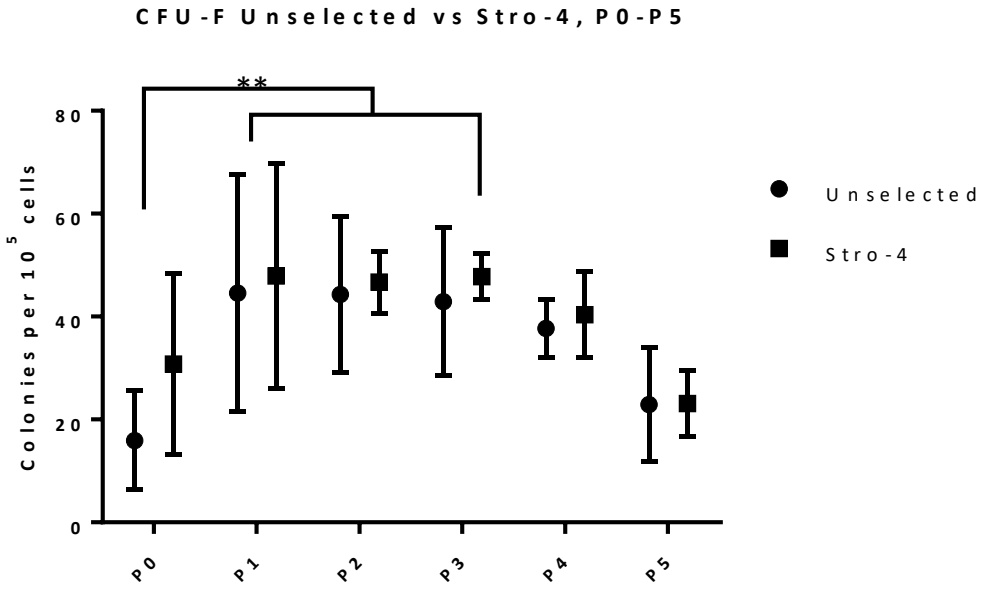

Figure 3-7 Stro-4 and Unselected Ovine-SSCs Colony Forming Unit capacity with passage. Stro-4 and unselected SSCs displayed similar colony forming capacity from early to late passage. P0 colony forming capacity was poor in comparison to that seen at P1 and sustained until P3, slowly tapering off at late passage (P5). Error bars = standard deviation (SD), N= 5, ANOVA, comparison between passage means.

3.3.2.4 Direct CFU-F comparison between passage zero Stro-4 enriched and unselected BMMNCs

Passage zero cells were isolated and cultured either unselected or after Stro-4 selection as described in methods, page 81 section 2.2

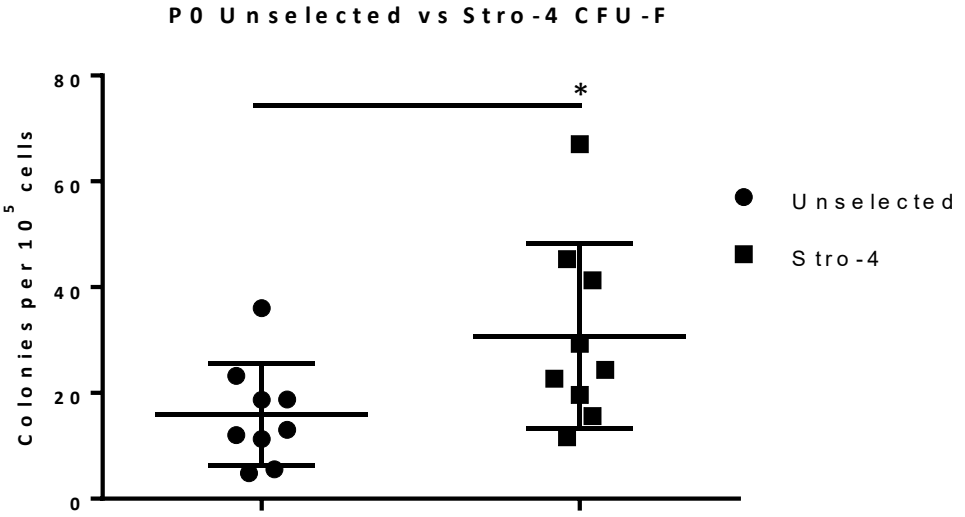

Figure 3-8 P0 Unselected vs Stro-4 CFU-F. The number of colonies formed by Stro-4 was significantly higher than unselected population at P0, n=9, unpaired t-test, P=0.0413

3.3.3 Tri-Lineage differentiation of ovine unselected and Stro-4 BMMNCs at early and late stage passage culture

Cells from both selected and unselected populations were successfully culture *in vitro*. There was a positive lineage specific differentiation response to osteogenic, chondrogenic and adipogenic conditioned media although adipogenic response was diffuse and sparse, Figure 3-9 and Figure 3-10. It was evident that a lineage bias presented towards a chondrogenic phenotype, a culture feature not seen in human adult Stro-1 selected cells.

Passage 2 osteogenic response. Unselected and Stro-4 BMMNCs responded to osteogenic differentiation media. Changes in morphology were noted from 3-5 days with visible mineral inclusions present from 10 days. Calcium content assessed by Alizarin red staining on day 21 cultured cells was present in both cell groups under conditioned media, Figure 3-9 middle row. There was a negligible background staining observed in basal controls.

Passage 2 chondrogenic response. Intense stain uptake of alcian blue was observed in both selected and unselected groups under conditioned media. There was a marked visual difference in intensity in Stro-4 over unselected cells. Proteoglycan (glycosaminoglycan) presence was detected in each of the cell groups cultured in basal conditions as well as chondrogenic conditioned media, the effect was macroscopically increased in the Stro-4 group, Figure 3-9 top row.

Passage 2 and 5 adipogenic response. Lipid accumulation as assessed by Oil Red O staining was negligible in both selected and unselected populations grown in adipogenic conditions for both passages. Lipid size was small and intermittently dispersed. There were no lipid accumulations observed under basal conditions**,** Figure 3-9 and Figure 3-10 bottom row.

Passage 5 osteogenic response. Alizarin red staining was present in both cell groups at later passage (P5) although staining was reduced compared with early passage (P2), both stain intensity and stain distribution was reduced, Figure 3-10, middle row.

Passage 5 chondrogenic response. The intense stain uptake observed in passage 2 cultures remained present in passage 5 cells. Glycosaminoglycan presence was clearly demonstrated in both cell groups under basal conditions. Staining intensity was overtly stronger in Stro-4 cells under chondrogenic conditions. When assessed by alcian blue staining, the chondrogenic potential of both cell groups did not appear to diminish between passage 2 and 5, see Figure 3-9 and Figure 3-10 for comparison.

3.3.3.1 Tri-lineage differentiation of passage 2 selected and unselected skeletal stem cells

Cell culture and differentiation, including description of reagents is given, page 80 paragraph 2.1.3

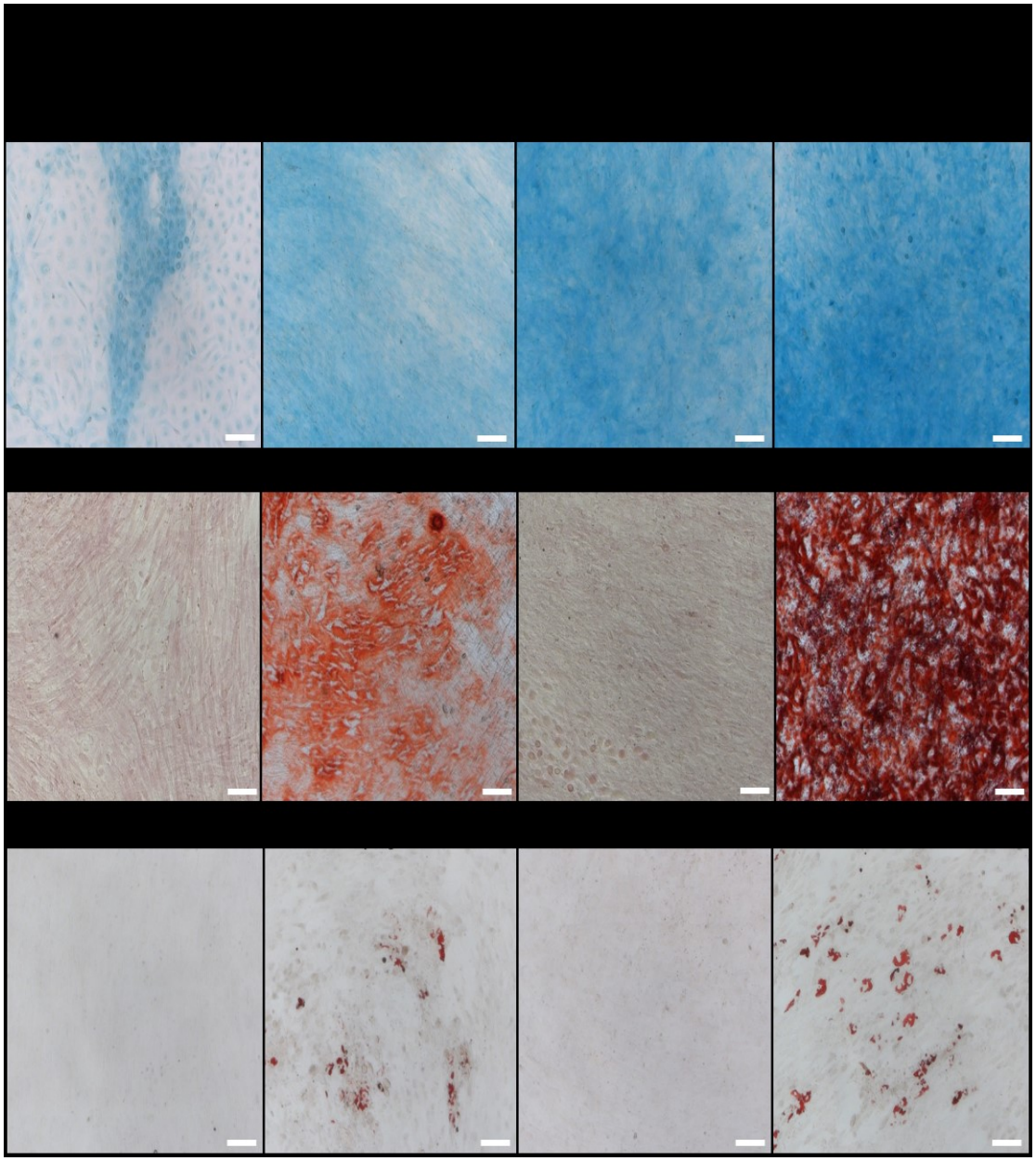

Figure 3-9 Tri-lineage Differentiation of passage 2 Unselected and Stro-4 enriched ovine BMMNCs. An enhanced osteogenic response observed in the Stro-4 population over unselected, alizarin red stain. Chondrogenic response was comparable between Stro-4 and unselected cell groups with inherent chondrogenic activity noted in the Stro-4 population under basal conditions, alcian Blue stain. Adipogenic response in both groups was present but unconvincing, assessed by Oil Red O staining. N = 4, both groups for each condition. Scale bar = 200µm.

3.3.3.2 Tri-lineage differentiation of passage 5 selected and unselected skeletal stem cells

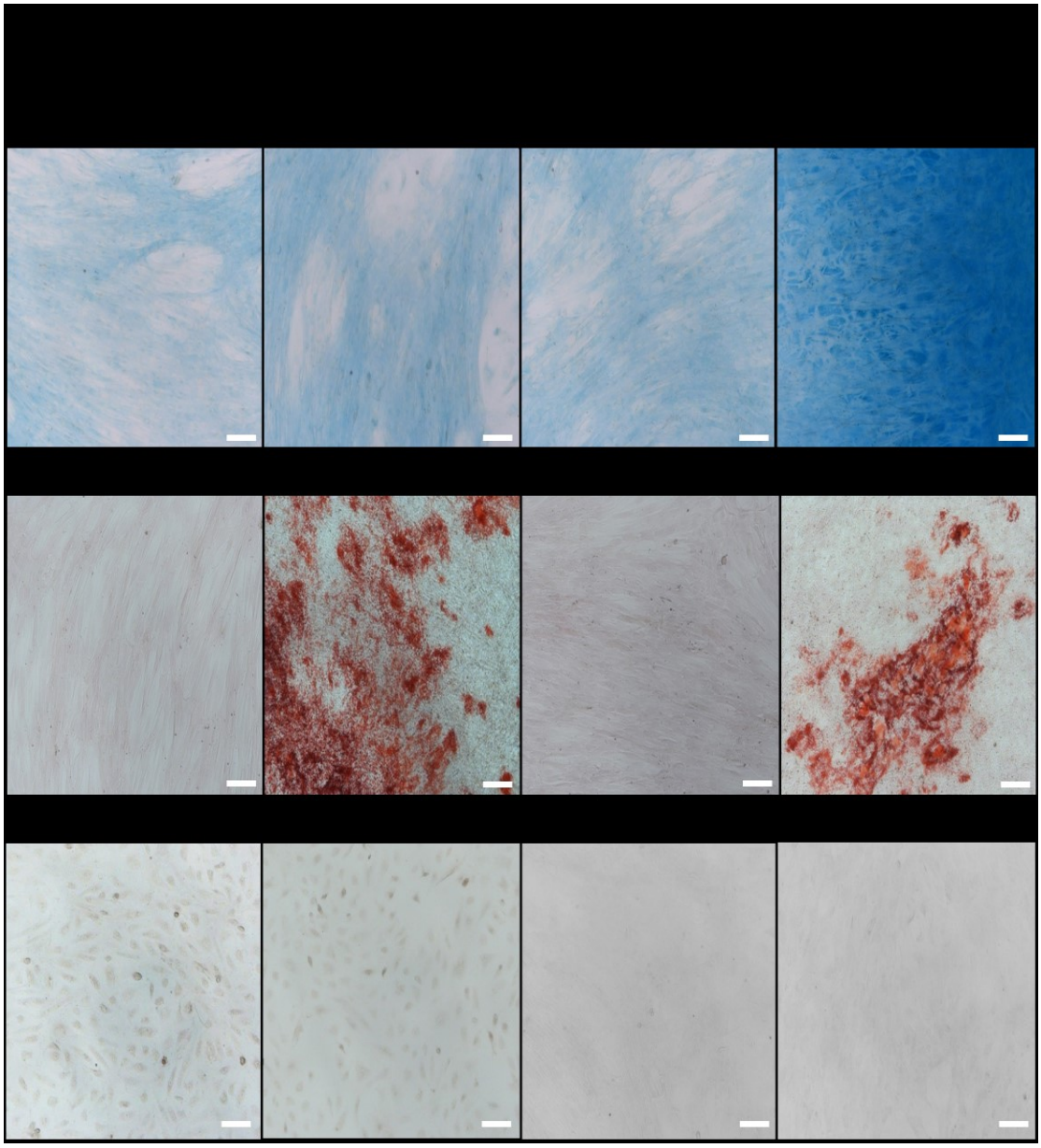

Figure 3-10 Tri-lineage Differentiation of Passage 5 unselected and Stro-4 enriched ovine BMMNCs. Response to osteogenic media was present in both cell groups although diminished compared to passage 2, Alizarin red. The chondrogenic response in unselected cells had diminished at passage 5 but was conserved in the Stro-4 enriched population, alcian blue. Adipogenic differentiation was not present in either populations. N = 4, both cell groups for each condition. Scale bar = 200µm.

3.3.4 Quantification of staining intensity by histomorphometry

Early passage cells (P2) responded actively to conditioned media for chondrogenic and osteogenic lineages. The chondrogenic response was marked, staining was detected under basal and conditioned media. Stro-4 cells demonstrated significantly more alcian blue stain uptake under basal conditions than unselected cells. Stro-4 also showed a clear difference in staining intensity over unselected cells in chondrogenic conditions, $p<0.005$ for both. Proteoglycan deposition in the Stro-4 population cultured in basal media was significantly higher than unselected cells cultured under chondrogenic conditions, $p=0.0007$, Figure 3-11.

Both cell populations responded to osteogenic conditioned media but neither group demonstrated a measurable osteogenic response under basal conditions. Selected and unselected groups had significantly stronger staining intensity under osteogenic conditions compared to basal conditions, $p<0.005$, there was no significance between Stro-4 and unselected groups, Figure 3-12.

The osteogenic response diminished dramatically in later passage (P5), alizarin red staining was detectable under osteogenic conditions but was not significant between basal and osteogenic media between unselected ($p=0.1150$) and Stro-4 ($p=0.0507$). Calcium accumulation noted in Stro-4 cells at passage 2 was significantly higher than at passage 5 ($p=0.0006$), Figure 3-16.

By comparison, the chondrogenic capacity of Stro-4 selected cells appears to maintain through until later passage (P5), Stro-4 cells in basal conditions showed an increase in stain intensity for proteoglycan over unselected cells in basal media ($p=0.0074$). Stro-4 also showed significant alcian blue staining intensity over unselected cells when cultured in chondrogenic media ($p=0.0369$). Proteoglycan deposition in Stro-4 cells cultured in basal media was significantly higher than unselected cells cultured in chondrogenic media ($p=0.029$). As seen in passage 2, there was no significant difference between Stro-4 cells cultured under basal and chondrogenic conditions. A clear chondrogenic capacity was noted in Stro-4 cells, which was maintained throughout passages. There was no statistically significant reduction in alcian blue staining intensity in selected and unselected cells between passage 2 and passage 5, Figure 3-15**.**

For all graphs, *$p<0.05$ **$p<0.01$ ***$p<0.001$ and ****$p<0.0001$ unless otherwise stated

3.3.4.1 Histomorphometry of alcian blue staining, P2

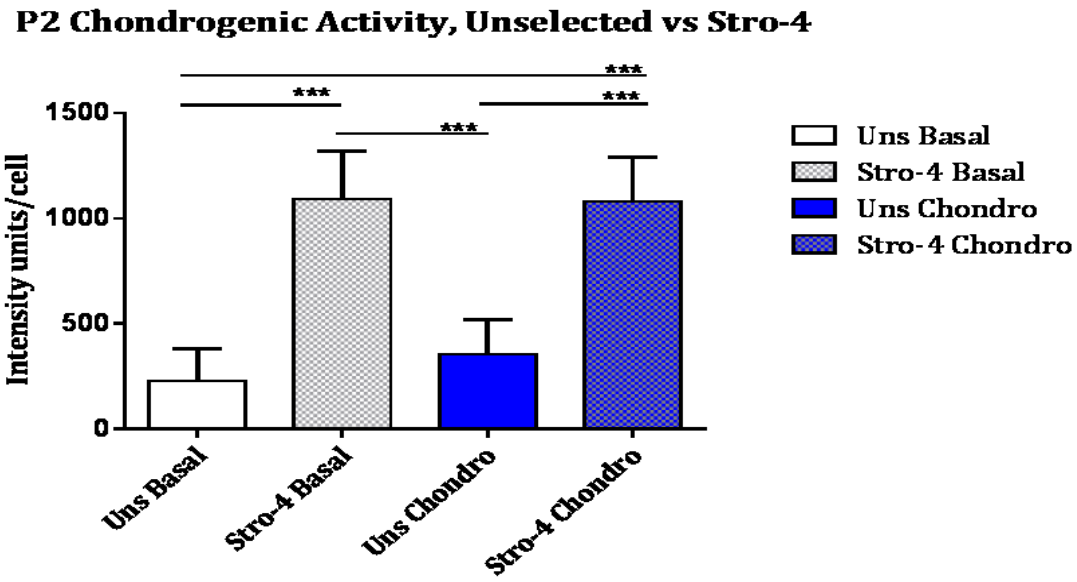

Figure 3-11 Quantification of alcian blue staining to assess *in vitro* chondrogenic response in passage 2 unselected and Stro-4 populations. Stro-4 enriched SSCs showed increased staining intensity compared to Unselected SSCs. Stro-4 enriched cells cultured in basal media expressed an innate chondrogenic response in the absence of exogenous growth factor cues. N = 4, data presented as means with error bar = SD.

3.3.4.2 Histomorphometry of Alizarin red staining, P2

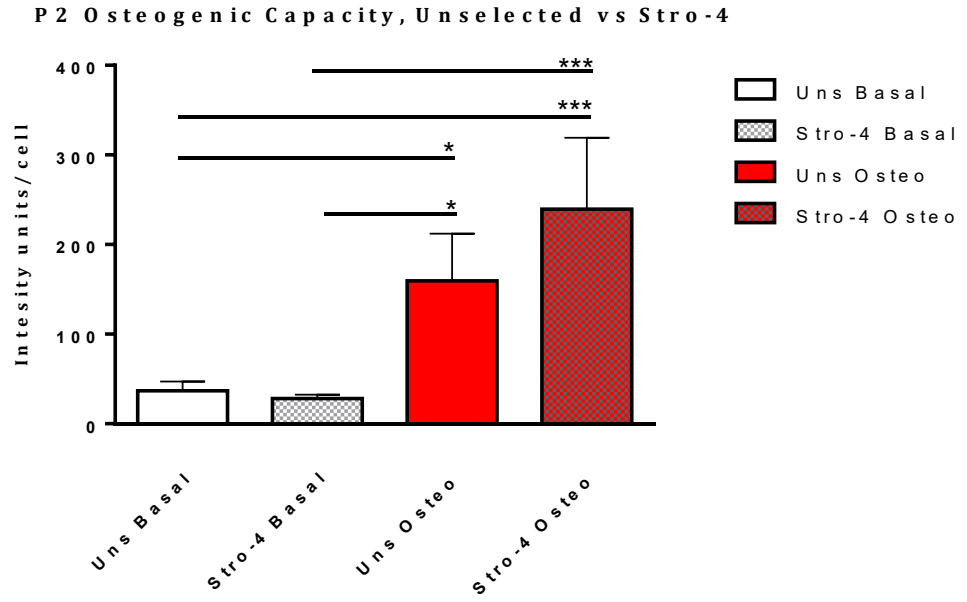

Figure 3-12 Quantification of Alcian Blue staining to assess *in vitro* chondrogenic response in passage 2 unselected and Stro-4 populations. Both populations showed a positive phenotypic change under osteogenic conditions but did not show a significant difference between unselected and enriched populations. In contrast to chondrogenic differentiation, no innate osteogenic response was noted under basal culture conditions. N = 4, data presented as mean with error bar = SD.

3.3.4.3 Histomorphometry of Alican Blue staining, P5

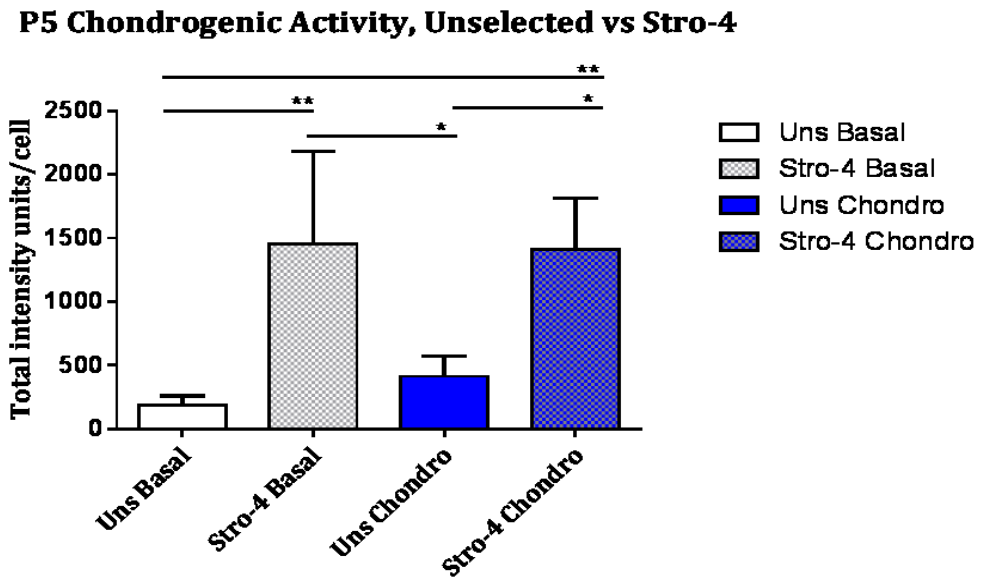

Figure 3-13 Cell Profiler Quantification of Alcian Blue staining to assess *in vitro* Chondrogenic response in passage 5 Unselected and Stro-4 populations. Under both basal and chondrogenic conditions, Stro-4 enriched SSCs responded positively showing significant increases in staining intensity compared to Unselected cells. The response pattern between groups appears similar to that seen at passage 2. N = 4, data presented as mean with error bar = SD.

3.3.4.4 Histomorphometry of Alizarin red staining, P5

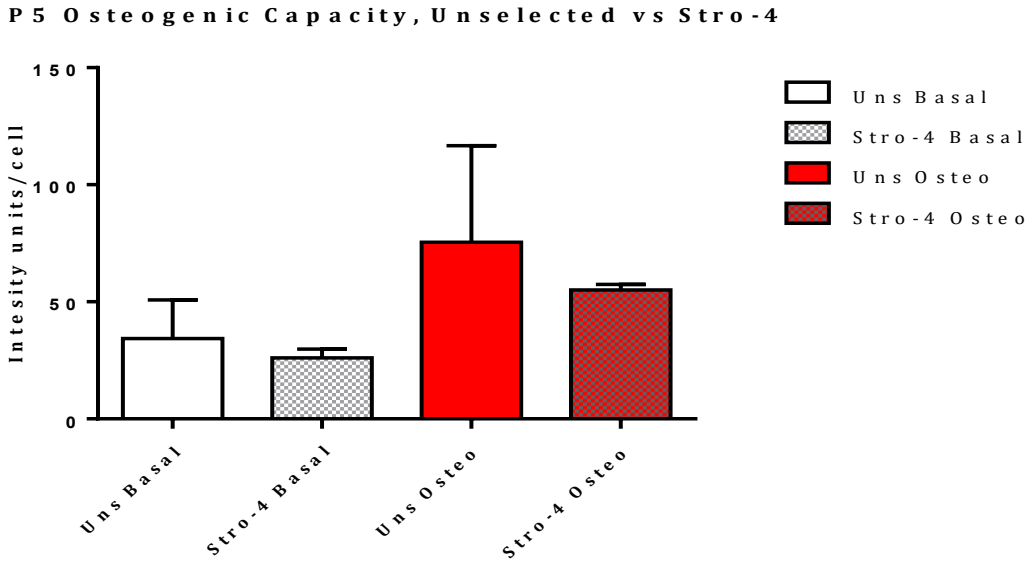

Figure 3-14 Cell Profiler quantification of alizarin red staining to assess *in vitro* Osteogenic response in passage 5 Unselected and Stro-4 populations. Cellular response to osteogenic media diminished in late passage. Although osteogenic response was present there was no significant difference in osteogenic response between conditioned and basal media. N = 4, data presented as mean with error bar = SD.

3.3.4.5 Comparison of Chondrogenic response P2 vs P5

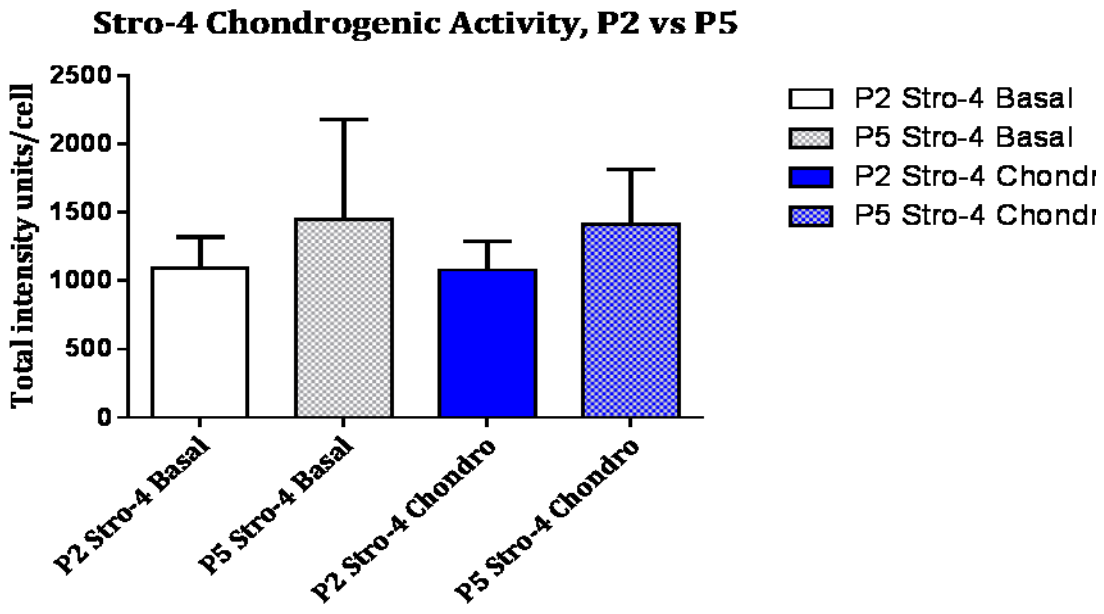

Figure 3-15 Cell Profiler quantification of alcian blue staining intensity, comparing early (P2) and late (P5) passage Stro-4 populations. Chondrogenic phenotypic change is noted in both basal and conditioned media in both early and late passages. Stro-4 enriched populations maintain chondrogenic capacity through cell culture passages. N = 4, data presented as mean with error bar = SD.

3.3.4.6 Comparison of Osteogenic response P2 vs P5

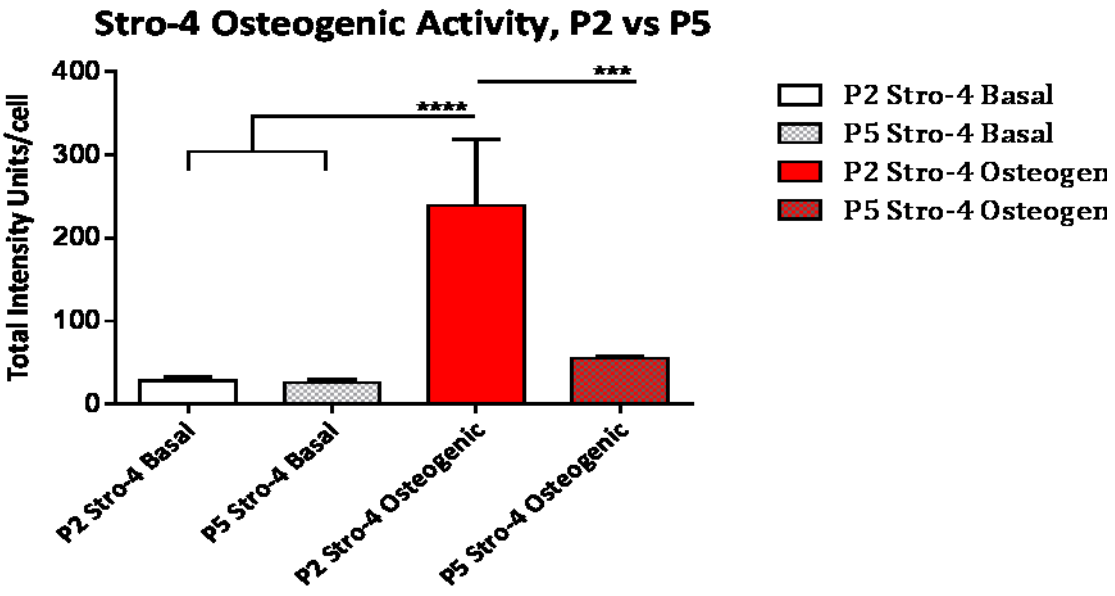

Figure 3-16 Cell Profiler quantification of alizarin red staining intensity, early (P2) compared to late (P5) passage Stro-4 populations. Osteogenic capacity of early passage Stro-4 cells was significantly stronger than at later passages. Early passage Stro-4 cells exhibited a stronger osteogenic response than unselected populations. N = 4, data presented as mean with error bar = SD.

3.3.5 Molecular analysis of Osteogenic, Chondrogenic- and Adipogenic gene expression

cDNA was produced using isolated RNA from lysed cells cultured under lineage specific conditions *in vitro* as previously described in methods. Samples were exposed to osteogenic, chondrogenic and adipogenic media and cultured in monolayer for a period of 21 days using established differentiation protocols routinely used in culture and differentiation of human BMMNCs. All samples (n=4) responded positively to media containing osteo-, chondro and adipogenic factors with subsequent lineage differentiation lineages, these data mirror that seen by histomorphometric analysis of 2-D cultures, see 3.3.4.

3.3.5.1 **Osteogenic gene expression in monolayer culture**.

Expression of *COL1A1*, the primary structural collagen in bone and Osteocalcin (OCN), an osteoblast specific regulatory protein, was variable between conditions and cell type. Stro-4 enriched cell cultures showed a 1.64 fold increase (SD 2.37) in *COL1A1* in osteogenic media maintained in basal conditions over 21 days with a non-significant 1.08 fold increase (SD=0.45) in *COL1A1* expression in unselected population, Figure 3-17. Two of the four samples showed minimal *COL1A1* expression under basal culture conditions. *COL1A1* was upregulated across both cell populations under chondrogenic and osteogenic culture conditions, Figure 3-18 and Figure 3-19. Unselected populations showed a 4.38 (SD=2.61) and 3.34 (SD=1.85) fold increase under chondrogenic and adipogenic conditions respectively, compared with a 5.36 (SD=8.44) and 2.55 (SD=1.36) in Stro-4 selected populations.

Osteocalcin expression was reduced under osteogenic media in both cell populations, 0.81 in unselected (SD=0.76) and 0.90 in Stro-4 (SD=0.83), not significant. There was a non- significant upregulation of OCN in unselected cells under chondrogenic conditions 6.50 fold with a SD of 15.18 and 3.04 fold in Stro-4 cells, SD= 28.30, Figure 3-18.

3.3.5.1.1 Osteogenic gene expression

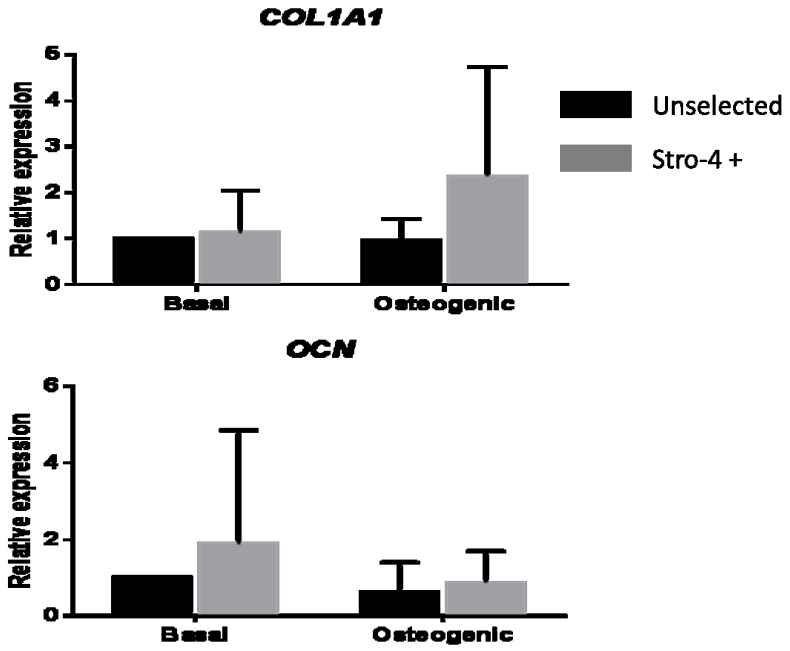

Figure 3-17 Osteogenic gene expression of unselected and Stro-4 enriched ovine-BMMNCs.
There was no significant difference in COL1A1 expression between selected and unselected populations cultured under basal and osteogenic conditions. Osteocalcin expression was low and variable in conditioned media in selected and unselected groups. N = 4, error bar =SD

3.3.5.1.2 Osteogenic gene expression from monolayer culture, basal, osteogenic and chondrogenic media

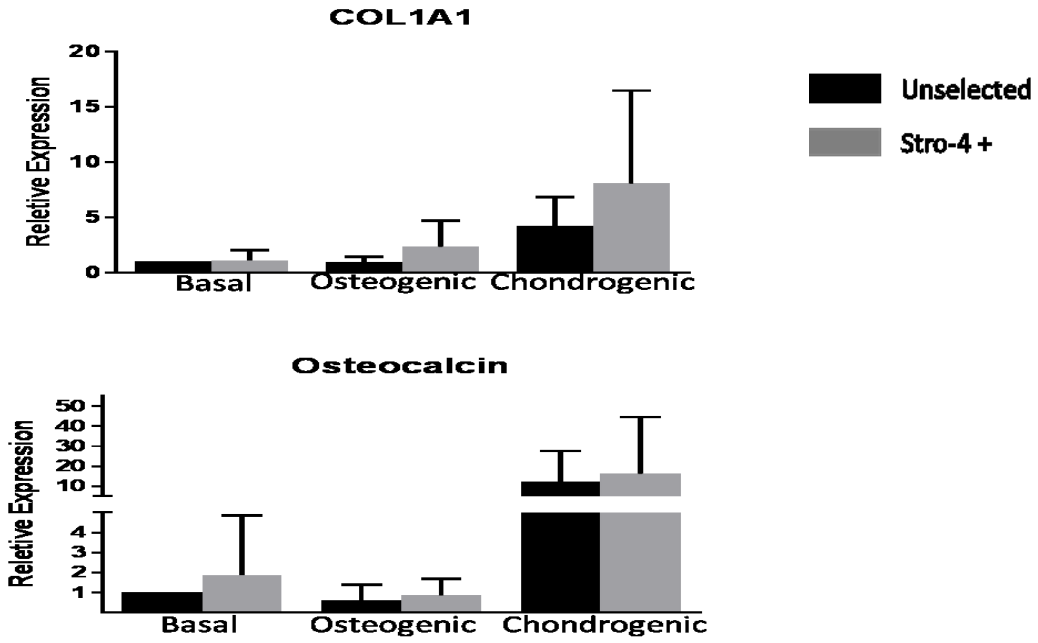

Figure 3-18 Osteogenic gene expression following culture in different media conditions.
COL1A1 expression in osteogenic and chondrogenic media failed to show a statistically significant difference between media conditions. A non-significant increase in COL1A1 expression following culture in chondrogenic media was observed. Osteocalcin expression increase under osteogenic media was not significant. N = 4, error bar = SD.

3.3.5.2 Chondrogenic gene expression in monolayer.

Cellular response to chondrogenic differentiation in 2-Dimensional monolayer was exceptional with significant increases in *COL2A1*, *ACAN* (Aggrecan) and *SOX-9* expression over basal conditions, Figure 3-19**.**

COL2A1 gene encodes for a component of type II collagen, found abundantly in cartilage. Under chondrogenic conditions, unselected cells expressed a mean 216 fold increase (SD=947.74) whilst Stro-4 selected cells demonstrated a relative upregulation of 1760.16 times control levels, SD = 9052.92. In both populations, all four samples expressed upregulation, but the large standard deviation in both groups is attributed to two out of four samples displaying an exceptional chondrogenic response. Stro-4 populations also showed a 6.12 fold increase in *COL2A1* gene expression when cultured in basal conditions, Figure 3-19**.**

Up regulation of *ACAN*, an integral cartilage extracellular matrix protein, paralleled *COL2A1* with relative expression of 630.34 fold (SD=9182.93) in unselected cells and 1831.34 fold (SD=17444.40) in the Stro-4 population under chondrogenic conditions. Four out of four unselected samples were in excess of 400 fold upregulation compared with four out of four Stro-4 samples which were in excess of a 1300 fold increase. *ACAN* was increased in Stro-4 cells under basal conditions (20.44 fold, SD=29.72) indicating a chondrogenic predisposition in the Stro-4 selected population.

SOX-9 is a regulatory protein in chondrocyte development working in concert with *COL2A1* during cartilage development. *SOX-9* expression was upregulated in chondrogenic conditions 5.98-fold in unselected populations and 6.34 in Stro-4 populations, SD of 6.98 and 6.43 respectively.

3.3.5.2.1 Chondrogenic gene expression, monolayer culture Figure 3-19

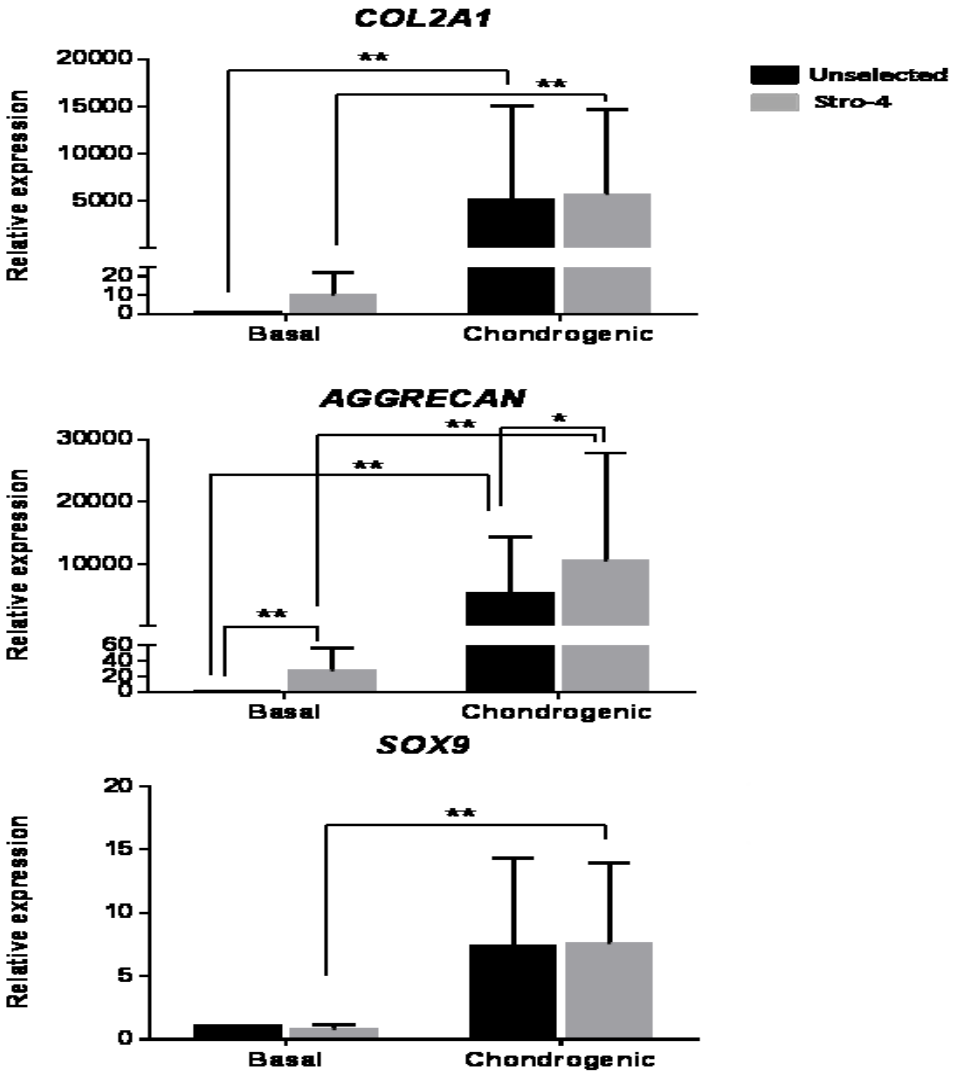

Figure 3-19 Chondrogenic gene expression. Selected and unselected cells groups cultured in monolayer. COL2A1 displayed a significant upregulation in both cell groups in basal vs chondrogenic conditions. ACAN expression was upregulated in basal vs chondrogenic conditions. SOX-9 expression was significantly upregulated between basal and chondrogenic conditions in selected cells, a non-significant upregulation was present in the unselected cell population. N = 4 Error bar = SD.

3.3.5.3 Adipogenic gene expression, monolayer.

Peroxisome proliferator-activated receptor gamma (*PPAR-γ*) is a type II nuclear receptor found in many tissue types throughout the body but is of particular importance in adipose metabolism and lipid storage. The absence of validated adipogenic gene primers in the sheep resulted in only *PPAR-γ* being investigated in the current study. Under basal conditions Stro-4 selected cells showed a very slight increase in expression (1.27-fold, SD= 0.26) compared with unselected equivalent. When cultured in an adipogenic environment unselected, (3.34 fold, SD=12.10), and selected (4.07 fold, SD=20.49) populations displayed a similar increase in *PPARG-γ* expression. No significant differences were noted between groups or between conditions, Figure 3-20.

Unusually there was an increase in *PPARG-γ* expression in cells cultured under osteogenic conditions. The unselected population showed a median 5.12 fold increase (SD=3.67). Stro-4 cells displayed a clear and significant 32-fold (SD=28.63) increase in *PPARG-γ* expression when cultured in osteogenic conditions. Figure 3-21**.**

3.3.5.4 Chondrogenic gene expression in 3-D micromass culture

The effect of micromass culture on unselected and selected populations upregulated *COL2A1* (1681.89, SD=2042.52 and 415.72, SD=699.76), *ACAN* (174.34, SD =131.73 and 118.57, SD=30419.96) and *SOX-9* (56.89, SD=41.48 and 22.65, SD= 23.05) when cultured in basal media. Micromass culture in chondrogenic media further increased *COL2A1* (9297.29, SD= 8605.48 and 4904.08, SD=5169.35) and *ACAN* (3935.52, SD=36770.89 and 2018.06, SD=140379.68) expression in both unselected and selected group. No significant increase in *SOX-9* expression was observed between micromass cultured in basal and chondrogenic media. This effect was seen in both unselected (17.84 fold increase, SD=11.20) and selected cells (10.50 fold, SD=4.64). Figure 3-22.

3.3.5.5 Peroxisome proliferator activated receptor gamma expression; basal and adipogenic media

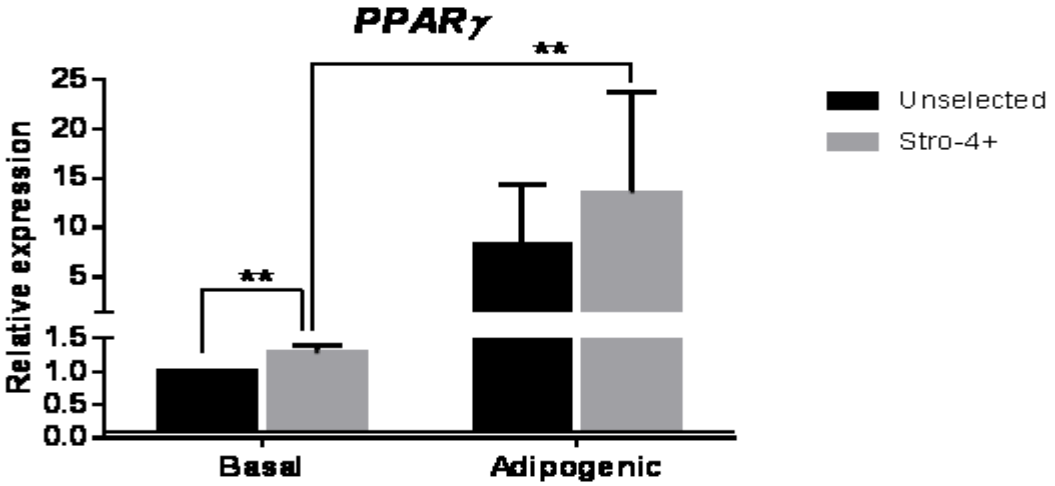

Figure 3-20 Peroxisome Proliferation Activated Receptor- Gamma expression. PPAR-γ was upregulated in response to adipogenic conditioned media. Significant upregulation was noted between unselected and selected populations in basal media and between Stro-4 in basal and conditioned media. N = 4, error bar = SD, ** p=<0.05.

3.3.5.6 Peroxisome proliferator activated receptor gamma expression; osteogenic and adipogenic media

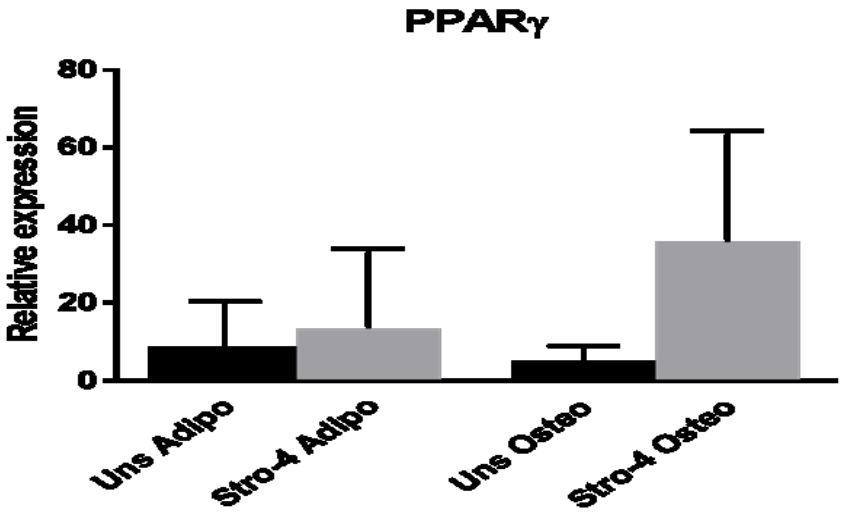

Figure 3-21 PPARγ expression under adipogenic and osteogenic conditions. Stro-4 selected and unselected ovine BMMNCs express PPARγ when cultured under adipogenic and osteogenic conditions. N = 4, error bar = SD.

3.3.5.6.1 Chondrogenic gene expression

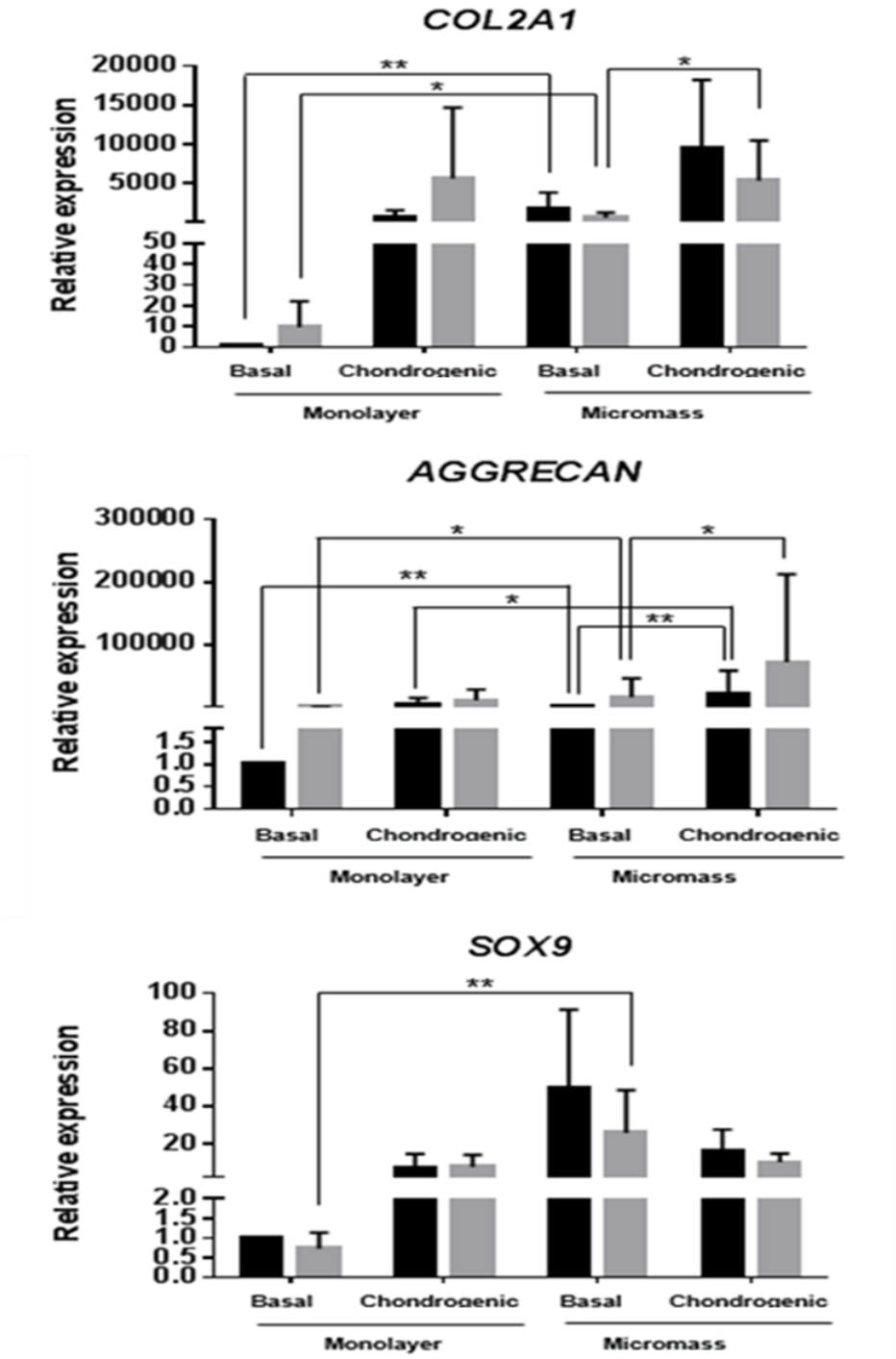

Figure 3-22 Chondrogenic expression of micromass and monolayer cultures. Chondrogenic gene upregulation was seen in micromass culture under basal conditions. Gene expression pattern between groups was variable, as described above. N =4, error bar = SD.

3.3.6 Stro-4 seeded and unseeded bovine extracellular matrix hydrogels localised by melt-electrospun PCL microfiber mesh; macroscopic and µCT description

Ex vivo day 18 chick femurs were combined with a proprietary PCL microfiber mesh (described in 3.2.5), ECM hydrogel mesh and Stro-4 ovine SSCs. The CAM femur model was chosen to provide functional assessment of Stro-4 within an *in vivo* environment, the model is used routinely in the Bone and Joint Research Group and provides a biologically dynamic alternative to other models such as ceramic chip and subcutaneous assays.

CAM survival was within accepted model tolerances, 60-70%., although a lower number of samples were integrated with the CAM membrane and were not included in analysis. Integration into the CAM is an essential aspect of the model, if it has not occurred then results are considered unreliable.

Images of samples at harvest demonstrate viability and membrane integration (when present), Figure 3-23. Further qualitative and analysis was provided by µCT, Figure 3-24 and histology, Figure 3-25, Figure 3-26 and Figure 3-27. A summary of experimental groups, survival and integration is given below:

3.3.6.1 Experimental groups, egg viability and membrane integration

Group	Seeded	PCL Mesh	ECM	Survived (out of 6)	Integrated
I	None	Yes	None	4	3
II	None	Yes	Yes	4	2
III	Stro-4 ovine	Yes	Yes	4	3

3.3.6.2 Group I: Blank femurs with PCL mesh

Femurs and mesh constructs showed integration with the CAM membrane with evidence of soft tissue and blood vessel invasion. 4/6 scaffolds were retrieved intact from a viable egg, with 3/4 viable samples clearly integrated into the CAM. µCT evaluation showed a clear boundary demarcation between femur segment ends, bone edges were squarely outlined showing no signs of new bone growth. Small nucleations of bone-density material was seen on outer boundaries of the scan region, but not in contact with sample femurs. It is not certain that these bone spicules are localised to mesh fibres but historical data shows blank control femurs do not contain ectopic bone accumulations of this nature. No bone growth within or around the defect boundaries was noted in any of the blank PCL mesh only control femurs.

3.3.6.3 Group II: Femurs with PCL mesh and bovine ECM Hydrogel

Group II only produced two samples which had both survived (4/6) and which had integrated into the membrane (2/4) the addition of bECM hydrogel did not adversely alter chick survival, although sample numbers were low. The defect space itself did not appear to have been maintained as no rigid fixation was employed to stabilise the femur constructs.

Along the bone periphery, in a region continuous with periosteum, amorphous cloudy low dense opacities were present proximal and distal to the defect area. Bone segments at either end of the defect were easily delineated, a small degree of “softening” to the defect edges was evident, linked to early new tissue formation. New bone outgrowth from both defect edges was clear in both the well-integrated samples, although the degree of bone formation was small, Figure 3-24. Bone outgrowth and periosteal reaction is confirmed by histology, Figure 3-25 B-1 and B-2, and clearly distinct from mesh only control, Figure 3-25, A-1 and A-2.

3.3.6.4 Group III: Femurs with PCL mesh and Stro-4 seeded bovine ECM hydrogel

In group III, 4/6 eggs were viable at harvest with 3/4 samples from viable eggs well integrated into the CAM, in these samples, blood vessel and soft tissue ingrowth was visible macroscopically, with a hierarchy of vessel size distributed ubiquitously over the mesh surface and smaller vessels appearing more numerous than in control and mesh/bECM groups.

When viewed on µCT, the defect was completely bridged and the defect substance filled with new bone. Sagittal cross-sectional views confirmed the presence of bone throughout defect region with new bone formation appearing structurally in longitudinal bone columns and nodules. The external texture of new bone was pitted in appearance, the significance of which is unknown but, as a matter of conjecture may relate to vessel invasion, this pattern has been noted historically in samples with proven strong vascular assimilation.

3.3.6.5 Femurs at time of harvest from viable egg, demonstrating CAM integration

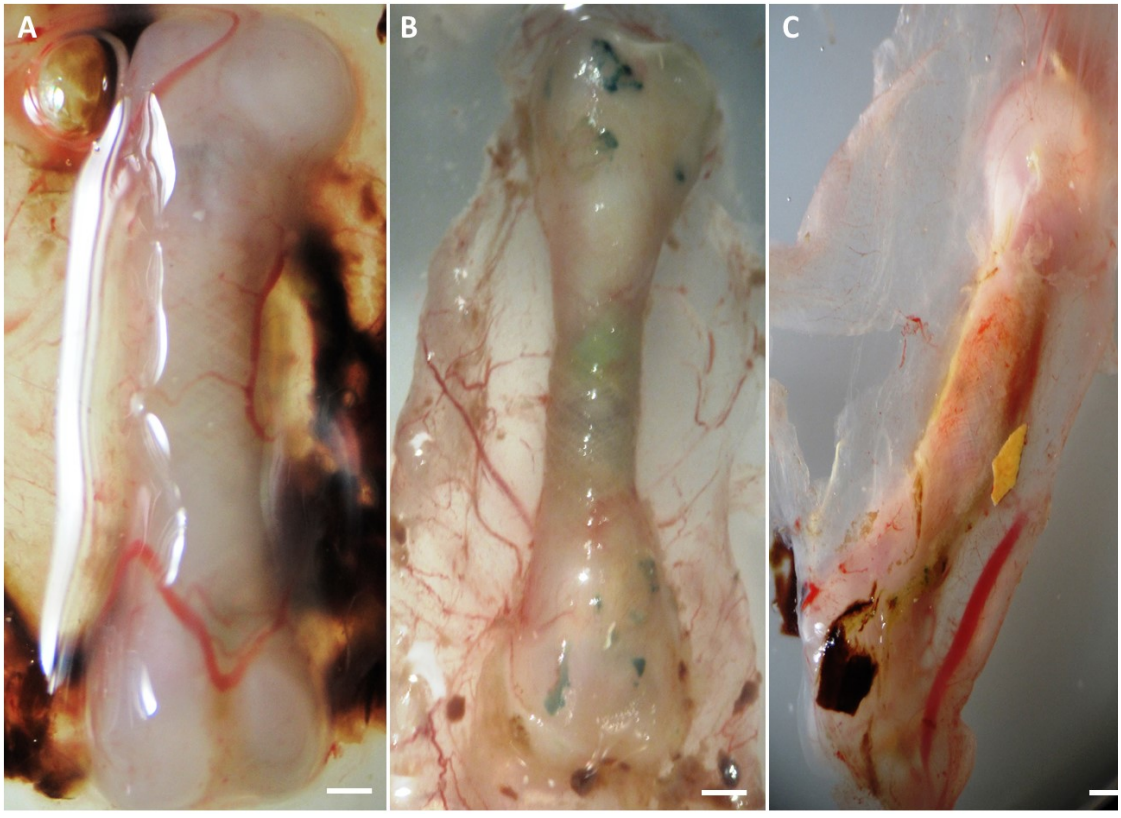

Figure 3-23 Chick femurs at harvest. Stro-4 PCL ECM study. A) Femur with blank mesh. B) Femur with mesh and ECM. C) Femur with PCL mesh, ECM hydrogel seeded with Stro-4 ovine SCCs. N =3, Scale bar = 2mm

3.3.6.6 Micro Computed Tomography; PCL, bECM, Stro-4 femur constructs

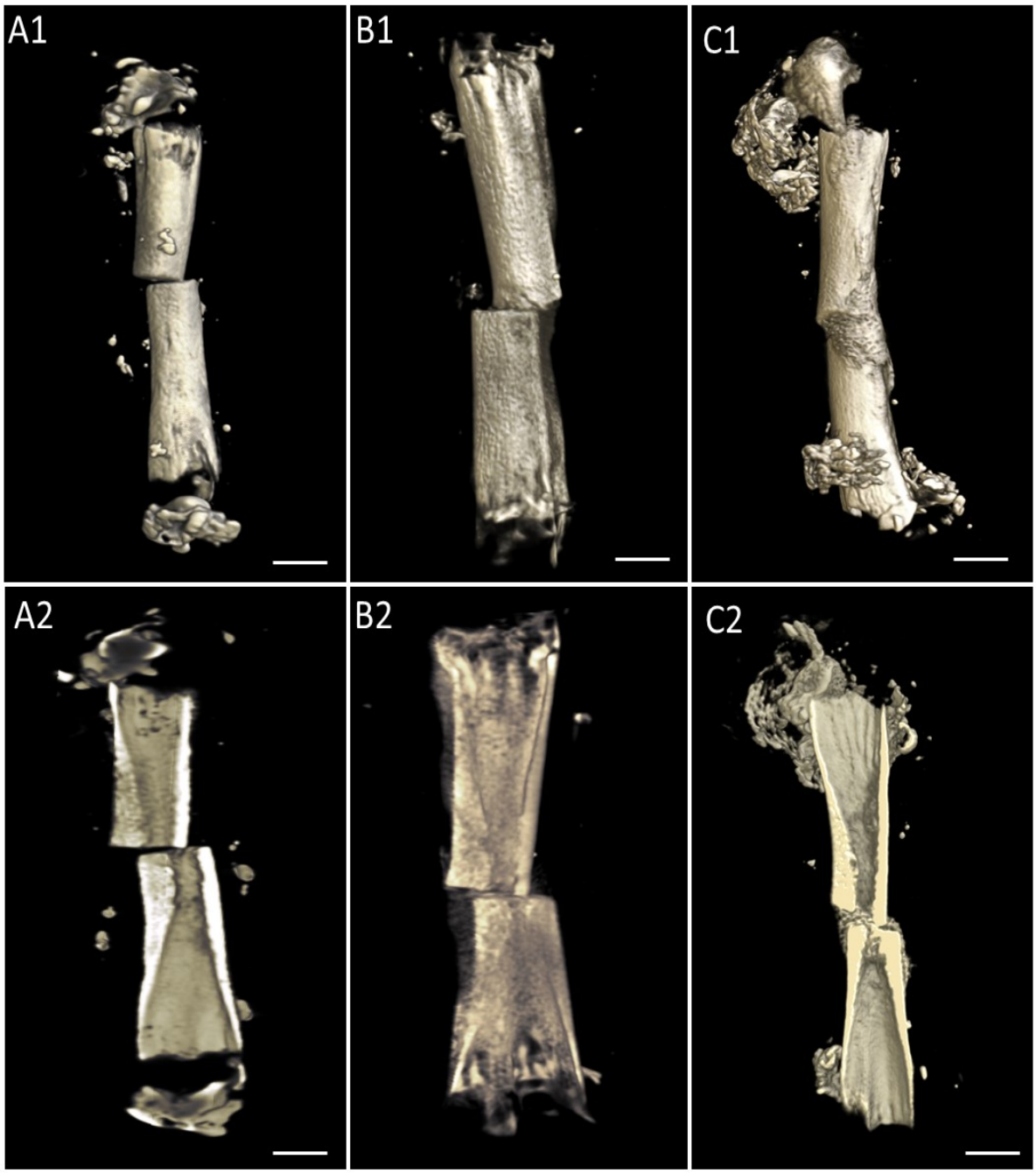

Figure 3-24 Micro-Computed Tomography images of day 18 CAM femurs. Stro-4 PCL Mesh ECM Hydrogel constructs. A) Unseeded Mesh alone. B) Unseeded Mesh and blank ECM. C) PCL Mesh and Stro-4 Seeded ECM. No new bone growth was noted in blank mesh. Areas of low opacity noted in the blank and blank ECM controls. New bone formation and bony bridging was observed in the Stro-4 seeded ECM/PCL mesh group. N =3, scale bar = 3mm.

3.3.6.7 Alcian blue and sirius red; blank mesh, unseeded bECM and Stro-4 bECM

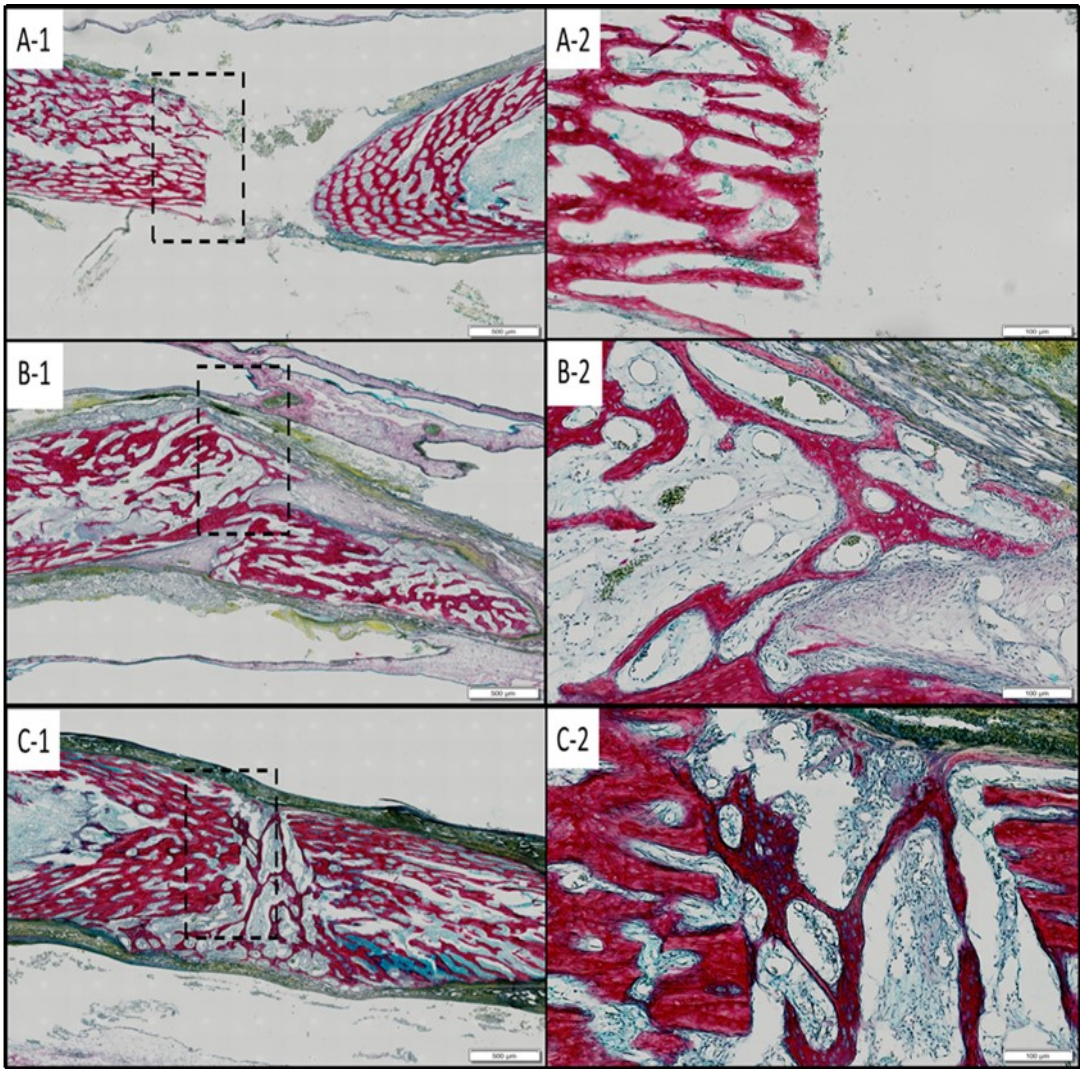

Figure 3-25. CAM ECM-PCL mesh histology, Alcian Blue and Sirius Red histology. A) Blank PCL mesh only. B) PCL mesh and unseeded bECM. C) PCL mesh with Stro-4 seeded ECM. A-1 to C-1 scale bar = 500µm. A-1 to C-2 scale bar = 100µm. Defect boundary demarcated by black dashed box.

3.3.6.8 PCL mesh with Stro-4 seeded bECM, CAM femurs. Alcian blue

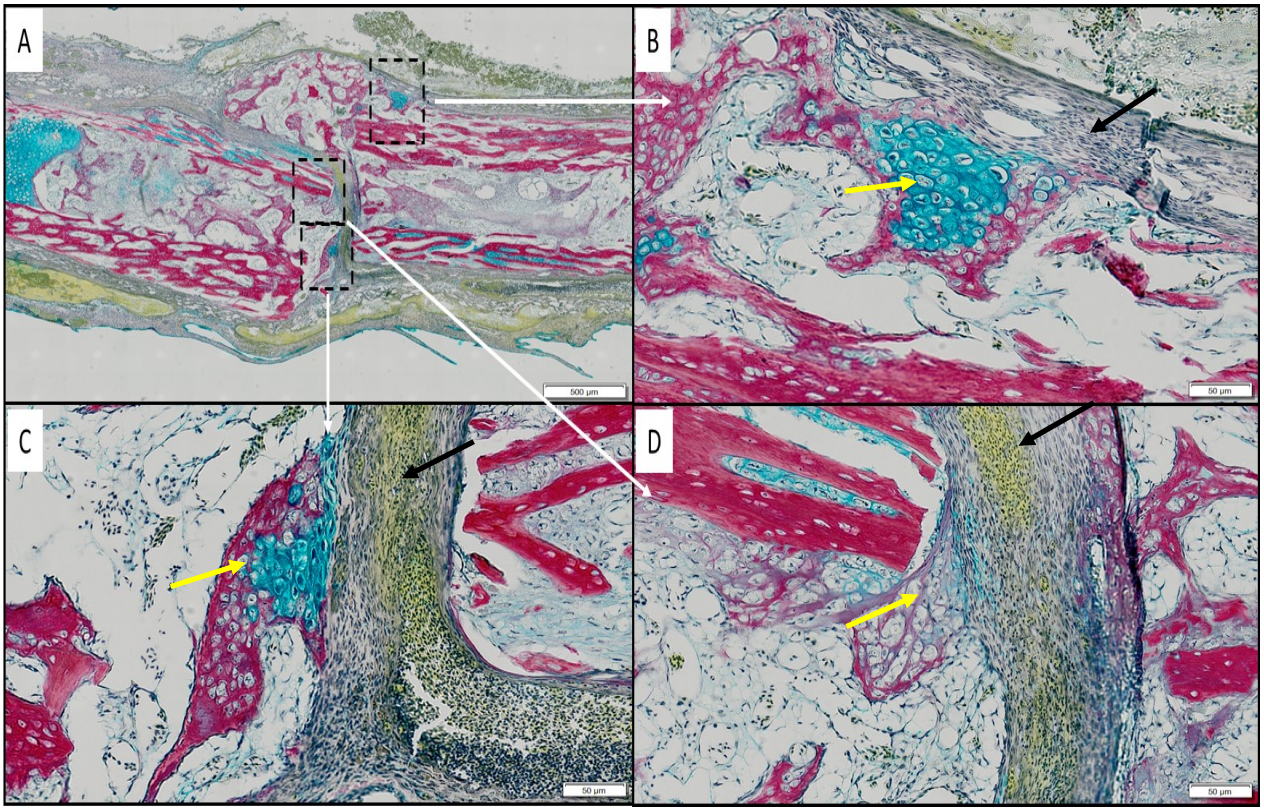

Figure 3-26 Stro-4 seeded ECM, A/S. A) 2x magnification sample overview, 3 regions of interest demarcated by dashed box. B) Cluster of proteoglycan producing cells (yellow arrow) associated with periosteum like membrane (black arrow). C) x15, Area of hypertrophic cells (yellow arrow) associated with invading fibrous sheet (black arrow), osteoid and proteoglycan visible. D) x15, cellular invasion of homogenous connective tissue-like material (black arrow), invading cells appear extra-femoral in origin and have begun collagen and proteoglycan matrix deposition (yellow arrow). Scale bar A =500µm, B, C and D = 50µm

3.3.6.10 PCL mesh with Stro-4 seeded bECM, CAM femurs. Goldner's Trichrome

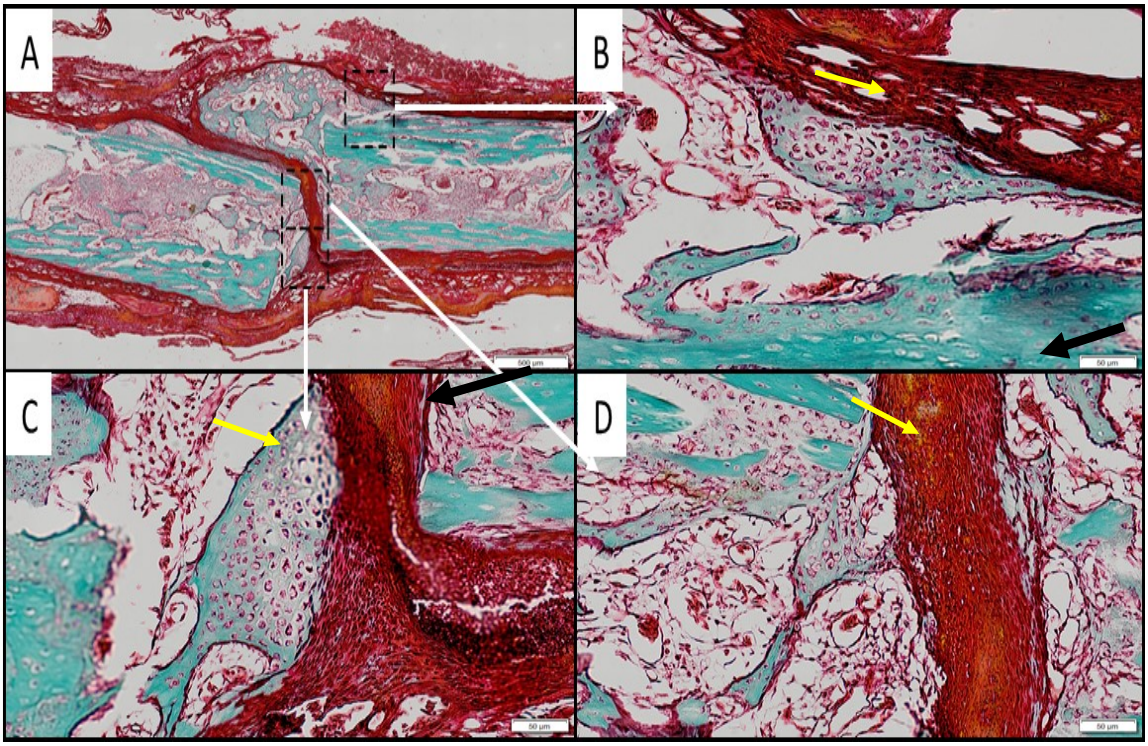

Figure 3-27 Stro-4 seeded ECM, Goldner's Trichrome stain. A) 2x magnification sample overview. B) Area of hypertrophic cells showing central region of osteoid production. C and D) Highlighted regions (x15) hypertrophic cells showing clear osteoid production (yellow arrows), cells are associated with invading collagen dense tissue (Black arrows). Scale bar A =500µm, B, C and D = 50µm

3.4 Discussion

3.4.1 Research in context

The development of novel tissue engineering therapies requires a comprehensive *in vitro* and *in vivo* review with particular attention given to using animal models capable of providing clinically relevant datasets. Orthopaedic research requires animals of comparative size, mass, biomechanics and physiology to the human and a model which corresponds to the clinical use. The sheep has emerged as a favourable candidate model species in recent years, fulfilling many of the favourable selection criteria in translational medicine. Ongoing use of ovine models has enhanced our understanding of species bone structure, anatomy, metabolism and physiology.

A comprehensive understanding of species specific cellular biology relating to that species model is essential to our understanding of the roll cells participate in self-renewal and repair. Along with other mononuclear cells of multiple adult tissue origins, the MSC has received enormous attention as a target cell in regenerative strategies. Although much is known about human MSC populations, debate remains surrounding the origin, phenotype, tissue location and function of this heterogeneous cell population, this debate extending to translational model species, in this case the sheep.

Recent work by Sanjurjo-Rodriguez and colleagues provides the most comprehensive data about the morphology, phenotype and function characterisation of ovine unselected MSCs to date, (Sanjurjo-Rodriguez et al., 2017), supporting and expanding on data published by Gronthos and others regarding ovine MSCs both *in vitro* and *in vivo* (McCarty et al., 2009; Niemeyer et al., 2010; Zscharnack et al., 2010). As knowledge about unselected ovine MSC populations increases, our understanding of specifically selected sub-populations lags behind.

Work in this chapter prospectively identifies and characterises Stro-4 enriched SSCs and compares them to unselected MSCs populations, detailing both Stro-4 and unselected cells *in vivo* potential as a cell target in musculoskeletal regenerative medicine.

3.4.2 Overview

The bone marrow of 7 adult sheep was harvested from fresh cadaveric sternal and pelvic bones, the non-haematopoietic mononuclear fraction was isolated by density gradient centrifugation of prepared mononuclear cell suspension. Magnetically conjugated Stro-4 positive cells were selected for by MACS, Stro-4 expression was confirmed by light microscopy immediately post selection and again through passage. Stro-4 expression declined with passage and was no longer detectable at passage 4. The persistence of Stro-4 in ovine SSCs has not yet been documented but is in keeping with the surface expression and recession of HSC-70 human Stro-1 positive BMMNCs (Fitter et al., 2017) and in Stro-1 expression as shown by earlier work in the same group (Gronthos et al., 1994b).

Growth rates, measured by population doubling time, in unselected and selected cells were comparable between populations at each passage between P1 and P5 and was also comparable to results by others in both the sheep (Gronthos et al., 2003; Lyahyai et al., 2012) and human (Friedenstein, 1982; Bruder et al., 1997) and (Gronthos et al., 2003), data for Stro-4 PDT was not available in the literature. The CFU-F capacity of whole, lymphoprep separated BMMNCs from ovine bone marrow presented with a morphological and colony forming potential comparable to findings by Bruder and Gronthos and similar to CFU-F data reported in human unselected MSCs (Castro-Malaspina et al., 1980; Friedenstein, 1982; Pittenger et al., 1999). Stro-4 CFU-F was documented by Gronthos et al*,* 2009 (Gronthos et al., 2009) on freshly sorted P0 cells although CFU-F formation with continued passage has not been recorded.

Results obtained on growth rate and colony forming capacity of ovine unselected MSCs, compare favourably with the literature and show close homology in the performance of MSCs between humans and sheep. Work characterising Stro-4 at early passage was echoed in the current study, this was enhanced by further work documenting growth through later passages.

Bulk cultures of bone marrow mononuclear cells are known to be heterogeneous containing a mixture of haematopoietic precursors, immunocytes, niche stromal elements, perivascular cells, osteogenic precursors and osteocytes, fibroblasts and adipocytes. A selection of a homogenous multipotential cell group is achieved by density independent culture under defined conditions as described by Haynesworth *et al* 1992 (Haynesworth et al., 1992a). A defined component of an MSC is its ability to differentiate into skeletal elements. *In vitro* differentiation on 2-D monolayer culture under defined conditions resulted in a demonstrable phenotypic change towards and osteogenic, chondrogenic and adipogenic phenotypes.

3.4.3 Gene Expression

In monolayer cultures both unselected and Stro-4 cell groups showed significantly enhanced *COL2A1*, aggrecan and *SOX-9* expression under chondrogenic culture conditions indicating a differentiation towards a chondrogenic lineage. A similar expression pattern was established in the micromass experiments although it appeared that micromass culture was less responsive to further stimulation by chondrogenic media. When examining chondrogenic matrix deposition by Alcian Blue staining, Stro-4 cells at early passage significantly outperformed unselected cells. Discordantly, upregulation in gene expression across both cell groups was observed without any clear improvement in chondrogenic potential between selected or unselected groups. The current studies indicate a propensity for ovine cells at the molecular level to differentiate more readily towards a chondrogenic lineage rather than an osteogenic or adipogenic phenotype.

This is in contrast to the predominance of stro-1 cells from adult human donors to differentiate along the osteogenic lineage (Gronthos et al., 1994b). Human foetal chondrocytes and MSCs are known to share common MSC markers and are known to express higher levels of stro-1 than adult cell population (Choi et al., 2016). The inclination of ovine selected, and to a lesser degree, unselected bone marrow stromal cells towards chondrogenesis may imply an early SSC phenotype. Further differences in the differentiation behaviour of ovine Stro-4 and adult human stro-1 populations were observed in when examining adipogenic and osteogenic expression.

Both selected and unselected populations were shown to express adipogenic genes when cultured under osteogenic conditions, an expression pattern further complicated by the non-significant upregulation of osteogenic genes when cultured under chondrogenic conditions. An innate chondrogenic preference combined with the expression of osteogenic, adipogenic and chondrogenic markers under a wide variety of growth conditions indicate a less committed lineage specific state of ovine MSCs. Work by Gotherstrom et al 2005 (Gotherstrom et al., 2005) demonstrated that the gene expression of human adult and foetal MSCs varied with foetal MSCs expressing a less lineage specific phenotype. One explanation for the difference in differentiation behaviour between human stro-1 and ovine Stro-4 may include a more primitive phenotype in ovine Stro-4 cells. Work examining comparing foetal and mesenchymal stem gene expression would be needed prior to drawing more definitive conclusions.

Gene expression was analysed on early passage cells cultured for 21 days under basal and lineage specific culture media. By comparison, histomorphometric analysis was performed on early and late passage cells which may account for observed differences in between staining intensity and gene expression. The significant osteogenic advantage seen in Alizarin red staining of early and late passage Stro-4 cells over unselected was not reflected in gene expression analysis. Neither Osteocalcin nor *COL1A1* expression were significantly different in basal and osteogenic conditions in either cell group. This was inconsistent with the strong Alizarin red staining noted in osteogenic media of early passage cells. *COL1A1* and Osteocalcin have a variable temporal expression in human MSCs *in vitro* (Kulterer et al., 2007). Gene expression was only performed on day 21 cultures of ovine selected and unselected BMMNCs and may not have captured peak *COL1A1* and OCN expression.

Stro-4 selected and unselected ovine cells have shown osteogenic and chondrogenic capacity. The significance of this ability differs between the analyses techniques used. Real time qPCR must be regarded as a more sensitive quantifiable technique and weight should be given to gene expression results. It is not unreasonable to suggest that a mismatch exists between protein expression, as measured histologically and gene expression as measured by qRT-PCR. Future work should include gene expression at time points throughout the differentiation protocol. This was not performed due to the limited yields of early passage Stro-4 cells.

3.4.4 *In vivo* functional assay, µCT and histology

The bone and cartilage forming ability of Stro-4 and unselected MSCs was assessed in a high-throughput orthotopic CAM femur assay. Previously, the *in vivo* bone and cartilage forming capacity of ovine MSCs has been shown on HA/TCP and Gelfoam models specific to lineage differentiation (McCarty et al., 2009). Osteogenic and chondrogenic validation was undertaken using a novel PCL mesh bECM hydrogel system, comparing potential of the known unselected MSC population and the undocumented Stro-4 population.

Prior work within the Bone and Joint Research group using bovine bone derived ECM hydrogels tested in an *in vivo* subcutaneous model demonstrated enhanced calcium deposition in hydrogels both containing and devoid of exogenous growth factors. This effect was superior to irradiated control material and attributed to the inherent growth factor content of bECM. Although the incorporation of SSCs into ECM hydrogels has demonstrated enhanced bone and cartilage regeneration *in vivo* (Bosnakovski et al., 2006; Liu et al., 2006; Zheng et al., 2010), previous experiments in the group with bone derived bECM *in vivo* were ambiguous regarding the Stro-1 SSC effect (Kanczler et al., 2010). Hydrogels containing vitamin D-2 loaded microparticles containing significantly more bone volume and mineral than controls, unexpectedly ECM gels supplemented with BMP-2 showed a paradoxical reduction in bone volume (Gothard et al., 2015). A significant degree of enhanced mineralisation was seen in Stro-1 seeded bECM devoid of exogenous growth factors, with stem cell related trends seen in tissue invasion and vascular growth. Our experiments utilised a growth factor free ECM formulation and sought to capitalise on the strong *in vitro* chondrogenic potential of Stro-4 ovine cells. Further modifications were made to the original system by allowing the gel to set without the addition of cross-linked alginate to encourage cell invasion and division.

In this study, unseeded hydrogels demonstrated a lesser degree of osteoinduction showing hypertrophic periosteal reaction and partial bone bridging. Significant new bone formation was observed in the cell seeded hydrogel which was qualitatively superior to bECM hydrogel alone. Aggregates of large elongated ovoid cells with abundant cytoplasm and prominent dark staining nuclei were present and indicative of metabolically active hypertrophic bone forming elements. Staining concurrently for proteoglycan and calcium aggregation indicates the presence of chondrogenesis centrally, with osteoblast differentiation and mineralisation peripherally supporting a description of endochondral ossification. New bone formation appears orientated along invading fibrous tissue and vascular structures and clear differentiation between innate bone and newly formed bone.

Invading fibrous structures appear intimate and consistent with femoral periosteum which leads to the presupposition that new bone is highly dependent on the nature of this invading tissue and its interaction with bECM and Stro-4 elements.

The clear cell effect could be attributed directly to the tissue forming effects of a cell source, with this effect driven by the oxygen and nutrient provision of the invading vasculature. A paracrine cell effect must also be considered in-which invading periosteal and perivascular cells are directed chemotactically and activated by the SSC secretome. It appears likely that new bone was in part periosteal in origin as the newly formed bone was orientated perpendicularly to innate cortical and trabecular bone and appear concurrently with infiltrative vascular structures.

MSCs release a number of mitogen growth factors including VEGF, IGF, EGF and TGFβ-1 and their paracrine effects on periosteum resident MSCs enhance wound healing *in vivo* (Chen et al., 2008). Periosteum derived MSCs are multipotent and responsive to both osteogenic and chondrogenic differentiation *in vivo* (Bari et al., 2006), periosteum and bone marrow derived MSCs have been shown to upregulate type II collagen production in response to TGF-β1 (Ballock et al., 1997). Furthermore, MSCs are responsive to chondrogenic and osteogenic factors (see introduction) and MSC exposure to chondroblast conditioned media enhances bone and cartilage formation *in vivo* (Hwang et al., 2007).

The clear *in vitro* osteogenic and chondrogenic advantage documented in Stro-4 populations suggests a direct cell building-block effect. Paracrine effects may be inferred by the degree of enhanced periosteal hypertrophy and association of new bone directly with none-bone tissues. *In vitro*, ovine Stro-4 displayed a chondrogenic phenotype even under basal conditions.

A periosteal reaction is clear in cell-seeded scaffolds although it was not possible to determine whether the cellular reaction was a result of cells within the bECM hydrogel proliferating and differentiating themselves or whether the cells were influencing the SSCs within the periosteum through a signalling effect.

Unfortunately, cell tracking was not employed and therefore the persistence of ovine Stro-4 cells *in vivo* and any direct contributions to new bone formation cannot be confirmed. It is clear based on extensive *in vitro* characterisation and preliminary *in vivo* data that Stro-4 cells positively upregulate chondrogenesis and osteogenesis by direct or paracrine effects.

The null hypothesis can be rejected as bovine ECM seeded with Stro-4 SSCs effected bony bridging in the CAM femur model. The role of Stro-4 in this effect was not sufficiently determined.

3.5 Conclusions

The current studies have documented the *in vitro* and *in vivo* growth characteristics of an enriched Skeletal Stem Cell population selected for by monoclonal IgG Stro-4 antibody. It documents an *in vitro* growth profile comparable with human SSCs.

The results indicate a clear preference for ovine unselected and Stro-4 enriched BMMNCs toward a chondrogenic phenotype. Stro-4 enriched cells show a clear chondrogenic phenotype *in vitro* when cultured on monolayer in basal media and as a 3-D micromass culture.

These results validate the use of Stro-4 and pave the way for *in vivo* evaluation of skeletal populations in tissue engineering and regenerative medicine. It advises the relevance of data obtained using Stro-4 in ovine models of bone repair and bone tissue engineering. The next phase of work will examine the translational potential of Stro-4 cells in a translational model of BTE.

The effective use of ovine Stro-4 in concert with bovine ECM in the vascularised CAM-femur model validates further investigation using a larger scale model.

Chapter IV, V and VI: developing ovine translational models

Chapter IV outlines the development of the ovine condyle defect model by the BJRG, which, in addition to holding its own research value as true large animal translational model was an essential step towards developing skills and understanding required to implement a more advanced segmental defect experimental set-up at the University of Southampton.

Chapters IV, V and VI describes the surgical and analytical techniques required to implement ovine translational models and seeks to outline the value and pitfalls of large animal bone defect models in BTE. The period of model development and optimisation was an opportunity to evaluate two distinct hydrogel based therapies for bone regeneration, both of which had been examined extensively *in vitro* and using small animal models *in vivo*.

Chapter IV describes the establishment and validation of an ovine condyle defect model, with consistent data provided for blank, allo- and autograft control conditions. In **Chapter VI** the validated model was used to investigate the performance of a nano-silicate hydrogel to deliver commercial BMP-2 and effect relevant bone repair, this work was an extension from previous *in vitro* and *in vivo* research published by the BJRG (Dawson et al., 2011; Gibbs et al., 2016b).

Chapter VI documents a segmental bone defect model performed by myself, alongside collaborators at Queensland University of Technology, to stringently examine the stem-cell ECM hydrogel system described in Chapter III. Expertise gained through the collaborative experience fulfilled a HO regulatory requirement and has prepared the BJRG to implement the model in-house in future.

Of the models used and described in this thesis, the critically sized tibial segmental defect model bares the most clinical relevance to scenarios of large volume bone loss; high energy trauma, tumour resection, fracture impaction, metabolic and infection linked bone loss. The execution of segmental defect models is resource, skills and financially intensive. The flow of chapters IV V and VI is intended to document what has been done to develop the model at the University of Southampton and what is required in future to permanently establish the model for ongoing clinically relevant *in vivo* therapeutic evaluation.

Chapter IV

4 Development of an ovine condyle defect model in an aged female sheep population for pre-clinical research in bone tissue engineering

Chapter IV investigates whether an ovine condyle model utilising exclusively aged female sheep is feasible as a reliable standardised protocol in translational medicine. This question will be addressed by documenting husbandry, surgical and data analytical procedures.

Acknowledgements

Dr. Janos Kanczler, laboratory manager and principle research fellow in the Bone and Joint Research Group (BJRG), leading all *in vivo* experimentation. Research staff member Julia Wells for her assistance during surgery and significant duties in cell culture and histology. I would like to acknowledge Dr. David Gothard for his academic and practical assistance during the proof of concept phase and preliminary work and Dr. David Gibbs for his valuable surgical contribution. Thank you to Gry Hulsart-Billström for her expert assistance in micro-CT analysis, helping design analysis procedures. Staff of the Bioscience Research Facility (BRF), facility manager Richard Reid and principle large animal technician Michael Broome for his high level of animal husbandry and post-operative care. Special thanks and acknowledgement to Paul and Lisa Dunning for their considerable co-operation with the Home Office in the housing, preparation and supply of experimental animals. Veterinary support provided by Named Veterinary Surgeon, University of Southampton.

4.1 Introduction

Chapters IV and V form two components of a coherent progressive research aim and are intended to be viewed as one continuous work described over two chapters. The primary goal of Chapter IV was to document the establishment of a large animal translational orthopaedic model in aged sheep, once validated the model was then used to evaluate the efficacy of a novel hydrogel based growth factor delivery approach to treating large volume bone loss, reported in Chapter V.

The following chapter details the process of establishing an ovine condyle defect model at the University of Southampton. Establishing the experimental model was considered a primary thesis objective requiring a great deal of administrative time, details of non-surgical and non-analytical aspects of implementing the model are included as a supplementary, including details on Home Office compliance, animal sourcing, housing and transport. Discussion of the protocols and their modifications over subsequent surgical and experiment setups has also been included.

It was intended that once the Bone and Joint research group had demonstrated surgical proficiency and was able to show reliable control data, model tolerance and validation that the model would be used to evaluate novel therapeutics in BTE. Chapter V follows directly, trialling a nano-silicate BMP-2 delivery system using the established model

4.1.1 Ovine condyle model

In context of the thesis aims, the development of an ovine femoral condyle model was outlined as the primary goal. Validation of the condyle model would satisfy a major Home Office check point towards development of a complete tibial segmental defect for the study of bone regeneration, Figure 4-1.

In vivo pipeline to hosting large animal studies

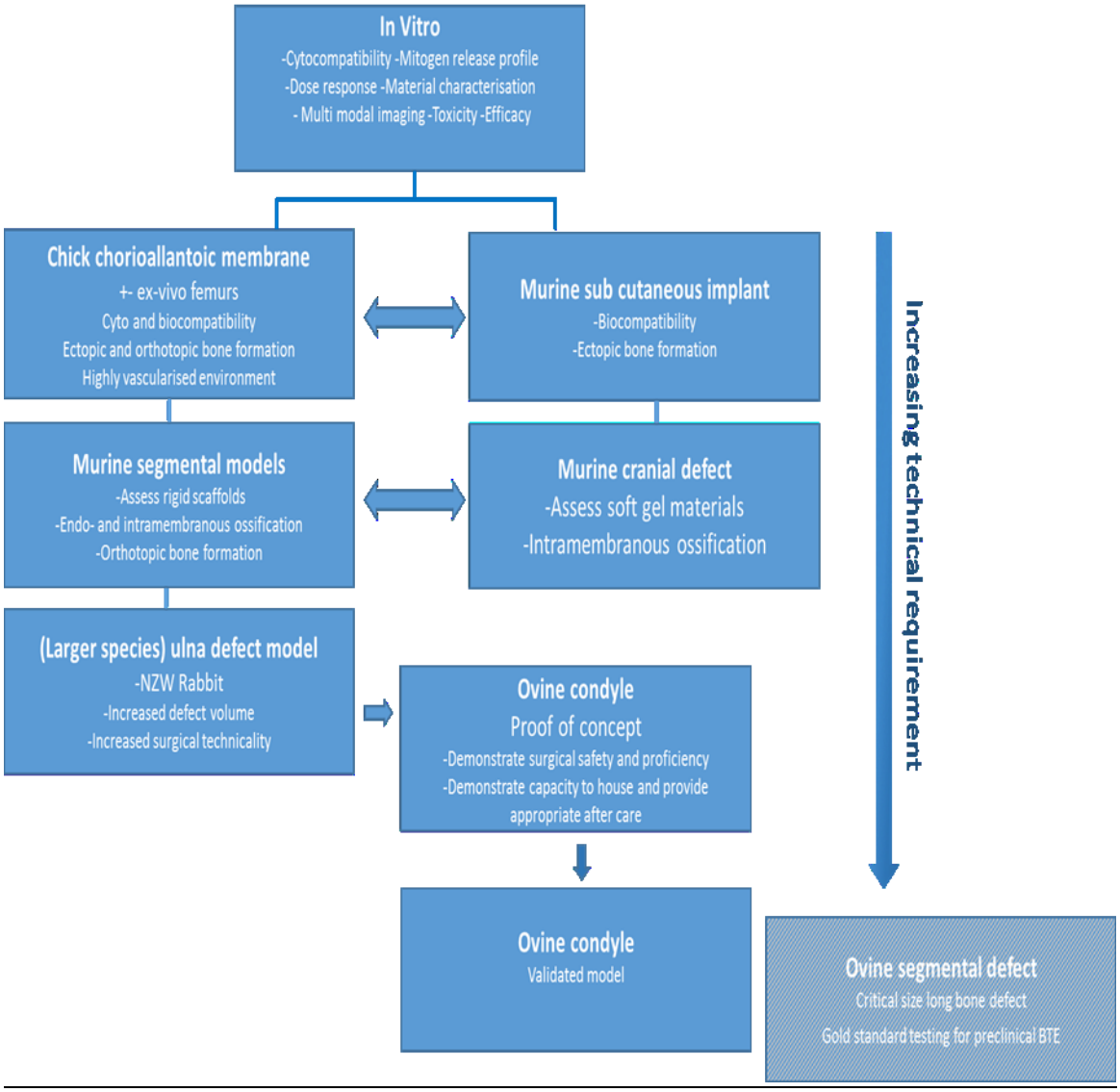

Figure 4-1 Legislative pathway to large animal use. Development of an ovine model was dependant on fulfilling milestones outlined by the Home Office.

4.1.2 The ovine femoral condyle defect

The model is suitable for testing tissue engineering strategies at a clinically relevant scale, the various merits and limitations of using the sheep in preference to other larger animal species such as the dog, goat and pig are discussed in the thesis introduction, 1.11. In particular, the choice between goat and sheep appears to be one of researcher preference and the suitability of facilities to host the chosen species (Li et al., 2015). Sheep are the most commonly used large animal species in musculoskeletal research (Neyt et al., 1998; Pearce et al., 2007a). Sheep share biomechanical similarity to humans, are skeletally large, share comparable body mass with humans (50-80kg), amenability in handling and resilience to surgical procedures and robust recovery (Pearce et al., 2007a). The use and development of an ovine model was justified by industry acceptance of sheep as a suitable species in developing biomaterials, biomedical devices and orthopaedic implants (Newman et al., 1995; Reichert et al., 2009; Woodruff et al., 2012).

The model was homologous to that published by Ding (Ding et al., 2012) and advised from detailed protocols by Nuss (Nuss et al., 2006a). In an advancement of the protocols already published, a model was developing using only an aged female population representative of the clinical demographic in humans. All animals used were female, entire and at least 7 years of age.

Bilateral defects were created in the distal medial femoral condyle, approximately 9mm in diameter x 11mm depth. The use of multiple defects in the proximal and distal femur, and proximal and distal humerus have been described (Nuss et al., 2006a; Liu et al., 2013). Up to eight defects have been performed in the same animal with further bilateral defects in metacarpal and metatarsal bones (Pobloth et al., 2016). Cylindrical drill defect models have also been reported in the ulna (Uebersax et al., 2013), vertebral bodies (Verron et al., 2014) and iliac crest (Lansdowne et al., 2014). Figure 4-2 presents recent use of the drill defect reported in the literature, many of which build on the methodology described by Nuss.

Malhotra *et al*. expanded on the model comparing defects of 8, 11 and 14 mm in diameter and 25mm depth, demonstrating a linear correlation exists between defect diameter and total new bone formed (Malhotra et al., 2014). Malhotra determined that an 8mm defect may be too small to be classed as a non-healing defect at 4 weeks. In contrast, Ding (Ding et al., 2012), von Rechenberg (von Rechenberg et al., 2013) and Apelt (Apelt et al., 2004) document defects varying from 8mm-10mm in diameter and 10-13mm in depth which had not healed by 6 months.

The design and location of any defect in the live animal must be carefully considered, particularly in models which do not include mechanical fixation. Edgerton et al. examined the relationship between defect diameter and torsional strength in ovine femurs, there was no impact on

torsional strength when a defect was less than 10% of the total bone diameter and a linear relationship between loss of torsional strength and defect diameter between 20 and 62% of total bone diameter (Edgerton et al., 1990).

Work by Amanatullah and colleagues supports Edgerton reporting a critical loss of torsional integrity when a defect diameter approached 50% of bone diameter (Amanatullah et al., 2014).

The mean diameter of condyles in welsh upland sheep was estimated at 35 -40mm, centred on the medial epicondyle and the creation of a 9mm x 11mm defect was less than 25% of the total condyle diameter. Initially a defect dimension of 9mm x 15mm was decided upon which was subsequently revised to a 9mm x 11mm as a 15mm depth occasionally penetrated the defect floor during preliminary surgery. It was decided to limit defect number to two per animal on welfare grounds; a bilateral distal femoral defect.

4.1.3 Alternative locations for bone defects

Defects created in the flat bones and axial skeleton such as iliac crest, vertebral bodies and mandible have been described, Figure 4-2. Such defects offer a far lower fracture risk in a non-weight bearing bone which may appear attractive on welfare grounds. Flat bones are composed predominantly of cortical bone and do not share the same biomechanical loading as long bones (Zioupos, 2001). Use of a flat-bone defect model would not directly address questions relating to cancellous bone growth and remodelling as a function of weight-bearing (Huiskes et al., 2000) and were therefore not considered.

Study	Defect location	Defect size	Duration	Sex/age
Ding *et al* 2012	Med. femoral condyle	10mm x 11mm	9 weeks	Fem. Skeletally mature.
Nuss *et al* 2006	Lat. Pr/Di Humerus, Femur	8mm x 13mm	2, 4 ,8, 16 and 24 weeks	Fem. 2-5yrs old
Malhotra *et al* 2014	Lat.Pr/Di Humerus Lat. proximal femur Med. distal femur	8mm x 25mm 11mmx 25mm 14mm x 25mm	4 weeks	Sex n/a, 18 months-5 years old
Liu *et al. 2012*	Lat. Pr/Di Humerus, Femur	8mm x 13mm	4 and 8 weeks	Fem. 2-4 years old
Uebersax *et al* 2013	Lat.Pr Humerus Lat. Pr/Di Femur Med. Pr Tibia	8mm x 13mm	8 weeks	Male. 2 years old
Pobloth *et al* 2016	Lat.Pr/Di Humerus, Femur Ant. Metacarpal and metatarsal	6mm x 13mm	2, 4 and 6 months	Female. 2.5 years old
Rechenberg *et al* 2013	Lat. Pr/Di Humerus, Femur	8mm x 13mm	2, 4 and 6 months	Female 2 years old
Apelt *et al* 2003	Lat. Pr/Di Humerus, Femur	8mm x 13mm	2, 4 and 6 months	Female 3-5 years old
Schneider *et al* 2011	Lat.Pr/Di Humerus, Femur	8mm x 13mm	8 weeks	Female 2.5 years
Verron *et al* 2014	Vertebral body, L3-L4 Osteoporotic model	Parallel drill holes: 2 x 8mm x 10mm	3 months	Female, ovariectomised. Adult, age n/a
Lansdowne *et al* 2014	Iliac crest Bilateral	17mm diameter, full thickness	3 months	Female. 2.5 years old
Shang et al., 2001	Skull, parietal bones Bilateral	20mm diameter, full thickness	18 weeks	Sex n/a. Adult

Figure 4-2 Published literature on the use of an ovine drill defect model. Pr Proximal, Di Distal.

4.2 Aims

1. →To develop and establish surgical, infrastructural and analytical protocols necessary to implement an ovine condyle defect experimental model.

2. →To satisfy Home office regulatory concerns entitling the Bone and Joint Research Group to utilise the model without restriction.

3. →To validate the model by demonstrating statistical significance between negative and positive controls.

4.3 Null hypothesis

The development of a validated ovine condyle defect model will not be possible

.

4.4 Development of the Ovine Sub-Condylar Defect Model.

Promising *in vitro*, *ex vivo* and small animal *in vivo* studies performed by the BJRG require experimentation in a large animal model to gauge any potential clinical application. Use of the Sheep in human orthopaedic research continues to gain popularity due to comparable adult weight, similar bone structure and tractable nature. The BJRG will use the sub-condylar model as a bridge in the effort to translate basic science into clinical application.

4.5 Sub-condyle defect study

The use of an ovine condyle defect in sheep as a model in orthopaedic research was not established at the University of Southampton prior to the work outlined below. As such, all aspects of the model development including regulatory approval, preparation of research facilities to accommodate experimental animals, surgical, anaesthetic and husbandry methodology were documented. The model was established over two experimental periods, collated data between these studies were reported and discussed.

A total of 13 adult sheep all aged 7 years or older were used over two extended experimental periods. Experimental groups are outlined in Figure 4-3 below. Experimental groups were designed to cover a proof of concept and competency stage, and once proficiency was satisfactorily demonstrated a second larger control cohort was performed.

Group	N (defect)	Experiment ID	Start	Finish
Blank	7	Proof of concept	12/03/2014	01/12/2014
Allograft	6	Proof of concept	12/03/2014	01/12/2014
Autograft	3	Proof of concept	12/03/2014	01/12/2014

Figure 4-3 Ovine condyle experimental timeline summary.

4.5.1.1 Experimental grouping and objectives.

Initial proof of concept.

A two-animal control study was undertaken, one defect per animal, blank defects only. Proof of concept aims were centred on rigorous testing of animal husbandry, facilities and surgical protocols. Strict animal welfare practices were maintained throughout whilst ensuring the scientific merit and justification of the experimental models in future experiments. Included in the preliminary element was the use of cadavers for initial testing of protocols without risk to live animals. Full transparency with the Home Office led to discussion and protocol amendments introduced prospectively aimed at improving animal welfare and experimental design. Animals were given a 2-week period of acclimatisation prior to surgery, the experimental time frame from surgery until end-point was 10 weeks.

Extended proof of concept and experimental trial: baseline control data

A total of eleven adult sheep were used, groups were staggered over two operational stages. All animals in the extended proof of concept phase were allocated between control groups, blank, allograft and autograft controls. A unilateral defect was created in five animals and a bilateral defect created in seven. The change from unilateral to bilateral defect was made on Home Office approval for the defect model, improving study numbers and applying 3Rs principles, defects were allocated uniformly between left and right limbs.

4.6 Materials and methods

4.6.1 Preparation of allograft

Material was obtained from cadaveric sheep femurs. Femoral heads were stripped of all soft tissue attachments and all connective tissue and cartilage was removed. The bulk bone material was cut into 3 x 2cm segments using a hand saw and clamp. Segments were washed in a 0.1% (v/v) Triton X (Sigma Aldrich, UK) solution for five minutes to remove excess fat and bulk soft tissue. Segments were rinsed twice in 1x PBS (Fisher Scientific, UK) for five minutes. Bone was milled using a Liebinger hand mill (Strkyer, USA), Figure 4-4 A. Morselised bone fragments were decellularised by five overnight washes in a 6% hydrogen peroxide solution (Fisher Scientific, UK), rinsed and stored in 5% Antibiotic/antimycotic (Sigma Aldrich, UK) solution until use. Allograft was placed in a plastic mould with dimensions matching the bone defect, allograft mass in each sample was a uniform 0.3g, Figure 4-4 B. Allograft was placed into the defect using the mould as a guide, pressed into place and the wound sutured closed.

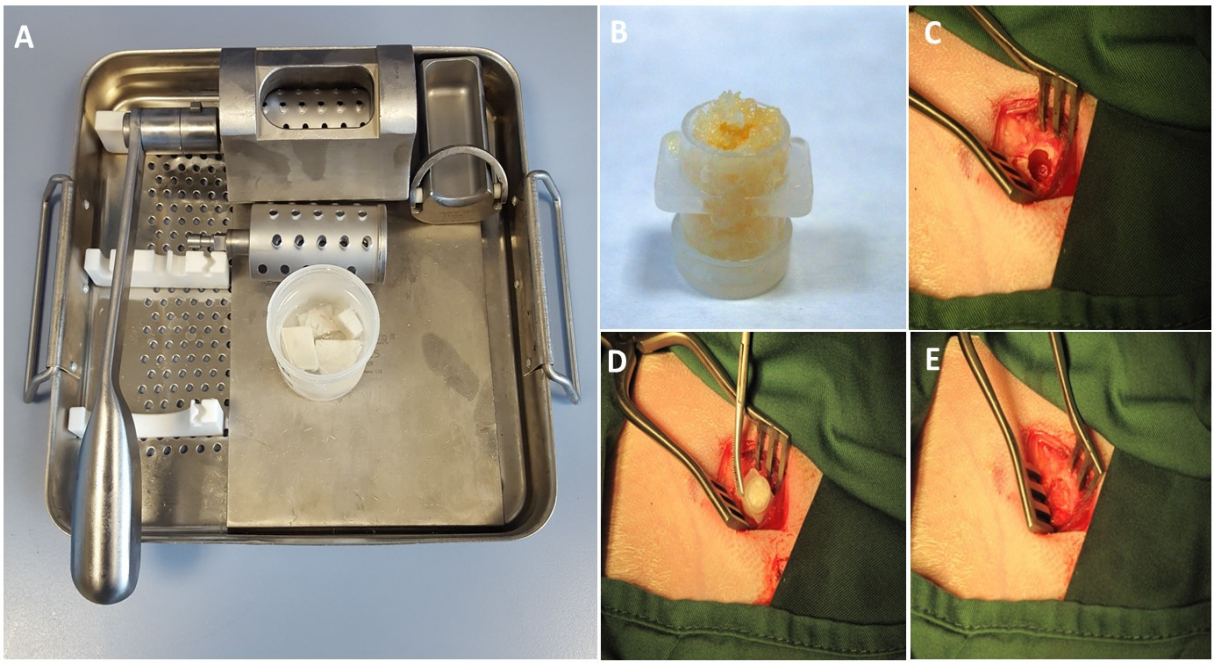

Figure 4-4 Allograft preparation. A) Lienbinger hand mill was used to produce morselised bone. B) Prepared allograft in sterile container. C) Ovine condylar defect. D) Allograft positioning over defect. E) Allograft in situ prior to wound closure.

4.6.2 Preparation of autograft

Autograft was prepared intraoperatively under aseptic conditions. After defect creation, one bone core (9mm x 12mm), was morselised using hand bone ronguers in a stainless-steel kidney dish. A small volume of sterile saline was added to prevent material from adhering to the bowl surface. In the follow up studies, two bone cores were combined to provide more material per defect.

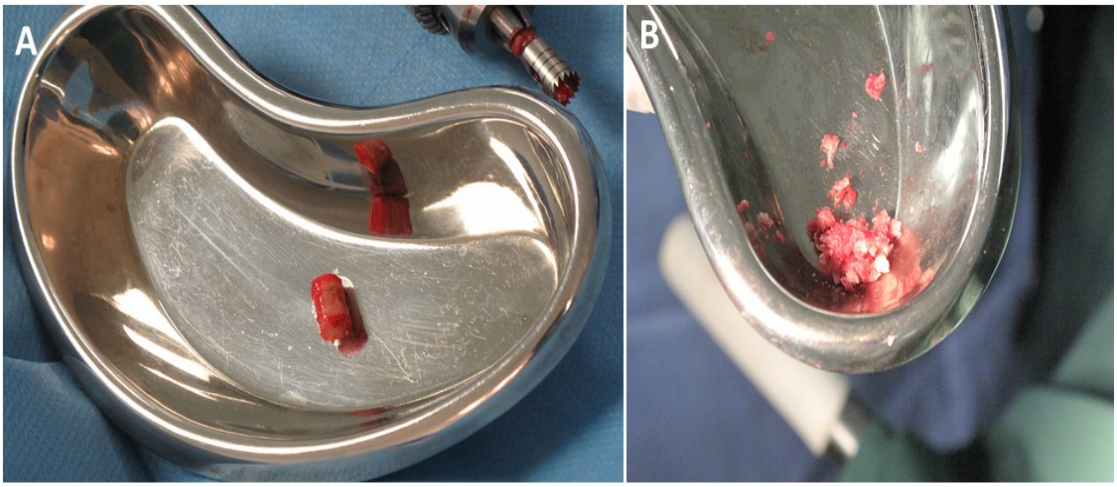

Figure 4-5 Autograft preparation. A) Bone core removed from defect. B) Autograft ready for implantation

4.6.3 Micro Computed Tomography

A new CT analysis protocol was developed, as detailed below, with assistance from Dr Gry Hullsart-Billstrom, Dr Janos Kanczler and Dr David Gibbs. All scanning was performed on a Skyscan 1176 (Bruker).

4.6.3.1 CT Scanning

Samples were trimmed to uniform size using a Biomet rotary saw and stored at 4°C in PBS. Samples were removed from storage pots and wrapped in moist paper towel to prevent sample desiccation for scanning. Samples were aligned and placed into the sample tray. Scanning parameters were set at 90kV and 278uA, with a 0.1mm Cu filter, a pixel size of 18µm, 360° scan with rotation at 1.5°.

4.6.3.2 CT Image reconstruction

Files were reconstructed using nRecon (Bruker), adjustments were made for ring artefact correction and beam hardening. A lower level greyscale of 118 was selected based on mean values obtained from Otsu threshold analysis (Otsu, 1975), the lower limit is the cut-off at which point the software separates calcified and non-calcified tissue. Reconstruction parameters were uniform for all samples across scanning occasions. Reconstructed files were orientated using DataViewer (Bruker) such that all samples were uniformly aligned centred on the defect.

4.6.3.3 Analysis

Analysis was performed in ctAn (Bruker). Three regions of Interest (ROIs) were identified on each sample. 1) A whole defect 9mm x 11 mm cylinder, 2) a smaller subset “mini-cylinder” measuring 6mm x 6mm and 3) an outer region of unaffected host bone termed the “standardisation” region, measuring 11mm inner diameter and 14mm outer diameter x 3mm in height.

The defect boundaries were determined by identifying the first slice which contained a complete ring of cortical bone, Figure 4-6, C. The bottom of the selection was determined to be the slice at which bone trabecular pattern appeared uninterrupted and congruent with host bone, this ROI was termed “Condyle, 9mm”.

An outer standardisation ROI of host bone was created to standardise results bone by limb and by animal. A donut-shaped ROI was selected with an inner diameter of 11mm, outer diameter of 14mm and height of 3mm, Figure 4-7, A and B.

The subset region “mini-cylinder” was created using the condyle 9mm as a template. The base of the defect was raised by 116 slices (2mm) and the top of the defect was reduced by 118 slices. The cylinder diameter was reduced from 9mm to 6mm. Total defect dimensions were reduced to 6mm diameter and approximately 6mm in height (depending on original defect depth). This ROI was selected to focus on new bone formation within the central most area of the defect, Figure 4-7, C.

Region of Interest identification, 9mm (top), standardisation and 6mm (below) ROIs

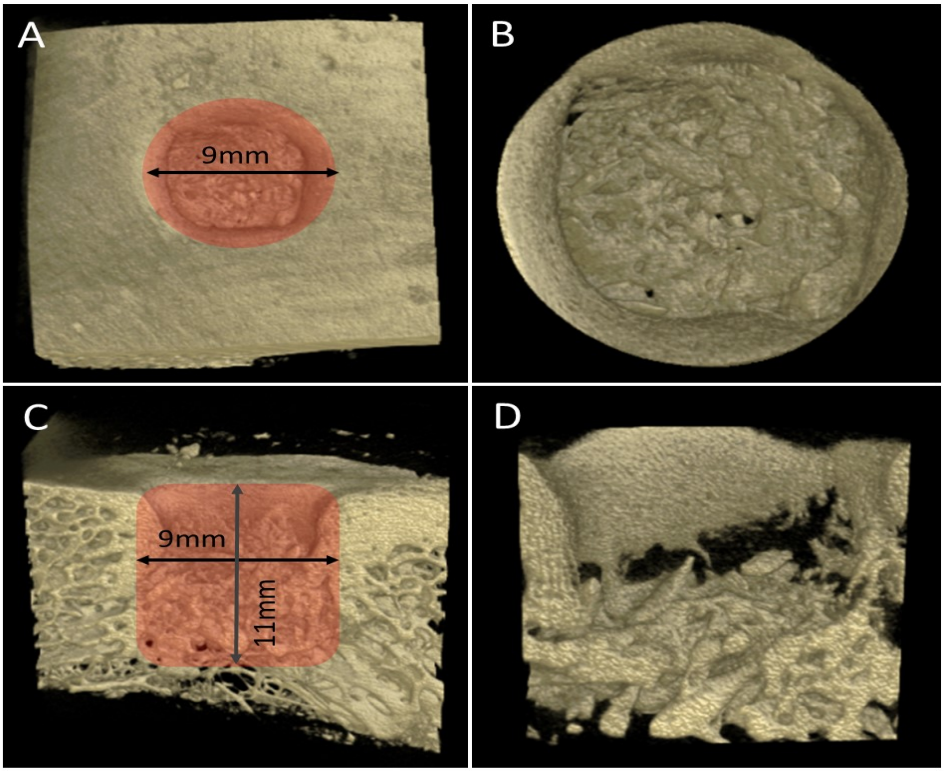

Figure 4-6 Micro-CT workflow, whole defect ROI. A) Transverse plane, 9mm defect ROI (red). B) Transverse view, whole defect render. C) Sagittal plane, defect ROI (red). D) Sagittal plane render.

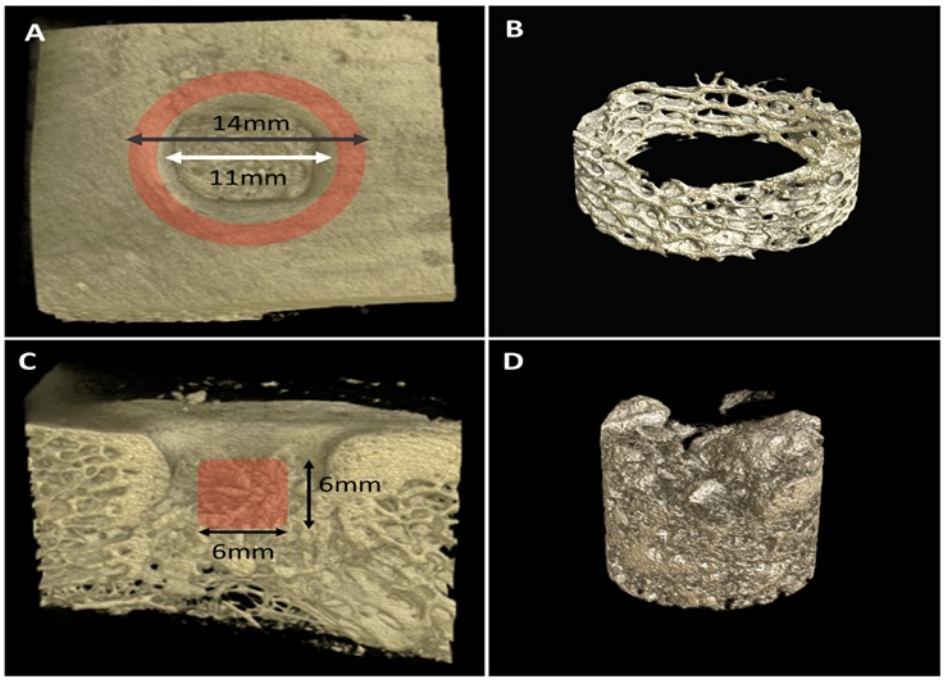

Figure 4-7 Standardisation and mini-cylinder ROIs.) Selection of an outer region, external diam. 14mm / internal diameter 11mm. B) Render of A. C) Mini-cylinder defect area selected within whole defect ROI. D) Render of 6mm defect

4.6.4 Statistical analysis

Statistical analysis was performed using GraphPad Prism and was based on methods described by Ding (Ding et al., 2012). A one-way ANOVA was used with Bonferroni post- hoc test comparing the means of each group with one another, $P < 0.05$ was considered significant. For all graphs presented below, * $p<0.05$, ** $p<0.01$, *** $p<0.001$, **** $p<0.0001$ indicated levels of significance

Sample size calculations were performed using open source software, Power and Size Calculations (Dupont and Plummer, 1990). A level of significance 0.05 ($\alpha = 5\%$) was chosen and power 0.8 ($1-\beta = 80\%$). Accepting a biological difference of a 50% increase in bone volumes between negative controls and test samples and a SD of 30%, a sample size of seven animals per group was required.

4.7 Development of surgical protocols, ovine condyle defect

All experiments were carried out under Home Office Project License (PPL) 30/2880, Protocol 5. All Bone and Joint Research Group members involved in handling, surgery and after care were current holders of a HO Personal License (PIL). PIL Cameron Black 30/10220, PIL Dr Janos Kanczler 70/19405

Protocols were written using the current University of Nottingham Project License as a reference, clinical advice from staff of the University of Glasgow Veterinary School, Large Animal Department, Royal Veterinary College Farm Animal service and the Parklands Veterinary Group The topic of surgery and anaesthesia is reviewed by White and Taylor, “Anaesthesia in Sheep”. Alternative drug protocols were provided in case of adverse response or contra-indication on an individual animal basis.

4.7.1 Pre-operative preparation

All animals were on site for a two-week period prior to surgery. Pre-operation health checks were performed the day before surgery, prior to food being withheld. Animals were starved for 24 hours prior to anaesthesia, access to water was restricted 2 hours prior to surgery. Pre-operative health checks were repeated prior to pre-medication. Pre-medication was administered intramuscularly (i.m.) and each animal was left in a holding pen for 20 minutes before being moved through to the pre-operative area. Pre-medicated animals were then microchipped and ear tag identifiers recorded. Animals were placed in a large animal stretcher (custom made for study purposes) Figure 4-8, A. The neck area was thoroughly clipped and scrubbed in two stages, with chlorhexidine 5% and ethanol 70%. A central venous catheter was placed by first injecting a local anaesthetic sub-cutaneous, allowing five minutes for effect, the central line was then introduced and secured, the animal was then induced and placed on maintenance anaesthesia.

4.7.2 Surgery

Preparation: The anaesthetised animal was placed on the surgical table in lateral recumbency, connected to intravenous fluids and monitoring equipment. Once the animal was stable under positive pressure ventilated gaseous anaesthesia it was placed in dorsal recumbency, Figure 4-8, B. Forelimbs, chest and hindlimbs were secured in place. All surgical fields were clipped and the animal cleaned. Skin covering left and right medial femoral condyles was clipped and shaved then scrubbed three times with chlorhexidine 5% solution and rinsed clean.

Each animal was then draped in sterile material drapes from sternum to distal limb, such that only the two defect areas were uncovered. Both undraped surgical "windows" were then covered with Ioban Incise® impregnated antibacterial adherent dressing, Figure 4-8, D.

Surgery: All care was taken to maintain haemostasis, sterility and to minimise tissue trauma to surgical site and surrounding soft tissue structures. Palpable land marks were identified as the tibial tuberosity, insertion of the straight patella ligament, patella, tibial plateau and medial femoral epicondyle. The point of incision was determined by first drawing a triangle connecting the medial epicondyle, distal border of the patella and the proximal portion of the tibial tuberosity. A central point was marked and the incision made from the marked point towards the medial epicondyle, approximately 3 cm in length, the incision was extended cranially and caudally as required, Figure 4-9, A.

Subcutaneous tissue and fascia were cut by stab incision and extended using round nosed scissors. The medial femoral condyle was exposed by blunt dissection of muscle fibres which were split by dissection parallel to muscle fibre orientation, taking care to conserve vascular and nervous structures. Transection of muscle tissue was avoided. Greater visualisation could be provided by partial transection of muscle tendinous attachments, which would later be sutured and reattached although this was rarely required. Drill site exposure was maintained by use of a Weitliner retractor, Figure 4-9, B.

The drill location was determined by manual palpation of the exposed medial condyle, locating the smooth flat surface linking medial epicondyle with medial trochlear. All soft tissue was cleared manually from the drill site bone surface using a moistened gauze swab. The drill guide, Figure 4-9 C, was secured in position. The bone defect was created using an Osteomed OsteoPower® orthopaedic drill with a trephine dental drill bit (Primadent®, UK), 9mm external diameter and 15mm in length. The drill bit was advanced through the guide until in contact with bone, the initial bone contact was performed at low drill revolutions.

Drill rpm was increased as the drill was advanced into the condylar bone, the drill area was continually irrigated with sterile saline to prevent thermal injury. The drill bit was kept perpendicular to the bone surface throughout and drilling stopped once the hub of the drill bit was in line with the bone surface (10mm). The drill bit was then withdrawn and the drill guide removed. Using the bone core removing tool custom made at the University of Southampton, Figure 4-10**,** A, the bone cylinder was gently rotated and removed from the bone, leaving a cylindrical empty defect approximately 9mm x 10mm in dimension. The defect was made uniform by use of a flat headed reaming bit Figure 4-10, B, at low rpm. The defect area was inspected for presence of a stable defect floor, adiposity, bleeding and trabecular density. At this stage, the defect is completed and either remains empty (blank control), filled with intervention, or filled with autograft material (positive control).

All connective tissue layers were closed sequentially using 2/0 Vicryl® in either a simple or uninterrupted pattern. Skin was closed using 3/0 Vicryl® in a sub-cuticular pattern or 2/0 horizontal mattress suture. The wound was then cleaned, dried and covered with adherent Ioban barrier dressing. The procedure was on contralateral limb.

4.7.3 Recovery

Each animal was closely supervised throughout recovery. Animals were placed in sternal recumbency within the stretcher, with ET tube in place and oxygen supply on. As laryngeal reflexes returned the ET tube was removed with cuff partially inflated to prevent aspiration, then gag reflex confirmed and independent breathing established. Once animals had been breathing independently for ten minutes, they were offered high energy food, this was an extremely reliable means of assessing recovery. Animals were monitored by clinical staff until conscious, capable of stable ambulation and able to maintain posture independently. All animals were given a post-recovery examination before being declared out of recovery. Animals were monitored hourly for the remainder of the surgical day. Operated animals were given a physical exam for three consecutive days with findings recorded.

Figure 4-8 Stages of surgery, induction through recovery. A) Animal in stretcher prior to central line placement. B) Positioned in dorsal recovery, limbs secured in place. C) Anaesthetised animal, monitoring and IVFT displayed. D) Draping of animal prior to first incision. E) Intraoperative, exposed condyle prior to drilling. F) Animal in stretcher during recovery, animals remained in position for a minimum of ten minutes after extubating.

4.7.3.1 Surgical protocol

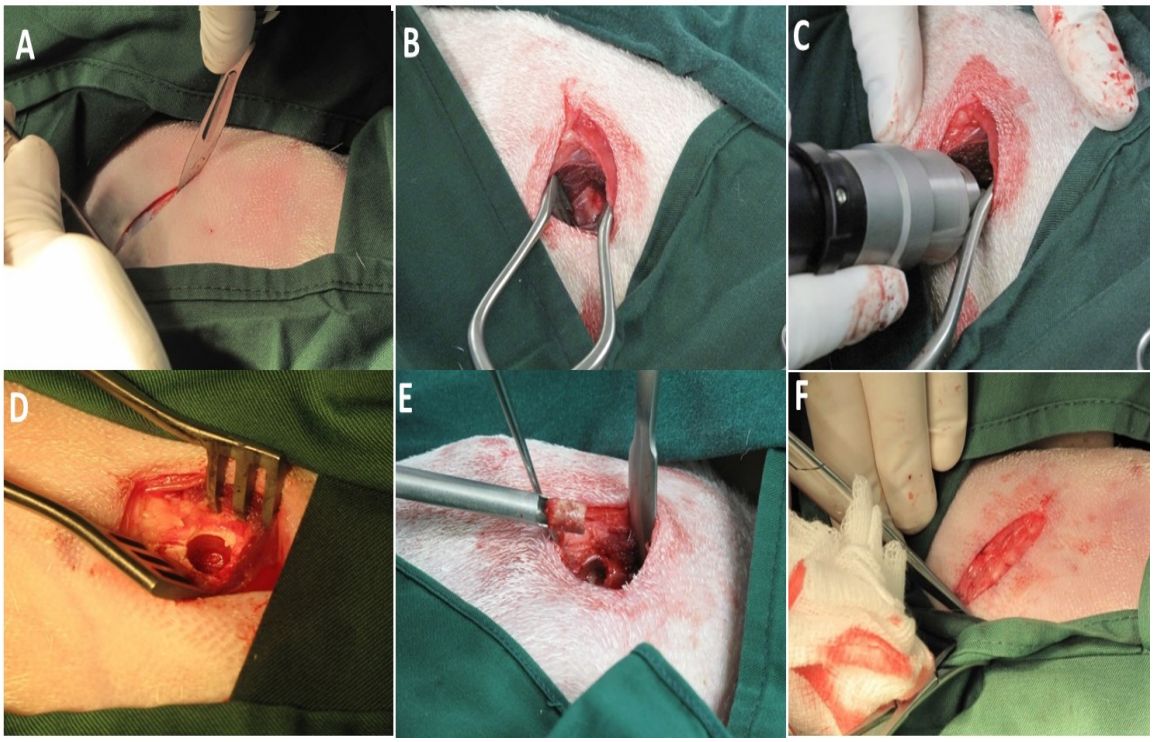

Figure 4-9 Surgical protocol, condyle defect creation. A) Skin incision. B) Blunt dissection through muscle fibres, placement of a Wietliner's retractor and exposed underlying bone. C) Creation of defect with OsteoPower® drill and trephine drill bit. D) Empty defect. E) Removal of bone core using core retrieval tool. F) Sequential closing of the wound.

4.7.3.2 Custom tools for condyle defect surgery

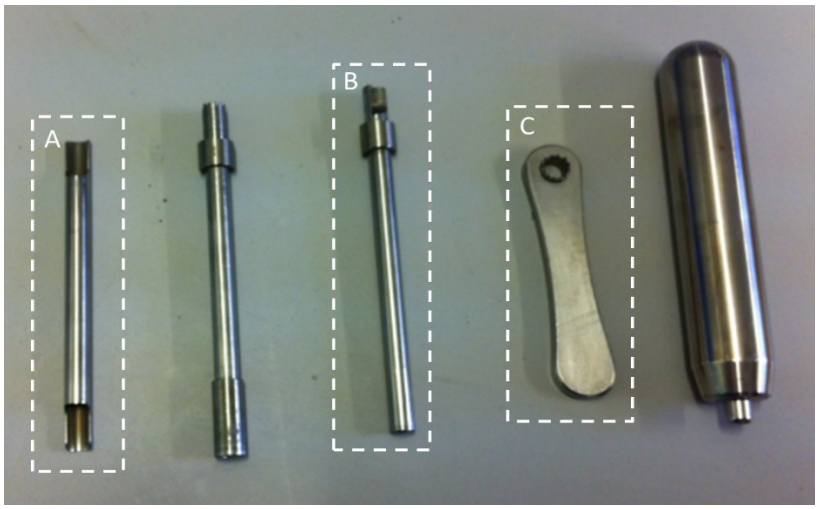

Figure 4-10 Custom made drill defect tools. A) drill guide (C), Blunt reamer (B) and bone core removing tool (A) were custom made for the study procedure. Each tool was designed on Solid Works and machined at the University of Southampton. Thanks To Dr Yu-Hin Man for assistance in CAD drawing.

4.7.4 Anaesthesia and Analgesia

4.7.4.1 Pre-medication

All animals received premedication after passing pre-operative health checks.

- Midazolam (0.2-0.4mg/kg) Buprenorphine (0.01mg/kg) was administered intra-muscularly (i.m.) twenty minutes before central line placement and induction.
- Ketamine (2-5mg/kg i.m.) was trialled in combination with Midazolam and buprenorphine separately but was discontinued due to undesirable effects on rumen function*:* Use of an alpha-2 agonist agent *(*Xylazine 2% 0.1mg/kg i.m.) alone or in combination was also trialled but rejected due to intraoperative cardiovascular instability.

4.7.4.2 Central line placement

A central line was placed in the left or right external jugular vein. An area approximately 20cm wide and 30cm long extending from the angle of the jaw to the manubrium was shaved using the trachea as a reference line. A 5cm x 5cm square in the middle of the clipped area was blocked using a 2% Lidocaine solution. A central venous catheter was inserted according to manufacturing guidelines (Arrows Corporation, central venous catheter). The large diameter guide catheter was inserted and the guide wire placed through the guide catheter, the outer guide catheter was then removed. A small 2-4mm dermal incision was made onto the guide wire to extend the catheter entry point. The central catheter was then placed over the guide wire, and sutured in place using a finger-trap pattern. The guide wire was removed, stoppers and a three-way tap were connected to the central catheter.

4.7.4.3 Antimicrobial protection

Duphapen and Strep, 1ml/25kg, s/c, administered at time of operation and 24 hours post providing 48 hours of broad-spectrum antimicrobial protection. Additional antimicrobial care was provided if indicated, based on clinical presentation and evaluation

4.7.4.4 Induction

Anaesthesia was induced by Propofol (3-5mg/kg), slow i.v. to effect, injection ports were flushed with sterile saline post induction. Ketamine induction (4-6mg/kg) was attempted after recommendation, but again rejected due to persistent ruminal tympani and spasmic paralysis of abdominal muscles and cardiac sphincter. A size 9 endotracheal tube (E.T.) was placed immediately upon induction. The larynx was visualised with a large-blade laryngoscope, sprayed with 1% lignocaine, E.T. tube placed and cuff inflated. Animals were placed on 0_2, HR confirmed and mucous membranes assessed for cyanosis. IVFT provided by lactated Ringer's solution at 10ml/kg/hr for duration of surgery. In cases of large volume regurgitation and potential acid/base imbalance, bicarbonate saline was available.

4.7.5 Anaesthetic maintenance

Animals were maintained on Isoflurane (2-4%) in O_2, and machine ventilated average tidal volume 4-6ml/kg. Nitrous Oxide (N_2O), was avoided due to associated risk of Ruminal Tympani. A full monitoring suite was available, heart rate (HR), electrocardiogram (ECG), oxygen saturation and exhaled CO_2% were assessed by Aestiva® monitoring systems. Oxygen saturation and heart rate were monitored by a secondary pulse oximeter as a redundancy measure. Mechanical monitoring was augmented by manual checks of HR, RR and mucous membranes every five minutes throughout surgery.

4.7.6 Analgesia

Fentanyl Patches (Durogesic), total dose of 0.2 +/- 0.01mg/kg. Patches were applied twelve hours prior to surgery to cleaned, clipped skin on the medial aspect of the forearm to deliver a dose rate of 2mcg/kg/hour. Patches were checked twice daily and repositioned as required. Patches were applied for sixty hours post-operatively providing up to seventy-two hours of opioid cover. **Lignocaine** 1-2% administered at 5mg/kg (not to exceed 10mg/kg), by subcutaneous perfusion of incision site, a line-block pattern was used. Local anaesthetic was administered to dermal ten minutes before first incision, and a second injection repeated at wound closure. **Buprenorphine** 0.01mg/kg i.m., administered as part of pre-medication and repeated during recovery. Effective analgesia provided for up to four hours and was repeated as required on an individual animal basis. Buprenorphine acts as a slow onset partial mu-agonist and suitable for co-administration with fentanyl at low doses, monitoring for opioid overdose was included as part of the aftercare plan.

.

4.8 Results

Overview: All animals survived surgery and recovered from anaesthesia. Uniformly, animals were observed to be stable on their feet and capable of un-aided eating and drinking within thirty minutes of anaesthetic cessation. All animals exhibited a degree of post-operative lameness ranging from 1/5th (mild gait abnormality) to 3/5th (obvious discomfort but remaining fully weight bearing) during the first twenty-four hours of recovery, there were no overt signs of lameness after seventy-two hours. Two animals developed moderate-severe 4/5th lameness (obvious discomfort with "toe-touching" weight bearing only) after being returned to the farm recovery, both animals were culled on welfare grounds in agreement with Home Office guidelines. As a result of complications arising from animal movement out of facility, future experimental animals were held in the BRF for the entire study duration, no further complications of this nature were experienced.

Data is presented in two parts; firstly, data from only the preliminary study is shown, demonstrating the validity of blank and allograft control datasets. In the second instance, control data accumulated from subsequent studies (data presented in Chapter V) is presented as a dataset pooled with the preliminary work, serving as the baseline historical data for the validated ovine condyle model.

Concerns were raised regarding the use of allograft as a positive control; variations in primary tissue, variability during milling, de-cellularisation, cost of storage and concerns regarding quality control. In subsequent experiments, autograft was used as the optimum positive control in keeping with clinical gold standard. Two autograft controls were performed in the preliminary study, bone volume values for the two samples was lower than had been expected, 266.10 mm^3 and 224.68 mm^3, Figure 4-11 both within the SE of allograft bone formation. In follow up defects the autograft protocol was updated to include more graft material within the defects, increasing bone volume and BV/TV values, presented in pooled data, Figure 4-14.

4.8.1 Pilot controls

In the whole 9mm defect region, allograft bone volumes (total bone 281.39 mm^3 SD = 67.40), were significantly greater ($p<0.005$) than blank defects (total bone 107 mm^3 SD 16.86). Bone volume in autograft samples (265.50 mm^3 SD = 34.37) was also significantly greater than blank controls with, although autograft sample numbers (n=2) were low and the test drastically under powered, (n=8 desired). Examination of the mini-cylinder ROI demonstrated significant differences between blank and allograft ($p<0.005$), and between blank and autograft ($p<0.05$), Figure 4-11 , Figure 4-12**.**

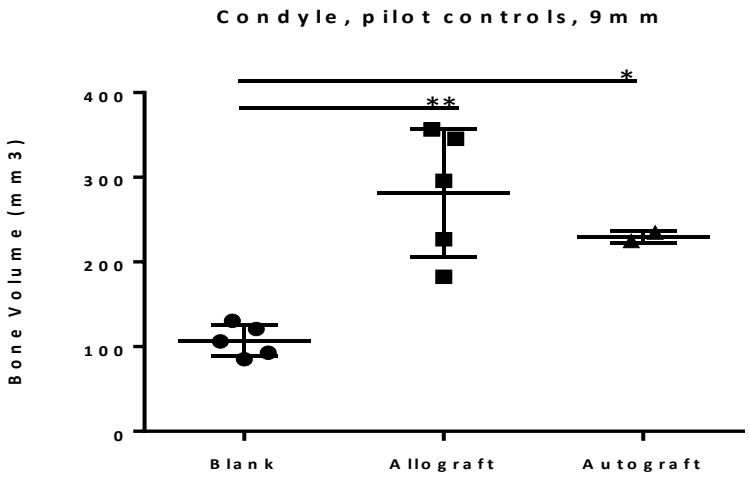

Figure 4-11 Pilot controls, 9mm ROI. Whole defect region of interest. Blank n=5, allograft n=5 and autograft n=2. Bone volume in Allograft and Autograft were significantly greater than blank defects. Error bar = SD**.**

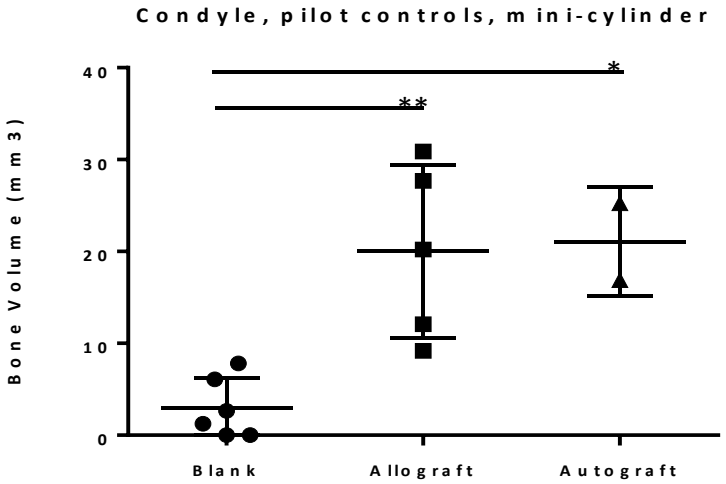

Figure 4-12 Pilot controls, 6mm ROI, mini-cylinder defect region of interest. Empty defect (blank) n=5, allograft n =5 and autograft n=2. Both allograft and autograft controls were significantly increased compared to blank defects. Error bar = SD.

4.8.1.1 Measurement of inter-sample bone density variation

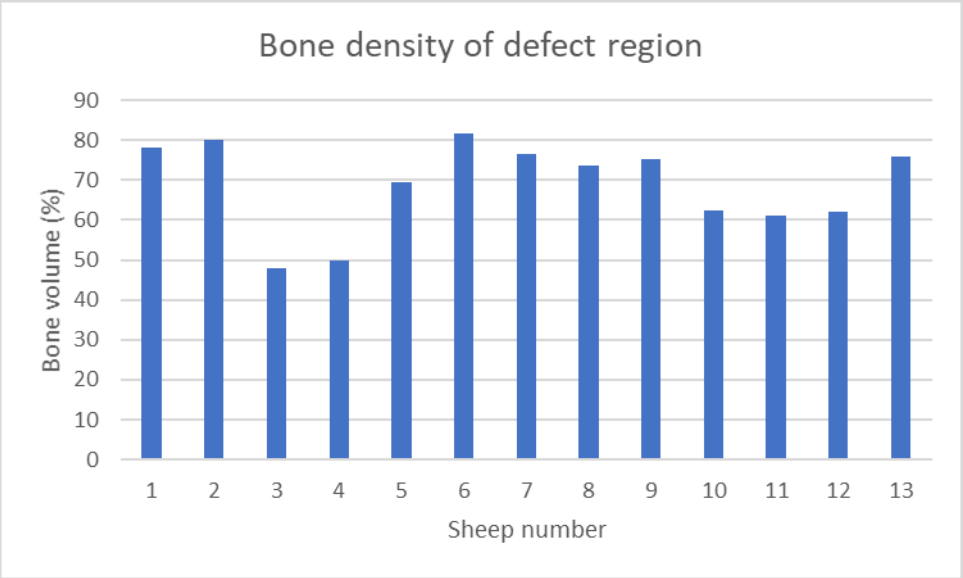

Figure 4-13. Bone volume of bone cores removed prior to implant placement. CT analysis of bone cores removed during surgery was used as a means of assessing variation between sheep in the cohort populaton. Bone density was measured as volume of bone as a percentage of the total defect.

4.8.2 Combined control data

Chapter V documents the use of the ovine condyle model to evaluate a hydrogel growth factor delivery system, experimental animals were split into two surgical batches with positive and negative controls allocated in each batch. Control data from these subsequent experiments was then combined with control data from the preliminary work and presented below.

Sample numbers in blank, n=9 and autograft, n=8 were augmented whilst those of allograft remained the same, n=5. The statistical difference between blank and autograft was increased in both the 9mm and 6mm ROIs, when examining total bone volume and bone volume/total volume or defect fill. Blank datasets were consistent, with a mean bone volume of 87mm^3, SD = 21, in the 9mm ROI and 3.93 mm^3, SD= 3.2 in the 6mm ROI. Autograft bone volumes increased from 265mm^3 (n=2) in the pilot data to 340mm^3 (n=8) in the 9mm ROI. Statistical significance between blank and autograft groups in both 9mm and 6mm ROIs altered from $p< 0.05$ in pilot data to $p<0.0001$ in the combined datasets.

Allograft sample numbers were not added to after the preliminary study, a decision was made to move from allograft to autograft as our control graft material. When comparisons were made between blank, allograft and autograft, mean allograft bone volume was demonstrated to be greater than blank and less than autograft in both 9mm and 6mm ROIs, and only significantly greater than blank in the 9mm ROI (pooled data). Figure 4-14, Figure 4-16.

4.8.2.1 Combined control data, 9mm ROI

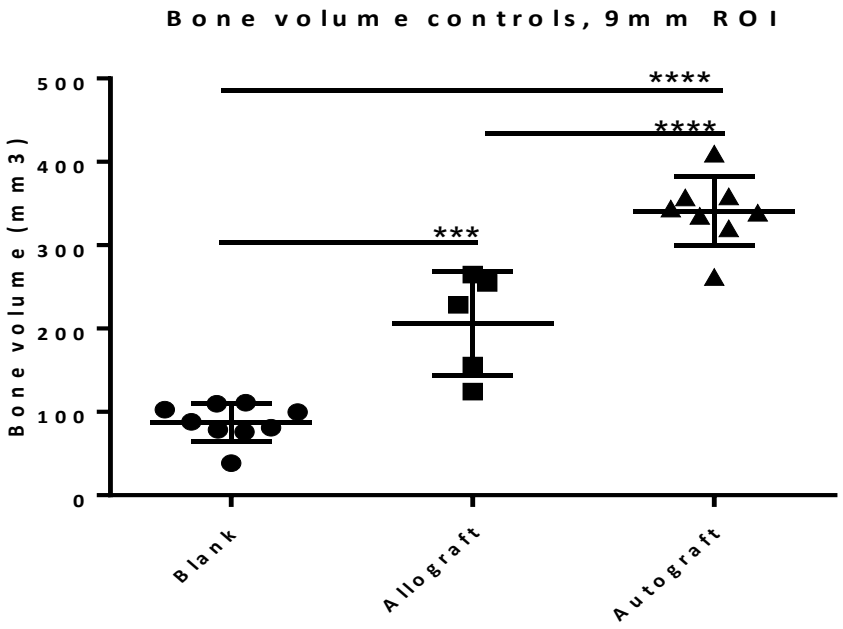

Figure 4-14. Control data, preliminary and follow up experimental data combined, bone volume, 9mm ROI. Statistical differences were demonstrated between blank (n=9) and allograft (n=5), blank and autograft (n=8) and between allograft and autograft.

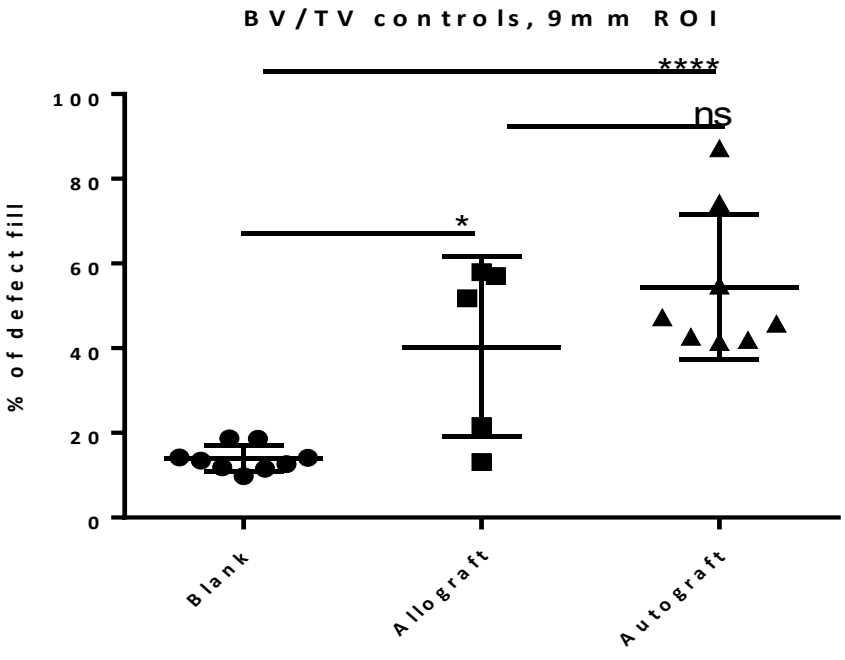

Figure 4-15. Control data, preliminary and follow up experimental data combined, BV/TV, 9mm ROI. Defects allograft and autograft had demonstrated a significantly higher percentage of defect filling, there was no difference between bone graft groups.

4.8.2.2 Combined control data, 6mm ROI

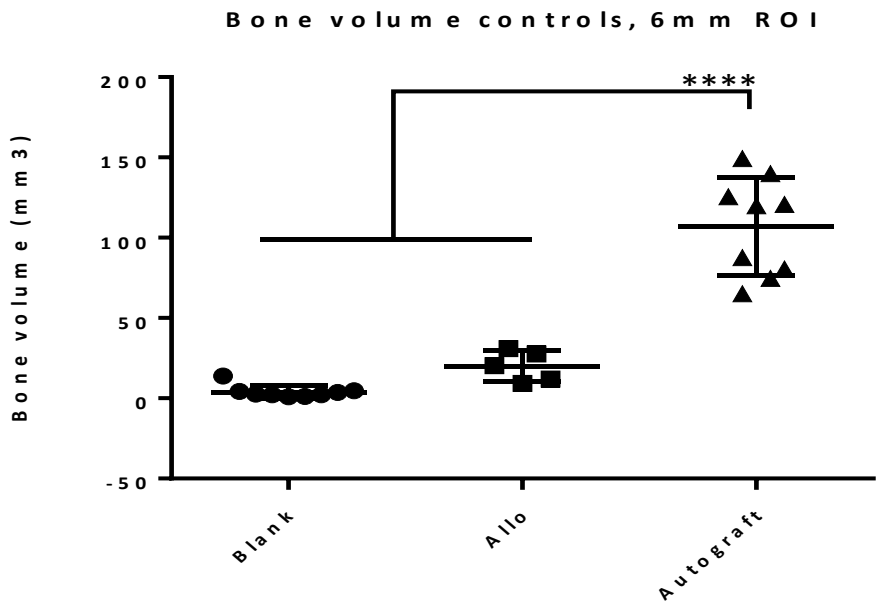

Figure 4-16. Control data, preliminary and follow up experimental data combined, bone volume, 6mm ROI. Autograft controls were significantly greater than blanks, with no difference between graft types.

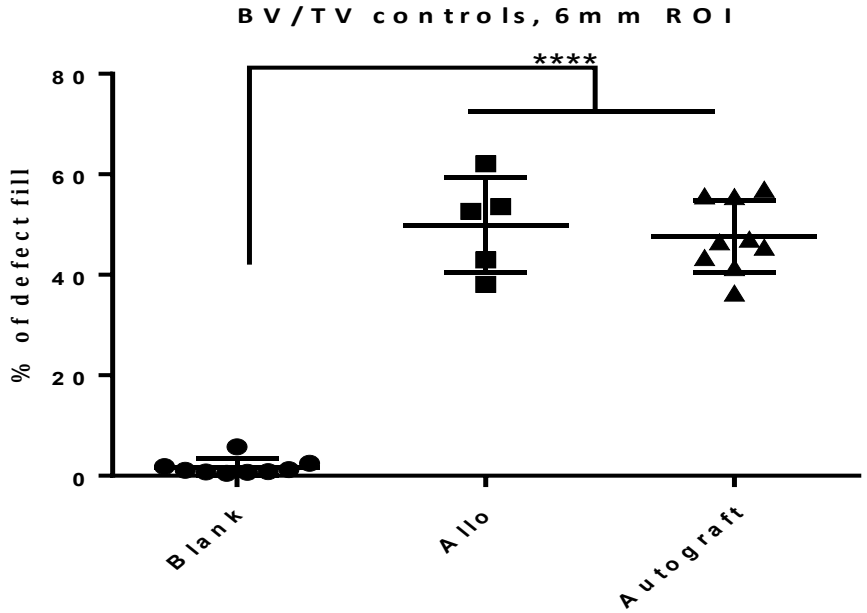

Figure 4-17. Control data, preliminary and follow up experimental data combined, BV/TV, 6mm ROI. When examining the percentage fill of defects, both allograft and autograft groups were significantly greater than blank controls, with no differences between bone graft materials.

4.8.3 Computed tomography, 2-D Renders

A panel of 2-D images from blank and autograft µCT scans is shown in Figure 4-18.

Blank and positive control numbers were increased to augment the previous dataset and led to a reliable and clearly separated significant difference in measured bone volume between negative and positive controls. The significance is evident on CT render, Figure 4-18, and when plotted graphically, Figure 4-14.

Blank Samples: In all five blank samples, a similar pattern of repair was seen. Bone formed at the top of the defect, growing from the periosteal boundary and folding inwards toward the defect base, in some cases forming a soft-edged rim, limited to the top of the defect. A small amount of new bone formed from the defect floor, rounding-out the bottom corners, turning the sagittal cross-section view from a square bottomed rectangle "□", to a curved "U", Figure 4-18. Empty controls did not show bone growth in the centre of the defect, this region was later focussed on in analysis, termed the "mini-cylinder" and was selected as a suitable location to assess new bone distinct to the innate healing response.

Autograft: The pattern of growth and repair for autograft was characterised by a dense and closely orientated pattern of bone spicules, appearing more compact when assessed visually. In all autograft samples, strong new bone growth was seen from the top of the defect inwards, this new bone was intimately associated with the non-defect periosteal region. Bone formation was almost exclusively continuous throughout the defect, including the central region away from the defect edges. Bone volume measured within the larger 9mm ROI was significantly greater in autograft over blank in 9mm and 6mm ROIs.

4.8.3.1 2-D Renders, empty and autograft samples

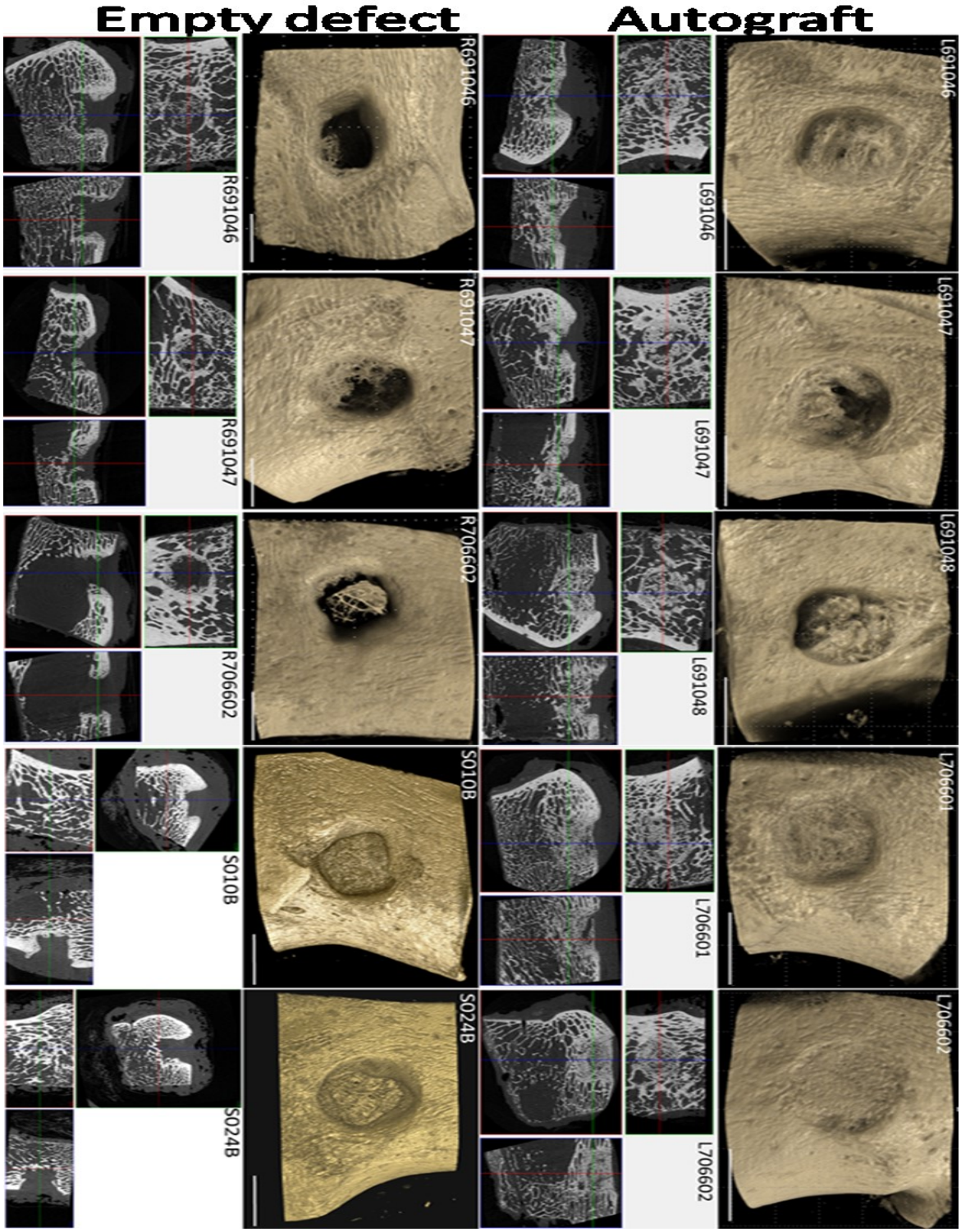

Figure 4-18 Two dimensional renders of high-resolution µCT scans. Representative images from blank and autograft groups are shown. Black and white images show 3 cross-sectional views whilst colour images are high resolution renders of transverse cross-sections. White scale bar = 8mm.

4.9 Discussion

4.9.1 Surgical model

The research team rapidly became accustomed to surgical protocols, defects were created uniformly and with minimal impact to research animals. Once a unilateral defect was established, the extension to bilateral defects did not excessively increase procedure duration and did not complicate intra or post-operative outcomes.

The choice of an upland hill ewe proved appropriate, the femoral length and diameter were shorter and narrower than expected but the reduced frame was balanced by a lower and more manageable body weight. In the proof of concept phase, Welsh Lleyns was used, these were replaced by the Llanwenog in subsequent experiments due to the breeds' comparatively docile nature and compact, shorter and broader, skeletal frame. Housing was modified over three experimental durations, with an adaptable, metal hurdle solution replacing the individual isolated lambing pens, which accommodated both individual recovery and easy intermixing. Feed and bedding were deemed appropriate, though animals were prone to post-operative weight gain.

A focus of surgical optimisation was the accurate identification of the drill defect site. A significant varying factor found during analysis was the extent to which the drill had penetrated trabecular bone and the curvature of the defect surface. This in-turn was linked to the reproducibility in defect location. Identifying reliable landmarks and a reproducible description of how to palpate the landmarks took time to develop and were the result of operator inexperience with the model, evidenced as samples in the second and third experimental setups were far more uniform in location.

A variation was noted regarding the trabecular density experienced whilst drilling. It is not known whether this variation was due to the location of the defect or the result of interpatient variation. Bone cores were scanned once extracted from the defect. The bone volume as a percentage of the total defect was calculated and used as a measure of bone density. This variation was between 47 and 75% with 11/13 samples greater than 62%. Similar measurements are not present for comparison in the literature and the significance of the variation is unknown.

Two animals were euthanased after developing lameness on turn-out to grass during the proof of concept stage. Both animals were of advanced age and on necropsy showed cortical thinning and almost complete loss of trabecular bone. Although anatomical/physiological and husbandry factors are likely to have contributed to the development of lameness, the mal-positioning of drill holes and potential cortical perforation proximal to the metaphyseal line must be kept in mind as

a potential cause, as reported by Nuss (Nuss et al., 2006b). A further animal was put to sleep on welfare grounds three days after surgery as it had developed non-weight bearing lameness. Post-mortem revealed the presence of underlying bone pathology which had fractured after surgery.

4.9.1.1 Improvements

Animals: A decision was made to move away from older females in future experiments. The combination of age and sex, although more representative of the intended clinical demographic, were of varying health status and in some fatal cases, had experienced age-related bone loss which were not suitable for surgery. Aged female animals were also not readily available for purchase and required a deal of investigation to source. 2-year-old females or males would be used in future, with males preferable should a segmental defect be undertaken.

Surgery: It may have been possible to identify many of these complications with the use of high resolution intra-operative imaging, and exclusion of these animals from the experimental cohort. The use of intra-operative imaging, such as high resolution X-ray or CT C-arm, would have increased data collection before and during the experimental period and help identify reasons for inter-patient sample variation. The same equipment would allow a form of longitudinal data collection, examining samples on a regular basis throughout the study duration.

The process was fluid with regular modifications made to items of surgical equipment, and improvements made to animal handling, anaesthesia, surgery and post-operative care. The protocols described in this chapter are the result of continual refinement and vary from those first used during the proof of concept phase. Two areas of ongoing need were identified i) intra and post-operative imaging, ideally by means of C-arm which would allow visualisation of defect position, identification of areas of low density trabecular bone and enable the surgeon to identify possible underlying bone pathology. ii) The ability to perform blood and biomarker analysis, both to improve pre-operative health checks but to aid with monitoring inflammation and repair response. These improvements are under consideration and hope to be incorporated in future experiments.

Further model developments could see the introduction of multiple defects in the proximal as well as distal femur and have also been documented in the humerus. Multiple defects would allow for increased sample number in fewer animals, it would also be possible to use on animal to examine different time points.

A portion of variation in defect volume resulted from the lack of accurate imaging. This resulted in samples varying in depth, cortical thickness, location in bloody or relatively fatty marrow areas and in more severe cases, not possessing a bone floor to the defect and being rendered not fit for purpose experimentally.

4.9.2 Analysis

The Bone and Joint Research Group, both independently and through facilities available through the University has an excellent capacity with qualitative and quantitative high resolution µCT. µCT is a sensitive imaging modality providing sensitive information regarding bone volume and structure but does not provided detail on the composition or physical properties of new bone or material formed.

Histology: Histology of control and experimental samples was underway at the time of writing but delays were experienced due the sample size, tough physical properties and the ovine origin of tissue. We are confident that effective protocols have been developed to process and produce high quality histology from decalcified tissue, however, to obtain accurate morphological descriptions of tissue, histology of calcified samples is required. The outlay in equipment, staff skill and budget to run a centre suitable for hard-tissue histology is significant and at present could not be justified by the sample caseload. These facilities are available through collaborative partners and are more applicable to samples obtained from segmental defect models then the smaller condyle defect.

Imaging directed mechanical evaluation: Non-invasive assessment of osteoporosis and fracture risk by dual-energy X-ray absorptiometry (DXA) and High Resolution Quantitative Computed Tomography (HR- QCT) are validated diagnostic tools clinically with supporting trial evidence. (Cheung et al., 2013; Sornay-Rendu et al., 2017). Using these techniques measurements of trabecular number, spacing, thickness and connectivity and areal BMD are combined to produce a virtual picture of the bone architecture which is compared with historical data and interpreted to form a diagnosis. Despite having the capacity to measure trabecular elements and BMD (although not DXA), these techniques were not applied to the condyle defect sample. It was decided that due to the restricted size of samples, the variation between host bone structure and the unusual patterns of bone growth that these measurements would be misleading with translational outcomes difficult to infer. These measurements were possible and a more in-depth picture created when combined with mechanical data, however the scope of work required to produce meaningful data in this regard was beyond the scope of the present work.

Mechanical testing: Traditional mechanical testing of whole bone samples such as axial compression, torsional moment assessment and 3-point bending are destructive and require excised bone for analysis (Coelho and Fernandes, 2000; Gallant et al., 2013). We chose not to employ traditional techniques in the condyle defect scenario because of the variation in host bone of our samples and the non-weight-bearing location of defects.

Although not included in Chapters IV or V, we are investigating the application of Micro-Indentation (MI) as a source of mechanical data. Reference Point Indentation (RPI) has been used clinically as a minimally invasive technique to assess mechanical properties of bone (Diez-Perez et al., 2010), antiretroviral and bisphosphonate related fracture risk in osteoporosis (Diez-Perez et al., 2010; Bedimo et al., 2012). The BJRG has published on the use of a hand-held RPI device and compared *in vitro* values obtained from femurs of varies species to human *in vivo* data (Jenkins et al., 2015) We will use this technique *in vitro* to obtain a suitable mechanical dataset and compare with known disease states *in vivo* and results from future *in vivo* experiments.

Model validation

Results obtained comparing bone volumes in negative blank controls and positive allograft controls were statistically significant, sample number in these groups were smaller than the desired n=8. Preliminary results for bone volume in autograft groups were higher than blank, but n=2 meant the data was not reliable. When control numbers were combined with values from follow up studies, a reliable significant difference in bone volume and BV/TV was demonstrated between blank, autograft and allograft. We are confident that these data support the claim of a validated bone defect model.

4.10 Conclusions

The BJRG has successfully developed the surgical, infrastructural and analytical protocols required to execute an ovine condyle defect model at the University of Southampton.

As in models using younger animals, bone healing in positive autograft and allograft was statistically significant validating the model for use in further *in vivo* testing.

All Home Office requirements were met and the BJRG may now implement the ovine condyle defect model as described without regulatory restriction.

The model has been validated with reliable reproduction of positive and negative control values

4.11 Appendix I

4.11.1 Husbandry, housing and animal source

4.11.1.1 Staff

PPL holder Dr Janos Kanczler has experience with *in vivo* experimentation and laboratory animal husbandry including small, medium and large (bovine) models spanning 20 years. **PIL Cameron Black**, veterinary surgeon with protocol specific proficiency achieved through cadaver specimen rehearsal combined with live animal training at FIRS, Nottingham University, under supervision form Dr Jane McLaren and Professor Brigitte Scammell. **Michael Broome** Member of the Institute of Animal Technology, registered Animal Technician and Named Animal Care and Welfare Officer. Prior experience included sheep work at the BRF under Dr Lucy Green. Refresher training was undertaken at the RVC during December 2013. **NVS** oversaw and approved surgical and husbandry protocols.

4.11.1.2 Animal breed, source and procurement

All housing and husbandry protocols were designed to comply with guidelines set out in EU directive 2010/63/EU Annex A, General Conditions and Section G Sheep and Goats.

4.11.1.3 Designated Site

"Designated site" refers to the farm premises licensed for the purchase, housing and post-operative management of experimental animals.

Animals: Skeletally mature adult sheep, aged but whole mouthed ewes of upland hill breed, e.g. Welsh Llynn, and Llanwenog, mature weight 60-75kgs were used in this programme of work. An upland type sheep breed was selected based on lower adult live-weights and skeletal dimensions. Low-land traditionally indoor housed breeds tend to be heavier with shorter limbs and a "stockier" build, making the animals less suitable for the model protocol.

As all animals would be taken from extensive hill farm environments the animals were required to spend a minimum of two weeks on-site at the HO designated site prior to movement into the Biomedical Research Facility (BRF), University of Southampton. During this time animals were acclimatised to indoor housing and halter trained for improved handling in the BRF. Each animal was held separate to main herd to assess and ensure biosecurity. During the preliminary study, six animals returned to designated site, fourteen days post-surgery and remained on-farm until study end-point, ten weeks post-surgery.

Haltering: In consultation with HO, all animals were acclimatised to indoor housing by a period of routine handling, a daily mock exam and a two-hour period of haltering within the pen environment. The acclimatisation process was performed by staff at the designated site. After the preliminary study, it was decided to limit halter training only to animals which failed to adjust to indoor housing.

Housing: Animals were barn housed with a total 18m x 12m floor footprint, 4.2m internal height, enclosed on three out of four aspects, shielding from prevailing wind. Sides were added as part of HO requirements and both lower full boarding and upper York boarding added. Housing ventilation was measured at approximately fifteen air changes per hour, in keeping with regulation.

Husbandry All animals were group penned indoors, each pen of size 3.5m x 4.5 m to hold up to five animals, providing 3.3m^2 floor area per animal. An animal with a specific health concern was penned individually in 1.8m x 1.8m pens. Animals were bedded with clean straw, changed as appropriate. Maintenance feed ration to comprise approximately 80% hay with 20% sheep concentrate feed with ad-lib fresh water.

Movement It was necessary to ensure that all animal movements on and from the designated site were registered and traceable by local Trading Standards Authority. It was ensured that: i) Transport type was appropriate to the number of animals transported. ii) No animal was transported individually and no more than six animals moved in any one day. The route and timing of transfers between designated site and the University of Southampton was designed to minimise the total duration of transport and ensure safety of individual animals. Delivery was scheduled during periods low staffing and minimal activity around the delivery point.

Biosecurity The designated site was under the care of a veterinary herd health scheme which included robust protocols in the prevention and transmission of communicable diseases both onto and within the site. All new stock, including experimental animals were examined prior to movement on-site and were isolated for a two-week period prior to integration with general population. All experimental animals were treated upon arrival with Zolvix (Monepantel, 1ml/kg) drench and Coopers Spot on (Deltamethrin, Cypralic and Cyric Triglyceride) providing comprehensive parasitic protection extending for a minimum of 4 weeks. Animals were inspected before movement into the BRF.

4.11.1.4 BRF housing

Movement: Transport between the farm and the BRF was identified as a major area of concern for both the Home Office and for the University hierarchy. The following procedure was developed to reduce movement issues. Animals were delivered during a time of minimal staff presence and activity around the entrance e.g. 5.00-6.00am. The PIL holders and designated Animal Technician were present for throughout movement, from arrival on-site to transport through the hospital into BRF large animal housing unit. Individual animals were moved within an enclosed, secure trolley. All reasonable precautions were taken to minimise the risk of visual exposure to the public.

Husbandry During the preliminary phase all animals were individually penned (Solway Pens), 6ft x 5ft (1.83m x 1.53m), providing 2.8m^2 floor space/ animal. No fewer than two animals to be housed within one room at any time. This was adjusted to an open pen setup with up to six animals in a 16m^2 environment.

Animals were fed on a maintenance ration of hay, supplemented with ewe concentrate feed (Champion Ewe Nuts 16, SCATS). Hay to be stored at the site designated site, placed in reusable autoclavable bags, transported to the BRF and autoclaved prior to storage within the facility.

Water was provided ad-lib, changed daily, immediately if soiled to all animals. Ample hay covering floor space was provided as bedding and cleaned daily (Bedding should be of sufficient to prevent formation of pressure related injuries when animal is at rest and provide absorption of excreta).

4.12 Appendix II

4.12.1 Surgical materials

Consumables

All consumables and drugs were supplied by Centaur Vet Supplies unless otherwise indicated by italics

Microchip ID (Pet ID Microchips, UK)

Central Venous Cather, (Arrows, Telefrex International, USA) - *NHS Supplies*

Ioban Incise drapes sterile drapes (3M Medical, USA)

Barrier drapes (3M Medical, USA)

Foliodrape (Hartman, UK)

Intravenous catheter 21G (Smith's Medical, Jelco, USA)

Syringe 2/5/10/20ml (Aniject, Millpledge Veterinary supplies, UK)

Needles 18g, 21g and 23g (Terumo medical, Japan)

Ringer's Lactate 500ml and 1L (Vetivex, Dechra USA)

Sterile saline, 500ml and 1L (Vetivex, Dechra USA)

Hypertonic Saline, 7.2% (Vetivex, Dechra USA)

Fluid giving set, 20 (Aqupharm, UK)

Three-way tap (Smith's Medical, Jelco)

Sterile disposable gown (3M Medical, USA)

Sterile surgical gloves, size 7 and 8 (Krutex, Kruuse Int. DEN)

Co-flex bandage (Medline, USA)

Soffban Plus bandage (BSN Medical, UK)

Tensoplast bandage (BSN Medical, UK)

Sterile Gauze swabs (Steroplast Healthcare)

Cotton wool 500g (Millsoft, UK)

Vicryl 2/0 and 3/0 suture (Polyglycolide 910, Ethicon)

PDS 2/0 and 3/0 suture, (Poly p-dioxanone, Ethicon)

Chlorhexidine, 5% (Krusan, Kruuse,DEN)

Iodine Vet (Kruuse, DEN)

Single use Surgical scrub brush (E-Z Scrub, BD Worldwide, USA)

Suction canister (GBUK, UK)

Equipment

Aestiva® 5 Anaesthetic machine, (Datex Ohmeda, GE Healthcare, USA)

OsteoPower® orthopaedic drill (OsteoMed, USA)

Eiketron® Electrosurgery unit (Eikemeyer, UK) - *Eikemeyer*

Veterinary pulse oximeter (LifeVet, Eikemeyer, UK) - *Eikemeyer*

Suction pump, SIP 3000 (Eikemeyer, UK) - *Eikemeyer*

9mm x 15mm trephine Drill bit (Primadent UK) - *Primadent Supplies*

Drill guide (custom)

Bone core remover (custom)

Flat head reamer (custom)

Laryngoscope, 12cm blade (Eikemeyer, UK) - *Eikemeyer*

Animal stretcher (custom)

Unifusor® Pressure Infusor (Statcorp Medical, USA) *Eikemeyer*

Wietliner Retractor (Eikemeyer, UK) - *Eikemeyer*

Homan's retractor (Eikemeyer, UK) - *Eikemeyer*

Size 4 scalpel handle (Eikemeyer, UK) - *Eikemeyer*

Size 15 scalpel blade

Artery forceps (Eikemeyer, UK) - *Eikemeyer*

Tissue forceps (2 teeth) (Eikemeyer, UK) - *Eikemeyer*

Gillies forceps (Eikemeyer, UK) - *Eikemeyer*

Needle forceps (Eikemeyer, UK) - *Eikemeyer*

Metzenbaum scissors curved 8cm (Eikemeyer, UK) - *Eikemeyer*

Metzenbaum scissors, straight, 10cm (Eikemeyer, UK) - *Eikemeyer*

Rongeurs, Leur-Friedman, (Eikemeyer, UK) - *Eikemeyer*

Periosteal elevator (Eikemeyer, UK) - *Eikemeyer*

Curette, 15cm handle, 6mm cup (Eikemeyer, UK) - *Eikemeyer*

Kidney dishes (Eikemeyer, UK) - *Eikemeyer*

Autoclave (L.E West Benchtop Autoclave, UK)

Pet ID chip reader (Pet ID Microchips, UK)

Pharmacological agents

Isoflurane 100% (Isoflo® Abbott Animal Health, USA)

Fentanyl patches 50mcg/hr (Durogesic®)

Buprenorphine 0.3mg/ml (Vetergesic®)

Lidocaine HCL 2%- (Fresenius Kabi, USA)

Propoflo 10mg/ml (Abbott Animal Health, USA)

Midazolam 10mg/2ml vials (Hypnovel®, Roche, CH)

Ketamine 100mg/ml (Ketaset®, Zoetis, USA)

Penicillin/Streptomycin (Duphapen/Strep®, Fort Dodge, USA)

Chapter V

5 Controlled delivery of a commercial Bone Morphogenic Protein-2 product "InductOS®" by a Laponite gel carrier

The nano-silicate hydrogel "laponite" has demonstrated a high affinity for protein binding and controlled release *in vitro*, in chapter V the capacity of Laponite to influence bone formation by the controlled spaciotemporal delivery of low concentration of BMP-2 is investigated in an ovine condyle model.

Acknowledgements

The following work required a broad collaboration across a varied skillset in the Bone and Joint Research Group. The surgical team comprised of Dr Janos Kanczler, Dr Jo McEwan and Miss Julia Wells, with Dr Jon Dawson preparing constructs and assisting in implant delivery. Sample retrieval was performed with Dr Janos Kanczler and post mortem cell isolation, cell culture and differentiation was shared along with Miss Julia Wells and Dr Jo McEwan. I am grateful to Dr Stuart Lanham who performed µCT scanning and image reconstruction and provided expert advice on the development of CT analysis protocols. The staff of the BRF, University of Southampton, in particular Mr Mike Broome for his daily care and husbandry of all experimental animals and Mrs Lisa Dunning for the purchase, housing and delivery of pre-experimental animals. University of Southampton Named Veterinary Surgeon for active consultation, protocol development and provision of veterinary care. The ongoing post-analysis including histology is being shared by all members of the Bone and Joint Research Group mentioned above: Dr Janos Kanczler, Miss Julia Wells, Dr Jo McEwan, Dr Stuart Lanham and Dr Jon Dawson. Finally, to thank group PI Professor Richard Oreffo for continual support, advice and expert opinion.

5.1 Introduction

The application of mitogenic, proliferative and morphogenic peptides in bone tissue engineering has developed rapidly in the past decade to include approaches to control the release and localisation of bio-active proteins. Clinically administered doses of BMP-2 are measured in milligrams, in marked contrast to the micrograms per kilogram measured in demineralised bone matrix (Bessa et al., 2008). The clinical application of such supra-physiological doses has been shown to trigger severe adverse effects including catastrophic swelling, heterotopic bone formation and osteolysis (James et al., 2016). The far lower physiological concentrations of BMP-2 located in the ECM intimates a control, activation and stabilisation role of BMP-2 binding domains within the ECM in the homeostasis and repair of healthy bone tissue. For a review of ECM in BMP-2 regulation see Umulis et al. 2009 (Umulis et al., 2009) .

Therapeutic outcomes of BMP-2 delivered in solution are unpredictable and do not always correlate to the dose response observed *in vitro*, the discrepancy is in part linked to a short *in vivo* half-life, rapid tissue clearance and complex localised cellular and molecular interactions at the target site (Kempen et al., 2008). Thus, it is necessary to develop carrier materials optimised to control the localisation and release kinetics of BMP-2 in a clinical setting. Although recombinant human BMP-2 can induce *de novo* bone *in vivo*, the osteogenic effects of BMP-2 are enhanced when delivered in combination with a biomaterial carrier (Uludag et al., 1999). Sustained BMP-2 release and enhanced osteogenic activity has also been demonstrated in a range of delivery vehicles including; fibrin glue (Li et al., 2016), colloidal hydrogels (Wang et al., 2013), functionalised organic polymer gels (Bhakta et al., 2012) and composite inorganic polymer systems (Seo et al., 2015).

Collagen scaffolds have a long history of use as carriers of BMP-2, demonstrating successful osteogenesis *in vivo* and are commercially available and licensed for clinical application (Spiller and Vunjak-Novakovic, 2015). Uludag (Uludag et al., 1999) demonstrated that the majority of BMP-2 activity, when applied in aqueous solution to a collagen sponge, was exhausted by 3-5 days *in vivo*, highlighting the need for approaches to sustain BMP-2 activity throughout the repair process.

The use of biodegradable carriers to mediate the spatio-temporal activity of growth factors, including BMP-2, demonstrated improved efficacy over the use of BMP-2 in solution. For example, Yamamoto and colleagues investigated the effect of gel hydration on the ability of gelatin gels to localise BMP-2 and induce ectopic bone formation (Yamamoto et al., 2003a), linking burst and sustained growth factor release to gel hydration in cross-linked gelatin hydrogels. Yamamoto found that the amount of new bone formation was inversely correlated to gel water content and, furthermore, that all hydrogels were significantly superior to BMP-2 in solution when assessed for ectopic bone and BMP-2 regional isolation.

Work by Kolambkar and colleagues showed a distinct advantage of controlled spatiotemporal administration of BMP-2 in a rat femoral segmental defect model (Kolambkar et al., 2011a), the authors demonstrated enhanced osteogenesis using a hybrid alginate BMP-2 hydrogel and PCL mesh system when compared to collagen sponge loaded with BMP-2 in solution.

Typically, a biomaterial delivery strategy aims to mimic the release-moderating effects of the ECM, stabilising and conveying the biological payload in a targeted and sustained manner. The release kinetics of peptides can be altered by manipulating degradation, erosion and absorption properties of the gel carrier (Drury and Mooney, 2003).

The release of biologically active peptides from a hydrogel is typically diffusion dependant with an initial burst release followed by a tapering off with much lower concentrations of the peptide/factor of interest (Spiller and Vunjak-Novakovic, 2015). Of particular interest, the release kinetics and degradation profiles of hydrogels can be modified, the complex interactions within nano-silicate gels further modulate release through cationic exchange, hydrophobic interactions, proton transfer and hydrogen bonding, potentially sustaining the release of bioactive proteins such as BMP-2 *in vivo* (Dawson et al., 2011).

5.1.1 Chapter in context

Work from Gibbs and colleagues has demonstrated the potential for self-organising nanoparticle clay gels to modulate the activity of BMP-2, demonstrating a binding affinity for BMP-2, producing a localised *in vivo* osteogenic response. (Gibbs et al., 2016b). In the first experimental scenario, a nanosilicate synthetic hydrogel, Laponite, was used to functionalise decellularised allogenic bone graft. In this set-up, the use of Laponite as a moderator of BMP-2 action and delivery was examined using sterilised decellularised cylinders of human trabecular bone in a mouse sub-cutaneous model.

Bone cylinders were allocated into blank control (PBS only), rhBMP-2 in PBS buffer (BMP-2 only), BMP-2 applied premixed into a 2.5% Laponite solution (encapsulated BMP-2) and BMP-2 first applied to the cylinders with Laponite applied secondarily (exogenous BMP-2). The use of Laponite as an enhancer of BMP-2 activity on a non-osteoinductive scaffold was selected due to the clear potential correlation to clinical application of allograft and allograft derived products.

In vivo results indicated that when BMP-2 was applied exogenously to Laponite, the osteogenic activity was enhanced compared with BMP-2 applied directly to bone without Laponite. Furthermore, there was enhanced bone formation within the Laponite encapsulated BMP-2 group, although not significantly greater than BMP-2 alone. Histologically, both encapsulated BMP-2 and exogenously applied BMP-2 groups demonstrated intramembranous and endochondral ossification respectively with hypertrophic chondrocytes, osteoblasts and osteoid matrix confirmed histologically.

Although these data were suggestive of the beneficial clinical use of Laponite in BMP-2 mediated bone repair, it was noted that the model may not have been sensitive enough to reliably identify an osteogenic effect as measured by new bone formation with CT.

The complex irregular shape of trabecular allograft bone was difficult to accurately analyse through CT co-registration and the problems of identifying new bone were compounded by the degree of bone absorption which was expected to be occurring concurrent with bone formation. The follow-up *in vivo* design sought to remove the confounding elements of the original study while still testing Laponite mediated BMP-2 release in a clinically relevant model.

5.1.2 Use of a collagen sponge substrate

The use of allograft cores in a mouse subcutaneous model obscured the detection of new bone formation by µCT, this complication was a likely consequence of the intricate pattern of trabecular bone and potentially the osteoconductive and inductive nature of allograft masking the osteogenic effects stimulated by BMP-2 delivery (Gibbs et al., 2016b). In the second set-up, Gibbs et al used a non-osteoinductive radiolucent scaffold material, in this case absorbable collagen sponge (ACS), increasing the sensitivity of the experimental set-up, as all bone measured could be directly attributed to the osteogenic effects of the hydrogel system. It was this ACS substrate approach that was translated into the ovine condyle model. A total dose of 100µg rhBMP-2 was used per defect at an approximate concentration of 160µg per ml of scaffold material across groups.

Collagen has been used as a delivery vehicle for BMP-2 both experimentally and clinically. In the second small-animal *in vivo* experimental set-up the ability of Laponite to induce osteogenesis by delivering low doses of BMP-2 on a collagen sponge carrier was examined. In this experiment two concentrations of BMP-2 (7µg/ml) and lower (0.7µg/ml) were compared using Laponite and standard BMP-2 buffer. The BMP-2 applied onto Laponite coated collagen sponge at high concentration level yielded a significant amount of new bone formation.

At a ten-fold reduction in BMP-2 concentration the osteogenic effect was maintained in Laponite encapsulated BMP-2 yet absent in the alginate (hydrogel control) carrier. These findings indicated a method to deliver BMP-2 which would overcome issues relating to prohibitive cost and deleterious off-target effects that have been associated with currently available products. The ability of Laponite to sustain and enhance the bone-forming effects of BMP-2 at low concentrations was indicative of a beneficial interaction between clay chemistry and the BMP2. The following work sought to expand upon these beneficial interactions and investigate the translational suitability of Laponite to deliver low-doses of BMP-2 using a large animal preclinical model- the recently established ovine femoral condyle model. Experimental groups were chosen to mimic the previous small animal models, comparing the BMP-2 delivery efficacy of Laponite and the standard BMP-2 buffer. A third group was also introduced to examine the possibility of using Laponite gel and BMP-2 alone as an osteogenic therapy in a large defect environment.

5.1.3 BMP-2 dosing

Medtronic InductOs® has been used clinically at a product dose of 1.5mg rhBMP-2/ml (Lissenberg-Thunnissen et al., 2011). Data for, InFUSE®, North American branding of InductOS®, references variable effective dose ranges depending on species and model (FDA P000058, 2002). In a rat femur critical defect model, the effective dose range was published at 0.025 -0.05 mg/ml and a dose-response of 0.2-0.5mg/ml recorded in a canine radius defect model.

The picture in non-human primates differed as no effective response was noted below 0.4mg/ml with no reliable dose-response between 0.4 and 1.5mg/ml. Without a clear distinction regarding a minimum effective dose in translational models we undertook to dose based on the known ability of Laponite to deliver bone formation at 10-fold dose reduction which in turn was advised by product information and literature search.

A literature search of hydrogel based BMP-2 delivery systems identified a range of experimentally effective BMP-2 doses. These findings substantiated the chosen experimental BMP-2 concentration and overall BMP-2 dose per defect. Table 5-1 details studies using non-polymer and organic hydrogel carriers to lower the effective BMP-2 dose in ectopic small animal models. Synthetic polymers (e.g. “PEG” hydrogel), solid scaffolds (e.g. CaP granules) and bone derivative products (e.g. DBM) were excluded to focus on systems similar in nature to those being tested.

Minimum effective dose (µg)	Minimum effective concentration (µg/cm³)	Carriers	Model	Species	Study
No bone	n/a (0.18 tested)	Alginate +- gelatin	Subcut.	Mouse	(Michelle T. Poldervaart et al., 2013)
5	6.4	Collagen sponge	Subcut.	Rat	(Wijdicks et al., 2009)
2	10	Collagen gel + BMP-binding peptide	Subcut.	Rat	(Hamilton et al., 2013)
0.5	26	Collagen sponge (+ collagen-binding BMP2)	Muscle	Rat	(Visser et al., 2009)
5	88	Collagen sponge	Subcut.	Rat	(Preativatanyou and Honsawek, 2011)
30	150	Hyaluronan hydrogel	Muscle	Rat	(Hulsart-Billstrom et al., 2013)
5	179	Collagen sponge	Subcut.	Mouse	(Nakamura et al., 2005)
5	179	Collagen sponge	Subcut.	Mouse	(Zhao et al., 2006)
5	357	Collagen sponge + dextran	Muscle	Rat	(Degat et al., 2009)
25	500	Collagen/DNA	Subcut	Rat	(Murata et al., 2002)
150	750	Hyaluronan hydrogel/ Chitosan hydrogel	Muscle	Rat	(Luca et al., 2011)
150	750	Chitosan hydrogel	Muscle	Rat	(Luca et al., 2010)

Table 5-1 Hydrogel delivery of BMP-2 in ectopic small animal models.

5.2 Aims

1) To successfully implement the validated ovine femoral condyle surgical protocol to examine growth factor mediated bone formation and to continue to develop and improve protocols as required.
2) To document the efficacy of Medtronic InductOS® at a reduced dose in an ovine cortical defect model.
3) To deliver BMP-2 using a 2.5% Laponite gel and compare efficacy to Medtronic InductOS® as described in (2) above.
4) To assess the potential use of Laponite gel as a sole delivery agent for bio-active peptides in bone regeneration, in this scenario, BMP-2.

5.3 Null hypothesis

The use of Laponite, either as a sole agent or combined with a college sponge carrier will not enhance the bone forming activity of BMP-2 when applied in an ovine condyle defect, and will not demonstrate significant new bone growth over empty controls.

5.4 Methods

Experimental design

All animals were allocated into one of the five groups outlined below. A total of 24 experimental animals were included in two surgical batches of 12 animals. The model protocol used was identical to the protocols outlined in Chapter IV. On completion of the final phase of defect surgeries a total of n=9 samples were available for each of the 5 experimental groups.

After harvest, each sample was scanned by micro-computed tomography prior to preparation for histology, at the time of writing histology is in progress but not completed. A marrow harvest was performed for each animal with CFU-F activity assessed by *in vitro* assay, methods given in 2.1, results were pooled with earlier work and presented both below and in Chapter III, page 89.

Experimental workflow

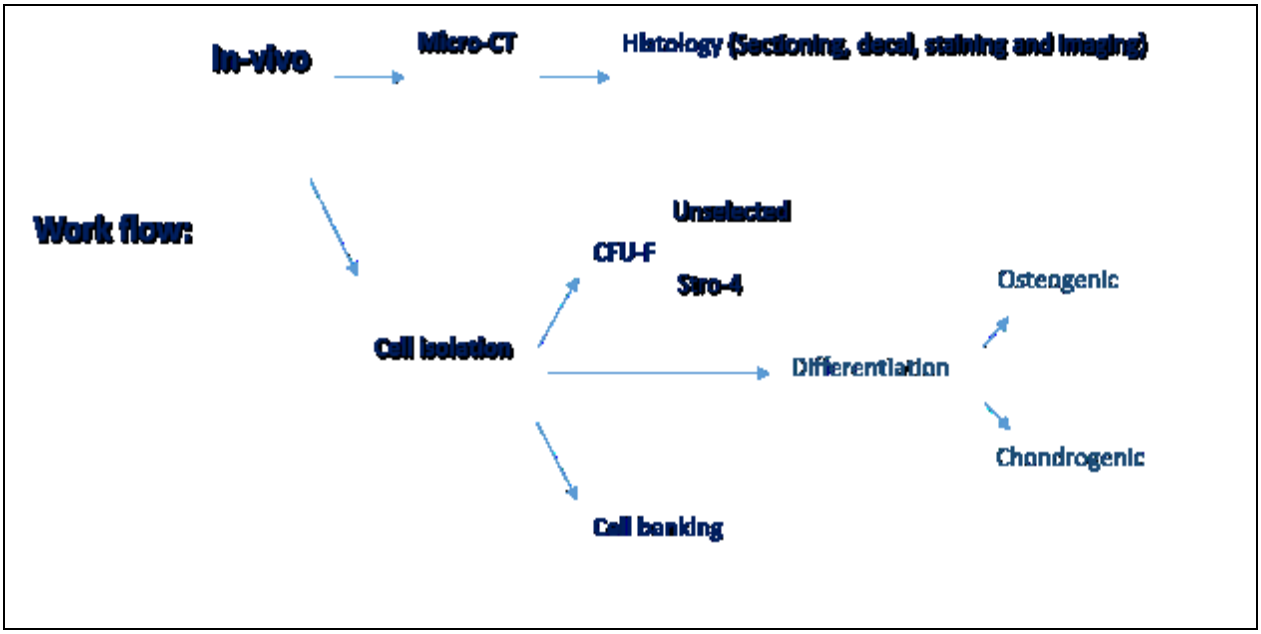

Product description, InductOS®: Work in this chapter utilises an FDA approved spinal fusion product, "InductOS®", manufactured by Medtronic Ltd, UK, as a source of growth factor and Absorbable Collagen Sponge (ACS) substrate. The InductOS® product consists of three elements, 1) absorbable collagen sponge, 2) recombinant human BMP-2 and, 3) proprietary buffer for BMP-2 application. For clarity, when the terms "collagen sponge", "buffer" and "BMP-2" are used, these terms refer to the individual components of the complete InductOS® product. At the time the study was performed, InductOS® was suspended from use in Europe due to quality control concerns with the ACS, the product remained licensed for use in spinal fusion in both USA and Canada.

5.4.1 *In vivo* set-up

Experimental groups were set-up to directly compare the use of a 2.5% Laponite hydrogel to facilitate delivery of a commercially licensed BMP-2 spinal fusion product, InductOS®. Three experimental groups were selected; two comparing the *in vivo* activity of InductOs® BMP-2 either delivered in proprietary InductOS® buffer or adsorbed onto a 2.5% Laponite gel, both conditions were applied on a collagen sponge substrate construct and placed into the condyle defect.

The third group investigated the osteogenic capacity of Laponite gel containing BMP-2 within a large bone defect in the absence of a collagen scaffold. Included in the experimental set-up were blank and autograft repeat control, acting as setup specific controls and further improving control data collection. Groups are set out in Table 5-2.

Collagen discs were prepared using an 8mm diameter biopsy punch (Kruuse UK LTD), discs measuring 4mm deep by 8mm in diameter were cut out under sterile conditions. The collagen sponge constructs were assembled by placing a disc of collagen sponge in a mould measuring 8mm x 12mm then adding 22µl of neat Medtronic BMP-2 (1.5mg/ml BMP-2) followed by either 47.1µl formulation buffer or 47.1µl of 2.5% Laponite. A second layer of sponge, BMP-2 and Laponite/formulation buffer was repeated identical to the first. A final 3rd collagen sponge disc was added and BMP-2 neat applied to the top layer (without Laponite or InductOS® buffer), see Figure 5-1.

A total of 66µl of BMP-2 (100µg) was applied per construct, each defect containing 100µg of InductOS® BMP-2. After assembly, scaffold constructs were stored sterile on ice and transferred to surgery. As accurately as possible, constructs were implanted into experimental animals within 30 minutes of assembly.

Experimental groups

Material	Substrate	Growth Factor	Delivery vehicle	BMP-2 / defect
Blank	None	None	None	None
Autograft	Autograft	None	None	None
InductOS® col. BMP-2	Collagen sponge	InductOS® BMP-2	InductOS® buffer	0.1mg
Laponite col. BMP-2	Collagen sponge	InductOS® BMP-2	2.5% Laponite	0.1mg
Laponite gel BMP-2	None	InductOS® BMP-2	2.5% Laponite	0.1mg

Table 5-2 Experimental groups and construct components

Set-up of Laponite InductOS® collagen sponge layers.

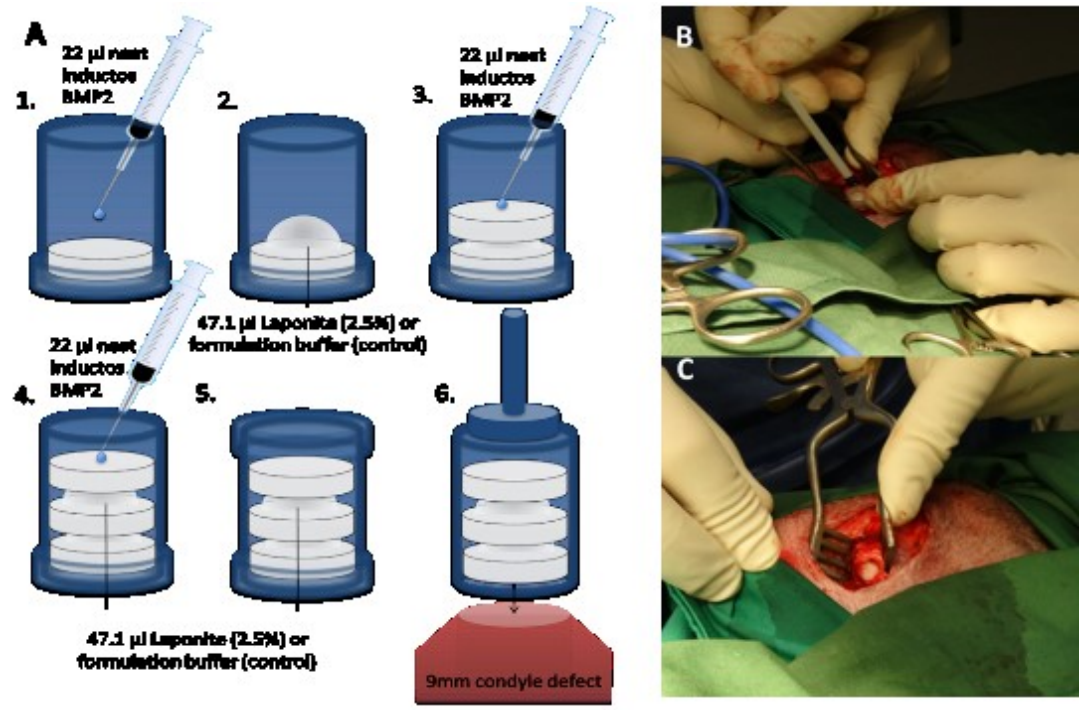

Figure 5-1 Schematic of multi-layered collagen sponge construct. A) A total of three 4mm x 8mm collagen sponge sections were sandwiched together with BMP-2 applied between layers. BMP-2 was applied in InductOS® buffer alone or with a 2.5% Laponite gel. B and C) Construct application in-vivo**.**

Application of Laponite BMP-2 without collagen sponge substrate

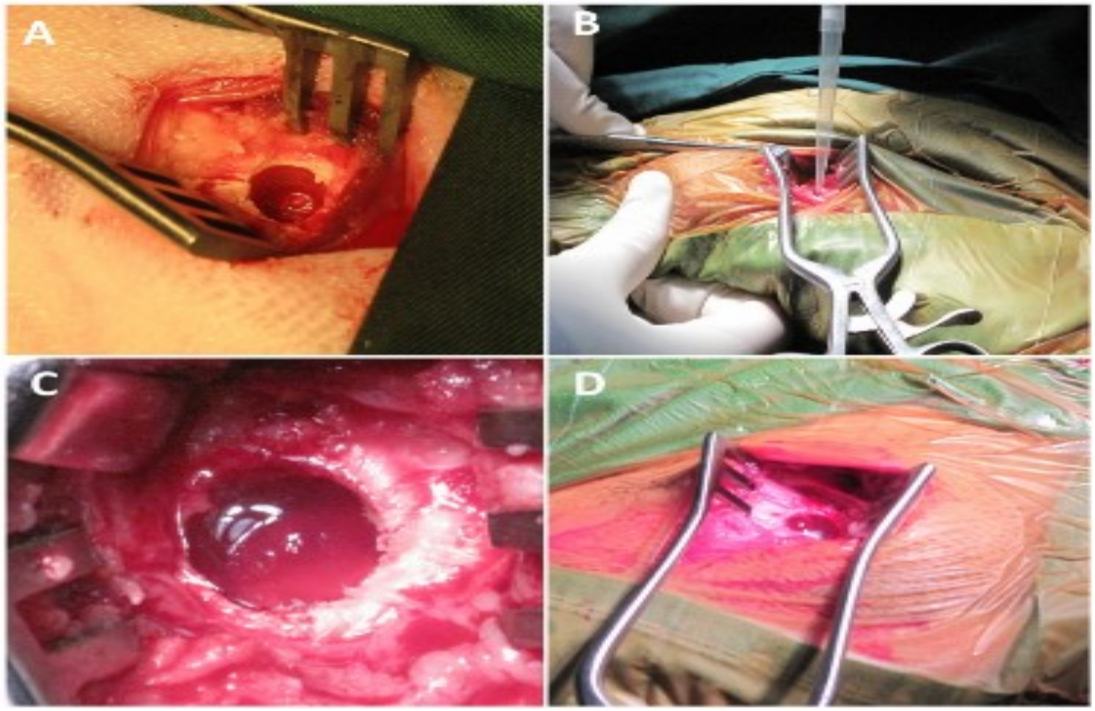

Figure 5-2 Application of Laponite gel BMP-2 *in vivo*. A) Exposed empty defect. B) Gel applied by sterile 1ml pipette. C and D) Gel in situ prior to wound closure.

Micro CT

Samples were scanned and analysed as described in Chapter IV, 4.6.3, two regions of interest (ROI) were created, one looking at a 9mm x 10 mm cylinder incorporating the entire original defect and a smaller 6mm x 6mm "mini cylinder", which focuses on a smaller region within the larger defect.

A global threshold was selected manually and used to separate soft tissue from calcified material, total Bone Volume (BV) and Bone Volume to Defect Volume percentage (BV/TV) data shown.

Unique to this chapter, a third ROI was used to help identify new tissue formation outside the defect borders. Qualitatively, defects in the Laponite gel BMP-2 group appeared to have a degree of bone resorption at the gel-defect bone interface. As a result of this restructuring, a proportion of newly formed bone was not identified using the conventional 9mm x 10mm cylinder approach. In an additional analysis, an "Adaptive Region of Interest" was created by manually selecting the defect boundary on a slice by slice basis and calculating both the total bone volume and bone volume % of the whole defect, justification for the adaptive ROI is shown in Figure 5-3 below.

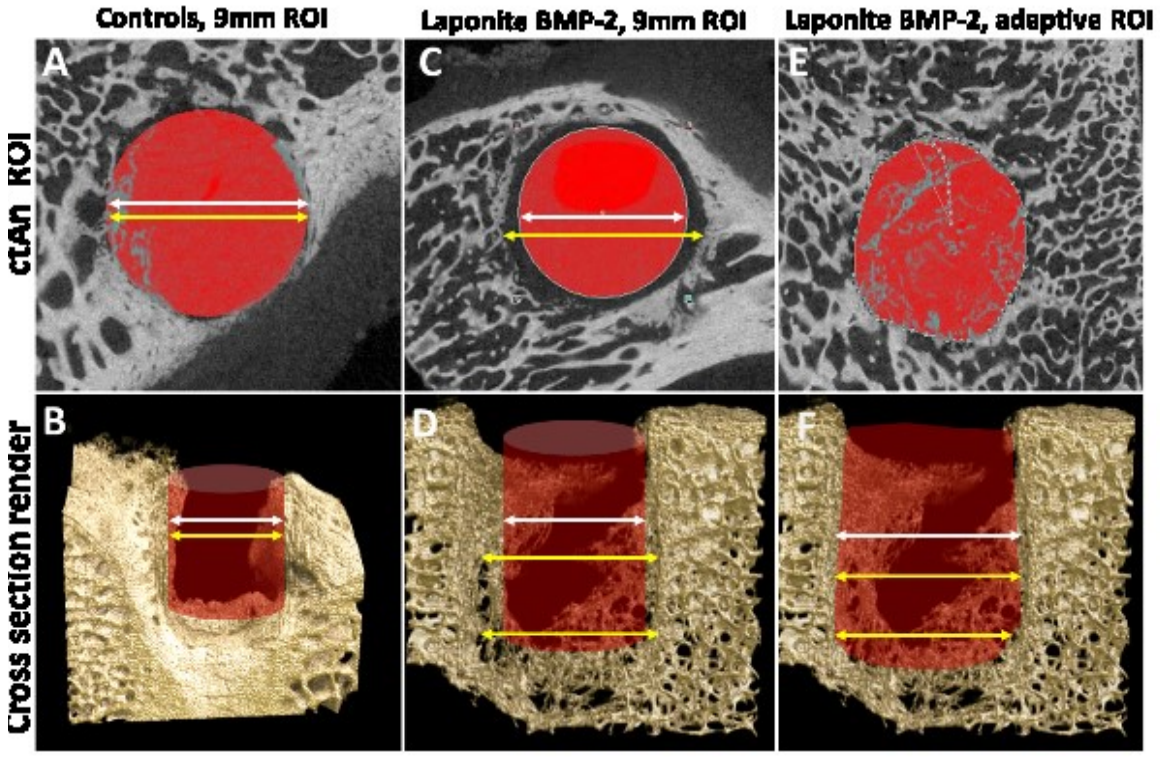

Figure 5-3. Region of interest variation between experimental groups. A) And B) Standard defect and 9mm region of interest (red circle), both the defect boundaries (yellow arrow) and ROI (white arrow) are closely matched. A mismatch between the standard 9mm ROI and the defect boundary (yellow line) can be seen on coronal (C) and sagittal (D) views of a Laponite gel BMP-2 containing sample. E) And F) The manually assigned "Adaptive" ROI incorporates the non-uniform defect boundaries seen in the Laponite gel BMP-2 experimental group.

5.4.3 Histology

Bone defect regions were removed from the medial condyle region at necropsy. Samples were fixed in 4% PFA at 4°C, a minimum volume of PFA of 20 times the bone volume material was used. PFA was change every 24 hours for 3 changes and fixed for 96 hours. Samples were rinsed in 1 x PBS for 30 minutes for three washes and placed in a decalcification solution (Histoline Medium Decalcification Solution, Histo-Line® Ltd.), samples were checked for mineral content by bench top X-Ray (Multifocus, Faxitron® Ltd.). Decalcified samples were washed in 3 washes of PBS for 30 minutes before being further trimmed to remove excess material. Samples were passed through ascending alcohols and cleared using Histoclear® (Agar Scientific, UK) and paraffin wax embedded overnight using a Leica automated embedding system.Birefringence was performed on A/S stained samples by placing a polarising light filter on the Lightsource outflow of a phase contrast inverted light microscope. 7µm section were cut from embedded sample and mounted onto treated Poly-prep slides (Sigma-Aldrich, UK). Samples were stained for Alcian Blue and Sirius Red (A/S) as well as Haematoxylin and Eosin (H and E) as described in methods, 2.4.2.

5.5 Results

Surgery was performed on 24 animals over two separate experimental periods. One animal was culled early on welfare grounds due to surgery related fracture, the fracture was found to have been a complication from a pre-existing bone injury. All remaining animals continued through to study end-point without any continuing concern.

5.5.1 Statistical analysis

Statistical analysis was performed using GraphPad Prism and was based on methods described by Ding (Ding et al., 2012). A one-way ANOVA was used with Bonferoni post-hoc test comparing the means of each group with one another, $P < 0.05$ was considered significant. For all graphs presented below, * $p<0.05$, ** $p<0.01$, *** $p<0.001$, **** $p<0.0001$.

5.5.2 Micro-CT quantitative assessment

5.5.2.1 9mm and 6mm Region of Interest (ROI)

Calcified tissue was selected by setting CT threshold values based on a global thresholding assessment performed in ctAN (Bruker). Global thresholding is a binary analysis whereby all tissue recognised above the lower limit is considered as calcified or bone material. Description of blank and autograft controls is given in chapter IV, 4.8, analysis of experimental groups and their relation to controls is given below.

InductOS® collagen BMP-2 and Laponite collagen BMP-2 groups shared a consistent statistical significance in comparison to blank and autograft control groups in both bone volume and bone volume/tissue volume as a percentage of defect fill in both the 9mm and 6mm ROIs.

In 9mm ROIs, InductOS® collagen BMP-2 displayed a mean BV of $202mm^{3,}$ SD=73 compared with a mean BV of $213.4mm^3$ and SD= 72 in the Laponite collagen BMP-2 group, Figure 5-4. BV/TV means were 31 and 29% respectively with standard deviations of 7 and 10, Figure 5-5. Bone volumes in both collagen sponge containing groups were greater than blank controls, with p= 0.0043 in the InductOS® group and p= 0.0021 in the Laponite, with BV/TV P values of p= 0.0030 and 0.0188.

5.5.2.2 6mm ROI

6mm ROIs repeated the pattern of significance over blank controls seen in the 9mm ROI in both BV and BV/TV with expectedly lower overall values. BV mean in InductOS® collagen BMP-2 was 55.2mm^3 (SD=22), with a BV/TV of 24.2% (SD=8.5%) compared with a BV mean of 46.2mm^3 and BV/TV of 18.6% (SDs of 27 and 10.7) in the Laponite collagen BMP-2 group, Figure 5-6 and Figure 5-7.

Comparisons between the Laponite gel BMP-2 and blank controls were different to those described above for collagen containing groups. No statistical difference was seen in BV or BV/TV in either the 9mm, Figure 5-4 and Figure 5-5, or 6mm ROIs, Figure 5-6 and Figure 5-7. In the 9mm ROI, although mean BV was higher (157mm^3 compared with 87mm^3 in blanks), the intra-group variation seen in the Laponite gel BMP-2 was very large, with a SD of 100 (the highest of any group). Again, in the 6mm ROI, mean BV in the Laponite gel BMP-2 was higher than blanks (29mm^3 vs 3.9mm^3) once more a large SD of 29.1 (compared with 3.7 in blanks) prevented any statistical significance between results.

Samples containing the Laponite gel BMP-2 treatment group, displayed trabecular resorption in the lower defect region, this created a variation in defect dimensions between gel and collagen sponge containing groups. To try and correct for the irregular defect dimensions noted in the Laponite gel BMP-2 group an Adaptive ROI analysis was introduced. Bone volume in this ROI significantly greater, 207.2mm^3 (although a large SD of 115) when compared to blanks, Figure 5-8. BV/TV of the adaptive ROI was 16.1%, Figure 5-9, and was not significantly different to blank defects. This result is important when determining the validity of the adaptive ROI against the blank results.

5.5.3 Results 9mm Region of Interest

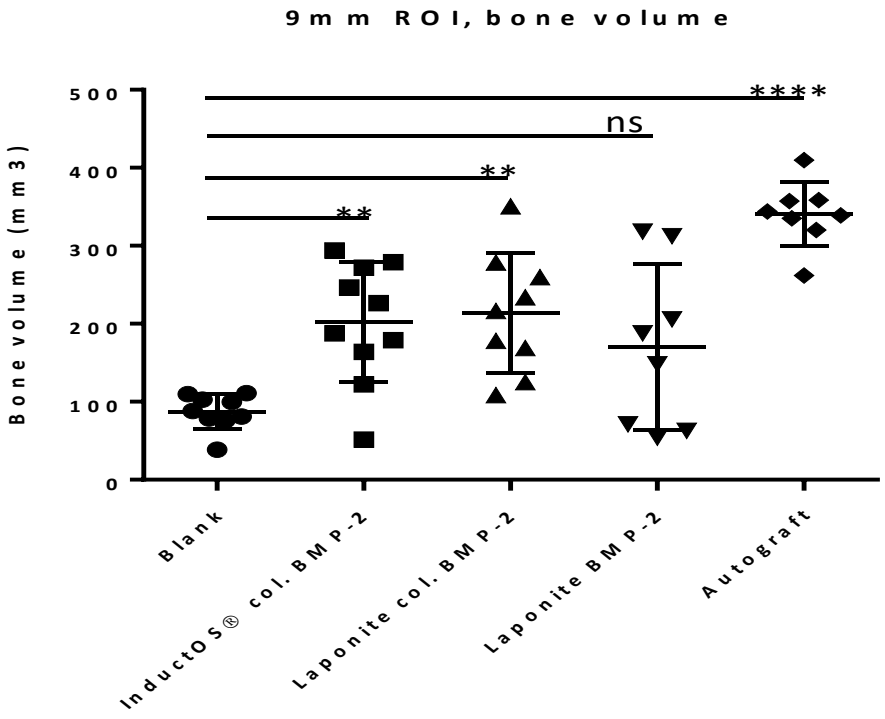

Figure 5-4. 9mm ROI, BV. BV In Both InductOS® (n=10) and Laponite BMP-2 (n=9) groups containing collagen sponge substrate was significantly higher than blank (n=9) defects. BV in Laponite gel BMP-2 was not significantly greater than blank.

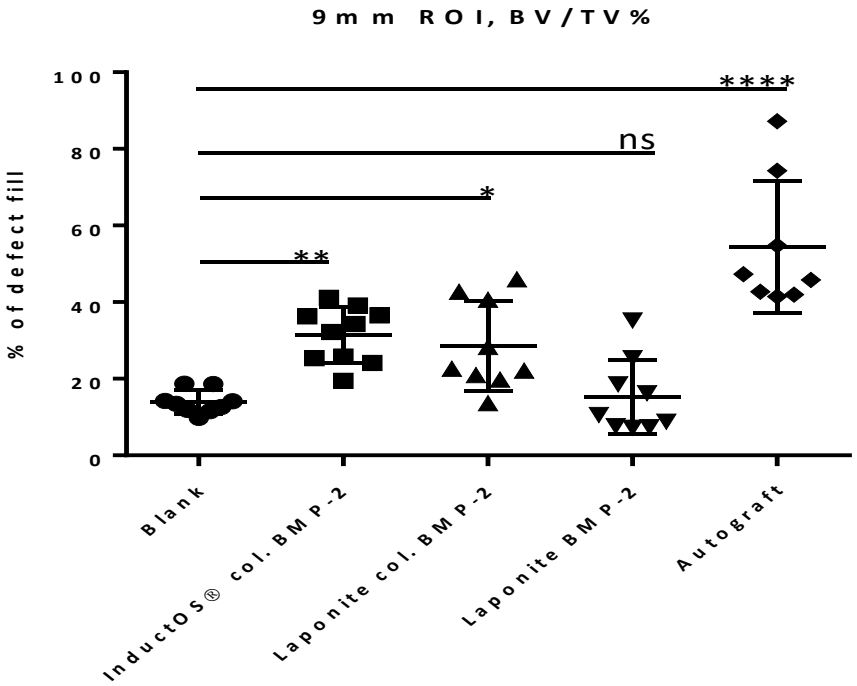

Figure 5-5. Percentage fill of the 9mm defect region. Analysis of the BV/TV produced the same pattern of significance seen in total BV. Collagen containing constructs in Laponite and InductOS® buffer groups were significantly greater than blank.

5.5.4 Results; 6mm Region of Interest

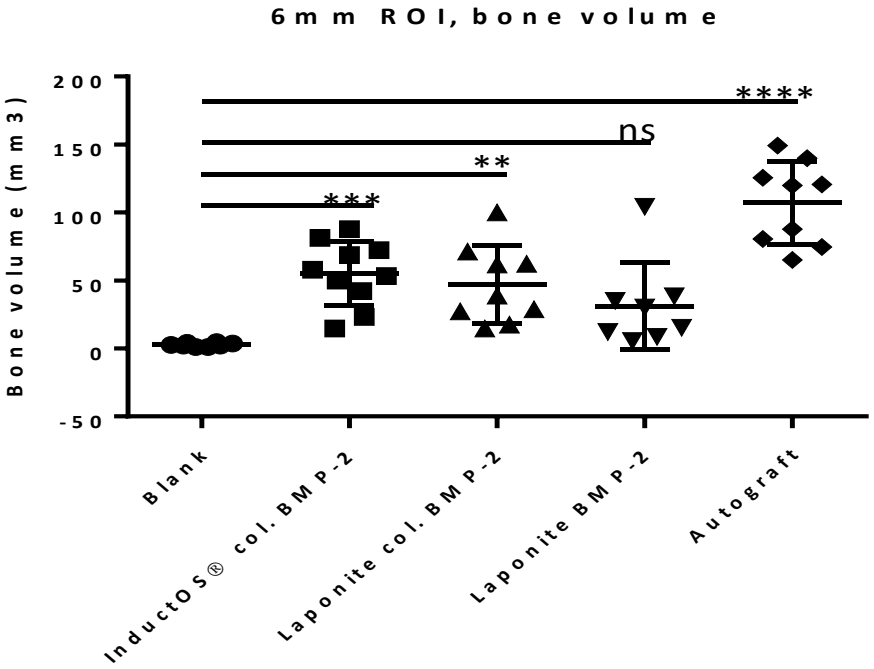

Figure 5-6. 6mm ROI, BV. Narrowing the ROI to focus on bone formation in a centralised area within the defect confirms the significance seen in the 9mm ROI, reducing the ROI did not change results between samples

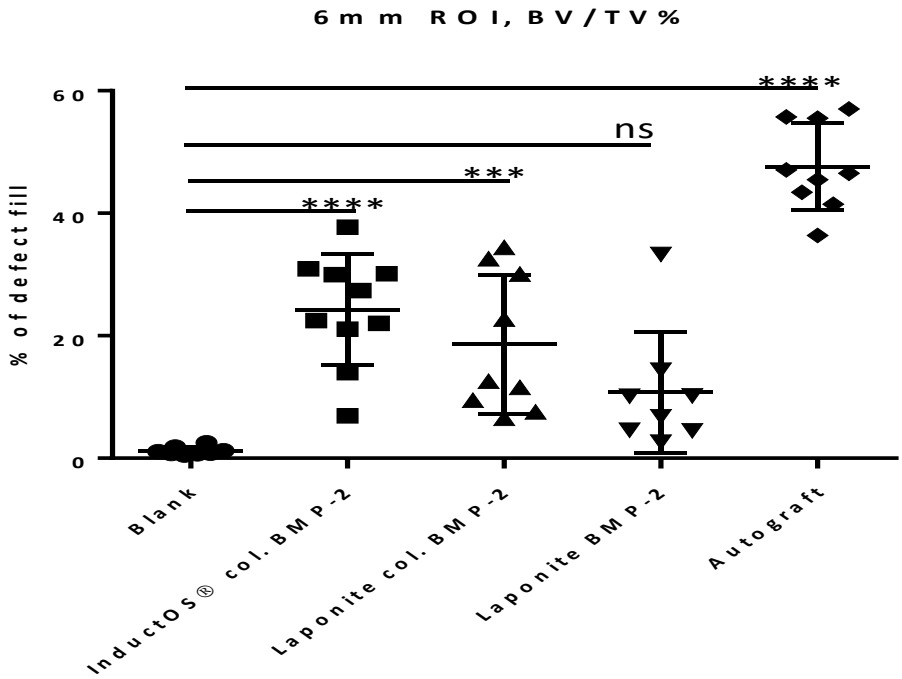

Figure 5-7. 6mm ROI, BV/TV. Comparing the BV/TV further increases the significance of collagen-containing groups vs blank defects. No statistical difference between Laponite gel BMP-2 and blank was found.

5.5.5 Results; Adaptive Region of Interest compared to 9mm ROI

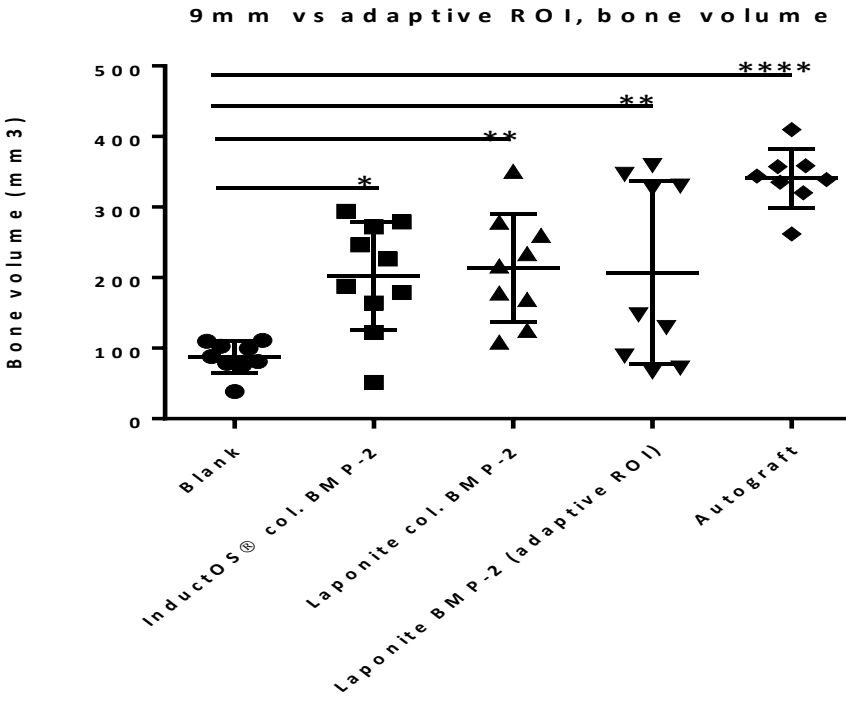

Figure 5-8. 9mm Adaptive ROI, Total BV. BV identified in all groups was statistically significant over blank defects, increasing the ROI in Laponite gel BMP-2 group classifies more new bone material and changes the pattern of significance seen in other analyses.

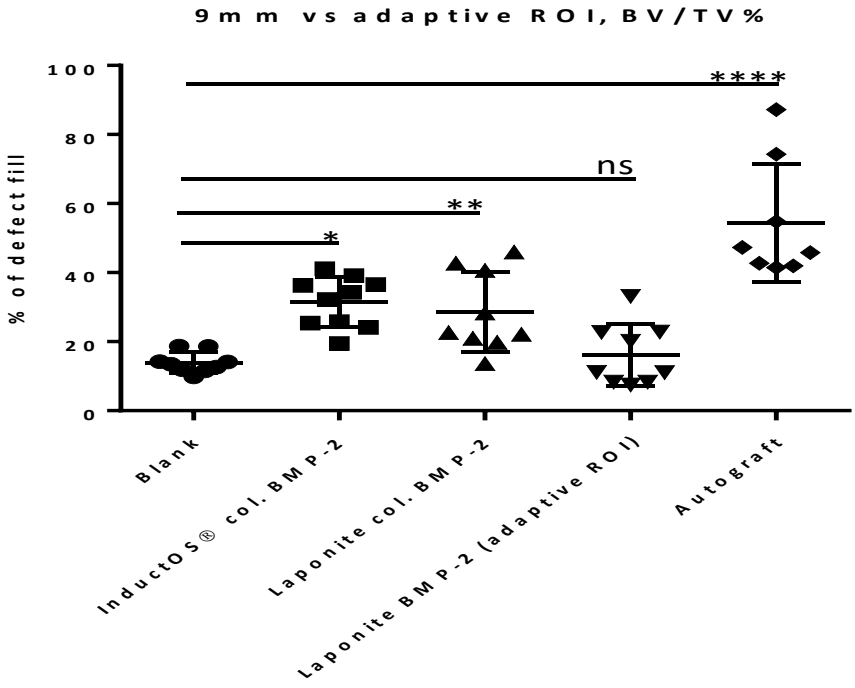

Figure 5-9. 9mm Adaptive ROI, BV/TV. When expressing bone volume as a percentage of the total ROI volume, the adaptive ROI is no longer significantly greater than blank defects. Remaining groups show significance as per standard 9mm ROI BV/TV.

5.5.6 Image renders from micro-CT reconstructions.

Image panels represent three examples from each *in vivo* group; the highest, mean and lowest bone volumes. Images are arranged as an overview with a narrow cross-sectional slice inset, followed by a “top-down” or coronal plane image adjoining. The sagittal and coronal views are purposely narrow “slices” through the defect to help visualise the volume and density of tissue within the repairing defect. In all renders, green is the lowest tissue density registered by analysis and highest density represented by red.

5.5.6.1 Autograft

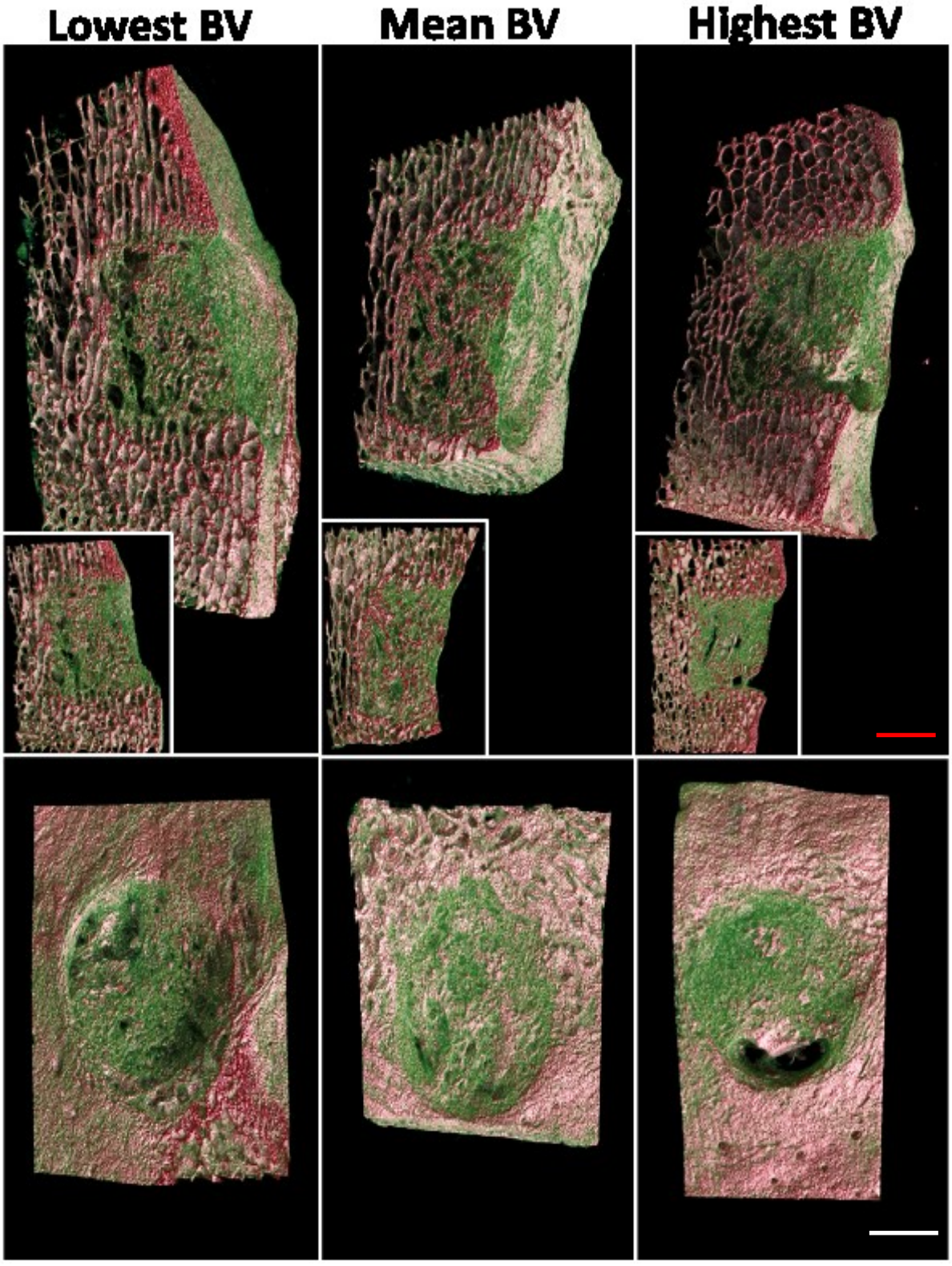

Figure 5-10. Autograft 2-D renders. Scale bar, white = 4mm, red = 5mm

5.5.6.2 Blank

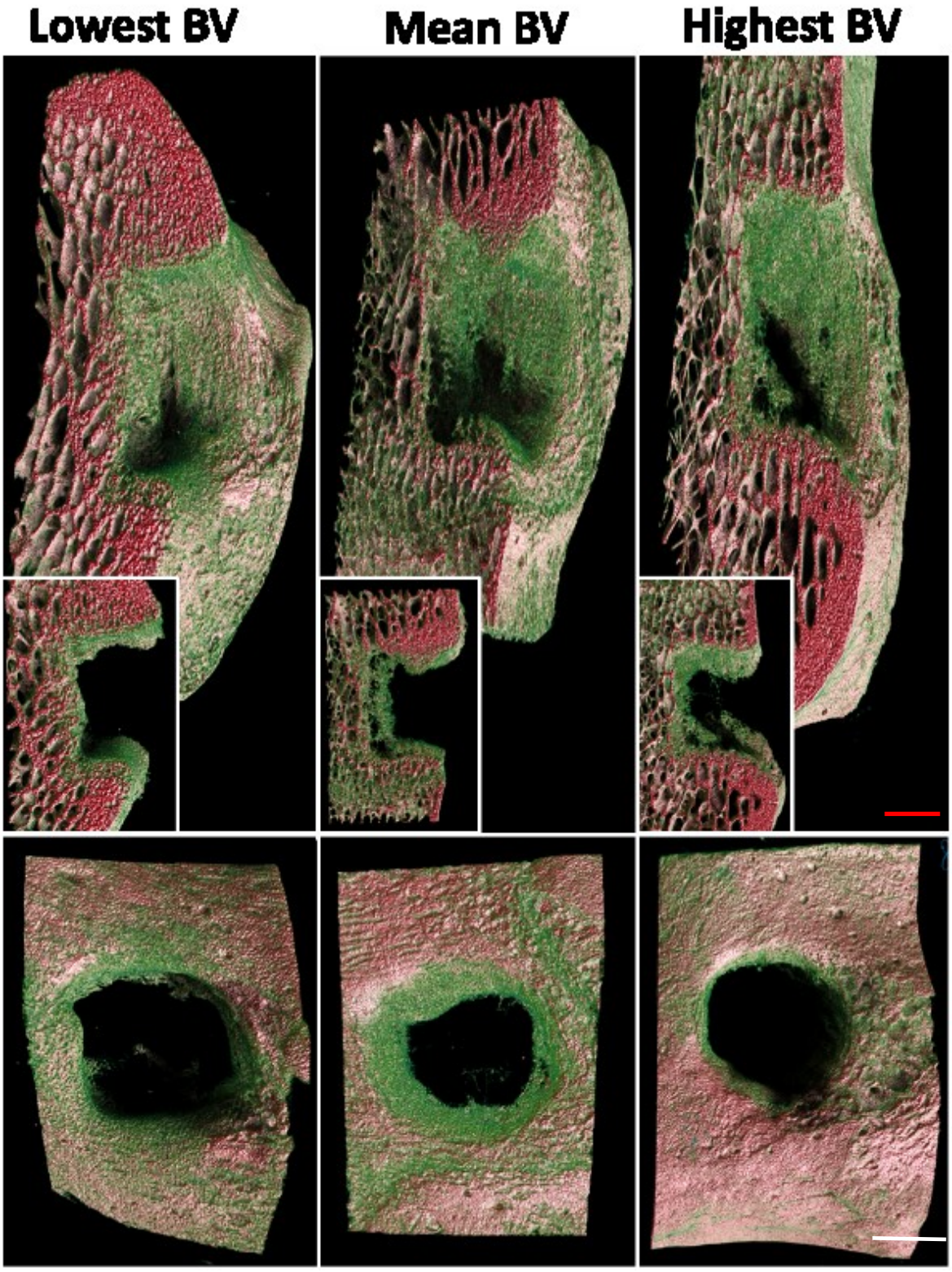

Figure 5-11. Blank 2-D renders. Scale bar, white = 4mm, red = 5mm

5.5.6.3 InductOS® collagen sponge and BMP-2

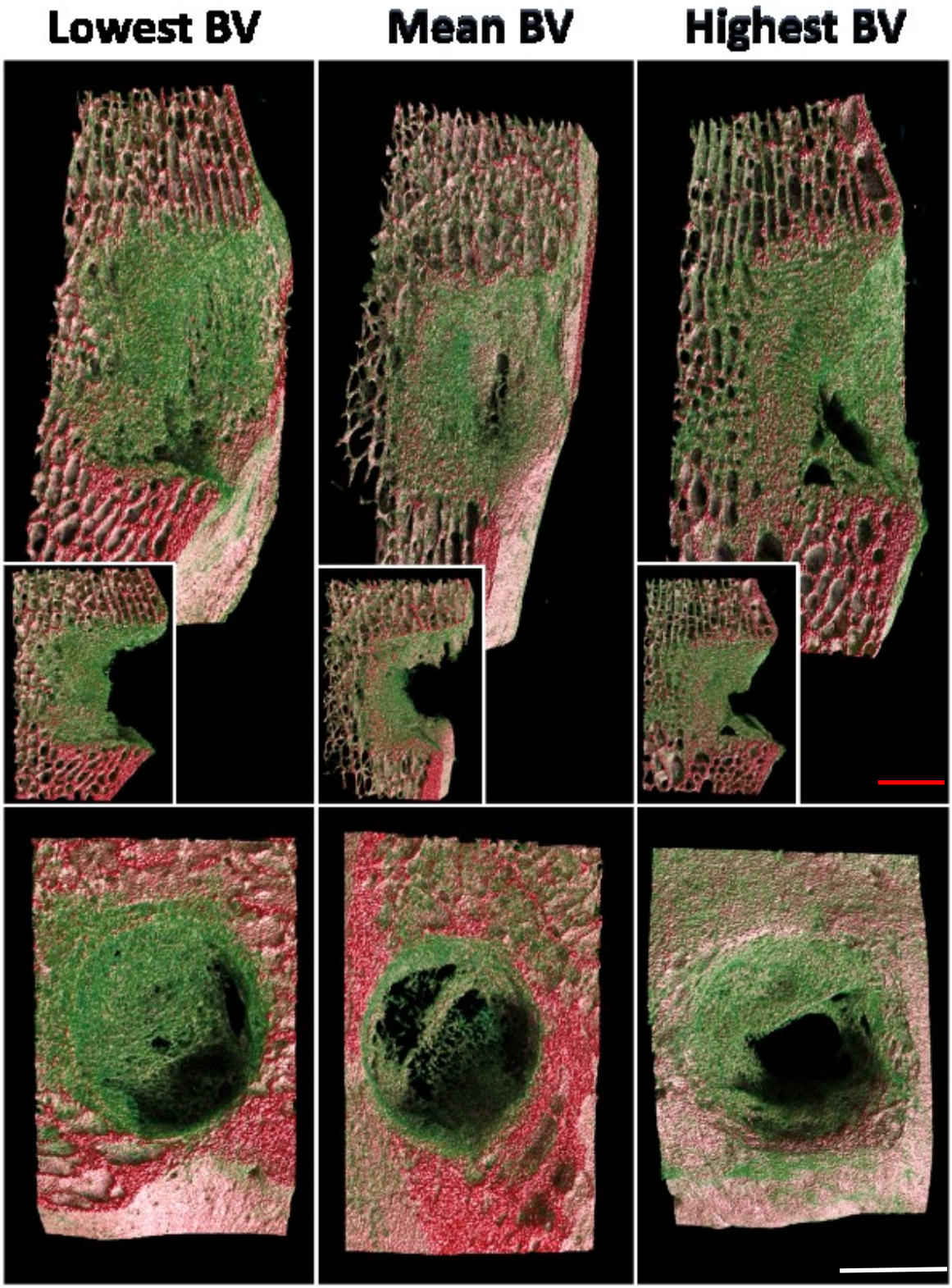

Figure 5-12. InductOS® collagen sponge BMP-2, 2-D renders. Scale bar, white = 4mm, red = 5mm

5.5.6.4 Laponite collagen sponge BMP-2

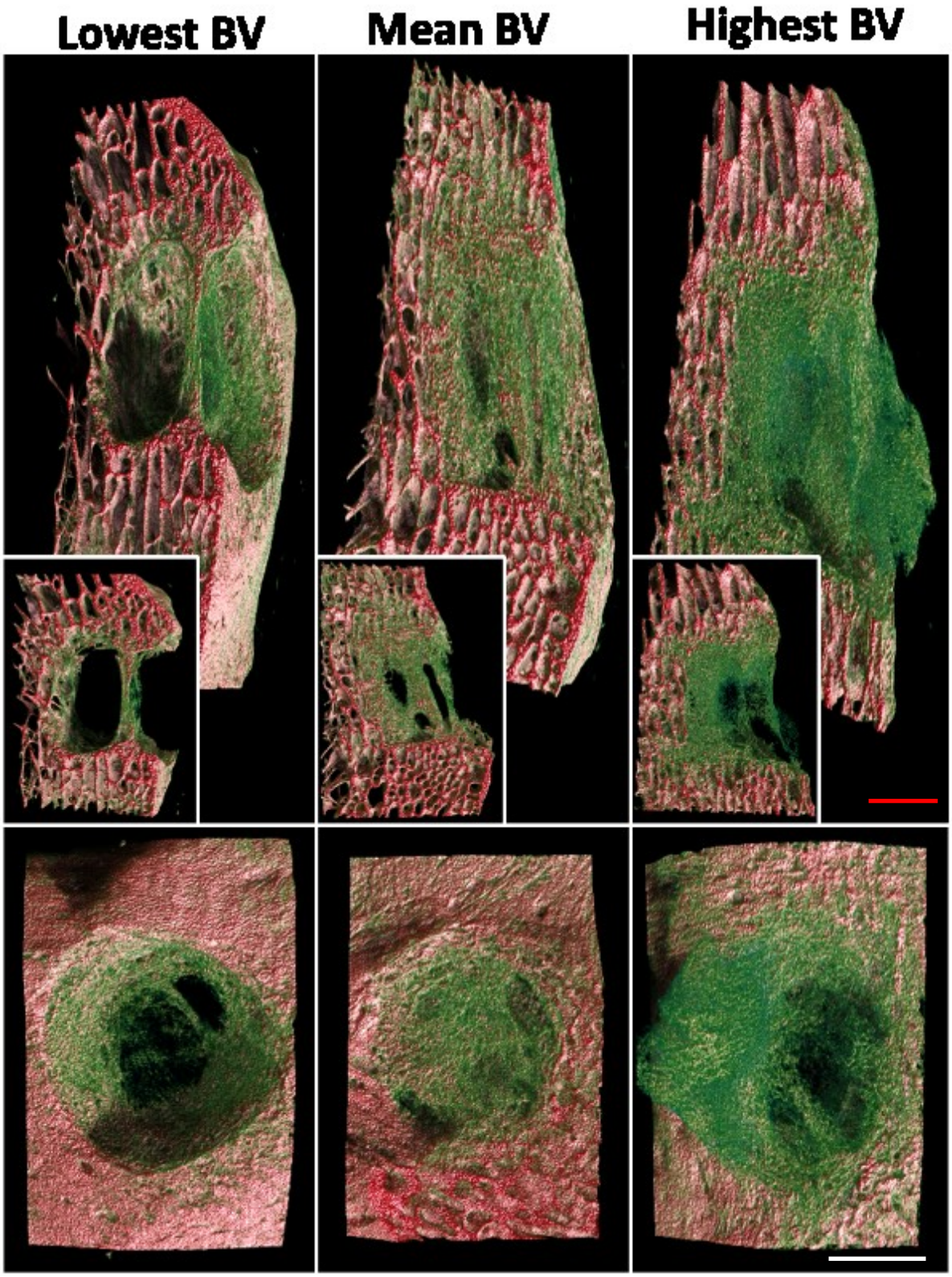

Figure 5-13. Laponite collagen sponge BMP-2, 2-D renders. Scale bar, white = 4mm, red = 5mm

5.5.6.5 Laponite gel BMP-2

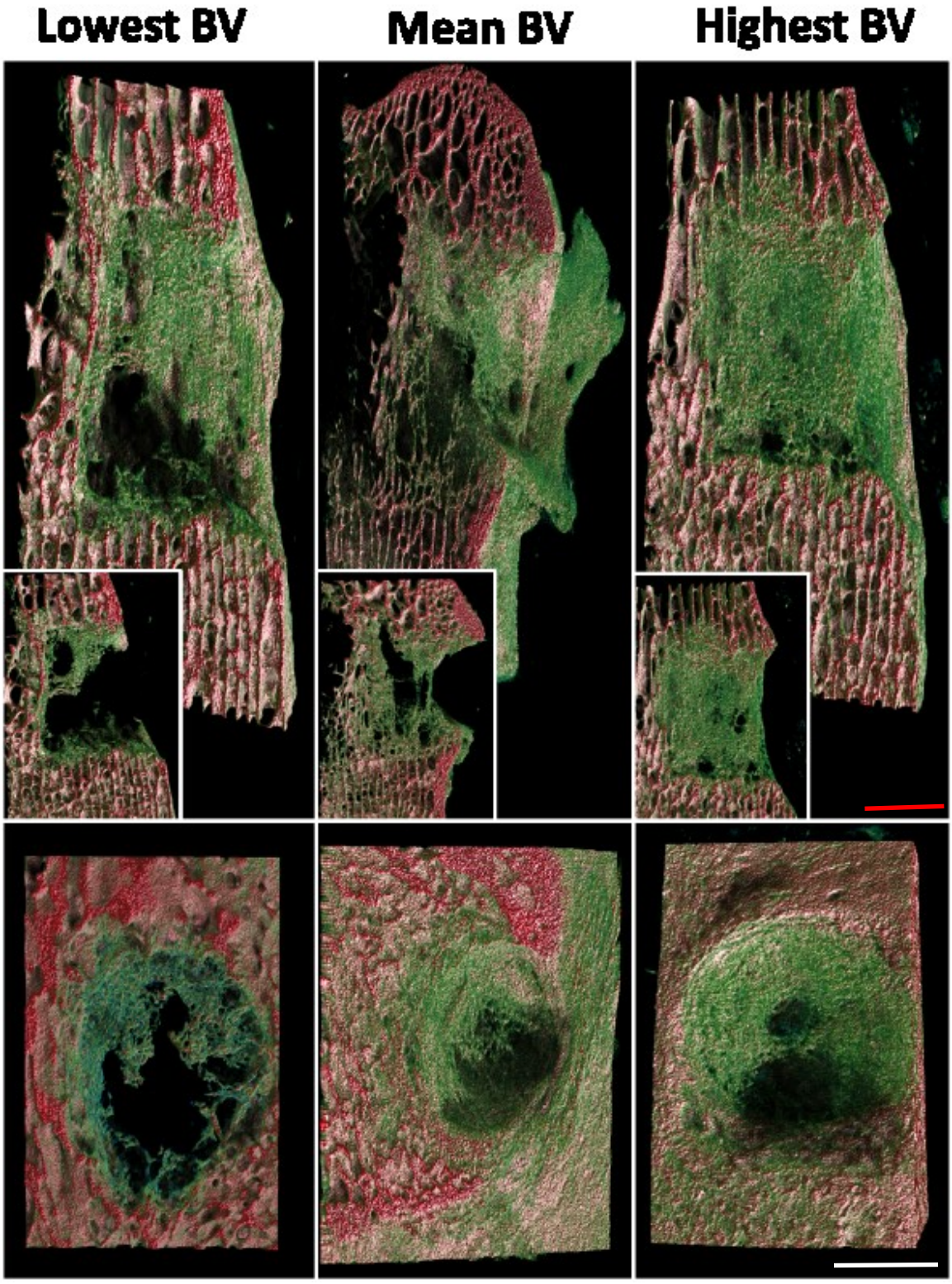

Figure 5-14. Laponite gel BMP-2, 2-D renders. Scale bar, white = 4mm, red = 5mm

5.5.7 Notable features of new bone formation by micro-CT anaylsis

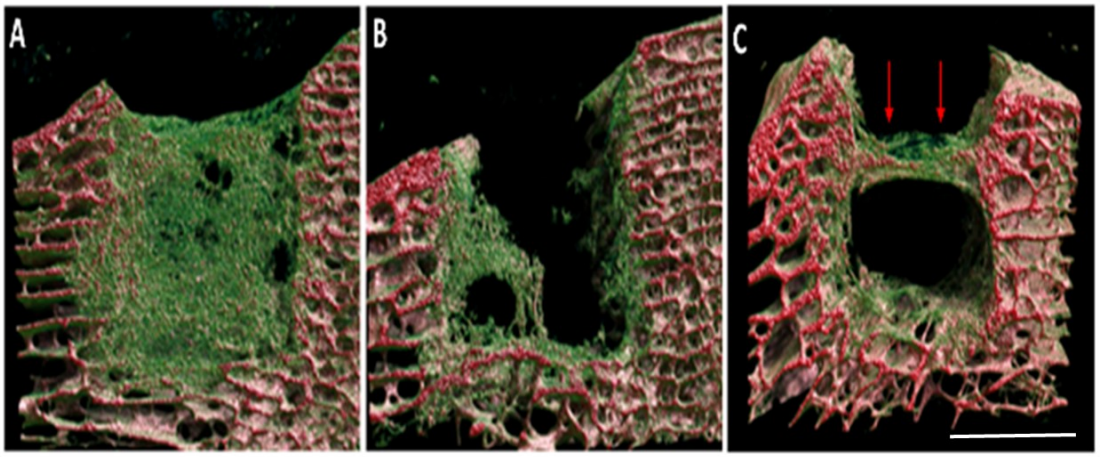

Figure 5-15 Examples of variable growth and unusual bone formation. A) and B) The variation in new bone formation between the highest (A) and lowest (B) values in the Laponite gel BMP-2 was considerable and was not easily accounted for. C) Demonstration of bone bridging spanning the defect edges (note arrows), it is thought this bridging occurred between sponge layers along the Laponite gel. Scale bar 9mm.

Consistent with BV and BV/TV values produced from µCT analysis, autograft samples, Figure 5-10, appeared near-completely full on cross sectional render, the bone pattern was dissimilar to innate bone but showed qualitatively the largest amount of higher density bone (red) out of all groups.

Blank samples, Figure 5-11, were predictably devoid of new bone tissue with only a small amount of bone growth seen “creeping” from the edges inwards and from the periosteal border down into the defect, there was little to no bone formation within the central area of the defects (as examined by the 6mm ROI).

InductOS® collagen BMP-2 two dimensional renders from high-mean-low represent the moderately reliable bone forming capacity of this experimental group, Figure 5-12. New tissue is lower in density (green>red) and contains very fine randomly orientated strands of mineralised tissue. Although a significant result, defect fill is incomplete as seen on sagittal and coronal sections.

Although Laponite collagen BMP-2 shared very similar values in BV and BV/TV to InductOS® collagen BMP-2, some notable differences were seen on cross sectional images. Tissue formation within the defects was characterised by alternating layers of lower density calcified tissue and soft tissue (below the bone threshold level) when view in 2-D, Figure 5-15, C. Viewed in 3-Dimensions, these appear with a high-density spheroid outer shell surrounding very low-dense soft tissue pockets. New bone appeared to have been encouraged from the defect edges across the defect diameter in fine strands with higher densities seen in the portions of bone immediately adjacent to the spheroid cavities described above, Figure 5-15, C.

5.5.8 Comparison of *in vitro* construct behaviour and *in vivo* bone formation

Constructs were placed in standard culture media for 30 minutes and examined macroscopically. The constructs maintained integrity although significant expansion was noted in the collagen sponge segments, Figure 5-16, A. The Laponite discs did not appear to swell maintaining their original volume.

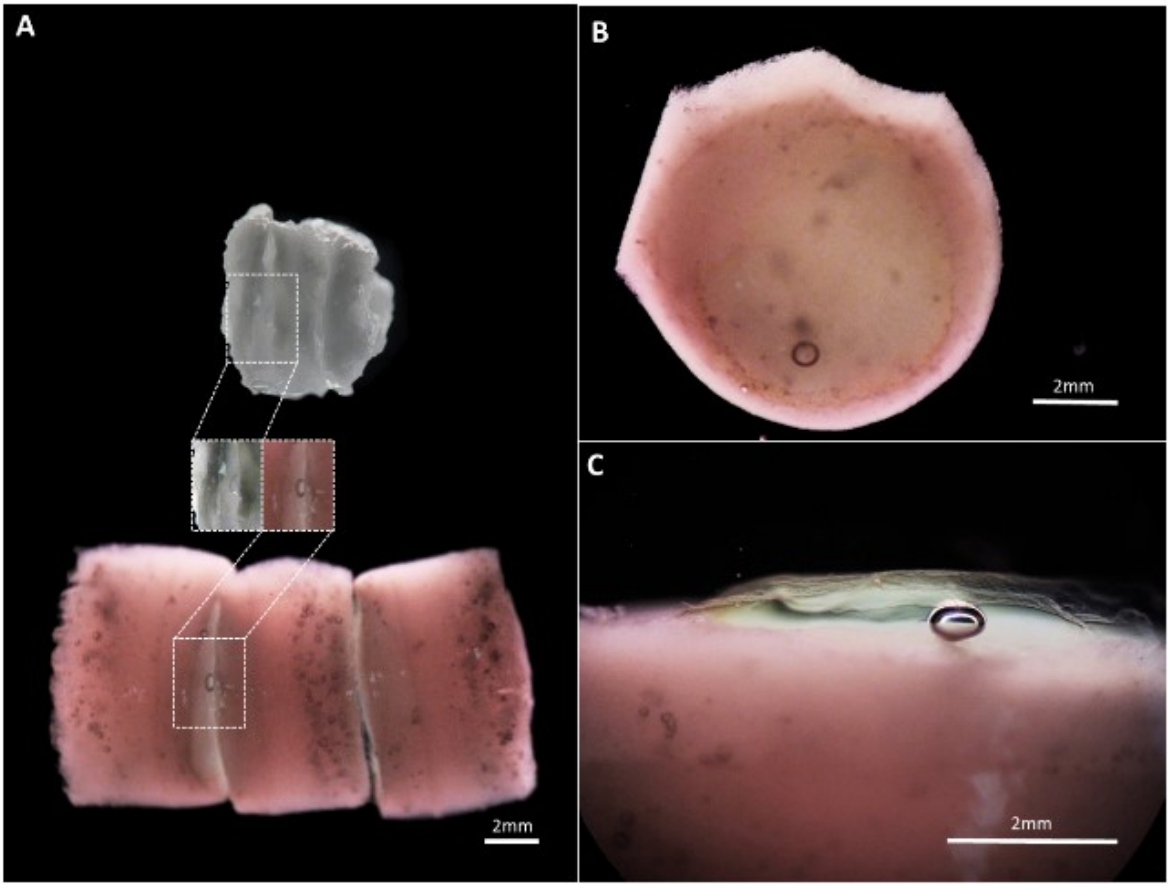

Figure 5-16. Behaviour of Laponite collagen sponge constructs *in vitro*. Constructs were exposed to a simulated physiological media to help determine construct behaviour in-vivo. A) The construct in white is prior to immersion in simulated buffer and pink 5 minutes after. Swelling of the collagen sponge was clear but Laponite layers maintained original dimension whilst Laponite remains unchanged. B) A top down view of the Laponite layer on a collagen sponge disc demonstrates the radial enlargement of collagen discs. C) A lateral profile of a collagen disc with Laponite layer on top. Images provided by Dr Jon Dawson.

5.5.9 Histology

5.5.9.1 Preliminary histology of blank control sample

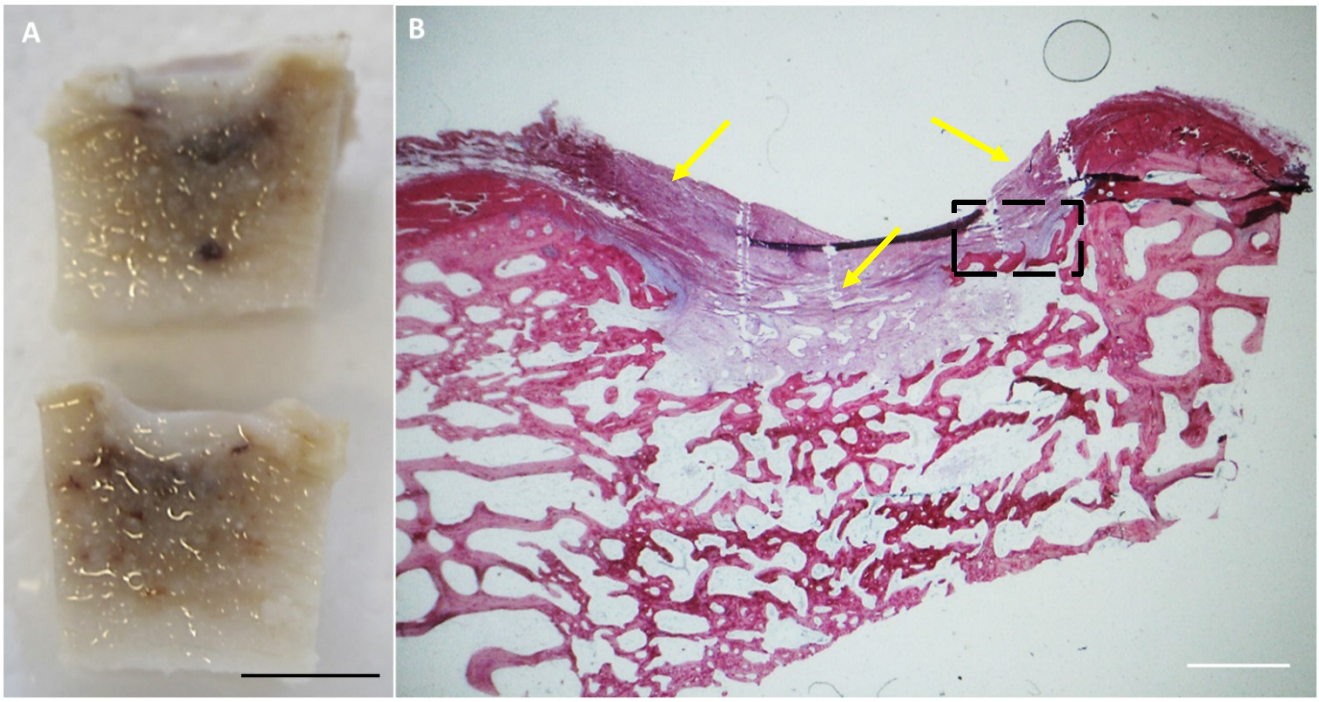

Figure 5-17 A) Macroscopic image of decalcified sample. B) A/S staining of blank control. A continous fibrous tissue infiltrate is present throughout the defect (yellow arrows). Spicule of bone remnant from surgery. Note that low density of staining near the defect floor compared to increased density fibrous network covering the defect entrace (at yellow arrows). Scale bar (black) = 10mm, white = 2mm.

5.5.9.2 Laponite BMP-2, overview.

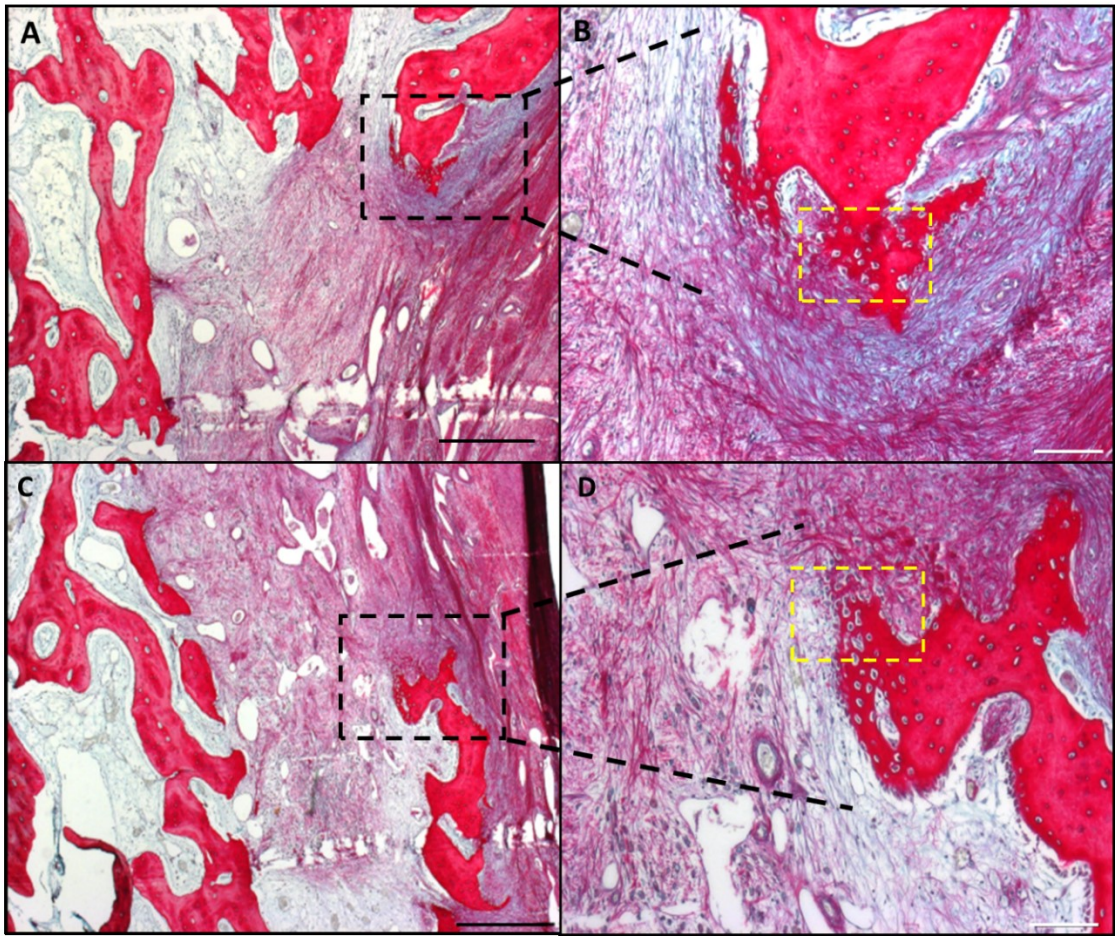

Figure 5-18. Alcian blue and Sirius red overview of defect infill. A) and C) Laponite BMP-2 defect sectioned transversely. Defect volume predominantly occupied by red staining collagen fibers with faint mucopolysaccharide background (blue hue, Alcian blue). Mild bony reaction present at defect periphery (black dashed boxes). B) and D) magnification of reaction area, hypertrophic cells surrounded by dense collagen network and enhanced alcian blue stain uptake consistent with collagenous glycoprotein network.

5.5.9.3 Tissue morphology, Laponite BMP-2

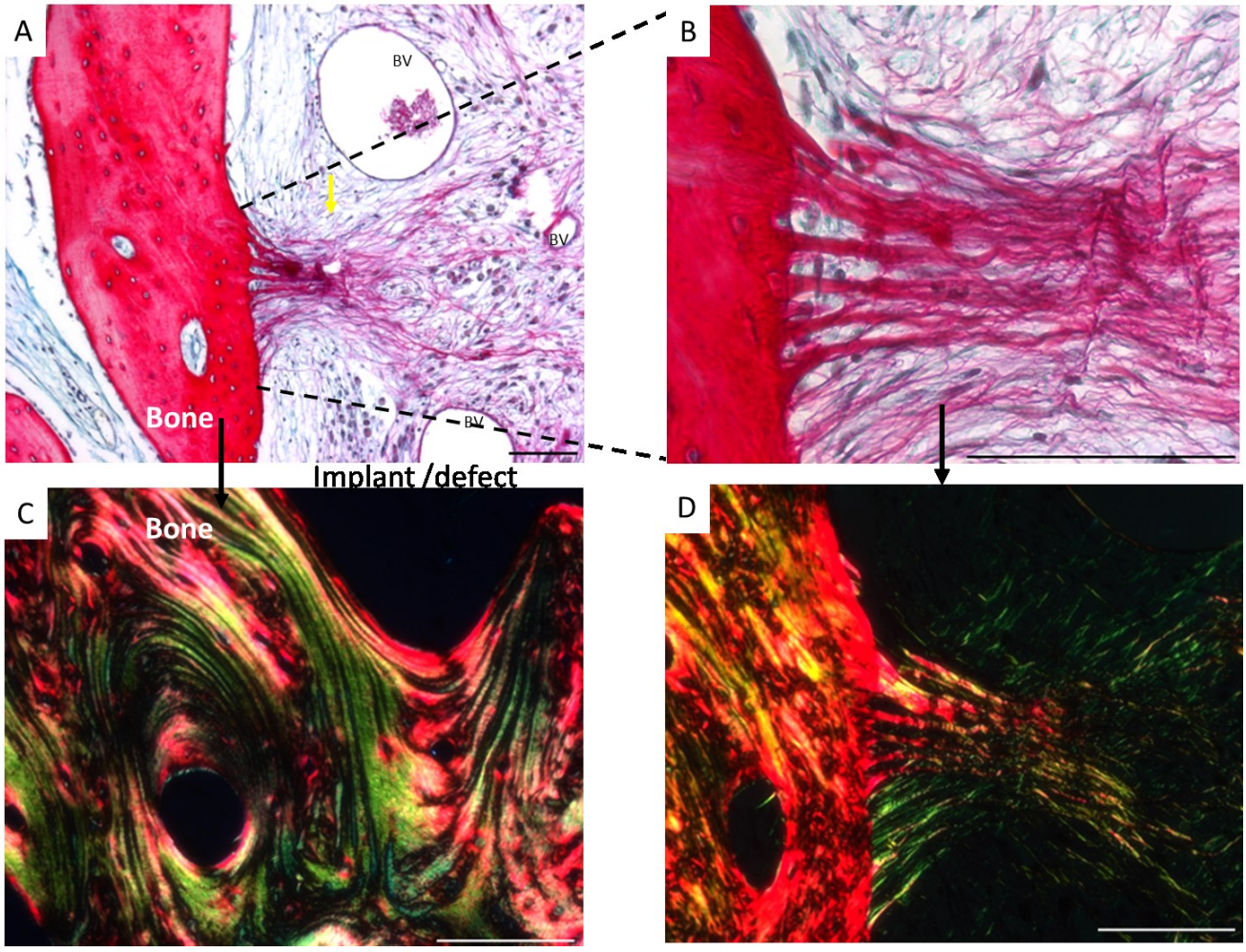

Figure 5-19. A) Mid-defect region demonstrating blood vessel formation (bv) and the outgrowth of intense staining strands of new tissue. Interrogation of tissue transference from innate bone into the defect substance. C) Birefringence of mature unaltered bone, red is indicative of positive birefringence infering paralellel fibre alignment (in the axis of the filter). D) Birefringence of region of fibre outgrowth, fibres are collagen dense (red on A/S) and aligned in parrallel (bright on birefringence). Scale bars = 1mm

5.6 Discussion

5.6.1 Summary and clinical relevance

Both InductOs® BMP-2 delivered with the proprietary Medtronic® InductOS® formulation buffer and InductOS® BMP-2 adsorbed onto Laponite induced a significant osteogenic response when applied to a collagen sponge substrate compared to blank control defects.

It is noteworthy that InductOs® was still efficacious in its native formulation buffer preparation when used at a ten-fold reduction from the manufacturer's guidelines, which is consistent with *in vivo* data supplied in FDA licensing literature (FDA pre-approval number P000058). Published clinical trial data for InductOS® used in spinal fusion strongly supports the use of the product with intervertebral body fusion success rates significantly higher than iliac crest bone graft (ICBG) at 24 months. There were no statistical differences in fusion rates at 6 and 12 months, and therefore claims regarding accelerated fusion were not possible, (EU, 2014). InductOS® has a justifiable clinical application based on improved long term fusion compared to ICBG, negating the need for bone grafting (and associated complications) and reducing the incidence of revision surgery and patient morbidity. The use of InductOS® clinically is not without shortcomings, the high BMP-2 concentration (1.5mg/ml) and high total BMP-2 dose requirements are prohibitively expensive, have been associated with off-target effects, demonstrated early trabecular bone resorption and is contra-indicated in patients with a history of neoplasia (MHRA) and may pose infection and immunological responses to the xenogenic nature of the collagen sponge matrix. Many of these complications potentially relate to all high dose BMP-2 products (James et al., 2016) and are not exclusive to InductOs® BMP-2.

Modifications which reduce the total BMP-2 required in a clinical application and which sustain growth factor release and activity *in vivo* would reduce product cost and limit unwanted non-therapeutic activity of the product. Our findings indicate that the product maintains bone forming efficacy at $1/10^{th}$ recommended BMP-2 concentration and that BMP-2 binding to Laponite does not ameliorate this effect. Crucially, due to Laponite's thixotropic and favourable rheological properties, intra-operative handling of Laponite was efficient with Laponite's physical properties lending to the use of Laponite as a sole agent for BMP-2 delivery, negating the requirement for further substrates or bone graft alternatives.

5.6.2 Hydrogels as principle agents of BMP-2 delivery in bone defects

Comparable formation of mineralised tissue between InductOS® and Laponite collagen sponge BMP-2 groups indicated a potential application of Laponite gel containing BMP-2 without a collagen sponge substrate, building on the hypothesis that BMP-2 release was modified by Laponite *in vivo* and that Laponite itself permitted cell infiltration and proliferation.

The use of materials to deliver peptides *in vivo* is well documented (see Table 5-1) although much of this work has taken place using small animal ectopic and only occasionally orthotopic models. Gel delivery systems are being developed to improve the mechanical properties and release kinetics for *in vivo* use (Nguyen and Alsberg, 2014; Utech and Boccaccini, 2015). Work by Yamamoto and colleagues demonstrated the correlation between the BMP-2 localising effect of hydrogel systems and prolonged BMP-2 activity *in vivo* (Yamamoto et al., 2003b).

In the sub-cutaneous model, Laponite localised ectopic bone formation more effectively than BMP-2 in an alginate carrier, an exciting feature with potential clinical applications.

The use of engineered gels to sequester growth factors has been shown to improve cell invasion and enhance engrafted cell survival at implant (Jha et al., 2015), this is one potential explanation for the capacity of Laponite gel to promote cell infiltration and facilitate new tissue growth within the gel substance. Hydrogels are often components in composite systems but less frequently as sole agents in bone tissue regeneration, we sought to investigate the application of Laponite as a sole delivery agent as an alternative to limited autograft, allograft and costly bone graft alternatives.

With a sole delivery agent approach in mind, Mariner et al (Mariner et al., 2013) sought to overcome the issues of high BMP-2 concentration and off target BMP-2 effects by administrating InFUSE® BMP-2 at the known effective dose range in rats (using a calvarial defect model), 0.025-0.05 mg/ml. In their work the calvarial defect volume was calculated at approximately 56µl, a total rBMP-2 dose of 2µg per defect (fitting within the 0.025-0.5mg/ml range) Mariner and colleagues selected two experimental doses, 2.0µg and 0.2µg, applied to collagen sponge and in a RGD-modified, functionalised PEG hydrogel alone. Their findings ably demonstrated comparable bone formation between hydrogel BMP-2 and InFUSE® groups at 2µg BMP-2 and a significantly higher volume of new bone in the 0.2µg BMP-2 hydrogel system over the InFUSE® equivalent.

To correlate the findings of the Mariner study to those of the current study knowledge of equivalent dosing is required. The scaled dose of BMP-2, using the 0.025-0.05mg/ml range quoted for rats, would equate to a total dose of 35-40µg BMP-2 per sheep condyle defect (approximately 750µl in volume), compared with the actual dose of 100µg used in the current study. In the supporting literature, no effective dose response in non-human primates was shown and no experimentation yet carried out in ovine species. Our selected dose of 100µg BMP-2 /defect is a concentration of 120 µg/ml, an approximate ten-fold reduction in the non-human primate effective range and guideline clinical dose given in InductOS® product information. In this comparison, both the lower effective dose range documented in the FDA report and the less challenging nature of a rat calvarial defect would contribute favourably to a successful *in vivo* outcome.

We detected a significant increase in bone volume when using a collagen sponge substrate in combination with Laponite, but not when Laponite was used as a sole agent for BMP-2 delivery, although large volumes of new bone were present in a number of Laponite gel BMP-2 samples. The large sample variation affected statistical analysis perhaps masking what 2-D renders show to be the potential for promising new bone growth.

5.6.3 Structure of new bone formation

On high resolution imaging, Laponite samples were seen to form new bone in a sandwich layer pattern. In contrast, InductOs® and autograft groups showed new bone formation as random, lower density calcified tissue, devoid of a readily identifiable distribution morphology. The pattern of bone formation in Laponite collagen sponge samples, particularly samples R706605 and R706610 (Figure 5-20, C and D), both show an unusual distribution of calcified tissue not seen in other groups, the pattern may indicate a function of Laponite gel in localising bioactive molecules *in vivo*.

The pattern of bone formation has yet to be satisfactorily explained, due in part to the absence of histology, but one hypothesis describes the "pocket" formation being caused by the strict localisation of BMP-2 onto the Laponite carrier in such a way that new bone growth occurred immediately within and adjacent to the Laponite bound BMP-2. As the Laponite was only applied to the surface of the sponge in the "sandwich" set-up, Figure 5-16, A-C, bone formation would only have taken place surrounding the sponge and not within the sponge substance.

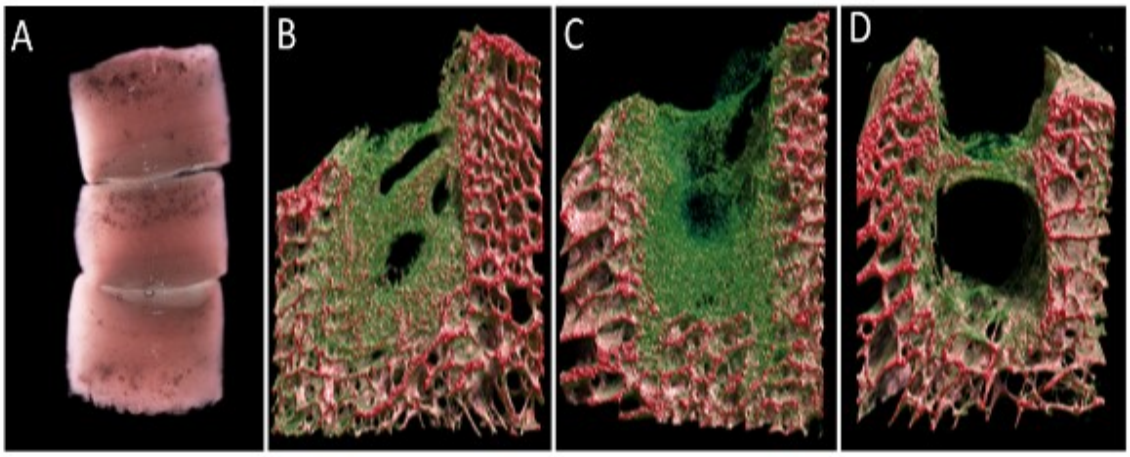

Figure 5-20. Correlation between collagen sponge construct and pattern of bone formation. A) Three sections of collagen sponge with 22µl of Laponite between layers. The sponge has swelled in the presence of physiological buffer but Laponite remains located in a disc shape as when first applied. B-D) Cross sections from highest (B), mean (C) and lowest (D) total bone volumes, from the Laponite collagen BMP-2 group, each demonstrating a portion of defect not filled with new material. It is proposed that unfilled areas of defect which are surrounded by new material correlate to sections of collagen sponge within the defect. Image (A) provided by Dr Jon Dawson.

Figure 5-20 Illustrates how the pockets of low-dense material encased in mineralising newly formed tissue may relate to the structure of the original layered construct at implantation (A), due to the large degree of collagen sponge swelling it could not be guaranteed that all three sponge layers persisted *in vivo,* this may form part of the inter-sample variation noted both in CT values and qualitatively on CT renders.

5.6.3.1 Role of construct properties in bone formation

Laponite was shown not to swell nor dissolve *in vitro*, the surrounding collagen sponge by comparison, absorbed simulated physiological buffer and swelled considerably, Figure 5-16, A. *In vitro*, Laponite can strongly localise model proteins (Dawson et al., 2011) (Gibbs et al., 2016b) and the pattern of mineralised tissue formation seen on CT in Laponite collagen BMP-2 samples closely follows the shape and structure of Laponite gel within the layered collagen construct. Laponite, by way of a variety of particle interactions, binds protein in such a way as to moderate its release kinetics *in vitro* enhancing the activity of BMP-2 *in vivo,* promoting osteogenesis at concentrations lower than that used in the current study.

We have also observed that Laponite induces endochondral ossification histologically although confirming this in our present work is ongoing as histology for the current study was not available at the time of writing.

BMP-2 is known to promote progenitor cell migration along a chemotactic gradient (Fiedler et al., 2002) and thixotropic biomaterials, including Laponite, have been shown to permit and facilitate cellular invasion, proliferation and differentiation both *in vivo* (Dawson et al., 2011; Gibbs et al., 2016b) and in 3-D culture systems (Pek et al., 2010). We propose that strong localisation of BMP-2 to Laponite which in turn is localised between collagen sponge layers, promotes cell infiltration and proliferation through the Laponite component, infiltrating cells then differentiate and mineralise under the stimulatory effects of BMP-2, forming shell-like structures surrounding collagen sponge blocks.

5.6.4 Sample variation

When viewing sagittal projections of µCT data, the volume of new bone formation appears irregular in Laponite groups, both collagen sponge and gel only groups. In the Laponite gel BMP-2 group there was high inter-sample variation in the amounts of new bone formed, this variation did not echo the inter sample variation seen in autograft nor empty controls and by extension it seemed unlikely the result of normal variation seen between animals and their individual propensity for healing.

An attempt was made to correlate the best and worst responders to the bone density in the defect at time of drilling. Again, no association could be seen between the bone density of the individual sheep and the new bone formation within the defect.

Confirmation that all sponges remained in place after implantation will inform potential causes of this variation, as will correlation to stem cell CFU-F performance and other factors such as bone mineral density (and its association with osteoporosis).

It was also considered whether the variation between construct preparation and implantation impacted on the bioactivity of BMP-2 at time of implant. The effect of active bleeding into the defect was also considered as Laponite had only previously been examined in a mouse sub-cutaneous model. The impact of large amounts of blood and exposure to inflammatory proteins has not yet been examined, although unpublished *in vitro* experiments have indicated that Laponite strongly and persistently binds proteins in solution, it is plausible this effect would extend to growth factors, cytokines and other small peptides *in vivo.*

Histology of BMP-2 and laponite only samples demonstrated a small amount of mineralised collagenous material branching from the defect wall, following the chemotaxic gradient. This material was parallel in orientation but did not demonstrate any cartilaginous anular. In control and Laponite samples, the defect is well demarcated with blood vessels present within a randomly orientated fibrous infiltrate. Further staining of samples is required to discern identifiable characteristics from tissue morphology.

5.6.5 Limitations

Unfortunately, it is possible that a well demarcated defect with rigid borders such as the one created in this model may not ideally demonstrate the ability of Laponite to provide an anatomical as well as biochemical localising effect as the defect itself will help localise installed therapies. It would be of interest in future work to examine the application of Laponite based carrier systems in a clinically analogous model such as a tibial or radial fracture model, clinical scenarios where an aqueous carrier would be unsuitable.

Further data on the behaviour of Laponite *in vivo* is required, it is not known whether Laponite persists in the defect location or whether factors such as haemorrhage, immune responses and shear forces may all accelerate elimination from the defect site therefore limiting *in vivo* activity.

Results presented are entirely based on µCT measurements of new bone only. The data as presented does not inform the reader about some of the favourable clinical application benefits of Laponite such as improved handling and ability of a gel to localise a payload to the target area, using lower concentrations and reduced overall dose, coupled with the benefits of using a bone forming gel through a minimally invasive technique such as transcutaneous injection, or used as an adjunct therapy in a delayed application. The absence of histology at this stage is limiting but is ongoing and will be available prior to intended publication.

5.7 Conclusions

Surgery was successfully carried out on 24 animals using protocols validated in Chapter IV, 23/24 animals were included in sample analysis. The 96% end-of-study survival rate was the highest of all large animal studies performed to date by the Bone and Joint Research Group.

Medtronic InductOS® was shown to have statistically significant osteogenic capacity at a tenfold dose reduction in BMP-2 concentration. Laponite was demonstrated to effectively deliver low dose of BMP-2 whilst also demonstrating clinically superior handling properties *in vivo.*

The use of Laponite as a sole delivery agent of BMP-2 in a cortical defect model did not yield statistically meaningful results due to high inter-sample variation, although several samples in the Laponite gel BMP-2 group demonstrated potent levels of new bone growth. Although limited by as-yet undetermined causes of high variation in its ability to generate an osteogenic response in a large animal model, Laponite has demonstrated a clear potential for application in this therapeutic area. Further work will need to determine the most effective mode of application, understand the *in vivo* physiological interactions between patient and material and reliably identify the causes of such large inter-sample variation. Although not conclusive, this study substantiates the claim that Laponite can be used as a vehicle for bioactive molecule delivery, as a sole agent or in combinations with composite solutions.

Chapter VI

6 Evaluation of Bovine ECM hydrogel and Stro-4 selected skeletal stem cells in a critical sized ovine tibial segmental defect

The use of *in vivo* models of increasing challenge is the proving ground for regenerative therapies en route to clinical trial or licensed application. The use of the ovine tibial segmental model poses one of the most significant tests in bone tissue engineering research. In chapter VI the ability of Stro-4 cells delivered with a novel extracellular matrix hydrogel to effect the formation of clinically relevant volumes of new bone in an ovine tibial segmental defect is examined.

Acknowledgements

The work detailed in this chapter was performed at the Queensland University of Technology in collaboration with Professor Dietmar Hutmacher. Surgery was performed at the Medical Engineering Research Facility, hosted by lead veterinarian Dr Siamak Saifzadeh with orthopaedic surgical protocol taught and supervised by Mr Jan Henkel.

I am grateful to Dr Mia Woodruff and the Bone Tissue Morphology group for assistance in mineralised tissue histology and micro-CT scanning. The protocols described were based on work by Mr Johannes Reichert who established the segmental defect model at the University of Queensland.

6.1 Introduction

The replacement of large volumes of bone damaged or resected due to metabolic, traumatic or neoplastic causes remains a major hurdle in orthopaedic surgery (Wiese and Pape, 2010; Kisiel et al., 2013). Severe bone loss can occur in highly comminuted high energy fractures and as a result of complications of healing in atrophic and hypertrophic non-union. In addition, primary osteosarcoma and secondary metastatic bone tumours are often highly invasive cancers requiring aggressive multimodal treatment and surgical resection, which can result in large volume bone loss in the affected limb. Traditionally the bone void is filled with autogenous or allogenic bone graft which possess osteoinductive and osteoconductive properties and, in the case of contained defects, graft can be impacted during application to enhance the mechanical contribution of graft material in-situ (Brewster et al., 1999). However, the use of bone graft has associated inherent problems relating to availability, donor site morbidity, risk of infection and incomplete graft integration.

Surgical interventions designed to address large volume bone loss have been led by techniques in distraction osteogenesis techniques (DO). DO harnesses the inherent bone forming capacity of the patient to form new bone in areas of bone loss. DO typically utilises an Ilizarov or Taylor Spatial Frame to drag or distract a bone fragment at a rate which allows the body to lay down new bone behind the segment (Alzahrani et al., 2014; Khunda et al., 2016). As the treatment progresses the volume of new bone formed increases. Although successful, these techniques are i) costly, ii) require prolonged periods of treatment and hospitalisation, iii) are susceptible to pin-site infections and, iv) cause extended patient morbidity (Khunda et al., 2016). The resultant need for clinically effective low-cost solutions has thus driven the development and translation of novel bone tissue engineering therapeutics.

6.1.1 Need for large animal models in clinical translation

In his 2011 review, Professor Hollister remarked upon the translation of therapies in bone tissue engineering as “bluntly, a failure.” (Hollister and Murphy, 2011). Hollister defended his claim by highlighting the relatively small numbers of novel therapeutics which had been introduced as approved clinically available products. Despite considerable progress in the field there currently exists no bone tissue engineering strategy capable of replicating the complexity of biological bone repair nor the clinical efficacy of autogenous bone graft transplantation. Furthermore, no alternative system exists which can accurately mimic the mechanical and physiological complexity of bone regeneration occurring within the human and other mammals. Examination using a large animal critical-sized defect model presents the most clinically analogous approach to comparative *in vivo* testing and remains an essential component of translational research.

Many technical, economic and regulatory barriers exist to prevent the progression of novel therapeutics from concept, through early development and into pre-clinical testing. Subsequently, many hydrogel-based systems, either used as a “growth factor free” approaches or as delivery vehicles for cells and bioactive peptides remain limited to the realm of small animal *in vivo* experimentation. The current work has sought to undertake experimentation in a weight bearing large animal model. For further information on the use of large animal models in bone tissue engineering see chapter I, 1.11.3 page 66.

6.1.2 Critical-sized defect

The complications arising from traumatic bone loss, reconstruction following tumour resection or tissue debridement as a sequelae to infection can be considered a form of critical sized defect; in which the damage to bone tissue or amount of tissue requiring regeneration exceeds the capacity of the body to replace the absent tissue. In translational models, the recreation of a critical sized defect is designed to simulate the complications experienced in the clinical scenario.

A critical-sized defect is described as “the smallest size intraosseous wound in a particular bone and species of animal that will not heal spontaneously during the lifetime of the animal” (Gugala and Gogolewski, 1999; Reichert et al., 2009) or, alternatively, as a defect which will not demonstrate more than ten percent bone healing during the lifetime of the animal (Gugala and Gogolewski, 1999).

A number of factors, not all of which are understood, contribute to the creation of a critical defect, including: Species, age, sex, bone type, surgical model performed and additional challenges made to the model such as removal of periosteum. Both definitions comment on the whole life course of the animal. In experimental scenarios, it would be unusual for the experimental period to extend throughout the natural course of an animals' life. A practical definition of a critical defect was proposed as being 2-2.5 times the diaphyseal diameter by Lindsey (Lindsey et al., 2006) although this itself offers no more than a guideline. Thus, it would be more accurate to state that a critical bone defect poses a regenerative challenge which reliably exceeds the reparative capacity of the host animal to repair more than 20% of the defect over the experimental time duration. In light of the inter-model variation, it is essential that every segmental or critical-sized defect study incorporates an empty control either as part of a historical dataset or included in each experimental set-up.

6.1.3 Methods of fixation

The choice of a 4.5mm broad dynamic compression plate for fixation was advised in whole by the work of Mr Johannes Reichert at Queensland University of Technology. In establishing the ovine tibial segmental defect model, the use of intramedullary nailing, LC-DCP plating, external fixation and DCP plating was compared. Reliably the broad DCP plate provided sufficient weight-bearing stability and resisted implant failure and fatigue over three and six month experimental periods (Reichert et al., 2009).

6.1.4 Hydrogels in bone tissue engineering

Tissue engineering approaches seek to harness the biomimetic properties of a scaffold material, simulating tissue matrix and providing a mechanical framework for the growth of new tissue. In context of translational medicine, a biomaterial needs to fulfil both biological and clinical pre-requisites. Biologically it must provide a biomimetic extracellular niche, promoting cell viability, conduction and induction whilst, clinically lending itself to production on a relevant scale, fulfil the requirements of appropriate regulatory framework and lend itself to use in a clinical setting (Dawson and Oreffo, 2008).

The scaffold framework can act as a sole agent, conducting and inducing new tissue formation from the surround host tissues or the scaffold can be augmented with an exogenous cellular component. In applications relating to large volumes of tissue loss, the cell choice should be amenable to high volume *in vitro* expansion whilst maintaining potential for lineage specific differentiation.

Hydrogels act as vectors in the delivery of bioactive molecules and osteogenic cellular elements. Critically, bECM has demonstrated efficacy in the formation of new bone in early stage *in vivo* experimentation (Gothard, 2014). Furthermore, bECM can be injected into the defect site potentially negating the need to surgically expose the underlying tissue surrounding an area of bone trauma or non-union or in the case of large bone loss, could be applied as a one off in concert with traditional fixation and solid scaffolds to augment fracture repair. The reduced need for surgical intervention combined with accelerated healing rates could therefore reduce hospitalisation periods, hospital visits and the total duration of treatment and morbidity a patient endures.

6.1.5 Role of extracellular matrix in bone tissue homeostasis and repair

In vivo, extracellular matrix is a multifunctional tissue constituent and in connective tissues, it is the ECM (not the cell), which forms the bulk tissue component by dry-weight. In bone, the osteoblast is responsible for ECM production and the ECM in turn is a major determinant of the overall skeletal mechanical properties. The primarily structural collagen proteins are secreted alongside supportive and signalling non-collagen proteins producing a diverse functional niche which facilitate molecular diffusion, providing a supportive framework directly and indirectly for cell responses (Alford et al., 2015).

6.1.6 Research in context of previous work

Decellularised bone matrix has been successfully produced by our collaborators at the University of Nottingham, providing a material inherently flush with collagen and non-collagenous proteins suspended within a self-assembling network without the necessity for a carrier fluid (Sawkins et al., 2013). Thus, the decellularised matrix provides an exciting biomaterial which may potentially be manufactured from processed and banked allogenic sources in addition to processed material of animal origin. Work in the Bone and Joint Research Group has shown bECM hydrogels are cytocompatible and can serve as a delivery vector for stem cells in bone tissue engineering (Gothard et al., 2015).

As demonstrated in chapter III, Stro-4 enriched ovine SSCs rapidly expand *in vitro* and respond to osteogenic and chondrogenic growth cues. A Stro-4 specific effect was also seen in femur repair using the CAM ex-vivo assay.

In chapter III a novel bovine bone derived ECM hydrogel therapeutic was examined in a functional *in vivo* CAM set-up. bECM gels were localised to a chick femur defect using a melt-electrospun PCL mesh and allowed to incubate on the membrane of a developing chick. µCT analysis identified comprehensive bone bridging within the bECM seeded with Stro-4 SSCs and unseeded when compared to empty controls.

In Chapter VI the ability of bECM hydrogels to augment new bone formation in a critical-sized ovine tibial segmental defect model was examined. A successful outcome would highlight the suitability of bECM as a feasible alternative to autograft, allograft and graft alternatives in a clinical application. Such an approach, would also lend credence to the combination of ECM hydrogels (including human) in augmenting bone formation when used in concert with traditional and manufactured graft materials.

6.1.7 Experimental set-up

Sixteen experimental animals were divided amongst two experimental groups, i) ECM hydrogel and PCL mesh constructs without cells and ii) ECM hydrogel and PCL mesh constructs seeded with Stro-4 ovine SSCs. Findings from the study were combined with historical data from empty and autograft controls.

Group	Material	Cell source	Number of samples
I (historical)	Empty defect	n/a	6
II	bECM Hydrogel PCL mesh	n/a	7
III	bECM Hydrogel PCL mesh	Stro-4 Ovine SSCs	6
IV (historical)	Autograft	Autologous heterogeneous population	7

Table 6-1 Experimental groups

6.2 Aims

1. To isolate and culture sufficient numbers of Stro-4 ovine skeletal stem for use in a tibial segmental model.
2. To establish a sixteen-animal segmental defect study comparing the bone forming capacity of seeded and unseeded bovine EXM hydrogels localised to a defect by use of a PCL microfiber mesh
3. To demonstrate the use of a bovine derived ECM hydrogel as an effective therapeutic in bone tissue engineering showing comparative efficacy to the clinical gold standard, autologous bone.
4. To demonstrate an enhanced bone forming effect in ECM hydrogels seeded with Stro-4 SSCs

6.3 Null hypothesis

The application of bovine bone derived extracellular matrix hydrogel, either alone or supplemented with an enriched stem cell population, does not enhance the repair of a critical-sized ovine tibial segmental defect.

6.4 Methods

6.4.1 Microfibre Mesh production

PCL Mesh production was generated as described in chapter III**.** For use in the ovine tibial defect, a 2cm diameter collecting mandrill was used and approximately 250 fibre layers were collected, allowed to cool, producing a mesh 6cm in length, 2cm in diameter and a wall thickness of 1mm. Each PCL mesh scaffold was etched and CaP coated.

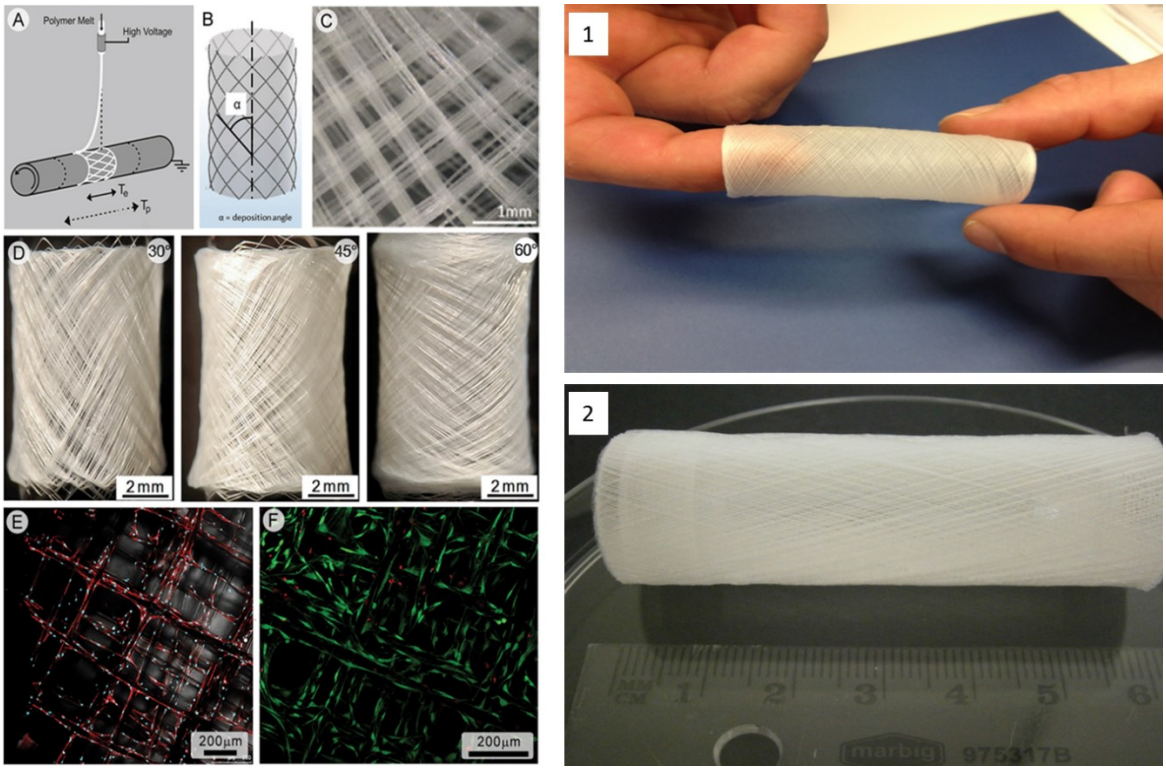

Figure 6-1 PCL microfiber mesh production. A) and B) Schematic of melt electrospinning production highlighting the importance of fibre orientation. C) Printed mesh with 60° fibre alignment. D) Macroscopic appearance of 30°,45° and 60° alignments. E) FITC-conjugated actin fibres of mesh adherent osteoblasts. F) LIVE/DEAD staining showing high cellular viability at 2 weeks. 1) Mesh printed for the current study 2) Showing approximate dimension, 6cm in length by 2cm in diameter. Images A-F used with permission from Prof Dietmar Hutmacher. Scale bars 200um-2mm, as detailed in C-F.

6.4.2 Stro-4 cell isolation and culture

Stro-4 MACS isolation was performed according to protocols outlined in Chapter II, 2.3. Bone marrow samples were washed in serum free α-MEM (Lonza, Australia) and passed through a 70µm cell strainer (Falcon, Corning, Australia) to form a single cell suspension. Single cell suspensions were layered onto density gradient separation medium (Lymphoprep, Stemcell Technologies, Australia), and centrifuged to isolate the mononuclear cell fraction.

Mononuclear cells were incubated with neat Stro-4 supernatant (kindly supplied by Professor Gronthos, University Adelaide). Following incubation, cells were washed and incubated with anti-mouse IgG MACS microbeads (Miltenyi Biotec, Australia). MACS labelled cells were passed through a QuadroMACS® (Miltenyi Biotec, Australia) magnet system and Stro-4 positive cells collected.

Isolated cells were seeded into 175cm^2 tissue culture flasks (Corning, Sigma-Aldrich, Australia) at a minimum density of 5 x10^5 per flask and a maximum density of 2 x 10^6 cells per flask, seeding density was dependant on sample yield. Cells were cultured in 10% FCS (Gibco, ThermoFisher, Australia), 1% Pen/Strep (Gibco, ThermoFisher, Australia) α-MEM. Cells were expanded over two passages and used at a total density of approximately 7 x 10^6 per ml of defect. Total cell number of passage 3 Stro-4 positive ovine mononuclear cells was 5-7 x 10^7 per sample.

6.4.3 Bovine ECM production

Production of bECM was performed as described in general methods, chapter II, 2.6 with adaptions to account for increased volume requirements and adaptions required for successful application during surgery. Each defect required 10-15ml of ECM hydrogel, to account for loss in application and material lost during transfer, 20ml was reconstituted for each defect surgery; a total of 320ml of ECM hydrogel for all animals. On the day of surgery, a 20ml aliquot of un buffered ECM was transferred to a 50ml Falcon tube and neutralised with NaOH. Buffered ECM was either used unseeded or seeded with 5 x 10^6 Stro-4 cells /ml and was kept on ice until surgery. ECM was drawn into a 12ml syringe using an 18g needle (Terumo, Australia) and injected into the PCL mesh lumen intra-operatively.

6.4.4 Surgical protocols

16 aged (>6 years old) male Merino cross sheep were allocated into two experimental groups, unseeded bECM (n=8) and Stro-4 seeded bECM (n=8). Surgical protocols were based in those published by Reichert *et al* 2012.

Anaesthetic and analgesic protocols for the tibial segmental defect share many similarities to protocols detailed in condyle defect surgeries. Notable additions are detailed below.

6.4.4.1 Pre-medication, anaesthesia and analgesia

Midazolam (0.2-0.4mg/kg) was administered i.m.. twenty minutes before central line placement and induction. A further bolus of midazolam at 0.1mg/kg was co-administered with Buprenorphine (0.01mg/kg) intravenously through the central line, the degree of sedation was assessed prior to induction. A Central line was placed as described for the ovine condyle defect creation, Figure 6-2**,** A and B.

All animals were given a final health check, which included baseline biomarker and blood count haematology from a sample drawn during central line placement. Induction was not commenced until confirmation of good health status. Bloods taken on day of surgery were a follow-up to full health screening performed one week prior to surgery.

Animals were intubated with a size 9mm ET tube, pre-oxygenated with a 100% O_2 and saturation monitored by pulse-oximetry. Each animal was then transferred to theatre and placed on Isoflurane at 2-3.5% in oxygen at 2L/min for anaesthetic maintenance. Animals were secured in right lateral recumbency and the surgical limb positioned with sandbags, foam pillow and rope (where needed).

6.4.5 Statistical analysis

Statistical analysis was performed using GraphPad Prism with graphs produced in the same software. A one-way analysis of variance ANOVA was used with Tukey's post-hoc test comparing the means of each group with one another, and Dunnett's post hoc comparing each group to blank controls. Significance was given at $p < 0.05$ was considered significant. Only autograft demonstrated significant bone growth, ****$p<0.0001$

6.4.5.1 Autograft harvest

Autograft was harvested from the iliac crest of eight animals. Pre-medication and anaesthesia was performed as for segmental defect surgeries 6.4.4. Anaesthetised animals were placed in sternal recumbency and secured in place. The sacrum and iliac wings were identified by palpation and an area surrounding the pelvic bones clipped, shaved and cleaned with Hibiscrub®. The animal was draped from the shoulders, extending beyond the tail with a window around the surgical area. Iodine impregnated adhesive dressings were placed over the surgical area. The right iliac wing was identified by palpation and an incision made along the iliac spine. Soft tissue attachments were removed from the iliac body by blunt dissection taking care to preserve vascular structures. The connective tissue capsule surrounding the ilium was leveraged from the bone, providing good exposure to underlying bone, Figure 6-3, A. A wedge osteotomy was created using an oscillating saw, with care taken not damage surround soft tissue and not to penetrate the abdominal wall, Figure 6-3, B. The osteotomy site was closed sequentially and animals recovered from anaesthesia. All animals were given a three-week healing period prior to tibial defect surgery. Autograft material was harvested from the osteotomy wedge and processed for Stro-4 isolation.

6.4.5.1.1 Surgical preparation and central line placement

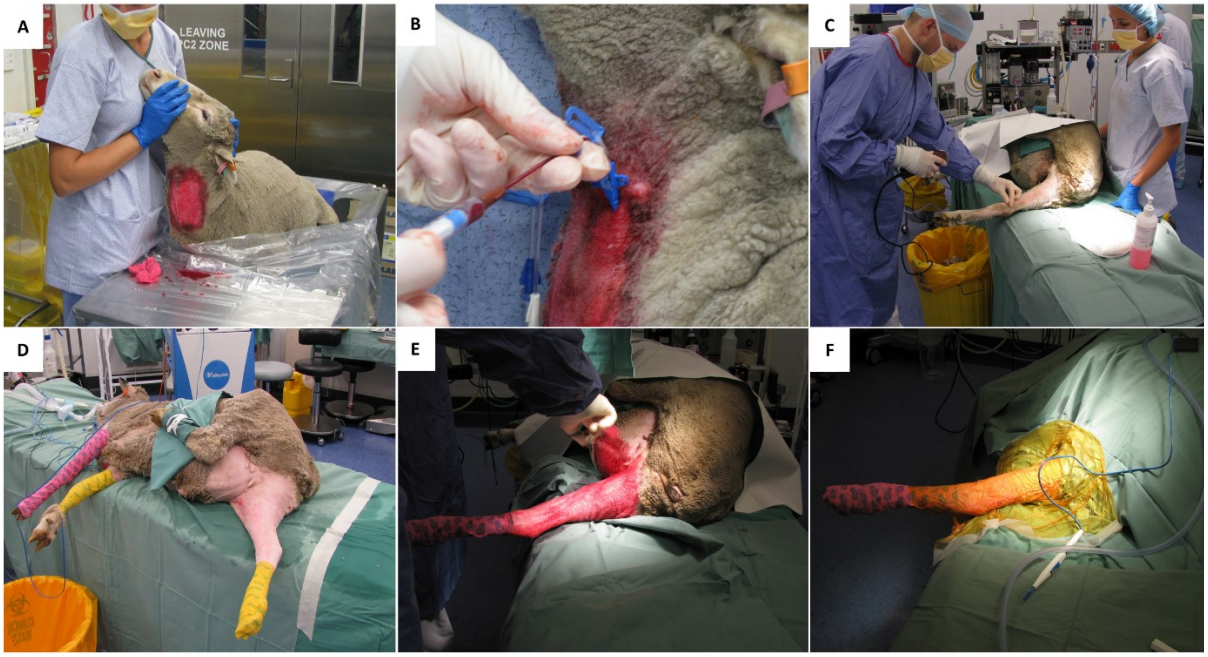

Figure 6-2 Surgical preparation. A) Sedated animal prepped for central line placement. B) Central line placed in left superior jugular vein. C) Animal placed in left lateral recumbency and wool clipped. D) Positioning of legs and application of monitoring equipment. E) Bandaging of limbs and surgical disinfection. F) Prepped animal, draped and surgical site covered with barrier dressing.

6.4.5.1.2 Autograft harvest and cell *in vitro* cell expansion

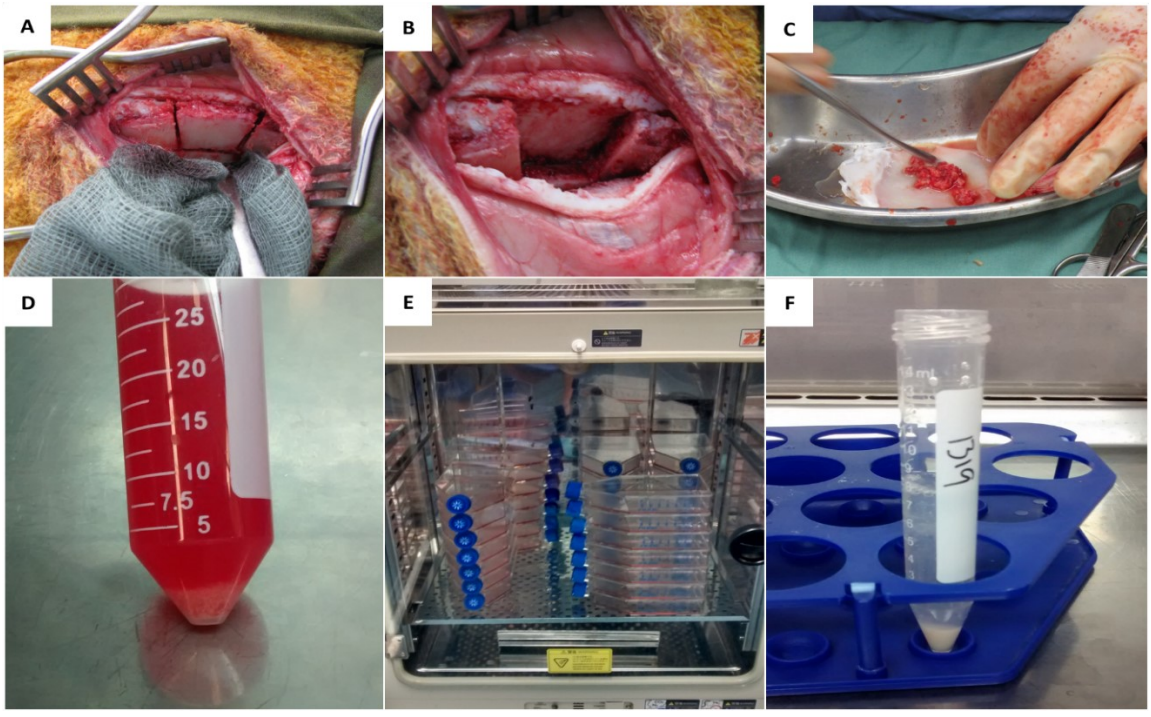

Figure 6-3 Cell isolation and expansion from Iliac crest autograft. A) Exposed Iliac crest, wedge defect cut using oscillating saw. B) Wedge osteotomy, iliac capsule intact. C) Autograft material isolated from bone wedge. D) Mononuclear cell pellet after autograft processing. E) *In vitro* culture of isolated Stro-4 mononuclear cells. F) Cell pellet prior to seeding of bECM.

6.4.6 Defect surgery

Each animal was prepared for surgery by carefully clipping an area of wool extending from the abdominal midline, left and right upper limbs with attention paid to the right upper and lower limbs. The animal was draped from thorax to lower limbs with the lower right limb remaining exposed. The right leg was disinfected and cleaned with 0.5% chlorhexidine and given a final preparation cleanse with 70 % ethanol. The prepared surgical field was covered with an impregnated barrier layer (Ioban®, 3M, Australia). Surgical preparation is shown in Figure 6-2.

A longitudinal incision, approximately 12 cm in length was made on the medial aspect of the limb, extending proximally from below the tibial plateaux and distally the medial malleolus. A Dynamic Compression Plate (4.5 mm broad, 10 holes, Synthes®) was adjusted to the morphology of the bone with a plate bending press (Synthes®) and the fit checked by pressing against the medial tibia. The distal end of all plates was placed exactly 2.5 cm proximal of the medial malleolus. Screws were placed in proximal and distal holes to lock the plate in place. The screw holes were pre-drilled, 3 proximally and 2 distally. A line marking the centre of the defect was made using a rasp. A point 1.5cm proximal and 1.5cm distal to the centre mark was made using the oscillating saw. These defined the precise osteotomy lines for a 3cm defect. The plate was subsequently removed to allow access to all soft tissue structures surrounding the bone. Soft tissue attachments surrounding the defect site were carefully removed. As the exposure to the postero-lateral aspect of the tibia was enhanced, a moistened gauze swab was placed between then bone and the periosteum, separating the bone from periosteum and deeper neurovascular tissue. Once soft tissue attachments were separated from the bone, a malleable blunt metal spatula was passed around the back of the tibia to protect structures during osteotomy (Figure 6-4 for surgery images).

A 3cm tibial diaphyseal defect was created by cutting parallel osteotomies perpendicular to the bone surface at pre-marked sites, Figure 6-4 B and C. A System 6 (Stryker) cordless power tool with sagittal saw under constant pressure was used to cut the bone, the osteotomy sites were continuously irrigated with sterile saline. The periosteum was stripped 1 cm proximal and distal the defect to inhibit the healing response and maximise the regenerative challenge.

Melt-electrospun mesh scaffolds were applied, sutured in place and secured by application of the DCP plate proximally, Figure 6-5 B-F. In both groups, 8ml of sterile bovine ECM hydrogel was injected into the defect lumen, localised by PCL mesh. Seeded ECM hydrogels were combined with cultured ovine Stro-4 selected skeletal stem cell progenitors at a density of 4 $x10^6$/ml of gel material. Seeded and unseeded treatments were warmed to room temperature immediately prior to application and allowed to cross-link in situ. Bone fragments were realigned and the limb secured in place by securing the remaining plate screws. The operated limb was cast in fibreglass tape which was split at the end of week one and used as a splint for a further two weeks. The animals were not immobilised following surgery and were permitted to weight bear immediately post recovery. The full extent of limb weight-bearing was minimised during the first 3 weeks post-operation using a leg cast and subsequent splint, Figure 6-4 E.

Animals were routinely examined for lameness, inflammation, infection and wound complication. All animals recovered successfully from surgery. Two animals were removed from the study after 6 weeks due plate bending, no fracture complications occurred. The remaining fourteen animals were sustained through to 3 months without incident.

6.4.6.1 Surgical protocol

Figure 6-4 Tibial defect surgical protocol. A) Exposed tibia. B) Osteotomy lines marked, wet gauze used to remove posterior soft tissue attachments, oscillating saw in position. C) Proximal and distal tibial portions without fixation. D) Defect secured by plate fixation, construct *in situ*. E) Cast leg. F) Animals 1 hour post-surgery.

6.4.6.3 ECM PCL Mesh construct application *in vivo*

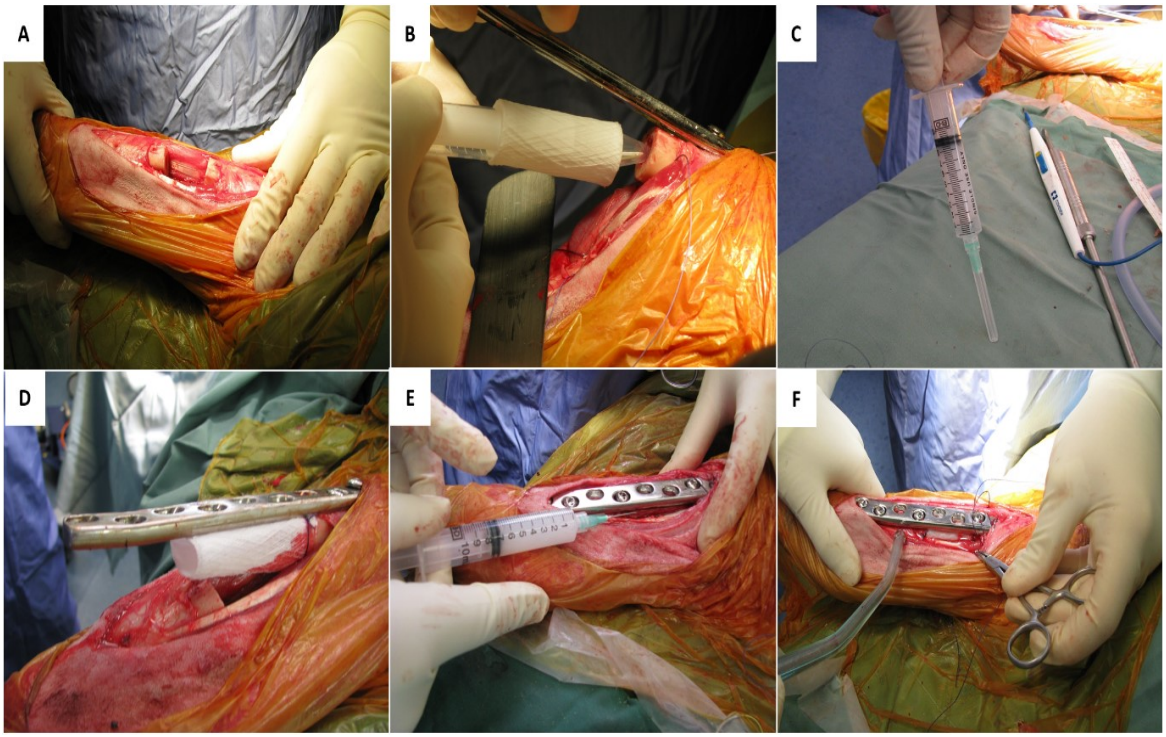

Figure 6-5 Mesh and ECM application. A) Completed osteotomy and defect. B) Application of ECM Mesh onto the proximal tibial segment. C) Syringe with 8ml of ECM. D) Mesh applied and secured by suture and plate, proximal segment. E) ECM injected into mesh lumen. F) Completed defect and construct.

6.4.7 Radiographs

Radiographs were taken using a Philips Varadius® C-ARM system. Radiographs were taken immediately post-operatively to confirm skeletal alignment, adequate screw penetration and plate orientation. Radiographs were repeated prior to cast removal at week three and four, and again at the study end-point of three months. In all cases medio-lateral and cranio-caudal projections were taken. Appropriate PPE was worn by all operators in proximity of the closed X-ray source.

6.4.8 Micro-CT analysis

6.4.8.1 Total bone volume

Samples were scanned at 18 μm resolution using a Scanco μCT 40 micro-CT, files were converted to .ISQ format and analysed in combination with control data at the University of Southampton using ctAN software (Bruker). The defect region was identified using the drill holes nearest to the defect boundary as landmarks, with the defect universally defined 0.5cm from the screw site. A global threshold was set using an Otsu weighted technique whereby a mean Otsu threshold was determined by automated calculation. The defect region was analysed in four segments, proximal, middle, distal and whole. Only values for the whole defect region were included due the absence on new bone formation demonstrated in test groups.

6.4.8.2 Bone distribution throughout defect sub-regions

Defect regions were further sub-divided into Proximal, Middle and Distal and distal ROIs. This was performed by measuring the total number of CT "slices" which constituted individual samples. 1mm of on the z-axis is represented by 55 slices on an 18μm resolution scan, i.e. each 3cm defect is comprised of approximately 1650 slices and each sub-region of 550 slices. The total number of slices was dived by three; then each of the three sub-regions (proximal, middle and distal) allocated according to the appropriate number of slices. Thus, each sample was analysed uniquely with the total volume of each sub-region differing between samples.

6.4.9 Histology; Resin embedding and immunohistochemistry

After micro-CT analyses, tibial bone specimens were frozen and trimmed to a 6 cm length. Samples were fixed in freshly made 4% Paraformaldehyde at 4°C for a minimum of one week and samples regularly checked for fixative penetration. The fixative was replaced every 72 hours. For histological analysis, the mid-defect regions were sectioned in the transverse and sagittal plane (see cutting guide Figure 6-6). Sections were divided between resin and paraffin embedding. Paraffin embedded sections were used for Immunohistochemistry (IHC). Samples for paraffin embedding were initially decalcified in 15% EDTA for 6-8 weeks at 4 °C with regular EDTA changes. Decalcified samples were then dehydrated by sequential rising percentages of ethanol using an automated tissue processor (Excelsior ES, Thermo Scientific, Franklin, MA, USA), and embedded in paraffin wax. Samples for IHC were sectioned into 5 μm slices using a microtome (Leica RM 2265). The slides were then deparaffinised with xylene and rehydrated prior to background haematoxylin and eosin staining (Sigma Aldrich). Samples were mounted with Eukitt (Fluka Biochemica, Milwaukee, WI, USA).

6.4.9.1 Immunohistochemistry

All histology was performed by staff of the Bone Tissue Morphology Unit, Queensland University of technology, led by Associate Professor, Mia Woodruff.

For immunohistochemical analyses, slides were rinsed in distilled water and washed in 0.2 M Tris-HCl buffer (pH 7.4). Endogenous peroxidase activity was removed by exposure to 3% H_20_2 diluted in 0.2 M Tris-HCL for 30 minutes at room temperature. Thereafter, sections were washed three times in Tris buffer for 2 minutes each. Slides were incubated with Proteinase K (DAKO, Botany, Australia) for 20 min at room temperature for antigen retrieval. Slides were then washed three times with Tris buffer for two minutes a wash. Washed slides were blocked using a 2% bovine serum albumin (BSA) (Sigma, Sydney, Australia) solution, applied for 60 minutes in a humidified chamber. Sections were gently washed in Tris buffer for two minutes prior to application of primary antibodies. Antibodies against osteogenic markers Collagen Type 1 (Saphire Bioscience, Waterloo, Australia), Osteocalcin (Saphire Bioscience, Waterloo, Australia) and endothelium-related von Willebrand-factor (Dako Australia, Campbellfield, Australia) were used and incubated at 4°C over-night. Sections were washed in Tris buffer three times before incubation with the secondary antibody.

Directly conjugated peroxidase-immunoglobulin linked secondary antibodies (DAKO EnVision+ Dual Link System Peroxidase, DAKO) were used as appropriate to the primary antibody used, incubated in humidified chambers at room temperature for one hour.

Samples were subsequently washed three times for two minutes in Tris buffer, colour development was performed using 3,3-diaminobenzidine (DAB, DAKO). A haematoxylin counterstain was applied for 5 minutes followed by Ammonium Hydroxide 0.1% for 30 seconds and gently rinsed under a tap to develop the colour. Coverslip's were applied using Keiser's glycerol gelatin (DAKO) as a mount and left to dry at room temperature over-night.

6.4.9.2 Resin embedding

Samples allocated for resin embedding were treated as detailed above for IHC. In brief, specimens were fixed in 4% paraformaldehyde, and dehydrated using an ethanol gradient from 70% for 30 minutes then 1 hour in 90%, 95% and 100% ethanol. The samples were then cleared by processing through xylene for 40 minutes and the step repeated three times. Samples were infiltrated with Methyl Methacrylate Monomer (MMA) for 3 hours at room temperature and embedded in MMA containing 3% PEG until set (up to 6 weeks). Seven micrometre sections were cut with using a sledge osteo-microtome (SM2500; Leica Microsystems, Wetzlar, Germany), stretched with 70% ethanol onto a polylysine coated microscope slide (Lomb Scientific). Stretched samples were covered with a plastic film and slides were clamped together and dried for 12 hours at 60°C. Sections were then stained using Von Kossa and Goldner's trichrome.

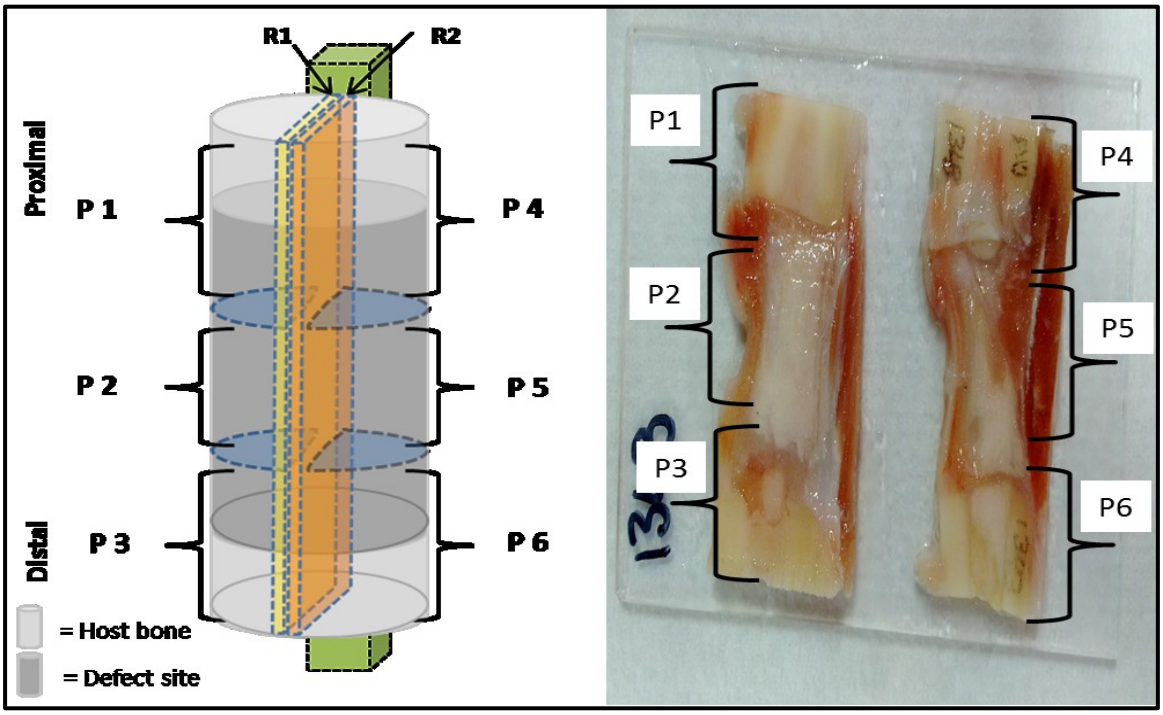

Figure 6-6 Sample sectioning template.

Left: Schematic outlining the regions each tibial sample was sectioned into prior to histology preparation. Each sample was cut longitudinally into R1 and R2 sections. R1 was resin embedded and prepared for ground sectioning. R2 was wax embedded and prepared for immunohistochemistry. Each R1 and R2 segment was further divided into P1; host bone/defect interface, P2; middle of defect and P3; defect/host bone interface. Right: gross samples with regions of interest marked. All undertaken at QUT.

6.5 Results

A total of sixteen experimental animals were used in the current study, eight animals allocated to each group, seeded and unseeded with bECM hydrogel and PCL mesh. All animals recovered from surgery without incident. Animals were ambulatory, capable of independent eating and drinking within one hour of anaesthesia cessation.

During the first week post-surgery, five out of eight animals in the cell seeded group and two out of eight animals in the unseeded group displayed a persistent mildly elevated body temperature. There were no other indications of ill health. Casts were split and wounds examined for suture integrity along with signs of inflammation and infection. Animals with a demonstrable raised body temperature also presented with localised superficial erythema focally associated with the defect location. There was no indication of pain, an absence of wound discharge and no evidence or indication of wound compromise. The animals were treated with NSAIDs (Carprofen) once a day for three days. At no stage was there any indication of wound complications such as i) suture break down, ii) dehiscence, iii) spread of inflammation or iv) reaction of regional lymph nodes. This localised response had dissipated by the start of week three post procedure.

Radiographs were taken of all animals as the casts/splints were removed, at week four post-operation. Concerning radiographic findings were observed in two animals - one animal from each of the unseeded and cell seeded experimental groups. In animal 1314 the implant had begun to bend with a medio-lateral deviation (bending in on itself), Figure 6-7**.** In 1340, the proximal three screws had loosened significantly, with three out of four screws pulling through the far cortex. Neither 1314 nor 1340 displayed signs of lameness but were excluded from the study and euthanased in the interests of preventing inevitable catastrophic failure and severe compromise to animal welfare. Of the remaining fourteen animals, 1320 was euthanased at week 10 due to persistent and unresponsive lameness, although no pathological radiographic changes were seen. Thirteen out of the sixteen animals continued until 3 months and were included in analysis, within the accepted experimental range of over an eighty percent success rate. Radiographs from all samples at 4 weeks are given in Figure 6-8 and Figure 6-9.

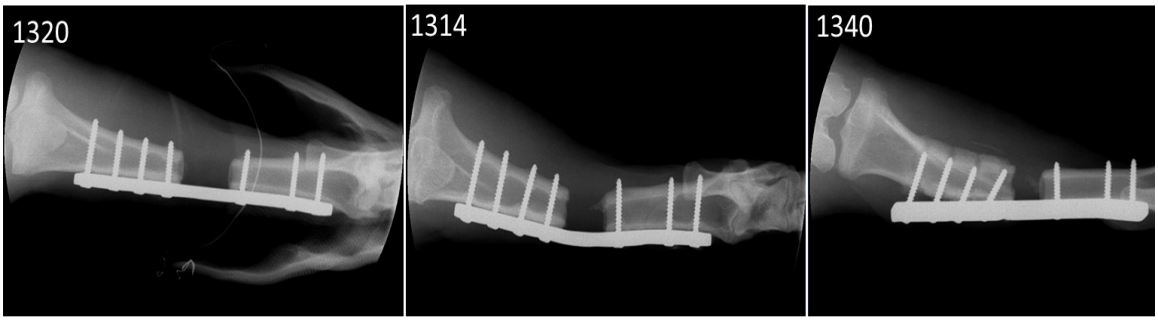

Figure 6-7 Radiographs detailing experimental complications. Radiographs of 1314 (Stro-4 seeded ECM) and 1340 (unseeded ECM). Implant failure and moderate plate bending was seen in 1314. Screw failure and was seen in 1340, radiographic changes indicate early fracture of the proximal cortices in apposition with the plate, probably as a result of overloading after splint removal. 1320 was excluded as a result of an unresponsive lameness noted at week 10, no radiographic abnormalities were seen.

6.5.1 Radiographs, four weeks post-surgery

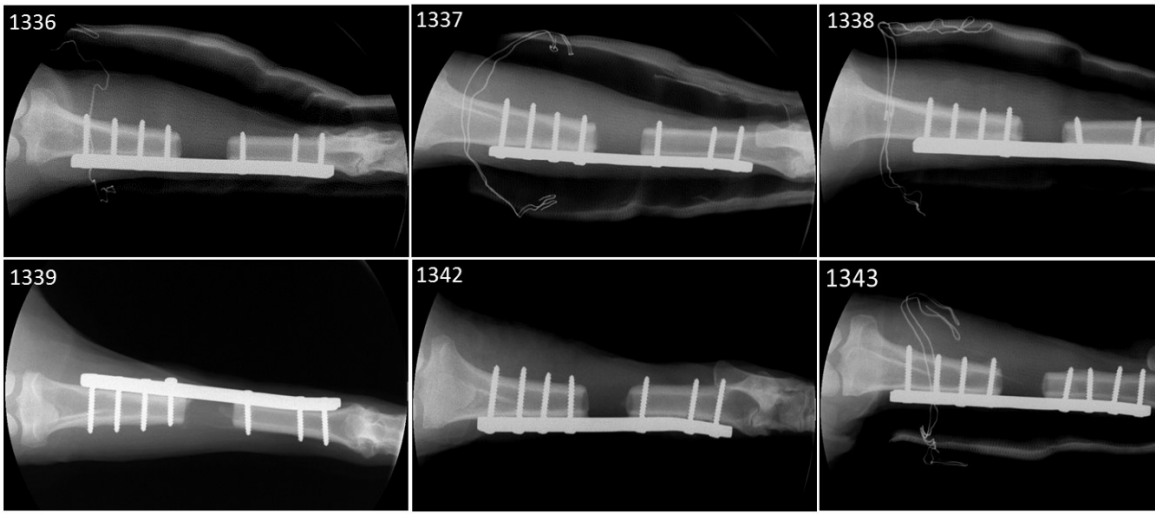

Figure 6-8 Radiographs, unseeded ECM. Radiographs were taken immediately prior to or post splint removal. Splints were removed between three and four weeks post-surgery. Cranio-caudal projections shown, n=6, all samples represented

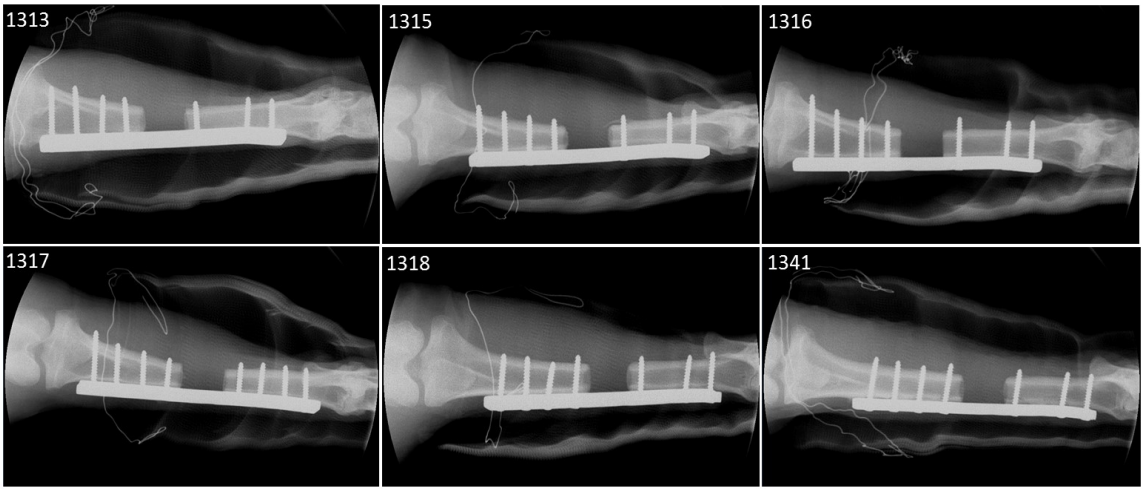

Figure 6-9 Radiographs, Stro-4 seeded ECM. Radiographs were taken immediately prior to, or post splint removal. Splints were removed between three and four weeks after surgery. Cranio-caudal projections shown, n=6, one sample is absent from image panel.

6.5.2 Micro-CT

Micro-CT analysis was performed on data from the current experiment and combined with historical control data provided by Prof Hutmacher (Reichert et al., 2010). 3-D renders were compiled for qualitative comparison and bone volume analysis performed for quantitative analysis.

The distinction between negative and positive controls was clear. The growth profile within blank samples was characterised by a low total amount of new bone and absence of bone bridging at the three-month time point. In all cases a degree of ossification was seen along the fixation plate. The total amount of bone in the area was variable but clearly distinguished from bone growth originating from the defect boundaries indicating “new bone”. Spicules of bone were also observed orientated along the line of the neurovascular bundle, unlike plate-related bone growth, although this was not always present. The degree of new bone originating from the bone medulla and cortical edges was minimal. New growth from these areas rarely projected in to the defect more than 5mm from the defect edges. In some cases, new bone was detected around the periphery of the defect, this was interpreted to be related to the PCL mesh. In no cases was any new bone present in the centre of the defect in the blank samples.

Autograft samples were clearly extremely successful evidenced by comprehensive bone bridging of the defect in all cases. There was a small variation in the diameter of the bone bridge, in only one sample the diameter of new bone was less than half of the intact cortices either side of the defect. Autograft samples also displayed large amounts of new bone around the plate - most evident on sample retrieval whereupon the plate was encased in new bone. The large volumes of new bone were readily distinguishable on micro-CT from un-operated bone by i) a change in cortical pattern internally and ii) a visually distinctive surface pattern externally.

Unseeded and seeded test samples were in most cases visually indistinguishable from empty control samples. In some cases, detailed below, there were potential indications of bone growth which did not match that observed in empty controls. These changes related to prominent bone outgrowth from the medullary canal (unrelated to intact cortices), low density irregular spiral patterned bone outgrowth from proximal and distal defect ends, and in one case, a consolidated high density bone fragment located centrally within the defect as highlighted in Figure 6-12.

6.5.2.1 Micro-CT renders, image panel 1 of 2

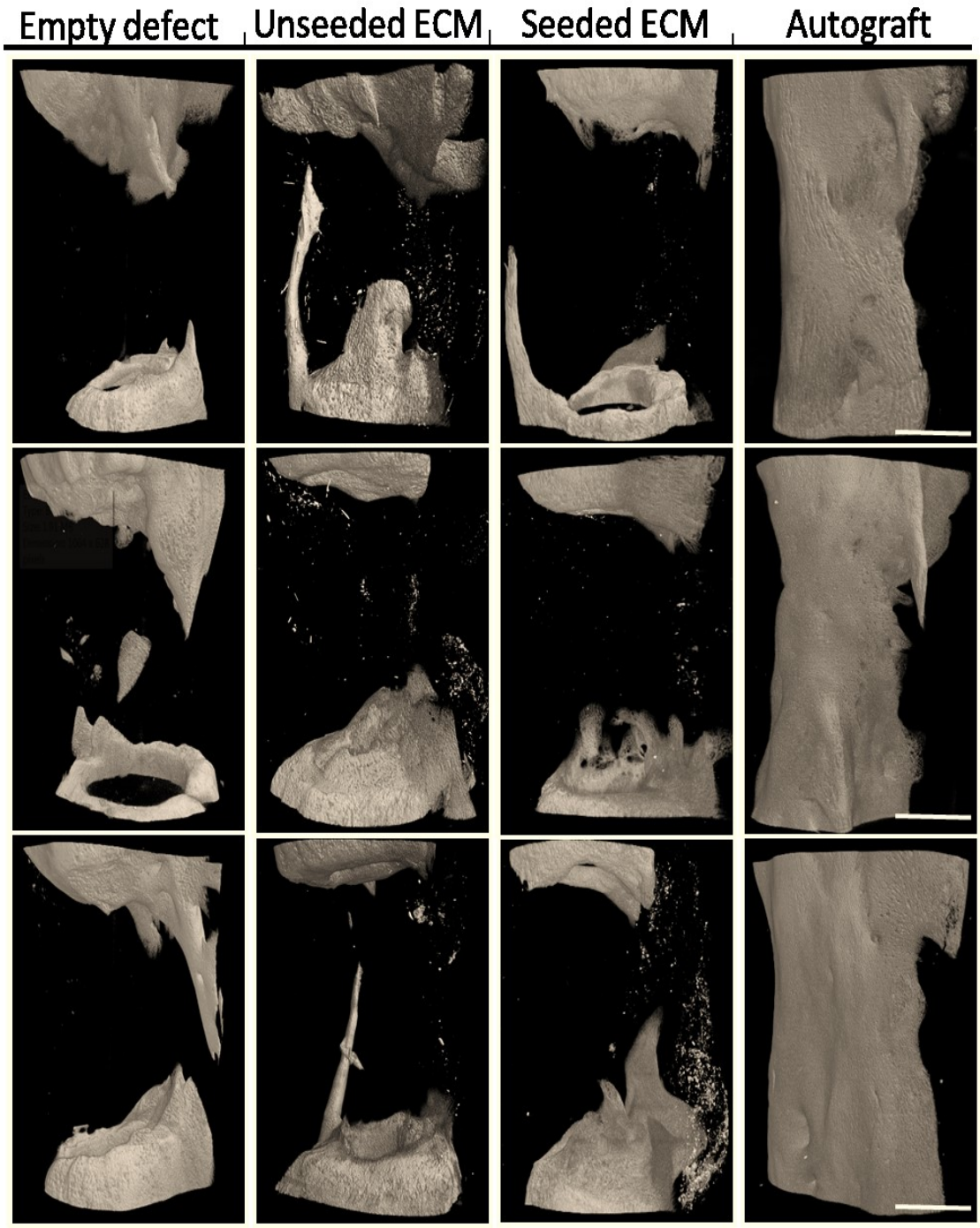

Figure 6-10 Micro-CT renders, panel 1 of 2. Images created using ctVox (Bruker). Empty defect 1-3 of 6 samples, unseeded ECM 1-3 of 6 samples, Stro-4 seeded ECM 1-3 of 6 samples and historical autograft control 1-3 of 6 samples. Scale bar = 1cm

6.5.2.2 Micro-CT renders, image panel 2 of 2

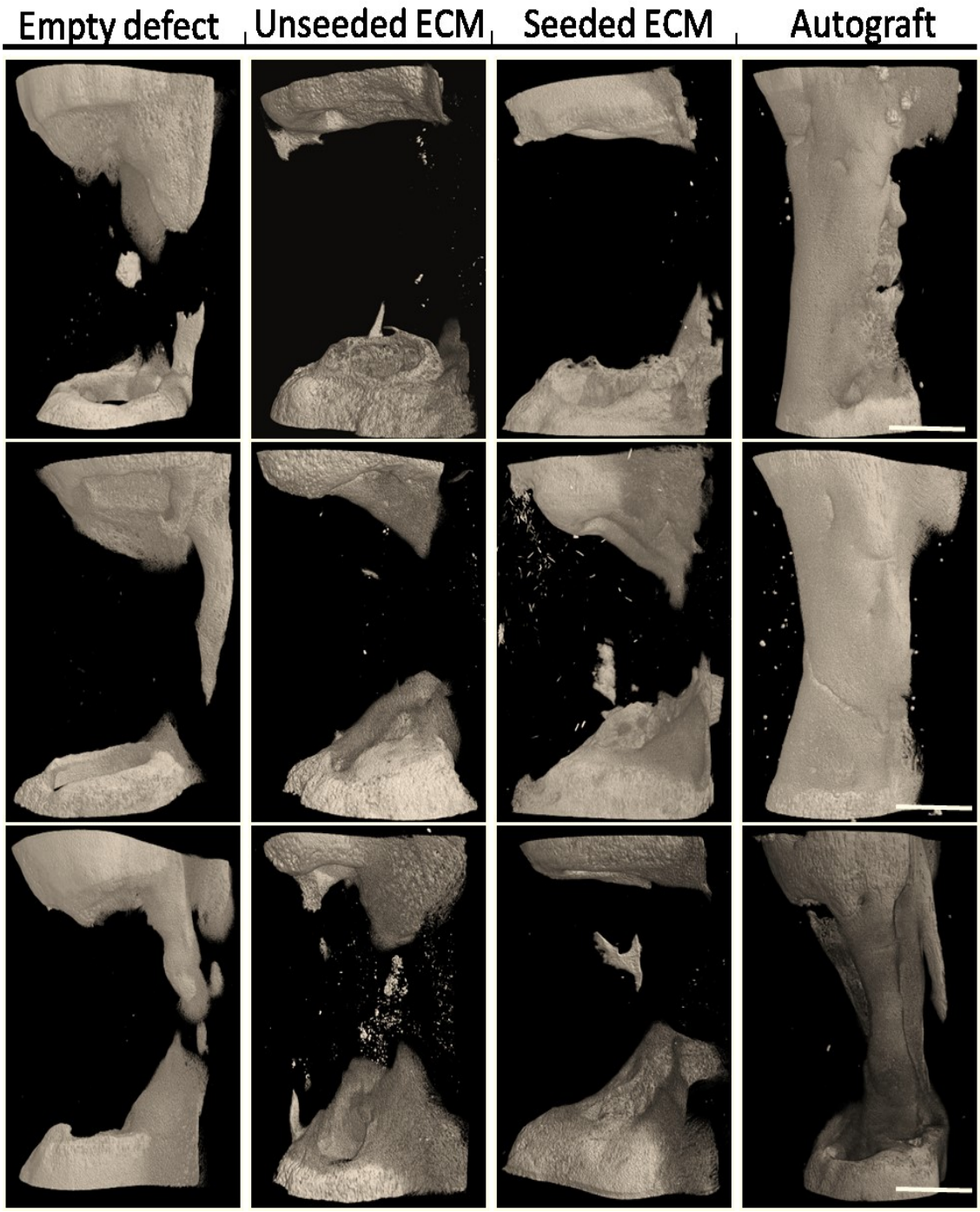

Figure 6-11 ECM PCL mesh micro-CT renders, panel 2 of 2. Images created using ctVox (Bruker). Empty defect 4-6 of 6 samples, unseeded ECM 4-6 of 6 samples, Stro-4 seeded ECM 4-6 of 6 samples and historical autograft control 4-6 of 6 samples. Scale bar = 1cm

6.5.2.3 Noteworthy patterns of new bone growth

To highlight features within experimental samples, images were selected using the highest µCT bone volumes as guidance, Figure 6-12. In all samples, there was evidence of bone growth associated with the fixation plate, (white arrows), it was advised that this pattern of growth was normal for the model based on published results (Reichert et al., 2010; Berner et al., 2013a; Cipitria et al., 2013).

In two out of six unseeded and two out of seven seeded samples, a distinct outgrowth of bone was observed as delineated in the red box in Figure 6-12. Bone growth originated centrally from the medullary canal, projecting into the defect, by contrast, new bone growth in empty defects appeared as either plate associated (white arrows) or from the cortical bone and periosteal region, but not from the central canal. A further area of bone growth was visible tracking along the neurovascular bundle (indicated by green arrows).

In two of six Stro-4 seeded samples, a small aggregate of bone was detected (yellow box). These small aggregates of bone appeared discrete and were not associated with peripheral regions of bone repair. Although not visible in a 2D image, the highlighted bone area was located centrally within the substance of the defect, at a point furthest away from the defect edges proximally and distally and axially through the axis of the defect.

In all cases, autograft produced bridging bone union across defect edges. In five out of six autograft defects the diameter of new formed bone was continuous with healthy bone. Autograft produced impressive healing at a three-month time point, Figure 6-12, D.

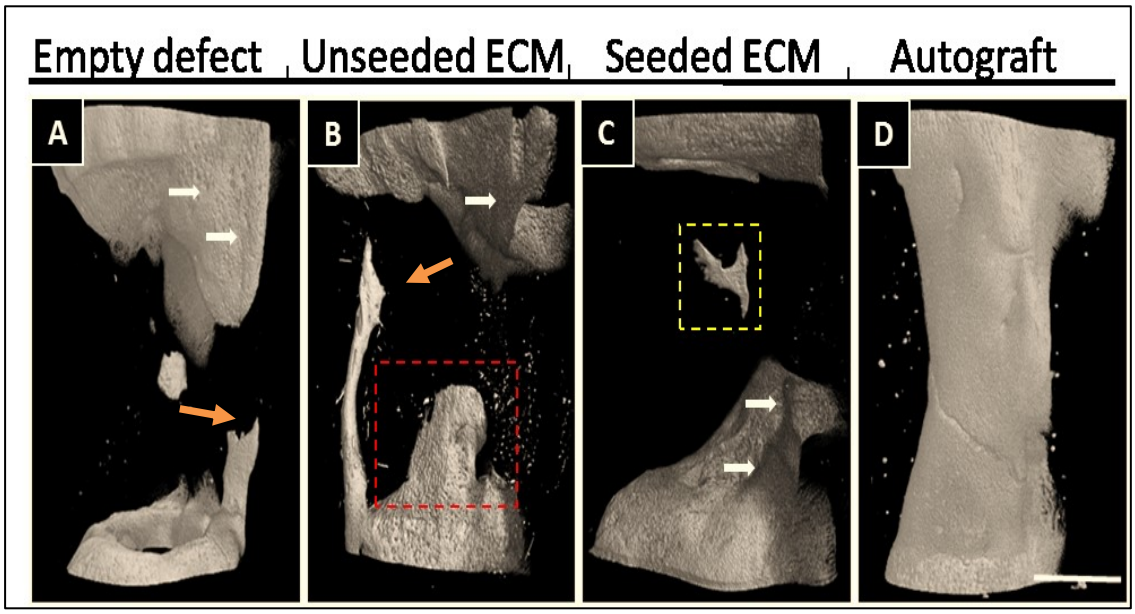

Figure 6-12 High-resolution images tibial segmental defect.

Images of the highest bone volume from each experimental group A) Empty defect. B) Unseeded ECM, region of new bone outgrowth originating from the distal medullary canal (red box). C) Stro-4 seeded ECM, new bone formation centrally within the defect (yellow box), unrelated to defect periphery or fixation plate. D) Autograft. White arrows indicate bone growth associated with fixation implant, orientated uniformly on the cranio-medial aspect of the tibia. Bone growth along the neurovascular bundle was present in many samples across all groups, orange arrow. Scale bar = 1cm

6.5.2.4 Bone volume analysis

Bone volume was calculated using Bruker Skyscan® ctAn software. Total bone volume was assessed using global threshold values of 85-255. Autograft samples contained significantly more bone, (4250.63 mm^3, SD = 1485.57) than blank (1045.29 mm^3, SD = 219.68) unseeded (1152.58 mm^3, SD = 191.95) and Stro-4 seeded ECM (1127.95 mm^3, SD = 166.44) groups, Figure 6-13. There was no significant difference in the volume of bone measured in blank, unseeded and seeded ECM groups.

A total of 6ml of autograft material was applied at the time of surgery. Autograft is a hydrated material which contains cellular, bone and connective tissue elements. Bone volumes in the autograft group varied between 2502mm^3 and 7466mm^3, the variation between autograft samples was attributed to the degree of bone remodelling and stage of healing.

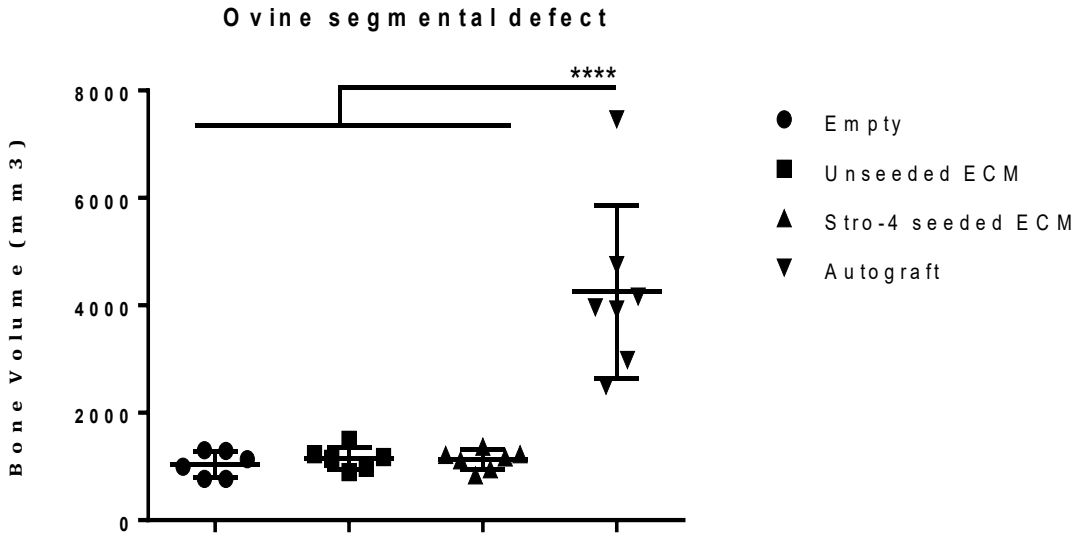

Figure 6-13 Ovine segmental defect, total bone volume. A statically significant difference in bone volume was observed between autograft (n=7) and blank (n=6), unseeded ECM (n=6) and Stro-4 seeded ECM (n=7). There were no significant differences amongst other groups.

6.5.2.5 New bone growth distribution through defect

Bone volume was analysed according the region with the defect. The total defect was sub-divided into proximal, middle and distal portions. This was undertaken to investigate whether a gravitational effect or displacement of hydrogel had occurred and if so, whether the effect translated into a variation in the location of new bone within the defect.

In all groups, the largest proportion of bone was located in the proximal segment. In seeded and unseeded groups, bone volume in the proximal segment was significantly larger than middle and distal portions. The proximal region of autograft samples was significantly great than middle sections only. A distinct feature of bone distribution in blank, unseeded and seeded groups was the near complete absence of bone measured in the middle portions. In the Blank samples, there were no differences between the three sub-regions, Figure 6-14.

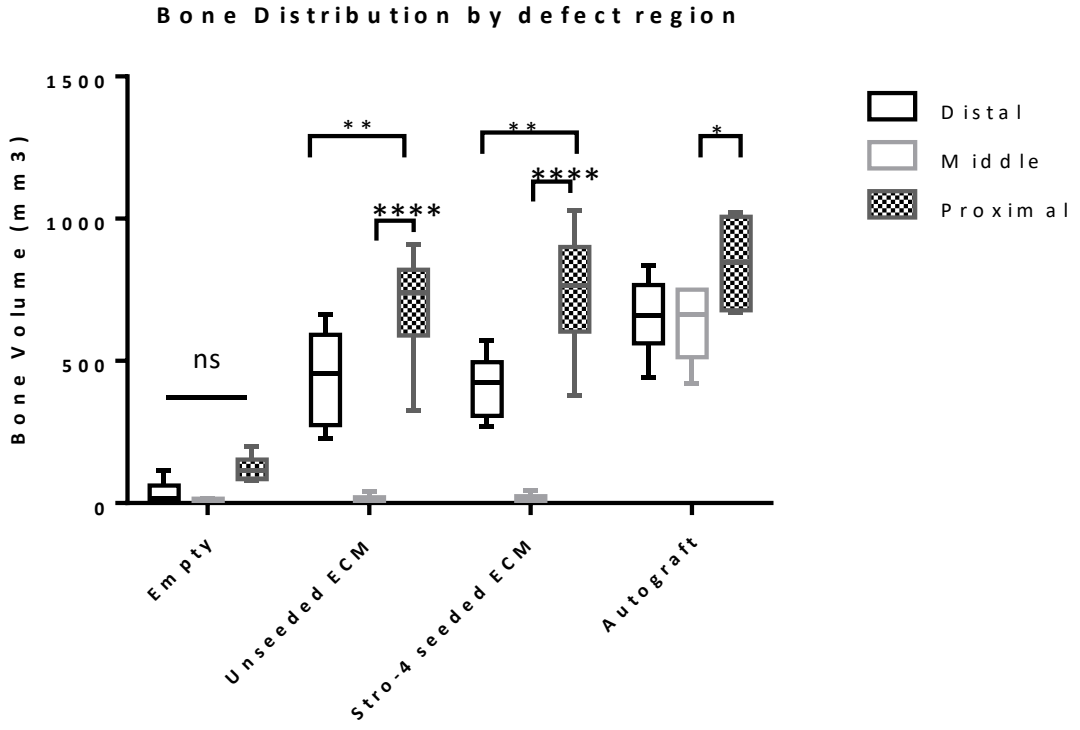

Figure 6-14 Bone distribution through tibial segmental defect. The distribution of new bone within the defect was examined. Defects were divided into "proximal", "middle" and "distal" regions. Blank n=6 per region, Unseeded n=6 per region, Stro-4 seeded n= 7 per region, autograft n=7 per region.

6.5.3 Histology

One sample from unseeded and seeded ECM groups were embedded and processed for resin embedding and immunohistochemistry by QUT

Unseeded ECM, sample ID 1338.

Goldner's Trichrome, Figure 6-15 E*,* staining was successfully performed on resin embedded, mounted and ground sections. The proximal and distal tibial segments of innate bone show strong blue/green osteoid staining. A small amount of open structured osteoid is visible sprouting from the bony defect edges. The centre of the defect appears devoid of nucleated tissue and an empty void was seen on section after processing. The central void was surrounded by a loose network of connective tissue staining orange-red. The region of fibrous tissue appears poorly cellularised, with randomly deposited matrix containing pockets of adipose like tissue.

Haematoxylin and Eosin, Figure 6-15 F, shows a pattern of poorly aligned low-cellularity tissue consistent with the amorphous fibrous description seen with Goldner's Trichrome. Proximal and distal segments demonstrated highly cellular marrow cavity components and orientated matrix which co-localised with innate bone.

Seeded ECM, sample ID 1320

Goldner's Trichrome, Figure 6-15*,* G*.* As in 1338 above, the presence of mineralised bone on the proximal and distal defect boundaries was observed. The defect substance was characterised by dense bundles of red/orange staining collagen fibres and cytoplasm. The fibre distribution was amorphous and disorganised and, as in 1338, contained a small amount of adipose like material. The fibre density in the seeded group was greater than that in the unseeded with a majority of the defect substance intensely staining, with only small areas lacking evidence of collagen.

Haematoxylin and Eosin, Figure 6-15*,* H*.* Findings on H and E were similar in morphology to the unseeded sample. The defect substance was characterised by a wash of non-distinct pink/purple eosinophilic material, with a low level of nuclear basophilic material. There are central areas lacking staining which may represent regions of dissolved lipids. Overall, the histological result description could be considered consistent with fibrous non-union.

Immunohistochemistry, Figure 6-16*.* IHC was available for 1320 only. VEGF expression was predominately limited to the boundary between host bone and defect, proximal and distal to the ostectomy site, faint staining was observed at the defect periphery associated with plate-related bone growth. *ALP* expression corresponded with BMP-2 and BMP-4.

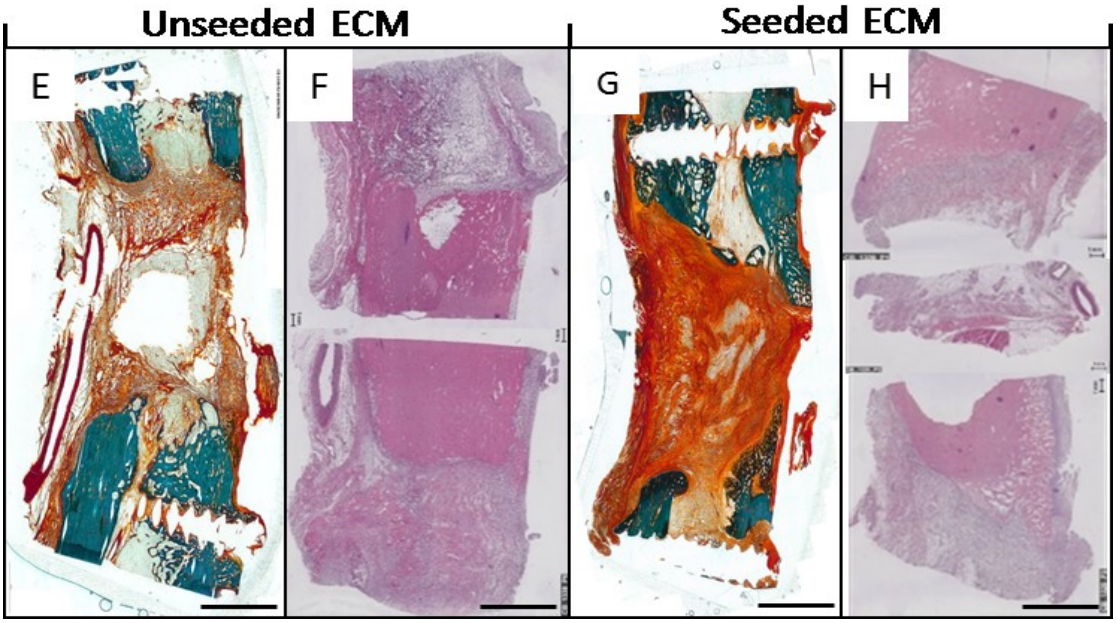

Figure 6-15 Histology ECM hydrogel PCL mesh. Unseeded ECM, Goldner's Trichrome (E), Haematoxylin and Eosin (F). Stro-4 seeded ECM, Goldner's Trichrome (G), Haematoxylin and Eosin (H). Goldner's Trichrome sections processed by resin embedding. H&E sections processed through decalcification and paraffin embedding. Scale bar 1 cm.

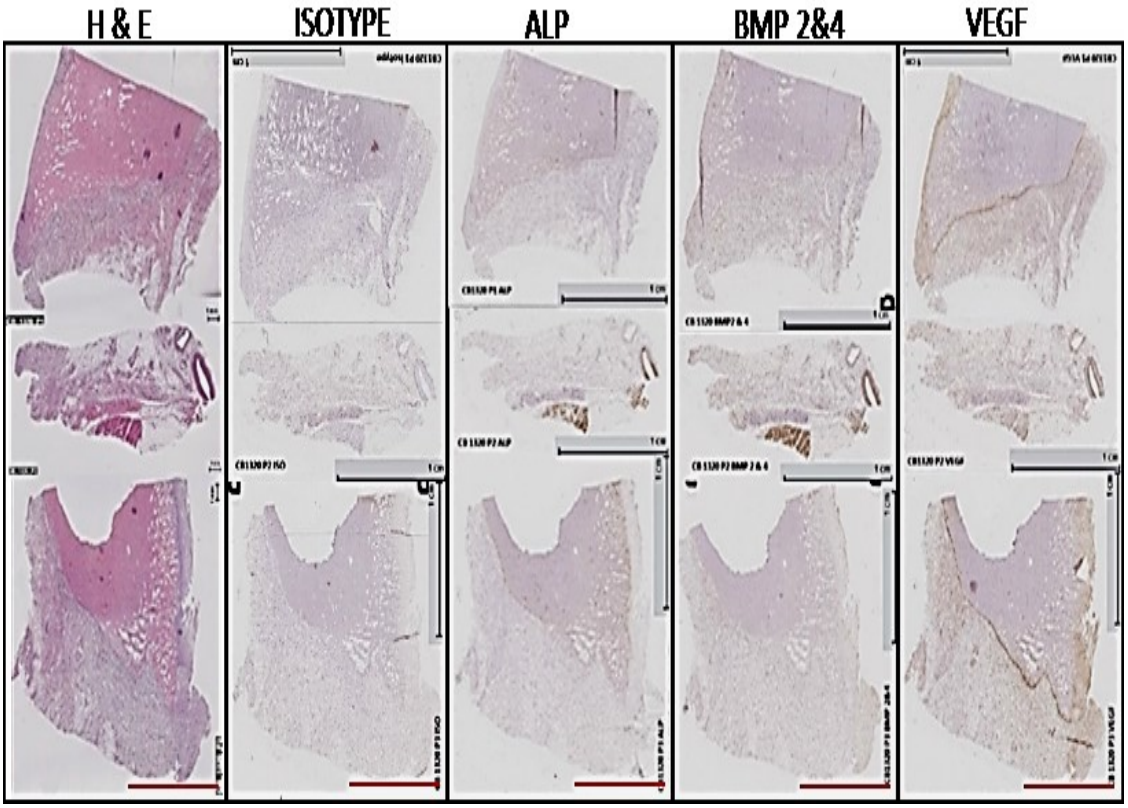

Figure 6-16 Immunohistochemistry sample 1320, Seeded ECM. IHC sections from sample 1320 only. Isotype control confirmed absence of non-specific antibody binding. ALP, A small area of ALP positive tissue was observed in the middle defect portion, this same tissue area showed positive staining for BMP-2 and 4. VEGF expression was limited to the boundary along innate bone tissue and was not observed in the defect tissue substance. Scale bar = 1cm

6.6 Discussion

6.6.1 Overview

The use of large animal models in pre-clinical translation continues to present a necessary yet challenging step in the development of novel therapeutics. All surgeries were completed and all experimental animals recovered from surgery. Despite the reproducibility of the model and the expertise provided by the host facility (over 200 animals in 5 years), three animals were excluded from the study as a consequence of defect related complications.

The production of bovine extracellular matrix hydrogel was previous limited to 10-20ml per batch, the, digestion and subsequent neutralisation appeared homogenous and reliably cross-linked as the temperature of the gel was increased to 37°C. For the present study, 400ml of hydrogel was required,an unexpected complication of producing larger volumes of ECM was the uneven distribution of pH measured by pH meter. As the NaOH and PBS buffer solution was added and the solution stirred, pH neutral pockets of crosslinking gel formed, even when maintained at 4°C, by contrast areas which did not cross-link demonstrated acid pH that was hard to distribute. This led to the formation of a bi-phasic “gelled” portion and acidic pockets of aqueous solution occurred in areas of the defect samples. When applied the aqueous phase was not retained by the PCL mesh and a reduced portion of hydrogel was retained. This phenomenon had been encountered by the collaborator, Dr White (University of Nottingham) and, to date, remains unresolved when producing higher volumes of bovine ECM hydrogel.

The role of the PCL mesh was to localise the ECM hydrogel. Melt Electrospun Micro-fibre PCL mesh has been produced, characterised *in vitro* and used successfully *in vivo* as previously published (Kolambkar et al., 2010; Brown et al., 2012; Zaiss et al., 2016). Previous applications documented the successful use of a PCL mesh to improve the localisation of incorporated autograft and platelet rich plasma in combination with BMP-7 (Berner et al., 2012). The same melt electrospinning technology was also used to produce scaffolds which localised a cross-linked alginate hydrogel containing BMP-2 (Kolambkar et al., 2011b). Mesh alginate constructs and mesh with increased pore size, produced complete bone bridging at four weeks with results indistinguishable from autograft at twelve weeks.

Findings using the CAM model indicate the capacity of bECM seeded with Stro-4 SSCs to result in new bone formation. On application of the PCL mesh constructs the mesh integrity was variable and in some cases whole sections of the mesh were friable and pulled apart on application. Unfortunately, no additional PCL mesh, which took 72 hours to prepare, was available and it was not possible to resolve this shortcoming within the study time frame. Furthermore, application of the hydrogel into the defect lumen was not satisfactory, with a variable amount of ECM material visibly escaping out of the defect upon injection. This observation held true to a degree for all samples and the degraded mesh structure was unable to reliably localise the ECM hydrogel within the defect which may have reduced the efficacy of ECM to stimulate new bone formation.

6.6.2 ECM incorporation and immunogenicity.

A potential explanation for the failed ability of the ECM hydrogel to stimulate an osteogenic effect could relate to the xenogenic nature of the matrix material. It was hypothesised that an acute inflammatory response was stimulated initiating the release of pro-inflammatory cytokines such as IL-1, IL-2 and TNFα against the collagenous and non-collagenous ECM gel components. Such an overwhelming inflammatory milieu would have reduced any pro-osteogenic signalling derived from matrix bound growth factors such as the TGF-β and BMP-2. The presence of a fibrous cellular capsule surrounding the cell-seeded and unseeded groups would support the pro inflammatory explanation of failed osteogenesis by bovine ECM. The use of bovine xenograft in human clinical applications has been extensively documented (Laurencin et al., 2006) with products available in various preparations including; ceramic (Bio-Oss®, Geistlich Biomaterials, Inc), allograft-ceramic combinations (EndoBon®, Merck, Inc) and as a collagen sponge and growth factor combination (Infuse®, Medtronic, Inc). Furthermore, the use of cancellous bovine xenograft has been reported clinically in tibial fracture repair (Bansal et al., 2009), maxillofacial reconstruction (Sartori et al., 2003) and reconstructive foot surgery (Shibuya et al., 2012). Although widely used and with reported improved efficacy over other common bone graft substitutes experimentally (Athanasiou et al., 2010), the efficacy and suitability of xenograft in orthopaedics remains contentious (Oryan et al., 2014).

A review of ECM xenograft materials failed to identify a reliable description of the human immune response to xenogenic ECM grafts (Badylak, 2004). Indeed as evidenced by the number of approved products of bovine and porcine origin, xenogenic ECM products were regarded as safe for clinical use, with significant discussion relating to product efficacy (Badylak, 2004; Badylak and Gilbert, 2008). A Small animal *in vivo* study indicated that although an immune response was evident in the presence of porcine decellularised ECM graft.

The response was t-cell type 2 dominated and may have actively encouraged host cell infiltration and graft remodelling (Allman et al., 2001). Although these findings are encouraging in defence of the use of xenogenic bovine ECM hydrogel, comprehensive data regarding the innate and acquired immune response to ECM products of xenogenic origin is required before conclusions can be drawn regarding efficacy and applicability the xenogenic material. Based on the widespread use of xenogenic ECM graft material in human clinics and the widespread documentation of xenogenic ECM material used experimentally, a catastrophic immune response would appear a less likely reason for the failure for new bone formation recorded.

As previously detailed in Chapter III, positive bone growth was observed in the CAM-femur studies. Importantly, when examining a xenograft related immunogenic response in an ovine model, work by Katz et al. (Katz et al., 2009) showed comparable osteogenesis between a decellularised xenograft and allograft.

The Immunogenicity of connective tissue grafts has been linked to the cellular component of the graft tissues. Critically, decellularisation and delivery of an acellular graft material mitigate the immune response of the host to donor material (Oryan et al., 2014). Immune responses to polymer and co-polymer hydrogels has been documented and optimised by modifications in the hydrogel surface structure (Sawhney and Hubbell, 1992). Interestingly, the use of hydrogels as a cell delivery vehicle has been implicated in generating an enhanced immune response. This was primarily linked to the adsorption of cell proteins and presentation to host immunocytes (Hugh Auchincloss and Sachs, 1998). In the current experiments, there was no significant new bone formation in either the cell seeded or unseeded groups indicating that there was no added benefit from using culture expanded SSCs.

6.6.3 Limitations

ECM: Based on guiding literature, it would seem unlikely that an immune response related to either the xenogeneic origin of ECM material or the delivered cell type was the primary issue in the lack of bone formation observed. Discussion remains about the *in vivo* bioavailability of ECM bond growth factors and whether these proteins are available from the ECM when produced in higher volumes, *in vitro* ELISA assays and protein characterisation techniques such as mass spectrometry characterising the protein component of reconstituted ECM would seem prudent.

Immune response: Further immunohistochemical evaluation of the immunocyte make up of inflammatory cells would prove valuable. The monocyte/macrophage response is an integral part of the host immune system in prevention of infection and the removal of waste cellular and molecular debris.

Macrophages are also important to how biomaterials incorporate with host tissue and they been shown to be present in response to many biomaterials including collagen containing scaffolds such as ECM hydrogels (Khouw et al., 1998) with both macrophages and multinucleate giant cells observed at the tissue-material interface (Brodbeck et al., 2002). The composition and polarisation of M1 and M2 macrophages in response to biomaterial implantation correlates to the degree of biomaterial integration and tissue regeneration (Boersema et al., 2016).

Profiling of the presence of macrophages in the defect/biomaterial area would advise whether an immunotolerated remodelling was prevalent or whether the implant elicited a pro-inflammatory reaction. Using the pan-macrophage marker CD63 and comparing M1 pro-inflammatory macrophages using CD80 to immunomodulatory CD163 positive M2 phenotype (Badylak et al., 2008), it would be possible to discern the macrophage compliment and characterise the type of immune response. This data would significantly aid discussion regarding the reasons for therapeutic insufficiency.

Cells: Stro-4 selected cells were isolated from matched patients and expanded to large numbers over 2 passages, *in vitro* work shown in Chapter III demonstrated osteogenic and chondrogenic potential in this cell population up to passage 5. What is not known is whether the effect if such large-scale expansion impacted the potential of Stro-4 cells and subsequent growth *in vivo*. *In vitro* differentiation, histology and molecular analysis of a representative portion of the cell population would have provided useful information in this regard. The survival of ovine Stro-4 within bulk Bovine ECM has been demonstrated by collaborators but again, it was not known whether the ECM used in this study, due to its large-scale production, possessed the same cytocompatibility as it had at our collaborators. Due to staffing and time restrictions, it was not possible to carry out these important *in vitro* tests.

PCL Mesh: In this experiment, ECM hydrogel failed to live up to its promise in large scale bone tissue engineering and it was unfortunate that steps to optimise the *in vivo* application of a bovine ECM hydrogel were identified post-experiment. Standardisation of PCL manufacturing, possibly with a higher number of layers and lower overall pore size, combined with a shorter etching period could improve the volume of ECM localised into the defect region. Regarding gel properties, it would be beneficial to combine ECM with another carrier hydrogel to improve its mechanical and gelation characteristics.

The BJRGP has expertise in the development of nanosilicate hydrogels which have highly adaptable mechanical properties and an ability to control protein adsorption and release (Dawson et al., 2011). By combining an ECM digest with a nanosilicate preparation, it may be possible to enhance gel viscosity, improving localisation during *in vivo* application and simultaneously extending the release of pro-osteogenic proteins. This work will need to progress from *in vitro* characterisation and demonstrate efficacy using small animal models before being introduced in a large model.

6.7 Conclusions

This study has demonstrated the successful isolation, selection and *in vitro* expansion of autologous ovine Skeletal Stem Cells and enrichment of the stem cell niche through the use of Stro-4 IgG antibody. The skeletal cells were culture expanded in numbers sufficient for use in large scale tissue engineering and incorporated into a bovine ECM hydrogel for use in a tibial segmental defect. A 3cm tibial defect was created and stabilised in sixteen experimental animals, all animals recovered from surgery although three were lost to implant failure. Two experimental groups comparing unseeded ECM with Stro-4 seeded were implemented.

There was no demonstrable advantageous bone formation in either of the ECM groups and the application of a seeded hydrogel was not superior to unseeded gel when examined by microCT or histological techniques. It was therefore not possible to reject the null hypothesise that the application of bovine bone derived extracellular matrix hydrogel, either alone or supplemented with an enriched stem population, does not enhance the repair of a 3cm ovine tibial segmental defect.

7 General conclusions and future directions

7.1 Chapter III- *In vitro* characterisation and *in vivo* functional assessment of a Stro-4 enriched ovine Skeletal Stem Cell populations

Characterisation of the enriched SSC stem cell sub-population has enabled the BJRG to move forward with prospective isolation and differentiation protocols utilising this cell type, it has enabled the prospective isolation of a cell population with considerable innate chondrogenic capacity and osteogenic potential, demonstrated *in vitro* and *in vivo*. The *in vitro* growth and differentiation characteristics are supported by published work from the providers of Stro-4 antibody and aid validation of work in this chapter.

The convincing chondrogenic preference of Stro-4 selected cells have already led to further work in the BJRG, investigating to chondrogenic potential of human BMMNCs selected for by Stro-4, and although this work is in its preliminary stages, the opportunity to isolate prospectively autologous cells with one marker type has practical implications in both research and clinical disciplines.

The rapid population doubling times and capacity to differentiate into osteogenic and chondrogenic lineages have identified the ovine Stro-4 population as exciting cell targets in BTE.

The functional *in vivo* testing of Stro-4 alongside the newly developed ECM hydrogel-mesh construct system demonstrated further promise. Sample numbers were limited by material production and availability but a clear endochondral effect was demonstrated in the production of complete bony bridging across the defect site in Stro-4 containing samples. This material-cell combination was identified as a promising therapy suitable for scaling up into a large animal defect model, as described in Chapter VI.

7.2 Chapter IV- Development of an ovine condyle defect model for pre-clinical research in bone tissue engineering-

The development of the ovine condyle defect model was a significant undertaking drawing together expertise across disciplines and faculties. It is now possible for the BJRG to host this experimental model routinely and have developed surgical and analytical techniques to obtain clinically relevant data.

All Home Office requirements were met and the BJRG may now implement the ovine condyle defect model as described as an ongoing activity, provided all ethical and regulatory standards continue to be met.

The model was validated through high-resolution µCT imaging, what has not been available and is required as the scope of the model and capacity with the BJRG, is capacity for histology mechanical data to match the high quality µCT. These concerns are being addressed and it is intended that both current and future studies will benefit.

Once validated the model was then employed to assess a promising nano-silicate growth factor delivery system as further step towards potential clinical translation.

7.3 Chapter V- Controlled delivery of a commercial Bone Morphogenic Protein-2 product "InductOS®" by a Laponite gel carrier

The validated ovine condyle defect model was implemented on a further 24 animals achieving a 96% end-of-study survival rate. We sought to deliver an effective dose of BMP-2 in combination with an Absorbable Collagen Sponge carrier at one tenth of the manufacturers' protocol dose.

The results were interesting if mixed, both the commercial Medtronic InductOS® collagen sponge and Laponite delivered BMP-2 with collagen sponge formed statistically significant new bone over negative controls. When BMP-2 was applied to the defect in Laponite alone, without the collagen sponge, no significance was found, although samples in the Laponite BMP-2 only group did demonstrate bone volume values comparable with highest recorded values in autograft groups.

Although limited by as-yet undetermined causes of high inter sample variation, Laponite was demonstrated as an effective growth factor delivery vehicle but further work is required to determine the most effective mode of application, understand the *in vivo* physiological interactions between patient and material and reliably identify the causes of such large inter-sample variation. Although not conclusive, this study substantiates the claim that Laponite has the potential application as a vehicle for bioactive molecule delivery, as a sole agent or in combinations with composite solutions.

7.4 Chapter VI- Evaluation of Bovine ECM hydrogel and Stro-4 selected skeletal stem cells in a critical sized ovine tibial segmental defect

The ovine tibial segmental defect model is currently the most physiologically and one of the most technically challenging bone defect models available to researcher; hosting facilities, veterinary care required, the volume of bone removed combined with removal of surrounding periosteum and the loss of collateral vascular supply are all contributing factors.

Use of this model allowed us to examine whether it was possible to isolate and expand sufficient Skeletal Stem Cells using Stro-4 selection to re-implant in a model of sufficient size as to represent a clinical application. After promising results *in vitro* and in a small animal model *in vivo* we examined the efficacy of Stro-4 seeded Bovine ECM hydrogel in the tibial model.

Stro-4 cells were successfully isolated and expanded *in vivo* for re-implantation at high cell density.

Bovine ECM hydrogel was produced in applied successfully *in vivo* both seeded and unseeded by patient matched Stro-4 selected SSCs. Rather disappointingly bECM hydrogel, seeded and unseeded, failed to produce any significant bone after 3 months. Stro-4 and Bovine ECM remains of interest as many reasons for this failure were identified and are discuss in Chapter VI.

Future work aims to combine the desirable physical and protein binding properties demonstrated by Laponite with the scaffold and growth factor content of human ECM. It is intended that Laponite will help localise the human ECM and enhance the effects of innate growth factors and other pro-osteogenic molecules.

Publications linked to this work:

Black CR, Goriainov V, Gibbs D, Kanczler J, Tare RS and Oreffo ROC (2015) Bone Tissue Engineering. MOLECULAR BIOLOGY OF SKELETAL TISSUE ENGINEERING (DW HUTMACHER, SECTION EDITOR). Curr Mol Bio Rep (2015) 1:132–140

Vaezi M, Black C, Gibbs DM, Oreffo RO, Brady M, Moshrefi-Torbati M, Yang S. Characterization of New PEEK/HA Composites with 3D HA Network Fabricated by Extrusion Freeforming. Molecules. 2016 May 26;21(6). pii: E687. doi: 10.3390/molecules21060687.PMID: 27240326 Free Article

Gibbs DM, Black CR, Hulsart-Billstrom G, Shi P, Scarpa E, Oreffo RO, Dawson JI. Bone induction at physiological doses of BMP through localization by clay nanoparticle gels. Biomaterials. 2016 Aug;99:16-23. doi: 10.1016/j.biomaterials.2016.05.010.PMID: 27209259

Gothard D, Smith EL, Kanczler JM, Black CR, Wells JA, Roberts CA, White LJ, Qutachi O, Peto H, Rashidi H, Rojo L, Stevens MM, El Haj AJ, Rose FR, Shakesheff KM, Oreffo RO. *In vivo* Assessment of Bone Regeneration in Alginate/Bone ECM Hydrogels with Incorporated Skeletal Stem Cells and Single Growth Factors. PLoS One. 2015 Dec 16;10(12):e0145080. doi: 10.1371/journal.pone.0145080. PMID: 26675008 Free PMC Article

Lindahl MAB, Gibbs DM, Dawson JI, Kanczler J, Black CRM, Tare RS, Oreffo RO. Cartilage and bone regeneration. 2015.

Gibbs DM, Black CR, Dawson JI, Oreffo RO. A review of hydrogel use in fracture healing and bone regeneration. J Tissue Eng Regen Med. 2016 Mar;10(3):187-98. doi: 10.1002/term.1968. Review.

West CC, Hardy WR, Murray IR, James AW, Corselli M, Pang S, Black C, Lobo SE, Sukhija K, Liang P, Hay DC, March KL, Ting K, Soo C, Peault B. Prospective purification of perivascular presumptive mesenchymal stem cells from human adipose tissue: process optimisation and cell population metrics across a large cohort of diverse demographics. Stem Cell Research and Therapy. 2016 doi: 10.1186/s13287-016-0302-7

8 References

OECD Health at A Glance 2015. OECD Indicators.

Aaron JE. 2012. Periosteal Sharpey's fibers: a novel bone matrix regulatory system? Frontiers in Endocrinology 3:98.

Aerssens J, Boonen S, Lowet G, Dequeker J. 1998. Interspecies differences in bone composition, density, and quality: potential implications for *in vivo* bone research. Endocrinology 139.

Alajati A, Laib AM, Weber H, Boos AM, Bartol A, Ikenberg K, Korff T, Zentgraf H, Obodozie C, Graeser R, Christian S, Finkenzeller G, Stark GB, Heroult M, Augustin HG. 2008. Spheroid-based engineering of a human vasculature in mice. Nat Meth 5:439-445.

Albrektsson T, Johansson C. 2001. Osteoinduction, osteoconduction and osseointegration. Eur Spine J 10.

Alford AI, Kozloff KM, Hankenson KD. 2015. Extracellular matrix networks in bone remodeling. The International Journal of Biochemistry & Cell Biology 65:20-31.

Allman AJ, McPherson TB, Badylak SF, Merrill LC, Kallakury B, Sheehan C, Raeder RH, Metzger DW. 2001. Xenogeneic extracellular matrix grafts elicit a TH2-restricted immune response. Transplantation 71.

Alzahrani MM, Anam EA, Makhdom AM, Villemure I, Hamdy RC. 2014. The Effect of Altering the Mechanical Loading Environment on the Expression of Bone Regenerating Molecules in Cases of Distraction Osteogenesis. Frontiers in Endocrinology 5:214.

Amado LC, Saliaris AP, Schuleri KH, St. John M, Xie J-S, Cattaneo S, Durand DJ, Fitton T, Kuang JQ, Stewart G, Lehrke S, Baumgartner WW, Martin BJ, Heldman AW, Hare JM. 2005. Cardiac repair with intramyocardial injection of allogeneic mesenchymal stem cells after myocardial infarction. Proc Natl Acad Sci U S A 102:11474-11479.

Amanatullah DF, Williams JC, Fyhrie DP, Tamurian RM. 2014. Torsional properties of distal femoral cortical defects. Orthopedics 37:158-162.

Amorin B, Alegretti AP, Valim V, Pezzi A, Laureano AM, da Silva MAL, Wieck A, Silla L. 2014. Mesenchymal stem cell therapy and acute graft-versus-host disease: a review. Human Cell 27:137-150.

An, Friedman. 1999. Animal Selections in Orthopaedic Research.

Anderson ML, Dhert WJ, de Bruijn JD, Dalmeijer RA, Leenders H, van Blitterswijk CA, Verbout AJ. 1999. Critical size defect in the goat's os ilium. A model to evaluate bone grafts and substitutes. Clin Orthop Relat Res:231-239.

Apelt D, Theiss F, El-Warrak AO, Zlinszky K, Bettschart-Wolfisberger R, Bohner M, Matter S, Auer JA, von Rechenberg B. 2004. *In vivo* behavior of three different injectable hydraulic calcium phosphate cements. Biomaterials 25:1439-1451.

Arrington ED, Smith WJ, Chambers HG, Bucknell AL, Davino NA. 1996. Complications of Iliac Crest Bone Graft Harvesting. Clin Orthop Rel Res 329:300-309.

Aslan H, Zilberman Y, Kandel L, Liebergall M, Oskouian RJ, Gazit D, Gazit Z. 2006. Osteogenic Differentiation of Noncultured Immunoisolated Bone Marrow-Derived CD105+ Cells. STEM CELLS 24:1728-1737.

Athanasiou VT, Papachristou DJ, Panagopoulos A, Saridis A, Scopa CD, Megas P. 2010. Histological comparison of autograft, allograft-DBM, xenograft, and synthetic grafts in a trabecular bone defect: an experimental study in rabbits. Med Sci Monit 16.

Badylak SF. 2004. Xenogeneic extracellular matrix as a scaffold for tissue reconstruction. Transplant Immunology 12:367-377.

Badylak SF, Freytes DO, Gilbert TW. 2009. Extracellular matrix as a biological scaffold material: Structure and function. Acta Biomater 5:1-13.

Badylak SF, Gilbert TW. 2008. Immune response to biologic scaffold materials. Seminars in Immunology 20:109-116.

Badylak SF, Tullius R, Kokini K, Shelbourne KD, Klootwyk T, Voytik SL, Kraine MR, Simmons C. 1995. The use of xenogeneic small intestinal submucosa as a biomaterial for Achille's tendon repair in a dog model. J Biomed Mater Res 29:977-985.

Badylak SF, Valentin JE, Ravindra AK, McCabe GP, Stewart-Akers AM. 2008. Macrophage Phenotype as a Determinant of Biologic Scaffold Remodeling. Tissue Eng Part A 14:1835-1842.

Bae DS, Waters. 2006. Free Vascularized Fibula Grafting:Principles, Techniques, and Applications in Pediatric Orthopaedics. Orthopaedic Journal at Harvard Medical School.

Bai L, Lennon DP, Eaton V, Maier K, Caplan AI, Miller SD, Miller RH. 2009. Human bone marrow-derived mesenchymal stem cells induce Th2-polarized immune response and promote endogenous repair in animal models of multiple sclerosis. Glia 57.

Baker LA, Jin P, Martin CR. 2005. Biomaterials and Biotechnologies Based on Nanotube Membranes. Critical Reviews in Solid State and Materials Sciences 30:183-205.

Ballock RT, Heydemann A, Izumi T, Reddi AH. 1997. Regulation of the expression of the type-II collagen gene in periosteum-derived cells by three members of the transforming growth factor-beta superfamily. J Orthop Res 15:463-467.

Bansal MR, Bhagat SB, Shukla DD. 2009. Bovine cancellous xenograft in the treatment of tibial plateau fractures in elderly patients. Int Orthop 33:779-784.

Bari CD, Dell'Accio F, Vanlauwe J, Eyckmans J, Khan IM, Archer CW, Jones EA, McGonagle D, Mitsiadis TA, Pitzalis C, Luyten FP. 2006. Mesenchymal multipotency of adult human periosteal cells demonstrated by single-cell lineage analysis. Arthritis & Rheumatism 54:1209-1221.

Barker JN, Wagner JE. 2003. Umbilical cord blood transplantation: current practice and future innovations. Critical reviews in oncology/hematology 48:35-43.

Barry FP, Boynton RE, Haynesworth S, Murphy JM, Zaia J. 1999. The Monoclonal Antibody SH-2, Raised against Human Mesenchymal Stem Cells, Recognizes an Epitope on Endoglin (CD105). Biochemical and Biophysical Research Communications 265:134-139.

Battula VL, Treml S, Bareiss PM, Gieseke F, Roelofs H, de Zwart P, Müller I, Schewe B, Skutella T, Fibbe WE, Kanz L, Bühring H-J. 2009. Isolation of functionally distinct mesenchymal stem cell subsets using antibodies against CD56, CD271, and mesenchymal stem cell antigen-1. Haematologica 94:173-184.

Bedimo R, Maalouf NM, Zhang S, Drechsler H, Tebas P. 2012. Osteoporotic fracture risk associated with cumulative exposure to tenofovir and other antiretroviral agents. AIDS 26:825-831.

Bellahcène A, Castronovo V, Ogbureke KUE, Fisher LW, Fedarko NS. 2008. Small Integrin-Binding LIgand N-linked Glycoproteins (SIBLINGs): Multifunctional proteins in cancer. Nature reviews Cancer 8:212-226.

Bergmann G, Graichen F, Rohlmann A. 1999. Hip joint forces in sheep. Journal of Biomechanics 32:769-777.

Bergmann G, Siraky J, Rohlmann A, Koelbel R. 1984. A comparison of hip joint forces in sheep, dog and man. Journal of Biomechanics 17:907-921.

Berner A, Boerckel JD, Saifzadeh S, Steck R, Ren J, Vaquette C, Zhang JQ, Nerlich M, Guldberg RE, Hutmacher DW, Woodruff MA. 2012. Biomimetic tubular nanofiber mesh and platelet rich plasma-mediated delivery of BMP-7 for large bone defect regeneration. Cell Tissue Res 347:603-612.

Berner A, Reichert J, Woodruff MA, Saifzadeh S, Morris A, Epari D, Nerlich M, Schuetz M, Hutmacher D. 2013a. Autologous vs. allogenic mesenchymal progenitor cells for the reconstruction of critical sized segmental tibial bone defects in aged sheep. Acta Biomaterialia 9:7874-7884.

Berner A, Reichert JC, Woodruff MA, Saifzadeh S, Morris AJ, Epari DR, Nerlich M, Schuetz MA, Hutmacher DW. 2013b. Autologous vs. allogenic mesenchymal progenitor cells for the reconstruction of critical sized segmental tibial bone defects in aged sheep. Acta Biomaterialia 9:7874-7884.

Bessa PC, Casal M, Reis RL. 2008. Bone morphogenetic proteins in tissue engineering: the road from laboratory to clinic, part II (BMP delivery). J Tissue Eng Regen Med 2:81-96.

Bhakta G, Rai B, Lim ZXH, Hui JH, Stein GS, van Wijnen AJ, Nurcombe V, Prestwich GD, Cool SM. 2012. Hyaluronic acid-based hydrogels functionalized with heparin that support controlled release of bioactive BMP-2. Biomaterials 33:6113-6122.

Bianco P. 2015. Stem cells and bone: A historical perspective. Bone 70:2-9.

Bianco P, Fisher, Robey PG. 1990. Expression and Localisation of the two small proteoglycans Biglycan and Decorin in developing human skeletal and non-skeletal tissues. Journal of Histochemistry and Cytochemistry 38:1549-1563.

Black CRM, Goriainov V, Gibbs D, Kanczler J, Tare RS, Oreffo ROC. 2015. Bone Tissue Engineering. Current Molecular Biology Reports 1:132-140.

Boersema GSA, Grotenhuis N, Bayon Y, Lange JF, Bastiaansen-Jenniskens YM. 2016. The Effect of Biomaterials Used for Tissue Regeneration Purposes on Polarization of Macrophages. BioResearch Open Access 5:6-14.

Bolt P, Clerk AN, Luu HH, Kang Q, Kummer JL, Deng Z-L, Olson K, Primus F, Montag AG, He T-C, Haydon RC, Toolan BC. 2007. BMP-14 Gene Therapy Increases Tendon Tensile Strength in a Rat Model of Achilles Tendon Injury. The Journal of Bone & Joint Surgery 89:1315-1320.

Bonewald LF. 2011. The amazing osteocyte. J Bone Miner Res 26:229-238.

Bornstein P, Sage EH. 2002. Matricellular proteins: extracellular modulators of cell function. Current Opinion in Cell Biology 14:608-616.

Bosnakovski D, Mizuno M, Kim G, Takagi S, Okumura M, Fujinaga T. 2006. Chondrogenic differentiation of bovine bone marrow mesenchymal stem cells (MSCs) in different hydrogels: Influence of collagen type II extracellular matrix on MSC chondrogenesis. Biotechnology and Bioengineering 93:1152-1163.

Bouxsein ML, Turek TJ, Blake CA, D'Augusta D, Li X, Stevens M, Seeherman HJ, Wozney JM. 2001. Recombinant Human Bone Morphogenetic Protein-2 Accelerates Healing in a Rabbit Ulnar Osteotomy Model. The Journal of Bone & Joint Surgery 83:1219-1230.

Boxall SA, Jones E. 2012. Markers for Characterization of Bone Marrow Multipotential Stromal Cells. Stem Cells International 2012:12.

Braithwaite RS, Col NF, Wong JB. 2003. Estimating Hip Fracture Morbidity, Mortality and Costs. Journal of the American Geriatrics Society 51:364-370.

Brewster, Gillespie, Howie, Madabhushi, Usmani, Fairbairn. 1999. Mechanical considerations in impaction bone

grafting. Journal of bone and Joint Surgery 81-B.

Brodbeck WG, Nakayama Y, Matsuda T, Colton E, Ziats NP, Anderson JM. 2002. BIOMATERIAL SURFACE CHEMISTRY DICTATES ADHERENT MONOCYTE/MACROPHAGE CYTOKINE EXPRESSION *IN VITRO*. Cytokine 18:311-319.

Brown TD, Slotosch A, Thibaudeau L, Taubenberger A, Loessner D, Vaquette C, Dalton PD, Hutmacher DW. 2012. Design and fabrication of tubular scaffolds via direct writing in a melt electrospinning mode. Biointerphases 7:13.

Bruder SP, Jaiswal N, Haynesworth SE. 1997. Growth kinetics, self-renewal, and the osteogenic potential of purified human mesenchymal stem cells during extensive subcultivation and following cryopreservation. Journal of Cellular Biochemistry 64:278-294.

Canalis E. Effect of insulinlike growth factor I on DNA and protein synthesis in cultured rat calvaria. The Journal of Clinical Investigation 66:709-719.

Cancedda R, Giannoni P, Mastrogiacomo M. 2007. A tissue engineering approach to bone repair in large animal models and in clinical practice. Biomaterials 28:4240-4250.

Cao W, Hench LL. 1996. Bioactive materials. Ceramics International 22:493-507.

Caplan Arnold I, Correa D. 2011. The MSC: An Injury Drugstore. Cell Stem Cell 9:11-15.

Carulli C, Matassi F, Civinini R, Innocenti M. 2013. Tissue engineering applications in the management of bone loss. Clinical Cases in Mineral and Bone Metabolism 10:22-25.

Castro-Malaspina H, Gay R, Resnick G, Kapoor N, Meyers P, Chiarieri D, McKenzie S, Broxmeyer H, Moore M. 1980. Characterization of human bone marrow fibroblast colony-forming cells (CFU-F) and their progeny. Blood 56:289-301.

Cheifetz S, Weatherbee JA, Tsang MLS, Anderson JK, Mole JE, Lucas R, Massagué J. 1987. The transforming growth factor-β system, a complex pattern of cross-reactive ligands and receptors. Cell 48:409-415.

Chen L, Tredget EE, Wu PYG, Wu Y. 2008. Paracrine Factors of Mesenchymal Stem Cells Recruit Macrophages and Endothelial Lineage Cells and Enhance Wound Healing. PLoS ONE 3:e1886.

Chen P-M, Yen M-L, Liu K-J, Sytwu H-K, Yen B-L. 2011. Immunomodulatory properties of human adult and fetal multipotent mesenchymal stem cells. Journal of Biomedical Science 18:1-11.

Cheng H, Jiang W, Phillips FM, Haydon RC, Peng Y, Zhou L, Luu HH, An N, Breyer B, Vanichakarn P, Szatkowski JP, Park JY, He T-C. 2003. Osteogenic Activity of the Fourteen Types of Human Bone Morphogenetic Proteins (BMPs). The Journal of Bone & Joint Surgery 85:1544-1552.

Cheung AM, Adachi JD, Hanley DA, Kendler DL, Davison KS, Josse R, Brown JP, Ste-Marie L-G, Kremer R, Erlandson MC, Dian L, Burghardt AJ, Boyd SK. 2013. High-Resolution Peripheral Quantitative Computed Tomography for the Assessment of Bone Strength and Structure: A Review by the Canadian Bone Strength Working Group. Current Osteoporosis Reports 11:136-146.

Chia HN, Wu BM. 2015. Recent advances in 3D printing of biomaterials. Journal of Biological Engineering 9:4.

Chichester CO, Fernández M, Minguell JJ. 1993. Extracellular Matrix Gene Expression by Human Bone Marrow Stroma and by Marrow Fibroblasts. Cell Communication & Adhesion 1:93-99.

Cho T-J, Gerstenfeld LC, Einhorn TA. 2002. Differential Temporal Expression of Members of the Transforming Growth Factor β Superfamily During Murine Fracture Healing. J Bone Miner Res 17:513-520.

Choe H, Inaba Y, Kobayashi N, Miyamae Y, Ike H, Saito T. 2015. Clinical utility of antibiotic-loaded hydroxyapatite block for treatment of intractable periprosthetic joint infection and septic arthritis of the hip. Modern Rheumatology 25:937-942.

Choi WH, Kim HR, Lee SJ, Jeong N, Park SR, Choi BH, Min B-H. 2016. Fetal Cartilage-Derived Cells Have Stem Cell Properties and Are a Highly Potent Cell Source for Cartilage Regeneration. Cell Transplantation 25:449-461.

Cipitria A, Reichert JC, Epari DR, Saifzadeh S, Berner A, Schell H, Mehta M, Schuetz MA, Duda GN, Hutmacher DW. 2013. Polycaprolactone scaffold and reduced rhBMP-7 dose for the regeneration of critical-sized defects in sheep tibiae. Biomaterials 34:9960-9968.

Coelho MJ, Fernandes MH. 2000. Human bone cell cultures in biocompatibility testing. Part II: effect of ascorbic acid, beta-glycerophosphate and dexamethasone on osteoblastic differentiation. Biomaterials 21:1095-1102.

Colón-Emeric CS, Saag KG. 2006. Osteoporotic fractures in older adults. Best practice & research Clinical rheumatology 20:695-706.

Committee AiS. 1986. Animals (Scientific Procedures) Act 1986.

Court-Brown CM, Caesar B. 2006. Epidemiology of adult fractures: A review. Injury 37:691-697.

Crisan M, Yap S, Casteilla L, Chen C-W, Corselli M, Park TS, Andriolo G, Sun B, Zheng B, Zhang L, Norotte C, Teng P-N, Traas J, Schugar R, Deasy BM, Badylak S, Bqhring H-J, Giacobino J-P, Lazzari L, Huard J, Péault B. 2008. A Perivascular Origin for Mesenchymal Stem Cells in Multiple Human Organs. Cell stem cell 3:301-313.

Cui X, Boland T, D'Lima DD, Lotz MK. 2012. Thermal Inkjet Printing in Tissue Engineering and Regenerative Medicine. Recent patents on drug delivery & formulation 6:149-155.

Culliford DJ, Maskell J, Kiran A, Judge A, Javaid MK, Cooper C, Arden NK. 2012. The lifetime risk of total hip and knee arthroplasty: results from the UK general practice research database. Osteoarthritis Cartilage 20:519-524.

Cypher TJ, Grossman JP. 1996. Biological principles of bone graft healing. The Journal of Foot and Ankle Surgery 35:413-417.

Dalby MJ, Gadegaard N, Oreffo ROC. 2014. Harnessing nanotopography and integrin-matrix interactions to influence stem cell fate. Nat Mater 13:558-569.

Davies OR, Lewis AL, Whitaker MJ, Tai H, Shakesheff KM, Howdle SM. 2008. Applications of supercritical CO2 in the fabrication of polymer systems for drug delivery and tissue engineering. Advanced Drug Delivery Reviews 60:373-387.

Dawson JI, Kanczler J, Tare R, Kassem M, Oreffo ROC. 2014. Concise Review: Bridging the Gap: Bone Regeneration Using Skeletal Stem Cell-Based Strategies—Where Are We Now? STEM CELLS 32:35-44.

Dawson JI, Kanczler JM, Yang XBB, Attard GS, Oreffo ROC. 2011. Clay Gels For the Delivery of Regenerative Microenvironments. Adv Mater 23:3304-+.

Dawson JI, Oreffo ROC. 2008. Bridging the regeneration gap: Stem cells, biomaterials and clinical translation in bone tissue engineering. Arch Biochem Biophys 473:124-131.

de Bakker E, Van Ryssen B, De Schauwer C, Meyer E. 2013. Canine mesenchymal stem cells: state of the art, perspectives as therapy for dogs and as a model for man. Veterinary Quarterly 33:225-233.

Degat MC, Dubreucq G, Meunier A, Dahri-Correia L, Sedel L, Petite H, Logeart-Avramoglou D. 2009. Enhancement of the biological activity of BMP-2 by synthetic dextran derivatives. J Biomed Mater Res Part A 88A:174-183.

Delaporte P, Alloncle A-P. 2016. [INVITED] Laser-induced forward transfer: A high resolution additive manufacturing technology. Optics & Laser Technology 78, Part A:33-41.

Delloye C, Cornu O, Druez V, Barbier O. 2007. Bone allografts. WHAT THEY CAN OFFER AND WHAT THEY CANNOT 89-B:574-580.

Diez-Perez A, Güerri R, Nogues X, Cáceres E, Peña MJ, Mellibovsky L, Randall C, Bridges D, Weaver JC, Proctor A, Brimer D, Koester KJ, Ritchie RO, Hansma PK. 2010. Microindentation for *in vivo* measurement of bone tissue mechanical properties in humans. J Bone Miner Res 25:1877-1885.

Ding M, Rojskjaer J, Cheng L, Theilgaard N, Overgaard S. 2012. The effects of a novel-reinforced bone substitute and Colloss(R)E on bone defect healing in sheep. Journal of biomedical materials research Part B, Applied biomaterials 100:1826-1835.

Dominici M, Le Blanc K, Mueller I, Slaper-Cortenbach I, Marini F, Krause D, Deans R, Keating A, Prockop D, Horwitz E. 2006a. Minimal criteria for defining multipotent mesenchymal stromal cells. The International Society for Cellular Therapy position statement. Cytotherapy 8:315-317.

Dominici M, Le Blanc K, Mueller I, Slaper-Cortenbach I, Marini F, Krause D, Deans R, Keating A, Prockop D, Horwitz E. 2006b. Minimal criteria for defining multipotent mesenchymal stromal cells. The International Society for Cellular Therapy position statement. Cytotherapy 8.

Dreger T, Watson JT, Dvm WA, Molligan J, Achilefu S, Schon LC, Zhang Z. 2014. Intravenous Application of CD271-selected Mesenchymal Stem Cells during Fracture Healing. Journal of orthopaedic trauma 28:S15-S19.

Drury JL, Mooney DJ. 2003. Hydrogels for tissue engineering: scaffold design variables and applications. Biomaterials 24:4337-4351.

Duda GN, Taylor WR, Ehrig RM, Heller MO, Schell H, Seebeck P. 2006. Tibio-femoral joint contact forces in sheep. Journal of Biomechanics 39:791-798.

Dupont WD, Plummer WD, Jr. 1990. Power and sample size calculations. A review and computer program. Control Clin Trials 11:116-128.

Edgerton BC, An KN, Morrey BF. 1990. Torsional strength reduction due to cortical defects in bone. J Orthop Res 8.

Egermann M, Goldhahn J, Schneider E. 2005. Animal models for fracture treatment in osteoporosis. Osteoporosis International 16:S129-S138.

Eggli PS, Moller W, Schenk RK. 1988. Porous Hydroxyapatite and Tricalcium Phosphate Cylinders with Two Different Pore Size Ranges Implanted in the Cancellous Bone of Rabbits: A Comparative Histomorphometric and Histologic Study of Bony Ingrowth and Implant Substitution. Clin Orthop Rel Res 232:127-138.

Einhorn TA. 1998. The Cell and Molecular Biology of Fracture Healing. Clin Orthop Rel Res 355:S7-S21.

Einhorn TA, Gerstenfeld LC. 2015. Fracture healing: mechanisms and interventions. Nat Rev Rheumatol 11:45-54.

Eitel F, Klapp F, Jacobson W, Schweiberer L. 1981. BONE REGENERATION IN ANIMALS AND IN MAN - A CONTRIBUTION TO UNDERSTANDING THE RELATIVE VALUE OF ANIMAL-EXPERIMENTS TO HUMAN PATHO-PHYSIOLOGY. Archives of Orthopaedic and Trauma Surgery 99:59-64.

Engler AJ, Sen S, Sweeney HL, Discher DE. 2006. Matrix Elasticity Directs Stem Cell Lineage Specification. Cell 126:677-689.

Erlebacher A, Filvaroff EH, Gitelman SE, Derynck R. 1995. Toward a molecular understanding of skeletal development. Cell 80:371-378.

EU CfMPfHU. 2014. Asessment Report Procedure No. EMEA/H/C/003850/0000. European Medicines Agency.

Even-Ram S, Artym V, Yamada KM. 2006. Matrix Control of Stem Cell Fate. Cell 126:645-647.

Fakhry A, Ratisoontorn C, Vedhachalam C, Salhab I, Koyama E, Leboy P, Pacifici M, Kirschner RE, Nah H-D. Effects of FGF-2/-9 in calvarial bone cell cultures: differentiation stage-dependent mitogenic effect, inverse regulation of BMP-2 and noggin, and enhancement of osteogenic potential. Bone 36:254-266.

Felsenberg D, Boonen S. 2005. The bone quality framework: Determinants of bone strength and their interrelationships, and implications for osteoporosis management. Clinical Therapeutics 27:1-11.

Feng B, Jinkang Z, Zhen W, Jianxi L, Jiang C, Jian L, Guolin M, Xin D. 2011. The effect of pore size on tissue ingrowth and neovascularization in porous bioceramics of controlled architecture *in vivo*. Biomedical materials 6:015007.

Ferrara N, Gerber H-P, LeCouter J. 2003. The biology of VEGF and its receptors. Nat Med 9:669-676.

Fiedler J, Röderer G, Günther K-P, Brenner RE. 2002. BMP-2, BMP-4, and PDGF-bb stimulate chemotactic migration of primary human mesenchymal progenitor cells. Journal of Cellular Biochemistry 87:305-312.

Fitter S, Gronthos S, Ooi SS, Zannettino ACW. 2017. The Mesenchymal Precursor Cell Marker Antibody STRO-1 Binds to Cell Surface Heat Shock Cognate 70. STEM CELLS 35:940-951.

Frantz C, Stewart KM, Weaver VM. 2010. The extracellular matrix at a glance. J Cell Sci 123:4195-4200.

Friedenstein AJ. 1982. Stromal bone marrow cells and the hematopoietic microenvironment.

Gallant MA, Brown DM, Organ JM, Allen MR, Burr DB. 2013. Reference-point indentation correlates with bone toughness assessed using whole-bone traditional mechanical testing. Bone 53:301-305.

Gallego L, Pérez-Basterrechea M, García-Consuegra L, Álvarez-Viejo M, Megías J, Novoa A, Costilla S, Meana Á, Junquera L. 2015. Repair of segmental mandibular bone defects in sheep using bone marrow stromal cells and autologous serum scaffold: a pilot study. Journal of Clinical Periodontology 42:1143-1151.

Gao C, Deng Y, Feng P, Mao Z, Li P, Yang B, Deng J, Cao Y, Shuai C, Peng S. 2014. Current Progress in Bioactive Ceramic Scaffolds for Bone Repair and Regeneration. International Journal of Molecular Sciences 15:4714-4732.

Garrigue-Antar L, Barbieux I, Lieubeau B, Boisteau O, Grégoire M. 1995. Optimisation of CCL64-based bioassay for TGF-β. Journal of Immunological Methods 186:267-274.

Gauvin R, Chen Y-C, Lee JW, Soman P, Zorlutuna P, Nichol JW, Bae H, Chen S, Khademhosseini A. 2012. Microfabrication of complex porous tissue engineering scaffolds using 3D projection stereolithography. Biomaterials 33:3824-3834.

Gerstenfeld LC, Cullinane DM, Barnes GL, Graves DT, Einhorn TA. 2003. Fracture healing as a post-natal developmental process: Molecular, spatial, and temporal aspects of its regulation. Journal of Cellular Biochemistry 88:873-884.

Ghert MA, Davis AM, Griffin AM, Alyami AH, White L, Kandel RA, Ferguson P, O'Sullivan B, Catton CN, Lindsay T, Rubin B, Bell RS, Wunder JS. 2005. The Surgical and Functional Outcome of Limb-Salvage Surgery With Vascular Reconstruction for Soft Tissue Sarcoma of the Extremity. Annals of Surgical Oncology 12:1102-1110.

Giannoudis PV, Dinopoulos H, Tsiridis E. 2005. Bone substitutes: An update. Injury-Int J Care Inj 36:20-27.

Gibbs DM, Black CR, Dawson JI, Oreffo RO. 2016a. A review of hydrogel use in fracture healing and bone regeneration. J Tissue Eng Regen Med 10:187-198.

Gibbs DMR, Black CRM, Hulsart-Billstrom G, Shi P, Scarpa E, Oreffo ROC, Dawson JI. 2016b. Bone induction at physiological doses of BMP through localization by clay nanoparticle gels. Biomaterials 99:16-23.

Giustina A, Mazziotti G, Canalis E. 2008. Growth Hormone, Insulin-Like Growth Factors, and the Skeleton. Endocr Rev 29:535-559.

Glass Ii DA, Bialek P, Ahn JD, Starbuck M, Patel MS, Clevers H, Taketo MM, Long F, McMahon AP, Lang RA, Karsenty G. 2005. Canonical Wnt Signaling in Differentiated Osteoblasts Controls Osteoclast Differentiation. Developmental Cell 8:751-764.

Gomes ME, Ribeiro AS, Malafaya PB, Reis RL, Cunha AM. 2001. A new approach based on injection moulding to produce biodegradable starch-based polymeric scaffolds: morphology, mechanical and degradation behaviour. Biomaterials 22:883-889.

Gothard D, Emma L. Smith, Janos M. Kanczler, Cameron R. Black, Julia A. Wells, Carol A. Roberts, Lisa J. White, Omar Qutachi, Heather Peto, Hassan Rashidi, Luis Rojo, Molly M. Stevens, Alicia J. El Haj, Felicity R. A. J. Rose, Kevin M. Shakesheff, Oreffo ROC. 2015. In-vivo Assessment of Bone Regeneration in Alginate Bone ECM Hydrogels with Incorporated Skeletal Stem Cells and Single Growth Factors PLOSONE.

Gothard DS, E.L; Kanczler, J;Rashidi, O; Qutachi, O; Henstock, M; Rotheram, A; El Haj, A; Shakesheff, K.M; Oreffo, R.O.C. 2014. Tissue Engineered Bone using select growth factors: A comprehensive review of animal studies and clinical translation studies in man Eur Cells Mater 28:166-208.

Gotherstrom C, West A, Liden J, Uzunel M, Lahesmaa R, Le Blanc K. 2005. Difference in gene expression between human fetal liver and adult bone marrow mesenchymal stem cells. Haematologica 90:1017-1026.

Gov U. 2009. Recognition and Alleviation of Pain in Laboratory Animals. National Academies Press (US).

Graham S, Leonidou A, Lester M, Heliotis M, Mantalaris A, Tsiridis E. 2009. Investigating the role of PDGF as a potential drug therapy in bone formation and fracture healing. Expert Opinion on Investigational Drugs 18:1633-1654.

Greenbaum MA, Kanat IO. 1993. Current concepts in bone healing. Review of the literature. J Am Podiatr Med Assoc 83:123-129.

Gronthos S, Graves S, Ohta S, Simmons P. 1994a. The STRO-1+ fraction of adult human bone marrow contains the osteogenic precursors.

Gronthos S, Graves SE, Ohta S, Simmons PJ. 1994b. THE STRO-1(+) FRACTION OF ADULT HUMAN BONE-MARROW CONTAINS THE OSTEOGENIC PRECURSORS. Blood 84:4164-4173.

Gronthos S, McCarty R, Mrozik K, Fitter S, Paton S, Menicanin D, Itescu S, Bartold PM, Xian C, Zannettino ACW. 2009. Heat Shock Protein-90 beta Is Expressed at the Surface of Multipotential Mesenchymal Precursor Cells: Generation of a Novel Monoclonal Antibody, STRO-4, With Specificity for Mesenchymal Precursor Cells From Human and Ovine Tissues. Stem Cells Dev 18:1253-1261.

Gronthos S, Zannettino ACW, Hay SJ, Shi S, Graves SE, Kortesidis A, Simmons PJ. 2003. Molecular and cellular characterisation of highly purified stromal stem cells derived from human bone marrow. J Cell Sci 116:1827-1835.

Guan X, Avci-Adali M, Alarçin E, Cheng H, Kashaf SS, Li Y, Chawla A, Jang HL, Khademhosseini A. 2017. Development of hydrogels for regenerative engineering. Biotechnology Journal 12:1600394-n/a.

Gugala Z, Gogolewski S. 1999. Regeneration of Segmental Diaphyseal Defects in Sheep Tibiae Using Resorbable Polymeric Membranes: A Preliminary Study. Journal of Orthopaedic Trauma 13:187-195.

Guntur AR, Rosen CJ. 2012. Bone as an Endocrine Organ. Endocrine practice : official journal of the American College of Endocrinology and the American Association of Clinical Endocrinologists 18:758-762.

Hamilton PT, Jansen MS, Ganesan S, Benson RE, Hyde-Deruyscher R, Beyer WF, Gile JC, Nair SA, Hodges JA, Grøn H. 2013. Improved bone morphogenetic protein-2 retention in an injectable collagen matrix using bifunctional peptides. PLoS One 8.

Harichandan A, Bühring H-J. 2011. Prospective isolation of human MSC. Best Practice & Research Clinical Haematology 24:25-36.

Hattori K, Dias S, Heissig B, Hackett NR, Lyden D, Tateno M, Hicklin DJ, Zhu Z, Witte L, Crystal RG, Moore MAS, Rafii S. 2001. Vascular Endothelial Growth Factor and Angiopoietin-1 Stimulate Postnatal Hematopoiesis by Recruitment of Vasculogenic and Hematopoietic Stem Cells. The Journal of Experimental Medicine 193:1005-1014.

Haynesworth SE, Goshima J, Goldberg VM, Caplan AI. 1992a. Characterization of cells with osteogenic potential from human marrow. Bone 13:81-88.

Haynesworth SE, Goshima J, Goldberg VM, Caplan AI. 1992b. Characterization of cells with osteogenic potential from human marrow. Bone 13.

Hench LL. 1998. Bioactive materials: The potential for tissue regeneration. J Biomed Mater Res 41:511-518.

Henkel J, Woodruff MA, Epari DR, Steck R, Glatt V, Dickinson IC, Choong PFM, Schuetz MA, Hutmacher DW. 2013. Bone Regeneration Based on Tissue Engineering Conceptions — A 21st Century Perspective. Bone Research 1:216.

Hoffman MD, Van Hove AH, Benoit DSW. 2014. Degradable hydrogels for spatiotemporal control of mesenchymal stem cells localized at decellularized bone allografts. Acta Biomaterialia 10:3431-3441.

Hollinger JO, Kleinschmidt JC. 1990. The Critical Size Defect as an Experimental Model To Test Bone Repair Materials. J Craniofac Surg 1:60-68.

Hollister SJ, Murphy WL. 2011. Scaffold Translation: Barriers Between Concept and Clinic. Tissue Engineering Part B, Reviews 17:459-474.

Huang W, Arai F, Kawahara T. 2015. Egg-in-Cube: Design and Fabrication of a Novel Artificial Eggshell with Functionalized Surface. PLoS ONE 10:e0118624.

Hugh Auchincloss Ja, Sachs DH. 1998. XENOGENEIC TRANSPLANTATION. Annual Review of Immunology 16:433-470.

Huiskes R, Ruimerman R, van Lenthe GH, Janssen JD. 2000. Effects of mechanical forces on maintenance and adaptation of form in trabecular bone. Nature 405:704-706.

Hulbert SF, Young FA, Mathews RS, Klawitter JJ, Talbert CD, Stelling FH. 1970. Potential of ceramic materials as permanently implantable skeletal prostheses. J Biomed Mater Res 4:433-456.

Hulsart-Billstrom G, Piskounova S, Gedda L, Andersson BM, Bergman K, Hilborn J, Larsson S, Bowden T. 2013. Morphological differences in BMP-2-induced ectopic bone between solid and crushed hyaluronan hydrogel templates. J Mater Sci-Mater Med 24:1201-1209.

Hutmacher DW. 2000. Scaffolds in tissue engineering bone and cartilage. Biomaterials 21:2529-2543.

Hwang NS, Varghese S, Puleo C, Zhang Z, Elisseeff J. 2007. Morphogenetic signals from chondrocytes promote chondrogenic and osteogenic differentiation of mesenchymal stem cells. J Cell Physiol 212:281-284.

Inzana JA, Olvera D, Fuller SM, Kelly JP, Graeve OA, Schwarz EM, Kates SL, Awad HA. 2014. 3D printing of composite calcium phosphate and collagen scaffolds for bone regeneration. Biomaterials 35:4026-4034.

Izadpanah R, Joswig T, Tsien F, Dufour J, Kirijan JC, Bunnell BA. 2005. Characterization of Multipotent Mesenchymal Stem Cells from the Bone Marrow of Rhesus Macaques. Stem Cells Dev 14:440-451.

James AW, LaChaud G, Shen J, Asatrian G, Nguyen V, Zhang X, Ting K, Soo C. 2016. A Review of the Clinical Side Effects of Bone Morphogenetic Protein-2. Tissue Engineering Part B: Reviews 22:284-297.

Jarocha D, Lukasiewicz E, Majka M. 2008. Adventage of mesenchymal stem cells (MSC) expansion directly from purified bone marrow CD105+ and CD271+ cells. Folia histochemica et cytobiologica / Polish Academy of Sciences, Polish Histochemical and Cytochemical Society 46:307-314.

Jenkins T, Coutts LV, Dunlop DG, Oreffo ROC, Cooper C, Harvey NC, Thurner PJ. 2015. Variability in reference point microindentation and recommendations for testing cortical bone: Maximum load, sample orientation, mode of use, sample preparation and measurement spacing. Journal of the Mechanical Behavior of Biomedical Materials 42:311-324.

Jha AK, Tharp KM, Ye J, Santiago-Ortiz JL, Jackson WM, Stahl A, Schaffer DV, Yeghiazarians Y, Healy KE. 2015. Enhanced survival and engraftment of transplanted stem cells using growth factor sequestering hydrogels. Biomaterials 47:1-12.

Jiang D, Gao P, Zhang Y, Yang S. 2016. Combined effects of engineered tendon matrix and GDF-6 on bone marrow mesenchymal stem cell-based tendon regeneration. Biotechnology Letters 38:885-892.

Jo CH, Lee YG, Shin WH, Kim H, Chai JW, Jeong EC, Kim JE, Shim H, Shin JS, Shin IS, Ra JC, Oh S, Yoon KS. 2014. Intra-Articular Injection of Mesenchymal Stem Cells for the Treatment of Osteoarthritis of the Knee: A Proof-of-Concept Clinical Trial. STEM CELLS 32:1254-1266.

Johnell O, Kanis JA, Oden A, Johansson H, Laet CD, Delmas P, Eisman JA, Fujiwara S, Kroger H, Mellstrom D, Meunier PJ, Melton LJ, O'Neill T, Pols H, Reeve J, Silman A, Tenenhouse A. 2005. Predictive Value of BMD for Hip and Other Fractures. J Bone Miner Res 20:1185-1194.

Jones AC, Arns CH, Sheppard AP, Hutmacher DW, Milthorpe BK, Knackstedt MA. 2007. Assessment of bone ingrowth into porous biomaterials using MICRO-CT. Biomaterials 28:2491-2504.

Kaigler D, Avila-Ortiz G, Travan S, Taut AD, Padial-Molina M, Rudek I, Wang F, Lanis A, Giannobile WV. 2015. Bone Engineering of Maxillary Sinus Bone Deficiencies Using Enriched CD90+ Stem Cell Therapy: A Randomized Clinical Trial. J Bone Miner Res 30:1206-1216.

Kaipel M, Schützenberger S, Schultz A, Ferguson J, Slezak P, Morton TJ, Van Griensven M, Redl H. 2012. BMP-2 but not VEGF or PDGF in fibrin matrix supports bone healing in a delayed-union rat model. J Orthop Res 30:1563-1569.

Kan L, Kessler JA. 2011. Animal Models of Typical Heterotopic Ossification. Journal of Biomedicine and Biotechnology 2011:8.

Kanczler JM, Ginty PJ, White L, Clarke NMP, Howdle SM, Shakesheff KM, Oreffo ROC. 2010. The effect of the delivery of vascular endothelial growth factor and bone morphogenic protein-2 to osteoprogenitor cell populations on bone formation. Biomaterials 31:1242-1250.

Kanczler JM, Smith EL, Roberts CA, Oreffo ROC. 2012. A Novel Approach for Studying the Temporal Modulation of Embryonic Skeletal Development Using Organotypic Bone Cultures and Microcomputed Tomography. Tissue Engineering Part C, Methods 18:747-760.

Karageorgiou V, Kaplan D. 2005. Porosity of 3D biomaterial scaffolds and osteogenesis. Biomaterials 26:5474-5491.

Katz J, Mukherjee N, Cobb RR, Bursac P, York-Ely A. 2009. Incorporation and immunogenicity of cleaned bovine bone in a sheep model. J Biomater Appl 24:159-174.

Keating JF, McQueen MM. 2001. Substitutes for autologous bone graft in orthopaedic trauma. J Bone Joint Surg (Br) 83.

Kempen DHR, Lu L, Hefferan TE, Creemers LB, Maran A, Classic KL, Dhert WJA, Yaszemski MJ. 2008. Retention of *in vitro* and *in vivo* BMP-2 bioactivities in sustained delivery vehicles for bone tissue engineering. Biomaterials 29:3245-3252.

Khademhosseini A, Langer R. 2016. A decade of progress in tissue engineering. Nat Protocols 11:1775-1781.

Khalil S, Nam J, Sun W. 2005. Multi-nozzle deposition for construction of 3D biopolymer tissue scaffolds. Rapid Prototyping Journal 11:9-17.

Khan SN, Cammisa FP, Jr., Sandhu HS, Diwan AD, Girardi FP, Lane JM. 2005. The biology of bone grafting. The Journal of the American Academy of Orthopaedic Surgeons 13:77-86.

Khouw IMSL, van Wachem PB, de Leij LFMH, van Luyn MJA. 1998. Inhibition of the tissue reaction to a biodegradable biomaterial by monoclonal antibodies to IFN-γ. J Biomed Mater Res 41:202-210.

Khunda A, Al-Maiyah M, Eardley WGP, Montgomery R. 2016. The management of tibial fracture non-union using the Taylor Spatial Frame. Journal of Orthopaedics 13:360-363.

Kim K, Yeatts A, Dean D, Fisher JP. 2010. Stereolithographic Bone Scaffold Design Parameters: Osteogenic Differentiation and Signal Expression. Tissue Engineering Part B: Reviews 16:523-539.

Kim KD, Wright NM. 2011. Polyethylene glycol hydrogel spinal sealant (DuraSeal Spinal Sealant) as an adjunct to sutured dural repair in the spine: results of a prospective, multicenter, randomized controlled study. Spine (Phila Pa 1976) 36:1906-1912.

Kim MB, Lee YH, Baek JK, Choi HS, Baek GH. 2015. Reconstruction of Large Femur and Tibia Defect with Free Vascularized Fibula Graft and Locking Plate. arms 24:68-74.

Kimble JE, White JG. 1981. On the control of germ cell development in Caenorhabditis elegans. Dev Biol 81:208-219.

Kinstlinger IS, Bastian A, Paulsen SJ, Hwang DH, Ta AH, Yalacki DR, Schmidt T, Miller JS. 2016. Open-Source Selective Laser Sintering (OpenSLS) of Nylon and Biocompatible Polycaprolactone. PLOS ONE 11:e0147399.

Kisiel M, Klar AS, Ventura M, Buijs J, Mafina MK, Cool SM, Hilborn J. 2013. Complexation and Sequestration of BMP-2 from an ECM Mimetic Hyaluronan Gel for Improved Bone Formation. Plos One 8.

Kokubo T, Yamaguchi S. 2016. Novel Bioactive Materials Derived by Bioglass: Glass-Ceramic A-W and Surface-Modified Ti Metal. International Journal of Applied Glass Science:n/a-n/a.

Kolambkar YM, Boerckel JD, Dupont KM, Bajin M, Huebsch N, Mooney DJ, Hutmacher DW, Guldberg RE. 2011a. Spatiotemporal delivery of bone morphogenetic protein enhances functional repair of segmental bone defects. Bone 49:485-492.

Kolambkar YM, Dupont KM, Boerckel JD, Huebsch N, Mooney DJ, Hutmacher DW, Guldberg RE. 2011b. An alginate-based hybrid system for growth factor delivery in the functional repair of large bone defects. Biomaterials 32:65-74.

Kolambkar YM, Peister A, Ekaputra AK, Hutmacher DW, Guldberg RE. 2010. Colonization and Osteogenic Differentiation of Different Stem Cell Sources on Electrospun Nanofiber Meshes. Tissue Eng Part A 16:3219-3230.

Kronenberg HM. 2003. Developmental regulation of the growth plate. Nature 423:332-336.

Kuboki Y, Takita H, Kobayashi D, Tsuruga E, Inoue M, Murata M, Nagai N, Dohi Y, Ohgushi H. 1998. BMP-induced osteogenesis on the surface of hydroxyapatite with geometrically feasible and nonfeasible structures: topology of osteogenesis. J Biomed Mater Res 39:190-199.

Kulterer B, Friedl G, Jandrositz A, Sanchez-Cabo F, Prokesch A, Paar C, Scheideler M, Windhager R, Preisegger K-H, Trajanoski Z. 2007. Gene expression profiling of human mesenchymal stem cells derived from bone marrow during expansion and osteoblast differentiation. BMC Genomics 8:1-15.

Lamerigts NM, Buma P, Huiskes R, Schreurs W, Gardeniers J, Slooff TJ. 2000. Incorporation of morsellized bone graft under controlled loading conditions. A new animal model in the goat. Biomaterials 21:741-747.

Lane JM, Tomin E, Bostrom MPG. 1999. Biosynthetic bone grafting. Clin Orthop Rel Res:S107-S117.

Langer R, Vacanti J. 1993. Tissue engineering. Science 260:920-926.

Lansdowne JL, Devine D, Eberli U, Emans P, Welting TJM, Odekerken JCE, Schiuma D, Thalhauser M, Bour, #xe9, L, Zeiter S. 2014. Characterization of an Ovine Bilateral Critical Sized Bone Defect Iliac Wing Model to Examine Treatment Modalities Based on Bone Tissue Engineering. BioMed Research International 2014:7.

Laurencin C, Khan Y, El-Amin SF. 2006. Bone graft substitutes. Expert Review of Medical Devices 3:49-57.

Le Blanc K, Rasmusson I, Sundberg B, Götherström C, Hassan M, Uzunel M, Ringdén O. 2004. Treatment of severe acute graft-versus-host disease with third party haploidentical mesenchymal stem cells. The Lancet 363:1439-1441.

Lee Y, Sah H. 2016. Simple emulsion technique as an innovative template for preparation of porous, spongelike poly(lactide-co-glycolide) microspheres with pore-closing capability. Journal of Materials Science 51:6257-6274.

Leichter I, Margulies JY, Weinreb A, Mizrahi J, Robin GC, Conforty B, Makin M, Bloch B. 1982. The Relationship between Bone-Density, Mineral-Content, and Mechanical Strength in the Femoral-Neck. Clin Orthop Rel Res:272-281.

Li G, Corsi-Payne K, Zheng B, Usas A, Peng H, Huard J. 2009. The Dose of Growth Factors Influences the Synergistic Effect of Vascular Endothelial Growth Factor on Bone Morphogenetic Protein 4–Induced Ectopic Bone Formation. Tissue Eng Part A 15:2123-2133.

Li Y, Chen S-K, Li L, Qin L, Wang X-L, Lai Y-X. 2015. Bone defect animal models for testing efficacy of bone substitute biomaterials. Journal of Orthopaedic Translation 3:95-104.

Li Y, Liu R, Hu J, Song D, Jiang X, Zhu S. 2016. Recombinant human bone morphogenetic protein-2 suspended in fibrin glue enhances bone formation during distraction osteogenesis in rabbits. Archives of Medical Science 12:494-501.

Liang D, Hsiao BS, Chu B. 2007. Functional electrospun nanofibrous scaffolds for biomedical applications. Advanced Drug Delivery Reviews 59:1392-1412.

Lieberman JR, Daluiski A, Einhorn TA. 2002. The Role of Growth Factors in the Repair of Bone. Biology and Clinical Applications 84:1032-1044.

Liebschner MAK. 2004. Biomechanical considerations of animal models used in tissue engineering of bone. Biomaterials 25:1697-1714.

Lin ASP, Barrows TH, Cartmell SH, Guldberg RE. 2003. Microarchitectural and mechanical characterization of oriented porous polymer scaffolds. Biomaterials 24:481-489.

Lindsey RW, Gugala Z, Milne E, Sun M, Gannon FH, Latta LL. 2006. The efficacy of cylindrical titanium mesh cage for the reconstruction of a critical-size canine segmental femoral diaphyseal defect. J Orthop Res 24:1438-1453.

Lissenberg-Thunnissen SN, de Gorter DJJ, Sier CFM, Schipper IB. 2011. Use and efficacy of bone morphogenetic proteins in fracture healing. Int Orthop 35:1271-1280.

Liu T, Wu G, Wismeijer D, Gu Z, Liu Y. 2013. Deproteinized bovine bone functionalized with the slow delivery of BMP-2 for the repair of critical-sized bone defects in sheep. Bone 56:110-118.

Liu Y, Shu XZ, Prestwich GD. 2006. Osteochondral defect repair with autologous bone marrow-derived mesenchymal stem cells in an injectable, in situ, cross-linked synthetic extracellular matrix. Tissue Eng 12:3405-3416.

Livingston A. 2010. Pain and Analgesia in Domestic Animals. In: Cunningham F, Elliott J, Lees P, editors. Comparative and Veterinary Pharmacology. Berlin, Heidelberg: Springer Berlin Heidelberg. p 159-189.

Lopes JH, Magalhães JA, Gouveia RF, Bertran CA, Motisuke M, Camargo SEA, Trichês EdS. 2016. Hierarchical structures of β-TCP/45S5 bioglass hybrid scaffolds prepared by gelcasting. Journal of the Mechanical Behavior of Biomedical Materials 62:10-23.

Lu SS, Zhang X, Soo C, Hsu T, Napoli A, Aghaloo T, Wu BM, Tsou P, Ting K, Wang JC. 2007. The osteoinductive properties of Nell-1 in a rat spinal fusion model. The Spine Journal 7:50-60.

Lubeck DP. 2003. The costs of musculoskeletal disease: health needs assessment and health economics. Best Practice & Research Clinical Rheumatology 17:529-539.

Luca L, L. RA, H. WB, R. G, O. J. 2010. The effects of carrier nature and pH on rhBMP-2-induced ectopic bone formation. Journal of Controlled Release 147:38-44.

Luca L, Rougemont AL, Walpoth BH, Boure L, Tami A, Anderson JM, Jordan O, Gurny R. 2011. Injectable rhBMP-2-loaded chitosan hydrogel composite: Osteoinduction at ectopic site and in segmental long bone defect. J Biomed Mater Res Part A 96A:66-74.

Luginbuehl V, Zoidis E, Meinel L, von Rechenberg B, Gander B, Merkle HP. 2013. Impact of IGF-I release kinetics on bone healing: A preliminary study in sheep. European Journal of Pharmaceutics and Biopharmaceutics 85:99-106.

Lukáš D, Sarkar A, Martinová L, Vodsed'álková K, Lubasová D, Chaloupek J, Pokorný P, Mikeš P, Chvojka J, Komárek M. 2009. Physical principles of electrospinning (Electrospinning as a nano-scale technology of the twenty-first century). Textile Progress 41:59-140.

Lyahyai J, Mediano DR, Ranera B, Sanz A, Remacha AR, Bolea R, Zaragoza P, Rodellar C, Martin-Burriel I. 2012. Isolation and characterization of ovine mesenchymal stem cells derived from peripheral blood. BMC Vet Res 8.

Mackie EJ, Ahmed YA, Tatarczuch L, Chen KS, Mirams M. 2008. Endochondral ossification: How cartilage is converted into bone in the developing skeleton. The International Journal of Biochemistry & Cell Biology 40:46-62.

Malhotra A, Pelletier MH, Yu Y, Christou C, Walsh WR. 2014. A Sheep Model for Cancellous Bone Healing. Frontiers in Surgery 1:37.

Mamalis AA, Cochran DL. 2011. The therapeutic potential of oxygen tension manipulation via hypoxia inducible factors and mimicking agents in guided bone regeneration. A review. Archives of Oral Biology 56:1466-1475.

Marcacci M, Kon E, Moukhachev V, Lavroukov A, Kutepov S, Quarto R, Mastrogiacomo M, Cancedda R. 2007. Stem cells associated with macroporous bioceramics for long bone repair: 6- to 7-year outcome of a pilot clinical study. Tissue Eng 13:947-955.

Marga F, Neagu A, Kosztin I, Forgacs G. 2007. Developmental biology and tissue engineering. Birth Defects Research Part C: Embryo Today: Reviews 81:320-328.

Mariner PD, Wudel JM, Miller DE, Genova EE, Streubel S-O, Anseth KS. 2013. Synthetic hydrogel scaffold is an effective vehicle for delivery of INFUSE (rhBMP2) to critical-sized calvaria bone defects in rats. J Orthop Res 31:401-406.

Marsell R, Einhorn TA. 2011. THE BIOLOGY OF FRACTURE HEALING. Injury 42:551-555.

Martin I, Wendt D, Heberer M. 2004. The role of bioreactors in tissue engineering. Trends in Biotechnology 22:80-86.

Martínez-Reina J, Domínguez J, García-Aznar JM. 2010. Effect of porosity and mineral content on the elastic constants of cortical bone: a multiscale approach. Biomechanics and Modeling in Mechanobiology 10:309-322.

Martini L, Fini M, Giavaresi G, Giardino R. 2001. Sheep model in orthopedic research: A literature review. Comparative Med 51:292-299.

McCarty RC, Gronthos S, Zannettino AC, Foster BK, Xian CJ. 2009. Characterisation and Developmental Potential of Ovine Bone Marrow Derived Mesenchymal Stem Cells. J Cell Physiol 219:324-333.

Meijer GJ, de Bruijn JD, Koole R, van Blitterswijk CA. 2008. Cell based bone tissue engineering in jaw defects. Biomaterials 29:3053-3061.

Melnyk M, Henke T, Claes L, Augat P. 2007. Revascularisation during fracture healing with soft tissue injury. Archives of Orthopaedic and Trauma Surgery 128:1159-1165.

Melton LJ, Atkinson EJ, O'Connor MK, O'Fallon WM, Riggs BL. 1998. Bone Density and Fracture Risk in Men. J Bone Miner Res 13:1915-1923.

Mi H-Y, Salick MR, Jing X, Jacques BR, Crone WC, Peng X-F, Turng L-S. 2013. Characterization of thermoplastic polyurethane/polylactic acid (TPU/PLA) tissue engineering scaffolds fabricated by microcellular injection molding. Materials Science and Engineering: C 33:4767-4776.

Michelle T. Poldervaart, Huanan Wang, Johan van der Stok, Harrie Weinans, Sander C. G. Leeuwenburgh, F. Cumhur Öner, Wouter J. A. Dhert, mail JA. 2013. Sustained Release of BMP-2 in Bioprinted Alginate for Osteogenicity in Mice and Rats. PLOSONE.

Mifune Y, Matsumoto T, Murasawa S, Kawamoto A, Kuroda R, Shoji T, Kuroda T, Fukui T, Kawakami Y, Kurosaka M, Asahara T. 2013. Therapeutic Superiority for Cartilage Repair by CD271-Positive Marrow Stromal Cell Transplantation. Cell Transplantation 22:1201-1211.

Mirhadi S, Ashwood N, Karagkevrekis B. 2013. Factors influencing fracture healing. Trauma 15:140-155.

Misch CM. 2010. Autogenous Bone: Is It Still the Gold Standard? Implant Dentistry 19:361.

Monroe DG, McGee-Lawrence ME, Oursler MJ, Westendorf JJ. 2012. Update on Wnt signaling in bone cell biology and bone disease. Gene 492:1-18.

Morrison SJ, Scadden DT. 2014. The bone marrow niche for haematopoietic stem cells. Nature 505:327-334.

Mroz TE, Joyce MJ, Steinmetz MP, Lieberman IH, Wang JC. 2008. Musculoskeletal allograft risks and recalls in the United States. Journal of the American Academy of Orthopaedic Surgeons 16:559-565.

Muramatsu K, Doi K, Ihara K, Shigetomi M, Kawai S. 2003. Recalcitrant posttraumatic nonunion of the humerus: 23 patients reconstructed with vascularized bone graft. Acta orthopaedica Scandinavica 74:95-97.

Murata M, Arisue M, Sato D, Sasaki T, Shibata T, Kuboki Y. 2002. Bone induction in subcutaneous tissue in rats by a newly developed DNA-coated atelocollagen and bone morphogenetic protein. British Journal of Oral & Maxillofacial Surgery 40:131-135.

Murphy SV, Atala A. 2014. 3D bioprinting of tissues and organs. Nat Biotechnol 32:773-785.

Murray IR, West CC, Hardy WR, James AW, Park TS, Nguyen A, Tawonsawatruk T, Lazzari L, Soo C, Peault B. 2014. Natural history of mesenchymal stem cells, from vessel walls to culture vessels. Cellular and Molecular Life Sciences 71:1353-1374.

Nakamura Y, Tensho K, Nakaya H, Nawata M, Okabe T, Wakitani S. 2005. Low dose fibroblast growth factor-2 (FGF-2) enhances bone morphogenetic protein-2 (BMP-2)-induced ectopic bone formation in mice. Bone 36:399-407.

Nanci A. 1999. Content and Distribution of Noncollagenous Matrix Proteins in Bone and Cementum: Relationship to Speed of Formation and Collagen Packing Density. Journal of Structural Biology 126:256-269.

Natta FJv, Hill JW, Carothers WH. 1934. Studies of Polymerization and Ring Formation. XXIII.1 ε-Caprolactone and its Polymers. Journal of the American Chemical Society 56:455-457.

Newman E, Turner AS, Wark JD. 1995. The potential of sheep for the study of osteopenia: current status and comparison with other animal models. Bone 16:277S-284S.

Neyt JG, Buckwalter JA, Carroll NC. 1998. Use of animal models in musculoskeletal research. The Iowa orthopaedic journal 18:118-123.

Nguyen MK, Alsberg E. 2014. Bioactive factor delivery strategies from engineered polymer hydrogels for therapeutic medicine. Progress in Polymer Science 39:1235-1265.

NHS. 2013. CCG Program Budgeting Benchmarking

Niemeyer P, Fechner K, Milz S, Richter W, Suedkamp NP, Mehlhorn AT, Pearce S, Kasten P. 2010. Comparison of mesenchymal stem cells from bone marrow and adipose tissue for bone regeneration in a critical size defect of the sheep tibia and the influence of platelet-rich plasma. Biomaterials 31:3572-3579.

Noth U, Osyczka AM, Tuli R, Hickok NJ, Danielson KG, Tuan RS. 2002. Multilineage mesenchymal differentiation potential of human trabecular bone-derived cells. J Orthop Res 20.

Nuss K, Auer JA, Boos A, Rechenberg B. 2006a. An animal model in sheep for biocompatibility testing of biomaterials in cancellous bones. BMC Musculoskelet Disord 15.

Nuss KM, Auer JA, Boos A, Von Rechenberg B. 2006b. An animal model in sheep for biocompatibility testing of biomaterials in cancellous bones. BMC Musculoskelet Disord 7:67.

Nyman JS, Roy A, Shen X, Acuna RL, Tyler JH, Wang X. 2006. The influence of water removal on the strength and toughness of cortical bone. Journal of biomechanics 39:931-938.

Oh SH, Park IK, Kim JM, Lee JH. 2007. *In vitro* and *in vivo* characteristics of PCL scaffolds with pore size gradient fabricated by a centrifugation method. Biomaterials 28:1664-1671.

ONS. 2015. National Population Projections: 2014-based statistical bulletin. Office of National Statistics.

Oryan A, Alidadi S, Moshiri A, Maffulli N. 2014. Bone regenerative medicine: classic options, novel strategies, and future directions. Journal of Orthopaedic Surgery and Research 9:1-27.

Otsu N. 1975. A threshold selection method from gray-level histograms. Automatica.

Ovsianikov A, Gruene M, Pflaum M, Koch L, Maiorana F, Wilhelmi M, Haverich A, Chichkov B. 2010. Laser printing of cells into 3D scaffolds. Biofabrication 2:014104.

Paley D, Maar DC. 2000. Ilizarov bone transport treatment for tibial defects. J Orthop Trauma 14:76-85.

Paolo Bianco XC, Paul S Frenette, Jeremy J Mao, Pamela G Robey, Paul J Simmons & Cun-Yu Wang. 2013. The meaning, the sense and the significance: translating the science of mesenchymal stem cells into medicine. Nature Medicine 19:12.

Papakostidis C, Kanakaris NK, Pretel J, Faour O, Morell DJ, Giannoudis PV. 2011. Prevalence of complications of open tibial shaft fractures stratified as per the Gustilo–Anderson classification. Injury 42:1408-1415.

Parr AM, Tator CH, Keating A. 2007. Bone marrow-derived mesenchymal stromal cells for the repair of central nervous system injury. Bone Marrow Transplant 40:609-619.

Patan S. 2004. Vasculogenesis and Angiogenesis. In: Kirsch M, Black PM, editors. Angiogenesis in Brain Tumors. Boston, MA: Springer US. p 3-32.

Pearce AI, Richards RG, Milz S, Schneider E, Pearce SG. 2007a. Animal models for implant biomaterial research in bone: A review. Eur Cells Mater 13:1-10.

Pearce AI, Richards RG, Milz S, Schneider E, Pearce SG. 2007b. Animal models for implant biomaterial research in bone: a review. Eur Cell Mater 13.

Pek YS, Wan ACA, Ying JY. 2010. The effect of matrix stiffness on mesenchymal stem cell differentiation in a 3D thixotropic gel. Biomaterials 31:385-391.

Perry CR. 1999. Bone repair techniques, bone graft, and bone graft substitutes. Clin Orthop Rel Res:71-86.

Phieffer LS, Goulet JA. 2006. Delayed Unions of the Tibia. The Journal of Bone & Joint Surgery 88:205-216.

Piard CM, Chen Y, Fisher JP. 2015. Cell-Laden 3D Printed Scaffolds for Bone Tissue Engineering. Clinical Reviews in Bone and Mineral Metabolism 13:245-255.

Pietrzak WS, Ali SN, Chitturi D, Jacob M, Woodell-May JE. 2011. BMP depletion occurs during prolonged acid demineralization of bone: characterization and implications for graft preparation. Cell and Tissue Banking 12:81-88.

Pittenger MF. 2013. MSCs: science and trials. Nat Med 19:811-811.

Pittenger MF, Mackay AM, Beck SC, Jaiswal RK, Douglas R, Mosca JD, Moorman MA, Simonetti DW, Craig S, Marshak DR. 1999. Multilineage potential of adult human mesenchymal stem cells. Science 284:143-147.

Pobloth A-M, Duda GN, Giesecke MT, Dienelt A, Schwabe P. 2015. High-dose recombinant human bone morphogenetic protein-2 impacts histological and biomechanical properties of a cervical spine fusion segment: results from a sheep model. J Tissue Eng Regen Med:n/a-n/a.

Pobloth A-M, Johnson KA, Schell H, Kolarczik N, Wulsten D, Duda GN, Schmidt-Bleek K. 2016. Establishment of a preclinical ovine screening model for the investigation of bone tissue engineering strategies in cancellous and cortical bone defects. BMC Musculoskelet Disord 17:1-12.

Pountos I, Georgouli T, Kontakis G, Giannoudis PV. 2010. Efficacy of minimally invasive techniques for enhancement of fracture healing: evidence today. Int Orthop 34:3-12.

Preativatanyou K, Honsawek S. 2011. RhBMP-2 and-7 combined with absorbable collagen sponge carrier enhance ectopic bone formation: An *in vivo* bioassay. Asian Biomedicine 5:85-92.

Prieto EM, Talley AD, Gould NR, Zienkiewicz KJ, Drapeau SJ, Kalpakci KN, Guelcher SA. 2015. Effects of particle size and porosity on *in vivo* remodeling of settable allograft bone/polymer composites. Journal of Biomedical Materials Research Part B: Applied Biomaterials 103:1641-1651.

Quarto R, Mastrogiacomo M, Cancedda R, Kutepov SM, Mukhachev V, Lavroukov A, Kon E, Marcacci M. 2001. Repair of Large Bone Defects with the Use of Autologous Bone Marrow Stromal Cells. New England Journal of Medicine 344:385-386.

Raab DM, Crenshaw TD, Kimmel DB, Smith EL. 1991. A histomorphometric study of cortical bone activity during increased weight-bearing exercise. Journal of bone and mineral research : the official journal of the American Society for Bone and Mineral Research 6:741-749.

Registry NJ. 2016. National Joint Registry Annual Report 2016. wwwnjrcentreorguk.

Reichert JC, Epari DR, Wullschleger ME, Saifzadeh S, Steck R, Lienau J, Sommerville S, Dickinson IC, Schutz MA, Duda GN, Hutmacher DW. 2010. Establishment of a Preclinical Ovine Model for Tibial Segmental Bone Defect Repair by Applying Bone Tissue Engineering Strategies. Tissue Eng Part B-Rev 16:93-104.

Reichert JC, Saifzadeh S, Wullschleger ME, Epari DR, Schutz MA, Duda GN, Schell H, van Griensven M, Redl H, Hutmacher DW. 2009. The challenge of establishing preclinical models for segmental bone defect research. Biomaterials 30:2149-2163.

Reifenrath J, Angrisani N, Lalk M, Besdo S. 2014. Replacement, refinement, and reduction: Necessity of standardization and computational models for long bone fracture repair in animals. J Biomed Mater Res Part A 102:2884-2900.

Ren JY, Blackwood KA, Doustgani A, Poh PP, Steck R, Stevens MM, Woodruff MA. 2014. Melt-electrospun polycaprolactone strontium-substituted bioactive glass scaffolds for bone regeneration. J Biomed Mater Res Part A 102:3140-3153.

Reneker D, Yarin A, Fong H, Koombhongse S. 2000. Bending instability of electrically charged liquid jets of polymer solutions

in electrospinning. JOURNAL OF APPLIED PHYSICS 87.

Rentsch C, Hess R, Rentsch B, Hofmann A, Manthey S, Scharnweber D, Biewener A, Zwipp H. 2010. Ovine bone marrow mesenchymal stem cells: isolation and characterization of the cells and their osteogenic differentiation potential on embroidered and surface-modified polycaprolactone-co-lactide scaffolds. *In vitro* Cellular & Developmental Biology - Animal 46:624-634.

Reznikov N, Shahar R, Weiner S. 2014. Bone hierarchical structure in three dimensions. Acta Biomaterialia 10:3815-3826.

Rho J-Y, Kuhn-Spearing L, Zioupos P. 1998. Mechanical properties and the hierarchical structure of bone. Medical Engineering & Physics 20:92-102.

Ridgway J, Butcher A, Chen P-S, Horner A, Curran S. 2010. Novel technology to provide an enriched therapeutic cell concentrate from bone marrow aspirate. Biotechnology Progress 26:1741-1748.

Roberts TT, Rosenbaum AJ. 2012. Bone grafts, bone substitutes and orthobiologics: The bridge between basic science and clinical advancements in fracture healing. Organogenesis 8:114-124.

Rogers GF, Greene AK. 2012. Autogenous bone graft: basic science and clinical implications. The Journal of craniofacial surgery 23:323-327.

Rosier RN, O'Keefe RJ, Hicks DG. 1998. The potential role of transforming growth factor beta in fracture healing. Clin Orthop Relat Res:S294-300.

Rouwkema J, Rivron NC, van Blitterswijk CA. 2008. Vascularization in tissue engineering. Trends in Biotechnology 26:434-441.

Rozemuller H, Prins H-J, Naaijkens B, Staal J, Bühring H-J, Martens AC. 2010. Prospective Isolation of Mesenchymal Stem Cells from Multiple Mammalian Species Using Cross-Reacting Anti-Human Monoclonal Antibodies. Stem Cells Dev 19:1911-1921.

Rubessa M, Polkoff K, Bionaz M, Monaco E, Milner DJ, Holllister SJ, Goldwasser MS, Wheeler MB. 2017. Use of Pig as a Model for Mesenchymal Stem Cell Therapies for Bone Regeneration. Animal Biotechnology:1-13.

Rundle CH, Wang H, Yu H, Chadwick RB, Davis EI, Wergedal JE, Lau KHW, Mohan S, Ryaby JT, Baylink DJ. 2006. Microarray analysis of gene expression during the inflammation and endochondral bone formation stages of rat femur fracture repair. Bone 38:521-529.

Rutz AL, Hyland KE, Jakus AE, Burghardt WR, Shah RN. 2015. A Multimaterial Bioink Method for 3D Printing Tunable, Cell-Compatible Hydrogels. Adv Mater 27:1607-1614.

Sachlos, Czernuszka. 2003. MAKING TISSUE ENGINEERING SCAFFOLDS WORK.

REVIEW ON THE APPLICATION OF SOLID FREEFORM FABRICATION

TECHNOLOGY TO THE PRODUCTION OF TISSUE ENGINEERING SCAFFOLDS. Eur Cells Mater 5.

Salgado AJ, Coutinho OP, Reis RL. 2004. Bone Tissue Engineering: State of the Art and Future Trends. Macromolecular Bioscience 4:743-765.

Samkoe KS, Cramb DT. 2003. Application of an ex ovo chicken chorioallantoic membrane model for two-photon excitation photodynamic therapy of age-related macular degeneration. BIOMEDO 8:410-417.

Sandhu HS, Grewal HS, Parvataneni H. 1999. Bone grafting for spinal fusion. The Orthopedic clinics of North America 30:685-698.

Sanjurjo-Rodriguez C, Castro-Vinuelas R, Hermida-Gomez T, Fernandez-Vazquez T, Fuentes-Boquete IM, de Toro-Santos FJ, Diaz-Prado SM, Blanco-Garcia FJ. 2017. Ovine Mesenchymal Stromal Cells: Morphologic, Phenotypic and Functional Characterization for Osteochondral Tissue Engineering. PLoS One 12:e0171231.

Santos ARC, Almeida HA, Bártolo PJ. 2013. Additive manufacturing techniques for scaffold-based cartilage tissue engineering. Virtual and Physical Prototyping 8:175-186.

Sartori S, Silvestri M, Forni F, Icaro Cornaglia A, Tesei P, Cattaneo V. 2003. Ten-year follow-up in a maxillary sinus augmentation using anorganic bovine bone (Bio-Oss). A case report with histomorphometric evaluation. Clinical Oral Implants Research 14:369-372.

Sawhney AS, Hubbell JA. 1992. Poly(ethylene oxide)-graft-poly(L-lysine) copolymers to enhance the biocompatibility of poly(L-lysine)-alginate microcapsule membranes. Biomaterials 13:863-870.

Sawkins MJ, Bowen W, Dhadda P, Markides H, Sidney LE, Taylor AJ, Rose FRAJ, Badylak SF, Shakesheff KM, White LJ. 2013. Hydrogels derived from demineralized and decellularized bone extracellular matrix. Acta Biomaterialia 9:7865-7873.

Sawyer AA, Song SJ, Susanto E, Chuan P, Lam CXF, Woodruff MA, Hutmacher DW, Cool SM. 2009. The stimulation of healing within a rat calvarial defect by mPCL–TCP/collagen scaffolds loaded with rhBMP-2. Biomaterials 30:2479-2488.

Schnabel LV, Fortier LA, Wayne McIlwraith C, Nobert KM. 2013. Therapeutic use of stem cells in horses: Which type, how, and when? The Veterinary Journal 197:570-577.

Schnell S, Friedman SM, Mendelson DA, Bingham KW, Kates SL. 2010. The 1-Year Mortality of Patients Treated in a Hip Fracture Program for Elders. Geriatric Orthopaedic Surgery & Rehabilitation 1:6-14.

Scott MA, Levi B, Askarinam A, Nguyen A, Rackohn T, Ting K, Soo C, James AW. 2012. Brief Review of Models of Ectopic Bone Formation. Stem Cells Dev 21:655-667.

Sen MK, Miclau T. 2007. Autologous iliac crest bone graft: Should it still be the gold standard for treating nonunions? Injury 38:S75-S80.

Seo B-B, Choi H, Koh J-T, Song S-C. 2015. Sustained BMP-2 delivery and injectable bone regeneration using thermosensitive polymeric nanoparticle hydrogel bearing dual interactions with BMP-2. Journal of Controlled Release 209:67-76.

Seyed Farid Seyed S, Samira G, Mehdi M, Hooman Y, Hendrik Simon Cornelis M, Nahrizul Adib K, Noor Azuan Abu O. 2015. A review on powder-based additive manufacturing for tissue engineering: selective laser sintering and inkjet 3D printing. Science and Technology of Advanced Materials 16:033502.

Shamblott MJ, Axelman J, Wang S, Bugg EM, Littlefield JW, Donovan PJ, Blumenthal PD, Huggins GR, Gearhart JD. 1999. Derivation of Pluripotent Stem Cells From Cultured Human Primordial Germ Cells. Obstetrical & Gynecological Survey 54:177-178.

Shang Q, Wang Z, Liu W, Shi Y, Cui L, Cao Y. 2001. Tissue-engineered bone repair of sheep cranial defects with autologous bone marrow stromal cells. The Journal of craniofacial surgery 12:586-593; discussion 594-585.

Shibuya N, Jupiter DC, Clawson LD, La Fontaine J. 2012. Incorporation of Bovine-based Structural Bone Grafts Used in Reconstructive Foot Surgery. The Journal of Foot and Ankle Surgery 51:30-33.

Shimomura K, Moriguchi Y, Murawski CD, Yoshikawa H, Nakamura N. 2014. Osteochondral Tissue Engineering with Biphasic Scaffold: Current Strategies and Techniques. Tissue Engineering Part B: Reviews 20:468-476.

Shin M, Yoshimoto H, Vacanti JP. 2004. *In vivo* bone tissue engineering using mesenchymal stem cells on a novel electrospun nanofibrous scaffold. Tissue Eng 10:33-41.

Simmons P, Torok-Storb B. 1991. Identification of stromal cell precursors in human bone marrow by a novel monoclonal antibody, STRO-1. Blood 78:55-62.

Simonet WS, Lacey DL, Dunstan CR, Kelley M, Chang MS, Lüthy R, Nguyen HQ, Wooden S, Bennett L, Boone T, Shimamoto G, DeRose M, Elliott R, Colombero A, Tan HL, Trail G, Sullivan J, Davy E, Bucay N, Renshaw-Gegg L, Hughes TM, Hill D, Pattison W, Campbell P, Sander S, Van G, Tarpley J, Derby P, Lee R, Boyle WJ. 1997. Osteoprotegerin: A Novel Secreted Protein Involved in the Regulation of Bone Density. Cell 89:309-319.

Smith EL, Kanczler JM, Oreffo ROC. 2013. A NEW TAKE ON AN OLD STORY: CHICK LIMB ORGAN CULTURE FOR SKELETAL NICHE DEVELOPMENT AND REGENERATIVE MEDICINE EVALUATION. Eur Cells Mater 26:91-106.

Sobral JM, Caridade SG, Sousa RA, Mano JF, Reis RL. 2011. Three-dimensional plotted scaffolds with controlled pore size gradients: Effect of scaffold geometry on mechanical performance and cell seeding efficiency. Acta Biomater 7:1009-1018.

Soleimani M, Nadri S. 2009. A protocol for isolation and culture of mesenchymal stem cells from mouse bone marrow. Nat Protocols 4:102-106.

Sornay-Rendu E, Boutroy S, Duboeuf F, Chapurlat RD. 2017. Bone Microarchitecture Assessed by HR-pQCT as Predictor of Fracture Risk in Postmenopausal Women: The OFELY Study. J Bone Miner Res:n/a-n/a.

Spiller KL, Vunjak-Novakovic G. 2015. Clinical translation of controlled protein delivery systems for tissue engineering. Drug Delivery and Translational Research 5:101-115.

Srouji S, Blumenfeld I, Rachmiel A, Livne E. Bone defect repair in rat tibia by TGF-β1 and IGF-1 released from hydrogel scaffold. Cell and Tissue Banking 5:223-230.

Srouji S, Rachmiel A, Blumenfeld I, Livne E. 2005. Mandibular defect repair by TGF-β and IGF-1 released from a biodegradable osteoconductive hydrogel. Journal of Cranio-Maxillofacial Surgery 33:79-84.

Starman JS, Bosse MJ, Cates CA, Norton HJ. 2012. Recombinant human bone morphogenetic protein-2 use in the off-label treatment of nonunions and acute fractures: a retrospective review. The journal of trauma and acute care surgery 72:676-681.

Stegen S, van Gastel N, Carmeliet G. 2015. Bringing new life to damaged bone: The importance of angiogenesis in bone repair and regeneration. Bone 70:19-27.

Story BJ, Wagner WR, Gaisser DM, Cook SD, Rust-Dawicki AM. 1998. *In vivo* performance of a modified CSTi dental implant coating. The International journal of oral & maxillofacial implants 13:749-757.

Strobel E-S, Gay RE, Greenberg PL. 1986. Characterization of the *in vitro* stromal microenvironment of human bone marrow. The International Journal of Cell Cloning 4:341-356.

Sutherland FWH, Perry TE, Yu Y, Sherwood MC, Rabkin E, Masuda Y, Garcia GA, McLellan DL, Engelmayr GC, Sacks MS, Schoen FJ, Mayer JE. 2005. From Stem Cells to Viable Autologous Semilunar Heart Valve. Circulation 111:2783-2791.

Tardif G, Hum D, Pelletier J-P, Boileau C, Ranger P, Martel-Pelletier J. 2004. Differential gene expression and regulation of the bone morphogenetic protein antagonists follistatin and gremlin in normal and osteoarthritic human chondrocytes and synovial fibroblasts. Arthritis & Rheumatism 50:2521-2530.

Tare RS, Mitchell PD, Kanczler J, Oreffo RO. 2012. Isolation, differentiation, and characterisation of skeletal stem cells from human bone marrow *in vitro* and *in vivo*. Bone Research Protocols:83-99.

Tatarova Z, Abbuehl J-P, Maerkl S, Huelsken J. 2016. Microfluidic co-culture platform to quantify chemotaxis of primary stem cells. Lab Chip.

Tavassoli M, Crosby WH. 1968. Transplantation of Marrow to Extramedullary Sites. Science 161:54.

Thorwarth M, Schultze-Mosgau S, Kessler P, Wiltfang J, Schlegel KA. 2005. Bone Regeneration in Osseous Defects Using a Resorbable Nanoparticular Hydroxyapatite. Journal of Oral and Maxillofacial Surgery 63:1626-1633.

Tsiridis E, Upadhyay N, Giannoudis P. 2007. Molecular aspects of fracture healing:Which are the important molecules? Injury 38:S11-S25.

Tsuruga E, Takita H, Itoh H, Wakisaka Y, Kuboki Y. 1997. Pore Size of Porous Hydroxyapatite as the Cell-Substratum Controls BMP-Induced Osteogenesis. Journal of Biochemistry 121:317-324.

Uebersax L, Apfel T, Nuss KMR, Vogt R, Kim HY, Meinel L, Kaplan DL, Auer JA, Merkle HP, von Rechenberg B. 2013. Biocompatibility and osteoconduction of macroporous silk fibroin implants in cortical defects in sheep. European Journal of Pharmaceutics and Biopharmaceutics 85:107-118.

Uludag H, D'Augusta D, Palmer R, Timony G, Wozney J. 1999. Characterization of rhBMP-2 pharmacokinetics implanted with biomaterial carriers in the rat ectopic model. J Biomed Mater Res 46:193-202.

Umulis D, O'Connor MB, Blair SS. 2009. The extracellular regulation of bone morphogenetic protein signaling. Development 136:3715-3728.

Urist MR. 1965. Bone: Formation by Autoinduction. Science 150:893-899.

Utech S, Boccaccini AR. 2015. A review of hydrogel-based composites for biomedical applications: enhancement of hydrogel properties by addition of rigid inorganic fillers. Journal of Materials Science 51:271-310.

Vaezi M, Seitz H, Yang S. 2013. A review on 3D micro-additive manufacturing technologies. The International Journal of Advanced Manufacturing Technology 67:1721-1754.

Vallet-Regí M, Ruiz-Hernández E. 2011. Bioceramics: From Bone Regeneration to Cancer Nanomedicine. Adv Mater 23:5177-5218.

van Gestel NAP, Geurts J, Hulsen DJW, van Rietbergen B, Hofmann S, Arts JJ. 2015. Clinical Applications of S53P4 Bioactive Glass in Bone Healing and Osteomyelitic Treatment: A Literature Review. BioMed Research International 2015:12.

van Leeuwen AC, Huddleston Slater JJR, Gielkens PFM, de Jong JR, Grijpma DW, Bos RRM. 2012. Guided bone regeneration in rat mandibular defects using resorbable poly(trimethylene carbonate) barrier membranes. Acta Biomaterialia 8:1422-1429.

van Staa TP, Dennison EM, Leufkens HGM, Cooper C. 2001. Epidemiology of fractures in England and Wales. Bone 29:517-522.

Verron E, Pissonnier M-L, Lesoeur J, Schnitzler V, Fellah BH, Pascal-Moussellard H, Pilet P, Gauthier O, Bouler J-M. 2014. Vertebroplasty using bisphosphonate-loaded calcium phosphate cement in a standardized vertebral body bone defect in an osteoporotic sheep model. Acta Biomaterialia 10:4887-4895.

Vert M, Li SM, Spenlehauer G, Guerin P. 1992. Bioresorbability and biocompatibility of aliphatic polyesters. Journal of Materials Science: Materials in Medicine 3:432-446.

Visconti RP, Richardson CD, Sato TN. 2002. Orchestration of angiogenesis and arteriovenous contribution by angiopoietins and vascular endothelial growth factor (VEGF). Proceedings of the National Academy of Sciences 99:8219-8224.

Visser R, Arrabal PM, Becerra J, Rinas U, Cifuentes M. 2009. The effect of an rhBMP-2 absorbable collagen sponge-targeted system on bone formation *in vivo*. Biomaterials 30:2032-2037.

von Bahr L, Batsis I, Moll G, Hägg M, Szakos A, Sundberg B, Uzunel M, Ringden O, Le Blanc K. 2012. Analysis of Tissues Following Mesenchymal Stromal Cell Therapy in Humans Indicates Limited Long-Term Engraftment and No Ectopic Tissue Formation. STEM CELLS 30:1575-1578.

von Rechenberg B, Génot OR, Nuss K, Galuppo L, Fulmer M, Jacobson E, Kronen P, Zlinszky K, Auer JA. 2013. Evaluation of four biodegradable, injectable bone cements in an experimental drill hole model in sheep. European Journal of Pharmaceutics and Biopharmaceutics 85:130-138.

Wagner W, Wein F, Seckinger A, Frankhauser M, Wirkner U, Krause U, Blake J, Schwager C, Eckstein V, Ansorge W, Ho AD. 2005. Comparative characteristics of mesenchymal stem cells from human bone marrow, adipose tissue, and umbilical cord blood. Exp Hematol 33:1402-1416.

Wang, Agrawal. 1998. An interspecies comparison of bone fracture

properties.

Wang H, Zou Q, Boerman OC, Nijhuis AWG, Jansen JA, Li Y, Leeuwenburgh SCG. 2013. Combined delivery of BMP-2 and bFGF from nanostructured colloidal gelatin gels and its effect on bone regeneration *in vivo*. Journal of Controlled Release 166:172-181.

Wang L, Zhang B, Bao CY, Habibovic P, Hu J, Zhang XD. 2014. Ectopic Osteoid and Bone Formation by Three Calcium-Phosphate Ceramics in Rats, Rabbits and Dogs. Plos One 9.

Warnke PH, Springer IN, Acil Y, Julga G, Wiltfang J, Ludwig K, Russo PAJ, Sherry E, Sivananthan S, Hedderich J, Terheyden H. 2006. The mechanical integrity of *in vivo* engineered heterotopic bone. Biomaterials 27:1081-1087.

Wedemeyer M, Parent S, Mahar A, Odell T, Swimmer T, Newton P. 2007. Titanium versus stainless steel for anterior spinal fusions - An analysis of rod stress as a predictor of rod breakage during physiologic loading in a bovine model. Spine 32:42-48.

Weiner S, Traub W. 1992. Bone structure: from angstroms to microns. The FASEB Journal 6:879-885.

WHO. 2012. Annual Technical Report 2012, World Health Organisation. http://appswhoint/iris/bitstream/10665/84992/1/WHO_RHR_1305_engpdf.

Wiese A, Pape HC. 2010. Bone Defects Caused by High-energy Injuries, Bone Loss, Infected Nonunions, and Nonunions. Orthopedic Clinics of North America 41:1-4.

Wijdicks CA, Virdi AS, Sena K, Sumner DR, Leven RM. 2009. ULTRASOUND ENHANCES RECOMBINANT HUMAN BMP-2 INDUCED ECTOPIC BONE FORMATION IN A RAT MODEL. Ultrasound in Medicine and Biology 35:1629-1637.

Wildemann B, Kadow-Romacker A, Haas NP, Schmidmaier G. 2007. Quantification of various growth factors in different demineralized bone matrix preparations. J Biomed Mater Res Part A 81A:437-442.

Williams EL, White K, Oreffo ROC. 2013. Isolation and Enrichment of Stro-1 Immunoselected Mesenchymal Stem Cells from Adult Human Bone Marrow. In: Turksen K, editor. Stem Cell Niche: Methods and Protocols. Totowa, NJ: Humana Press. p 67-73.

Wolfe SW, Pike L, Slade Iii JF, Katz LD. 1999. Augmentation of Distal Radius Fracture Fixation With Coralline Hydroxyapatite Bone Graft Substitute. The Journal of Hand Surgery 24:816-827.

Wolpert L. 2004. Much more from the chicken's egg than breakfast--a wonderful model system. Mech Dev 121:1015-1017.

Woodruff MA, Lange C, Reichert J, Berner A, Chen FL, Fratzl P, Schantz JT, Hutmacher DW. 2012. Bone tissue engineering: from bench to bedside. Mater Today 15:430-435.

Woods HM, Silva MMCG, Nouvel C, Shakesheff KM, Howdle SM. 2004. Materials processing in supercritical carbon dioxide: surfactants, polymers and biomaterials. Journal of Materials Chemistry 14:1663-1678.

Wright DE, Cheshier SH, Wagers AJ, Randall TD, Christensen JL, Weissman IL. 2001. Cyclophosphamide/granulocyte colony-stimulating factor causes selective mobilization of bone marrow hematopoietic stem cells into the blood after M phase of the cell cycle. Blood 97:2278-2285.

Xavier M, Oreffo ROC, Morgan H. 2016. Skeletal stem cell isolation: A review on the state-of-the-art microfluidic label-free sorting techniques. Biotechnology Advances 34:908-923.

Yamada Y, Ueda M, Naiki T, Nagasaka T. 2004. Tissue-engineered injectable bone regeneration for osseointegrated dental implants. Clinical Oral Implants Research 15:589-597.

Yamamoto M, Takahashi Y, Tabata Y. 2003a. Controlled release by biodegradable hydrogels enhances the ectopic bone formation of bone morphogenetic protein. Biomaterials 24:4375-4383.

Yamamoto M, Takahashi Y, Tabata Y. 2003b. Controlled release by biodegradable hydrogyels enhances the ectopic bone formation of bone morphogenetic protein. Biomaterials 24:4375-4383.

Yang S, Leong KF, Du Z, Chua CK. 2001. The design of scaffolds for use in tissue engineering. Part I. Traditional factors. Tissue Eng 7:679-689.

Yang XBB, Whitaker MJ, Sebald W, Clarke N, Howdle SM, Shakesheff KM, Oreffo ROC. 2004. Human osteoprogenitor bone formation using encapsulated bone morphogenetic protein 2 in porous polymer scaffolds. Tissue Eng 10:1037-1045.

Yelin E. 2003. Cost of musculoskeletal diseases: impact of work disability and functional decline. The Journal of Rheumatology 68:8-11.

Yuan H, Kurashina K, de Bruijn JD, Li Y, de Groot K, Zhang X. 1999. A preliminary study on osteoinduction of two kinds of calcium phosphate ceramics. Biomaterials 20:1799-1806.

Zaiss S, Brown T, Reichert J, Berner A. 2016. Poly(ε-caprolactone) Scaffolds Fabricated by Melt Electrospinning for Bone Tissue Engineering. Materials 9:232.

Zellin G, Linde A. 2000. Effects of recombinant human fibroblast growth factor-2 on osteogenic cell populations during orthopic osteogenesis *in vivo*. Bone 26:161-168.

Zhang X, Guo J, Wu G, Zhou Y. 2015. Effects of heterodimeric bone morphogenetic protein-2/7 on osteogenesis of human adipose-derived stem cells. Cell Proliferation 48:650-660.

Zhang Y, Fan Y, Wang Z, Wan Y, Zhou Z, Zhong B, Wang L, Wang F. 2012. Isolation, characterization, and gene modification of dairy goat mesenchymal stem cells from bone marrow. *In vitro* Cellular & Developmental Biology Animal 48:418-425.

Zhao B, Katagiri T, Toyoda H, Takada T, Yanai T, Fukuda T, Chung U-i, Koike T, Takaoka K, Kamijo R. 2006. Heparin potentiates the *in vivo* ectopic bone formation induced by bone morphogenetic protein-2. J Biol Chem 281:23246-23253.

Zhao F, Ma T. 2005. Perfusion bioreactor system for human mesenchymal stem cell tissue engineering: Dynamic cell seeding and construct development. Biotechnology and Bioengineering 91:482-493.

Zheng L, Fan HS, Sun J, Chen XN, Wang G, Zhang L, Fan YJ, Zhang XD. 2010. Chondrogenic differentiation of mesenchymal stem cells induced by collagen-based hydrogel: An *in vivo* study. J Biomed Mater Res Part A 93A:783-792.

Zhou H, Green TB, Joo YL. 2006. The thermal effects on electrospinning of polylactic acid melts. Polymer 47:7497-7505.

Zimmermann G, Moghaddam A. 2011. Allograft bone matrix versus synthetic bone graft substitutes. Injury 42.

Zioupos P. 2001. Ageing Human Bone: Factors Affecting its Biomechanical Properties and the Role of Collagen. J Biomater Appl 15:187-229.

Zong C, Xue DT, Yuan WJ, Wang W, Shen D, Tong XM, Shi DY, Liu LY, Zheng QA, Gao CY, Wang JF. 2010. RECONSTRUCTION OF RAT CALVARIAL DEFECTS WITH HUMAN MESENCHYMAL STEM CELLS AND OSTEOBLAST-LIKE CELLS IN POLY-LACTIC-CO-GLYCOLIC ACID SCAFFOLDS. Eur Cells Mater 20:109-120.

Zscharnack M, Hepp P, Richter R, Aigner T, Schulz R, Somerson J, Josten C, Bader A, Marquass B. 2010. Repair of Chronic Osteochondral Defects Using Predifferentiated Mesenchymal Stem Cells in an Ovine Model. The American Journal of Sports Medicine 38:1857-1869.